Technical Report 1245
August 1988

Graphite-Fiber-Reinforced Plastic Pressure Hull Mod 2 for the Advanced Unmanned Search System Vehicle

J. D. Stachiw
NOSC

B. Frame
Oak Ridge National Laboratory

NAVAL OCEAN SYSTEMS CENTER

San Diego, California 92152-5000

E. G. SCHWEIZER, CAPT, USN
Commander

R. M. HILLYER
Technical Director

ADMINISTRATIVE INFORMATION

The work in the report was performed for the Naval Sea Systems Command, Washington, DC 20362, by the Marine Materials Technical Staff (Code 9402), under program element 63713N, project number MS16, agency accession number DN588521.

Released by
J. D. Stachiw, Head
Marine Materials Technical Staff

Under authority of
N. B. Estabrook, Head
Ocean Engineering Division

LO

DISCLAIMER NOTICE

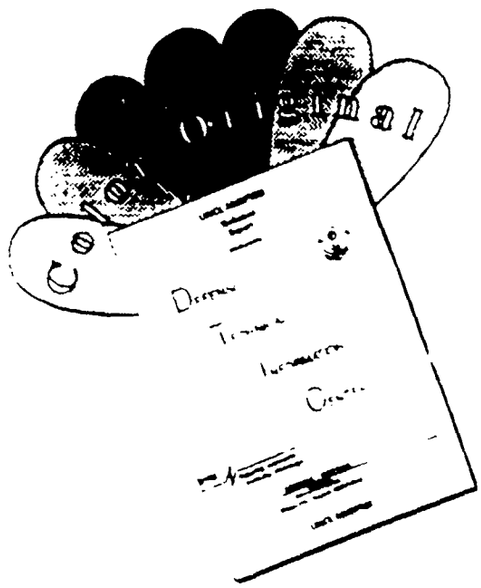

THIS DOCUMENT IS BEST QUALITY AVAILABLE. THE COPY FURNISHED TO DTIC CONTAINED A SIGNIFICANT NUMBER OF COLOR PAGES WHICH DO NOT REPRODUCE LEGIBLY ON BLACK AND WHITE MICROFICHE.

REPORT DOCUMENTATION PAGE

1a. REPORT SECURITY CLASSIFICATION UNCLASSIFIED	1b RESTRICTIVE MARKINGS
2a. SECURITY CLASSIFICATION AUTHORITY	3. DISTRIBUTION/AVAILABILITY OF REPORT Approved for public release; distribution is unlimited.
2b DECLASSIFICATION/DOWNGRADING SCHEDULE	
4. PERFORMING ORGANIZATION REPORT NUMBER(S) NOSC Technical Report 1245	5. MONITORING ORGANIZATION REPORT NUMBER(S)
6a. NAME OF PERFORMING ORGANIZATION Naval Ocean Systems Center 6b. OFFICE SYMBOL (if applicable) Code 9402	7a. NAME OF MONITORING ORGANIZATION
6c. ADDRESS (City, State and ZIP Code) San Diego, California 92152–5000	7b. ADDRESS (City, State and ZIP Code)
8a. NAME OF FUNDING/SPONSORING ORGANIZATION Naval Sea Systems Command 8b. OFFICE SYMBOL (if applicable) 05R41	9 PROCUREMENT INSTRUMENT IDENTIFICATION NUMBER
8c. ADDRESS (City, State and ZIP Code) Washington, DC 20362	10 SOURCE OF FUNDING NUMBERS PROGRAM ELEMENT NO. 63713N; PROJECT NO. MS16; TASK NO S0397; AGENCY ACCESSION NO. DN588521

11. TITLE (include Security Classification)
GRAPHITE-FIBER-REINFORCED PLASTIC PRESSURE HULL MOD 2 FOR THE ADVANCED UNMANNED SEARCH SYSTEM VEHICLE

12 PERSONAL AUTHOR(S)
J. D. Stachiw (NOSC) and B. Frame (Oak Ridge National Laboratory)

13a. TYPE OF REPORT	13b. TIME COVERED	14 DATE OF REPORT (Year, Month, Day)	15. PAGE COUNT
Final	FROM TO	August 1988	232

16 SUPPLEMENTARY NOTATION

17 COSATI CODES			18 SUBJECT TERMS (Continue on reverse if necessary and identify by block number)
FIELD	GROUP	SUB-GROUP	weight-to-displacement ratio wet winding graphite-fiber-reinforced plastic glass fiber reinforced plastic

19 ABSTRACT (Continue on reverse if necessary and identify by block number)

This report summarizes the fabrication and testing of the AUSS Mod 2 cylindrical pressure hull with a 30.75-inch outer diameter X 25.75-inch diameter X 65.0-inch length that successfully met the 20,000-foot design depth requirement of the AUSS vehicle. The AUSS Mod 2 pressure-hull assembly, consisting of a wet-wound graphite-fiber epoxy composite cylinder capped with adhesive-bonded titanium coupling rings, and closed off with titanium hemispherical bulkheads has a weight-to-displacement ratio of 0.58. The pressure-hull assembly provides the AUSS vehicle with a 950-lb positive buoyancy.

20 DISTRIBUTION/AVAILABILITY OF ABSTRACT	21 ABSTRACT SECURITY CLASSIFICATION
☐ UNCLASSIFIED/UNLIMITED ☒ SAME AS RPT ☐ DTIC USERS	UNCLASSIFIED

22a NAME OF RESPONSIBLE PERSON	22b TELEPHONE (Include Area Code)	22c OFFICE SYMBOL
J D Stachiw	(619) 553-1875	Code 9402

DD FORM 1473, 84 JAN — 83 APR EDITION MAY BE USED UNTIL EXHAUSTED ALL OTHER EDITIONS ARE OBSOLETE

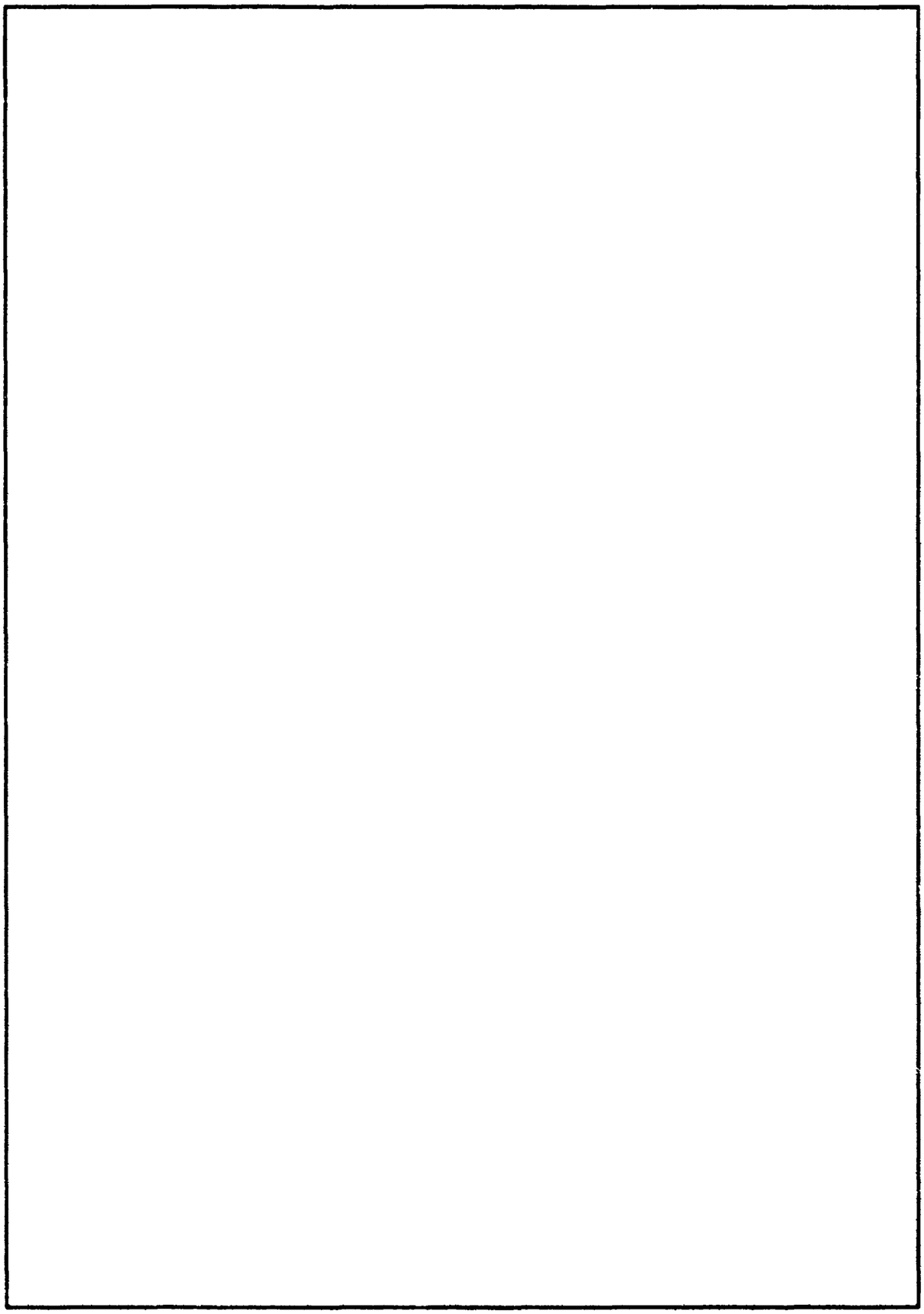

CONTENTS

CONTENTS (continued)

OBJECTIVE

Fabricate and test the AUSS Mod 2 cylindrical pressure hull that would successfully meet the outside diameter, inside diameter, length, and depth requirement of the AUSS vehicle.

RESULTS

The AUSS Mod 2 pressure-hull assembly, consisting of a wet-wound graphite fiber epoxy composite 25.75-inch (inside diameter) ID × 30.75-inch (outside diameter) OD × 65.0-inch length (L) cylinder, capped with adhesive-bonded titanium coupling rings, and closed off with titanium hemispherical bulkheads was found to satisfy operational requirements of the autonomous, deep-submergence AUSS vehicle. The AUSS Mod 2 pressure-hull assembly with the 0.58 weight-to-displacement ratio provides the vehicle with a 950-lb positive buoyancy. The weight-to-displacement ratio of the composite cylinder with titanium coupling rings, but without the bulkheads, is only 0.48.

RECOMMENDATIONS

1. Incorporate the composite AUSS Mod 2 cylindrical-hull assembly into the pressure housing of the AUSS vehicle for service to a 20,000-foot depth.

2. Apply the design, materials, and fabrication procedure used in the AUSS Mod 2 cylindrical hulls to the construction of deep-submergence cylindrical hulls for remotely operated or autonomous vehicles with external diameters less than three feet.

3. Initiate a research and development program to investigate the feasibility of applying the AUSS Mod 2 pressure-hull design, materials, and fabrication procedures to the construction of pressure hulls with greater length and external diameter.

4. Develop lightweight graphite-fiber epoxy composite hemispherical bulkheads to replace the heavy titanium bulkheads.

INTRODUCTION

The Navy, among other organizations and institutions, is very interested in acquiring the most effective and efficient submersibles and remotely operated vehicles (ROVs) for deep submergence operations. The three factors that determine if such submersibles or vehicles meet mission standards are the following: (1) payload, (2) operational range, and (3) speed. Each factor is a direct function of the system's buoyancy.

Buoyancy is the critical issue. Optimally, buoyancy is provided by a well-designed pressure hull. If the buoyancy provided by the pressure hull is inadequate, corrective measures are taken. However, these usually reduce the effectiveness of the submersible in fulfilling its mission task. For instance, additional buoyancy can be provided by attaching blocks of syntactic foam or soft-shell tanks filled with lighter-than-water fluids to the pressure hull. This approach has an overall negative impact on system cost and effectiveness.

Thus, the design and materials used in fabricating pressure hulls are of critical concern. The optimization of shape and the use of premium material in the construction of the hull are required to obtain a pressure hull with low weight-to-displacement ratio (a large positive buoyancy). The low weight-to-displacement ratio maximizes payload while maintaining optimum range and speed. For instance, assume a given payload volume is bound by the interior of a pressure hull. For a higher weight material, a weightier hull might require additional exterior buoyancy, thus changing the design shape and propulsion, speed, and range capabilities. A lower weight, high-strength hull material could permit the same payload volume and maintain optimum range and speed. The choice of materials is limited as only a few materials are light in weight, corrosion resistant, and strong in compression.

The characteristics of premium structural materials for external pressure housings are shown in Table 1, and housing-assembly material characteristics in terms of design pressure and of weight-to-displacement ratio are presented in Figures 1 2, and 3.

A quick glance at the numbers is sufficient to recognize that high-strength steel does not meet the rigid requirements. Stated simply, the poor weight-to-strength ratio will sink deep-submergence vehicles constructed from steel. Other metallic materials, like high-strength aluminum or titanium alloys, result in buoyant pressure hulls, but their buoyancy is inadequate for the payload requirements of a high-performance vehicle.

Only glass, ceramics, and fiber-reinforced epoxy composites possess the potential of providing the pressure hull for a 20,000-foot operational depth with a weight-to-displacement ratio less than 0.5, which is considered to be the minimum acceptable ratio for high-performance vehicles. Small (up to 12 inches in diameter and 92 inches in length) cylindrical pressure hulls with hemispherical end closures fabricated from 94-percent alumina ceramic have, to date, undergone more than 2000-pressure cycles to 9000 psi without implosion (References 1, 2, 3), substantiating the potential of ceramics to meet the 0.5 weight-to-displacement ratio for deep-submergence pressure hulls. There is, however, an industrial capacity limit to construction of alumina ceramic cylindrical and spherical pressure hulls with diameters in excess of 26 inches, and a technology barrier for diameters in excess of 10 feet. For glass ceramics, the

industrial capacity limit and technology barrier for cylinders and hemispheres lies beyond 10 feet.

Table 1. Premium structural materials for external pressure housings.

Material	Weight (lbs/in^3)	Compressive Strength (kpsi)	Strength Weight	Safety Factor
Steel (HY80)	0.283	80	280	1.25
Steel (HY130)	0.283	130	460	1.25
Aluminum (7075-T6)	0.10	73	730	1.25
Titanium (6AL-4V)	0.16	125	780	1.25
Glass (PYREX)	0.08	100	1250	2.0
Glass Composite	0.075	100	1330	2.0
Graphite Composite	0.057	100	1750	2.0
Beryllia Ceramic 96%	0.104	225	2160	2.0
Alumina Ceramic 94%	0.130	300	2310	2.0
Glass Ceramic (PYROCERAM 9606)	0.093	350	3760	2.0

There appears to be no industrial capacity limit for composites, or technological barrier for fabrication of cylinders in any size with deep-submergence capability. To date, however, only small (less than 12 inches in diameter and 24 inches in length) composite cylindrical pressure hulls have been fabricated from glass, or graphite-fiber-reinforced epoxy plastic and successfully pressure cycled to 9000 psi (References 4 to 12). Of these two composites, the graphite-fiber-reinforced plastic (GFRP) cylinders appear to be the only ones with a potential of meeting the 0.5 weight-to-displacement ratio requirement (Figure 4).

The GFRP composite was chosen by NOSC in 1982 for the fabrication of a cylindrical pressure hull for the Advanced Unmanned Search System (AUSS) vehicle with a 20,000-foot operational depth (Figure 5) based on the following criteria: (1) the favorable test results from the small size GFRP cylinder (Reference 12); (2) existing industrial capacity to fabricate cylinders up to 10 feet in diameter and 50 feet in length; and (3) absence of any intrinsic technological barrier.

The requirement for a cylindrical pressure hull with a 25.75-inch ID and a 45- to 90-inch L seemed to fall comfortably within the industrial fabrication capability, and the scaling up of fabrication processes developed for 6- to 8-inch diameter cylinders to 25- to 30-inch diameter cylinders appeared to be within the scope of existing technology. These assumptions turned out to be too optimistic and it was only after three changes in design, two contractors, and six fabrication attempts that, in 1987, the efforts were crowned with success (References 13, 14).

This report summarizes the fabrication and testing of the AUSS Mod 2 cylindrical pressure hull with a 30.75-inch OD x 25.75-inch ID x a 65.0-inch L that successfully met the 20,000-foot design depth requirement of the AUSS vehicle. The 0.477 weight/displacement ratio of the GFRP cylindrical pressure hull is better than the minimum acceptable 0.5 ratio of deep-submergence pressure hulls. However, when mated with titanium hemispherical end closures, its weight-to-displacement

ratio increases to 0.58. Although this weight-to-displacement ratio does not meet the 0.5 requirement of deep-submergence hulls, it is the lowest ratio achieved to date with a full-size GFRP pressure housing for remotely, or autonomously operated underwater vehicles. Replacement of titanium end closures with GFRP end closures should lower the weight-to-displacement ratio to 0.5, providing that lightweight GFRP hemispherical end closures are developed in the future.

PRESSURE-HULL DESIGN

The AUSS Mod 2 pressure-hull design for the AUSS vehicle consists of a GFRP cylinder, two titanium coupling rings, two aluminum split clamps, and two titanium end bells that serve as pressure-resistant bulkheads (Figure 6).

The Mod 2 design differs from Mod 1 design (Figure 7) by having the ends of the GFRP cylinder totally, instead of partially, enclosed by the seat in the titanium coupling ring. By enclosing the ends totally, instead of partially, (1) better sealing is achieved, (2) the adhesive is restrained from extrusion, (3) the ends of the cylinder are restrained from delamination, and (4) stronger bond is achieved between the titanium coupling ring and the GFRP cylinder.

CYLINDER

The 30.75-inch OD × 25.75-inch ID × 65.0-inch monocoque cylinder is fabricated from GFRP composite. The GFRP composite with 0.057 lb/cubic inch density results in a cylinder with 820 lb weight that provides the hull with an upward positive buoyancy of 966 lb when immersed in seawater. The 0.459 weight-to-displacement ratio of the GFRP cylinder surpasses the goal of 0.5 chosen for high-performance deep-submergence pressure hulls. When the cylinder is equipped with titanium coupling rings, its weight-to-displacement ratio increases to 0.477 which still surpasses the minimum goal ratio. The 0.477 weight-to-displacement ratio represents the lowest ratio reached to date with a full-scale GFRP cylindrical pressure-hull assembly (cylindrical GFRP hull with titanium coupling rings) for an unmanned vehicle with 9000-psi design pressure.

The ends of the cylinder are machined flat within 0.005 inch and parallel to each other within 0.010 inch (Figure 8) Since the GFRP does not lend itself to machining of grooves for sealing with o-rings, or joining with split wedge clamps, the ends of the cylinder are encased in titanium coupling rings securely bonded to the composite (Figure 9).

The cylinder wall thickness of 2.5 inches has been selected on the basis of 60,750-psi compressive stress in hoop direction on the interior surface at midbay and 32,250 psi compressive stress in axial direction on the exterior surface at midbay under 9000-psi design pressure. If the compressive strength of the composite in hoop direction exceeds 120,000 psi as specified, the cylinder will not implode due to material failure at pressures below 18,000 psi. The 0.097 thickness-to-interior diameter ratio also provides the monocoque GFRP cylinder with a critical instability pressure rating in excess of 30,000 psi even when it is not radially supported at its ends. The high critical pressure provides more than adequate margin of safety against elastic instability at the pressures below 18,000 psi.

COUPLING RINGS

The function of the titanium coupling rings Mod 2 is the following: (1) protect the ends of the GFRP cylinder from splitting; (2) serve as a smooth seal surface for the cylinder end; (3) provide a hard bearing surface for radial and axial support of the cylinder ends; and (4) act as a mechanical coupling device between the titanium end bells and the cylinder (Figure 9). Titanium was selected as structural material to match the modulus of elasticity and compressive strength of GFRP.

Lugs on the interior surface of the coupling rings serve as attachment points for rails connecting the coupling rings. These rails support the cage to which payload components are subsequently mounted. Specially formulated epoxy adhesive was selected for bonding the coupling rings to the GFRP cylinder. The radial clearances between the walls of the seat cavity in the coupling ring and the surfaces of the cylinder were kept to less than 0.030 inch to minimize extrusion of epoxy through the annular spaces when the epoxy layer is exposed to high-compressive bearing stress.

The Mod 2 coupling rings differ from Mod 1 rings (Figure 10) used with the AUSS Mod 1 pressure hull in two ways: (1) the seat on the coupling ring encloses the end of the cylinder totally instead of partially, and (2) the attachment lugs for interior rails present a smaller discontinuity on the interior surface of the ring.

The titanium coupling ring weighs 50 lb, resulting in a negative buoyancy of 13. If 7075-T6 aluminum alloy is substituted for the 6Al4Va titanium alloy, the weight of the coupling ring would decrease to 32 lb resulting in a positive buoyancy of 5 lb. Use of hard coatings on the aluminum surfaces could minimize corrosion in service. Substitution of aluminum for titanium in the coupling rings is, however, not recommended for the AUSS cylinder as the vehicle will be exposed to a marine environment for extended periods of time and the frequent disassembly and reassembly of the vehicle for charging of batteries will remove the protective coatings from the joint surface, causing it to corrode.

END BELL

Two hemispherical end bells serve as lightweight bulkheads for the GFRP cylindrical pressure hull (Figures 11, 12). The bells were cast from 6Al4Va titanium alloy and subsequently machined both on the exterior and interior surfaces by OREMET, Albany, Oregon. Castings, instead of forgings, were chosen because it resulted in substantial cost savings while at the same time provided a guaranteed compressive yield strength of 125,000 psi.

GFRP composite also was considered for this application as it had the potential of resulting in a lighter end bell. However, economical manufacturing techniques were not found that would guarantee predictable structural performance of a GFRP hemisphere under external design stress of 50,000 psi. This is the minimum stress level at which a GFRP hemisphere (equipped with titanium penetration inserts and coupling ring) becomes weight competitive with an optimally proportioned formed titanium end bell that has been designed with a 1.25 safety factor.

The cast-titanium end bells were designed with a 1.5 safety factor as there were some doubts about the accuracy of the design calculations and the ability of the fabricator to maintain the tight dimensional tolerances specified for the spherical

surfaces. Each of the cast-titanium end bells was provided with 8 holes whose diameters range from 1.125 to 1.875 inches. These holes are subsequently plugged with electrical and hydraulic bulkhead penetrators. If, in the future, the AUSS vehicle requires a larger number of bulkhead penetrators, the number of holes in each end bell can be increased from 8 to 16.

The equatorial edge of the end bell incorporates a flange that provides axial and radial support to the coupling ring on the GFRP cylinder. A separate equatorial ridge serves as the retainer for composite fairing (Figure 6). The end bells are clamped to the coupling rings on the GFRP cylinder with a split clamp band made out of aluminum. Some weight and cost savings, as well as decrease in corrosion, could be achieved by substituting molded Kevlar-fiber-reinforced plastic for aluminum clamp bands.

The cast-titanium end bells weigh approximately 218 lb and displace 234 lb each. This results in a positive buoyancy for each end bell of only approximately 16 lb each. The calculated weight-to-displacement ratio for both end bells is 0.93, significantly less than that of the GFRP cylinder. This weight-to-displacement ratio could be reduced approximately to 0.70 by optimizing the design and increasing the peak design stress to 100,000 psi at 9000-psi design pressure. Further reduction in weight cannot be achieved because of the many reinforcements around penetrations.

CLAMP BANDS

Spit clamp bands (Figure 13) with inclined bearing surfaces are used for attachment of the titanium end bells to the titanium coupling rings bonded to the ends of the GFRP cylinder (Figure 6). The two bands were fabricated from 6061-T6 aluminum alloy to minimize fabrication costs while at the same time keep down the weight increase of the vehicle to only 20 lb. Since the total displacement of clamp bands is 7 lb, their presence adds a negative buoyance of 13 lb to the pressure hull. The galvanic corrosion due to contact with titanium was not considered to be a serious drawback as seriously corroded clamps can be replaced often, and economically, with new ones.

STRUCTURAL EVALUATION

The structural evaluation of the AUSS Mod 2 pressure-hull design, composite material selection, and fabrication process was performed in two stages.

Stage One: A 1:4.95 model-scale GFRP cylinder (Figures 14, 15) was to be fabricated by Martin Marietta Energy Systems using the design, composite constituents, and fabrication process selected for the full-scale AUSS Mod 2 cylinder This model-scale cylinder would subsequently be outfitted at NOSC with titanium end rings (Figure 16) and end bells (Figure 17) to simulate the AUSS Mod 2 pressure-hull assembly. The model-scale pressure hull would then be instrumented and pressure cycled 100 times to 9000-psi design pressure. The hydrostatic pressure testing would culminate with a proof test to 10,000 psi, followed by an implosion test If the performance of the model-scale pressure hull during hydrostatic pressure testing was acceptable, a decision would be made to proceed with the fabrication of the full-scale AUSS Mod 2 pressure hull.

Stage Two: A full-scale GFRP cylinder would be fabricated by Martin Marietta Energy Systems utilizing the same composite constituents as in the model-scale cylinder. Whenever feasible, the fabrication process would follow the parameters and utilize the procedures developed during the fabrication of the model-scale cylinder. The completed cylinder would be equipped at NOSC with titanium coupling rings and end bells and, after instrumentation with electric resistance straingages and acoustic-emission transducers, would be subjected to an extensive test program. During this test program, the AUSS Mod 2 pressure hull would be subjected to 10,000-psi proof pressure, followed by 10 pressure cycles to design pressure of 9000 psi. If the AUSS Mod 2 pressure hull performs successfully during pressure testings, the GFRP cylinder would be considered to have met the structural performance requirements of an unmanned vehicle with a 20,000-foot design depth.

EVALUATION OF MODEL-SCALE AUSS CYLINDER

FABRICATION OF MODEL-SCALE AUSS CYLINDER

The 6.34-inch OD × 5.320-inch ID × 13.42-inch L model-scale cylinder was entirely wet-wound (Figures 18, 19) from Hercules IM6-G-12k carbon fiber tow and ERL 2258-mPDA epoxy resin. The precise cylinder layup schedule is shown in Figure 20. The layer thicknesses indicated in Figure 20 are the target values that were used in the design iteration. To decrease the magnitude of stresses in the cylinder, a 2.4:1 ratio was initially selected for the layers of fibers with 90/0 degree orientation in the first 40 percent of wall thickness, followed by a 1.97:1 ratio for the remaining 60 percent of wall thickness. The final fiber orientation ratios selected for the construction of the model-scale AUSS cylinder were 2.5:1 in the first 35 percent of thickness, followed by a 2:1 ratio for the remaining 65 percent of wall thickness (Reference 15, Appendix A). These values were based on measurement obtained in previous process trials by Martin Marietta Energy Systems, Inc.

The cylinder fabrication was divided into three stages in which approximately one-third of the total wall thickness was wound and fully cured at a time. The layup stopping points between fabrications were adjusted to occur at the middle of a hoop layer and are indicated in Figure 20. After each stage was wound, the composite was precured without removal from the mandrel for a minimum of 16 hours at 120 to 130°F to gel the epoxy resin. Once the composite jelled, the mandrel with the GFRP cylinders were removed from the winding machine, placed in an oven, and cured for 2 hours at 185°F and 4 hours at 300°F.

The measured density of the model-scale AUSS cylinder composite is 0.563-lb per cubic inch. The estimated average composition of the cylinder is 65 to 67 volume percent IM6 fiber. The longitudinal modulus-to-density ratio of the cylinder was experimentally determined to be 155E6 lb_f -in/lb_m via an acoustical-frequency technique. Based on the preceding information, the cylinder's longitudinal modulus is 8.76E6 psi. Visual inspection of the cylinder ends shows the individual layers to be of uniform thickness, tightly packed, free of wrinkles and resin-rich areas (Figures 21 and 22). The thickness of hoop- and axial-oriented fiber laminas did not deviate significantly from the thickness values specified in the fabrication drawing (Figure 20).

An estimate of the cylinder's circumferential and longitudinal modulus was made using a 2-D laminate code called CLASS. Based on the cylinder layup and

estimated composition, CLASS predicts that the cylinder circumferential modulus is 16.7E6 psi and the longitudinal modulus is 8.5E6 psi.

A comparison between the CLASS-predicted longitudinal modulus and the experimentally measured longitudinal modulus of 8.7E6 psi shows a fairly good agreement between the two values. In addition, based on the calculated stresses on the internal surface of the AUSS subscale cylinder at 10,0000-psi external pressure, CLASS predicts that the circumferential and longitudinal strains are respectively –3880 and –3742 in/in, respectively.

The weight-to-displacement ratio of the model-scale 7.0-lb AUSS cylinder equipped with titanium end rings weighing 0.833 lb was 0.48. When the ends of the cylinder were closed off with the titanium model-scale hemispheres weighing 2.971 lb, the weight-to-displacement ratio of the model-scale AUSS pressure-housing assembly increased to 0.528. This weight-to-displacement ratio fails to meet the 0.5 minimum ratio, but is still close enough to it to make this pressure-housing design acceptable for an AUSS vehicle.

A second, dimensionally identical model-scale AUSS Mod 2 cylinder was wet wound utilizing S2 glass fibers instead of IM6 graphite fibers. The glass-fiber-reinforced plastic (GRP) model-scale AUSS Mod 2 cylinder provided a less costly, and less difficult alternate approach to the construction of the full-scale AUSS Mod 2 hull. The GRP model-scale AUSS Mod 2 cylinder would also be instrumented and tested to destruction to validate the alternate construction method (Appendix B).

If both the GFRP and GRP model-scale AUSS Mod 2 cylinders performed successfully under 9000-psi design pressure, only the GFRP construction would be considered for the construction of the full-scale AUSS Mod hull. The weight-to-displacement ratio of the GRP model-scale cylinder is significantly higher than that of the GFRP model-scale cylinder. The weight-to-displacement ratio of the GRP hull is 0.626 for bare cylinder, 0.685 for cylinder with titanium end rings (Figure 16), and 0.695 for cylinder with titanium end rings and end closures (Figure 17).

Only if the performance of the GFRP model-scale cylinder was found to be unacceptable would the GRP construction be considered for construction of the full-scale AUSS Mod 2 hull. The 48-percent larger weight-to-displacement ratio of the GRP cylinder would necessitate increasing the length of the pressure hull by 70 percent, which would severely restrict the dynamic performance of the AUSS vehicle in accomplishing bottom surveillance missions.

INSTRUMENTATION OF THE MODEL-SCALE AUSS CYLINDER

The model-scale AUSS cylinder of GFRP composite was instrumented on its interior surface with 20 electric resistance straingages (Figure 23). The objective of this instrumentation was to do the following: (1) detect incipient elastic instability, (2) measure the magnitude of mismatch in radial contraction between the cylinder and bulkheads when pressurized, and (3) measure the magnitude of creep in GFRP composite under sustained design pressure.

In addition, an acoustic-emission detector was placed inside the pressure-housing assembly to monitor the acoustic emissions generated inside the GFRP composite by external hydrostatic loading.

The instrumentation leads from the acoustic-emission detector and the electric resistance straingages subsequently would be fed from the interior of the model-scale AUSS pressure-housing assembly to its exterior through custom-made bulkhead penetrators designed to withstand 10,000-psi external pressure. The other end of the instrumentation leads would be fed through another bulkhead connector designed to fit into the cover of the deep-ocean pressure simulator.

PRESSURE TESTING OF MODEL-SCALE AUSS PRESSURE HOUSING

The GFRP model-scale cylinder was converted into a pressure housing by bonding titanium end rings to its ends and closing off the cylinder with titanium hemispherical bulkhead (Figures 24 to 26). The titanium hemispheres, model-scale versions of the bulkheads for a full-scale AUSS pressure hull, were equipped with penetrations that accommodated the bulkhead penetrators with instrumentation leads (Figure 27). The assembled model-scale AUSS pressure-housing assembly was placed inside a deep-ocean pressure simulator and the instrumentation leads were fed to the exterior of the vessel through a bulkhead penetrator in the pressure-vessel end closure.

The pressure testing of the model-scale AUSS pressure-housing assembly was accomplished by filling the interior of the pressure vessel with tap water and pressure cycling it with an air-operated pump to the desired pressure level. The first pressure cycle consisted of pressurizing the test assembly to 10,000-psi proof pressure, maintaining this pressure for 60 minutes, dropping the pressure to 0 psi, and allowing the assembly to relax for 60 minutes before commencing with pressure cycling to 9000-psi design pressure. Strains and acoustic emissions were recorded at 1000-psi intervals during pressurization, and at 15-minute intervals during sustained pressure loading and relaxation.

The pressure cycles to 9000-psi design pressure were of 60-minute duration (30 minutes of sustained loading at 9000 psi followed by 30 minutes of relaxation at 0 psi). Strains were read only during the first and last cycles. The test assembly was submitted to a total of 100 cycles. Acoustics emissions were monitored continually.

The cyclic testing concluded with pressurizing the test assembly to destruction. For this test, the titanium spherical bulkheads were replaced with flat steel bulkheads whose critical pressure exceeded that of the GFRP cylinder (Figures 28 and 29).

RESULTS OF MODEL-SCALE AUSS PRESSURE-HOUSING TESTS

Strains

The maximum strains on the GFRP cylinder assembly were recorded on its interior surface at midbay in hoop direction (Table 2). Their magnitude at 10,000-psi hydrostatic pressure varied from -3880 to -4150 microinches/inch (Figure 30). The axial strains at the same locations varied from -3400 to -3500 microinches/inch. The observed creep was only 30 microinches/inch after 60 minutes of sustained pressurization at 10,000 psi.

The hoop strains at the ends were only somewhat smaller, averaging –3500 microinches/inch. No creep was observed at the ends. (Figure 31).

The comparison between the CLASS computer program predicted strains and the measured strains is good. The predicted –3880 microinches/inch hoop and –3742 microinches/inch axial strains compare well with the measured average hoop strain of –3977 and axial strain of –3442 microinches/inch on the interior surface at midbay. The predicted hoop 16.7×10^6 and axial 8.5×10^6-psi moduli of elasticity also correlate well with the 17.2×10^6-psi and 8.7×10^6-psi moduli of elasticity calculated on the basis of experimentally measured strains.

Based on the inspection of recorded strains one may conclude that:

(1) Hemispherical end closures are well matched elastically to the cylinder; the hoop strains at the ends of the cylinder differ by only 12 percent from those at midbay.

(2) The hoop-to-axial fiber layup ratio of approximately 2.2:1 selected for the winding of the model-scale AUSS cylinder is approximately correct as the hoop strains at midbay differ from the axial strains only by 13 percent. With an ideal fiber layup, the magnitude of hoop and axial strains would be the same.

(3) There is no creep or incipient elastic instability at 10,000-psi proof pressure since the recorded hoop strains around the circumference of the cylinder at midbay were very uniform and experienced no measurable increase under sustained loading.

Acoustic Emission

The number of acoustic events increased linearly with pressure during the first pressure cycle to 10,000 psi. During subsequent pressure cycling to 9000 psi, the number of events during each cycle was repetitive, and significantly less than during the first cycle. There was no sudden increase in acoustic emissions prior to critical failure during implosion testing.

Material Failure

The GFRP model-scale AUSS cylinder assembly imploded catastrophically at 12,600 psi. The strains at midbay were linear to the moment of implosion, indicating that the implosion was not caused by elastic instability (Figures 32, 33). The calculated stresses at midbay prior to implosion were –85,000 in hoop and –36,500 in axial direction. It is postulated that the implosion (Figure 34) was triggered by uneven sliding of the titanium end rings upon the flat steel plates. With elastically matched bulkheads, the critical pressure of the GFRP cylinder is calculated to be in excess of 15,000 psi.

Table 2. Strains on the interior surface of AUSS model-scale GFRP cylinder ETAC Mod 1 Sn 1 under hydrostatic proof test to 10,000 psi.

	;<-----				Mid-bay				---------->	
Pressure	GAGE 1		GAGE 2		GAGE 3		GAGE 4		GAGE 5	
(PSI)	Axial	Hoop	Axial	Hoop	Axial	Hoop	Axial	Hoop	Axial	Hoop
0	0	0	0	0	0	0	0	0	0	0
1000	-334	-358	-325	-376	-326	-379	-338	-391	-338	-402
2000	-685	-746	-688	-764	-668	-767	-678	-783	-688	-809
3000	-1025	-1122	-997	-1141	-996	-1138	-999	-1157	-1013	-1185
4000	-1362	-1489	-1320	-1505	-1312	-1500	-1315	-1526	-1338	-1564
5000	-1713	-1879	-1663	-1900	-1655	-1894	-1656	-1927	-1689	-1975
6000	-2064	-2271	-2008	-2299	-2001	-2291	-2000	-2330	-2041	-2391
7000	-2416	-2666	-2354	-2700	-2347	-2691	-2343	-2735	-2394	-2812
8000	-2780	-3084	-2770	-3127	-2714	-3115	-2707	-3164	-2766	-3260
9000	-3158	-3510	-3099	-3573	-3095	-3560	-3086	-3611	-3154	-3733
10000	-3498	-3881	-3418	-3951	-3415	-3935	-3403	-3987	-3479	-4135
10000	-3509	-3900	-3431	-3973	-3429	-3954	-3414	-4008	-3497	-4135
10000	-3500	-3890	-3424	-3976	-3433	-3953	-3413	-4006	-3498	-4151
10000	-3520	-3910	-3444	-3985	-3443	-3965	-3427	-4021	-3513	-4167
10000	-3533	-3921	-3456	-3998	-3456	-3977	-3440	-4034	-3526	-4180
10000	-3509	-3894	-3434	-3969	-3439	-3949	-3418	-4006	-3503	-4149
10000	-3521	-3902	-3443	-3978	-3443	-3958	-3427	-4014	-3513	-4161
9000	-3177	-3522	-3108	-3584	-3106	-3566	-3091	-3622	-3173	-3740
8000	-2814	-3117	-2752	-3168	-2748	-3152	-2737	-3207	-2813	-3301
7000	-2438	-2699	-2383	-2739	-2379	-2774	-2368	-2776	-2438	-2849
6000	-2091	-2312	-2044	-2344	-2037	-2330	-2030	-2378	-2092	-2435
5000	-1728	-1906	-1686	-1932	-1679	-1920	-1675	-1962	-1730	-2004
4000	-1378	-1517	-1343	-1537	-1335	-1526	-1334	-1562	-1380	-1592
3000	-1023	-1122	-994	-1138	-987	-1128	-988	-1156	-1024	-1176
2000	-669	-729	-647	-740	-640	-732	-642	-752	-667	-763
1000	-333	-358	-317	-364	-314	-358	-316	-370	-327	-376
0	-11	-9	-8	-11	-10	-5	-3	-8	-8	-8
0	4	13	8	12	6	17	11	14	8	14

NOTES: 1. The strain readings during subtained pressurization at 10,000 psi and 0 psi levels were taken at 10 minute intervals
2. Ends of the cylinder were simply supported by titanium end bells

Table 2. (continued) Strains on the interior surface of AUSS model-scale GFRP cylinder ETAC Mod 1 Sn 1 under hydrostatic proof test to 10,000 psi.

	<----- Mid-Bay to Ring A ----->									
Pressure	GAGE 6		GAGE 7		GAGE 8		GAGE 9		GAGE 10	
(PSI)	Axial	Hoop	Axial	Hoop	Axial	Hoop	Axial	Hoop	Axial	Hoop
0	0	0	0	0	0	0	0	0	0	0
1000	-341	-407	-345	-398	-340	-392	-338	-383	-337	-370
2000	-689	-815	-694	-801	-682	-796	-672	-787	-638	-760
3000	-1009	-1193	-1017	-1176	-998	-1171	-983	-1162	-925	-1120
4000	-1332	-1574	-1341	-1552	-1315	-1548	-1295	-1538	-1218	-1482
5000	-1679	-1987	-1690	-1959	-1656	-1956	-1631	-1945	-1535	-1873
6000	-2030	-2405	-2043	-2372	-2001	-2370	-1971	-2359	-1857	-2269
7000	-2380	-2827	-2396	-2789	-2346	-2787	-2311	-2774	-2180	-2666
8000	-2753	-3278	-2771	-3235	-2713	-3233	-2672	-3218	-2521	-3090
9000	-3138	-3751	-3160	-3702	-3093	-3701	-3046	-3682	-2872	-3571
10000	-3462	-4155	-3487	-4093	-3412	-4098	-3359	-4077	-3166	-3905
10000	-3481	-4173	-3505	-4120	-3428	-4118	-3373	-4094	-3172	-3925
10000	-3476	-4165	-3499	-4112	-3422	-4108	-3367	-4084	-3165	-3917
10000	-3492	-4103	-3515	-4129	-3437	-4124	-3382	-4100	-3178	-3932
10000	-3507	-4199	-3530	-4144	-3450	-4138	-3396	-4114	-3191	-3946
10000	-3485	-4167	-3507	-4114	-3428	-4108	-3374	-4084	-3171	-3919
10000	-3496	-4180	-3518	-4125	-3439	-4120	-3386	-4096	-3182	-3930
9000	-3157	-3760	-3177	-3712	-3105	-3706	-3058	-3685	-2873	-3571
8000	-2796	-3318	-2813	-3276	-2748	-3271	-2708	-3251	-2543	-3128
7000	-2424	-2868	-2438	-2832	-2382	-2825	-2347	-2807	-2202	-2704
6000	-2079	-2452	-2091	-2422	-2042	-2414	-2012	-2398	-1884	-2313
5000	-1718	-2021	-1728	-1996	-1687	-1988	-1661	-1972	-1550	-1906
4000	-1370	-1607	-1377	-1587	-1344	-1578	-1372	-1563	-1225	-1513
3000	-1018	-1191	-1022	-1175	-998	-1166	-979	-1153	-897	-1118
2000	-665	-776	-668	-766	-651	-755	-636	-743	-568	-723
1000	-332	-387	-333	-380	-324	-369	-313	-358	-263	-351
0	-18	-15	-17	-15	-13	-9	-13	-2	-14	-3
0	2	7	0	6	1	13	0	17	6	15

Table 2. (continued) Strains on the interior surface of AUSS model-scale GFRP cylinder ETAC Mod 1 Sn 1 under hydrostatic proof test to 10,000 psi.

	|<----- ----- End Ring B ---------- ----->|			
Pressure (PSI)	GAGE 11 Hoop	GAGE 12 Hoop	GAGE 13 Hoop	GAGE 14 Hoop	GAGE 15 Hoop
0	0	0	0	0	0
1000	-318	-428	-410	-488	-374
2000	-674	-760	-780	-910	-852
3000	-984	-1070	-1110	-1236	-1278
4000	-1306	-1384	-1446	-1530	-1690
5000	-1650	-1728	-1800	-1834	-2110
6000	-1990	-2070	-2170	-2140	-2520
7000	-2334	-2418	-2522	-2430	-2904
8000	-2694	-2770	-2900	-2726	-3296
9000	-3062	-3134	-3276	-3034	-3696
10000	-3362	-3438	-3598	-3284	-4024
10000	-3384	-3440	-3624	-3242	-4060
10000	-3372	-3430	-3614	-3220	-4054
10000	-3378	-3440	-3626	-3220	-4066
10000	-3384	-3446	-3634	-3222	-4078
10000	-3354	-3410	-3606	-3186	-4048
10000	-3362	-3414	-3604	-3192	-4050
9000	-3034	-3080	-3262	-2864	-3714
8000	-2672	-2730	-2904	-2520	-3346
7000	-2300	-2354	-2522	-2170	-2964
6000	-1966	-2010	-2174	-1848	-2606
5000	-1602	-1662	-1810	-1510	-2224
4000	-1260	-1320	-1444	-1186	-1844
3000	-910	-970	-1074	-854	-1432
2000	-564	-644	-710	-492	-988
1000	-256	-342	-348	-216	-490
0	42	42	42	36	56
0	60	68	54	54	70

Table 2. (continued) Strains on the interior surface of AUSS model-scale GFRP cylinder ETAC Mod 1 Sn 1 under hydrostatic proof test to 10,000 psi.

	|<----- ----- End Ring A ---------- ----->				
Pressure (PSI)	GAGE 16 Hoop	GAGE 17 Hoop	GAGE 18 Hoop	GAGE 19 Hoop	GAGE 20 Hoop
0	0	0	0	0	0
1000	-398	-310	-252	-420	-294
2000	-830	-650	-676	-790	-592
3000	-1236	-970	-1038	-1130	-872
4000	-1706	-1296	-1366	-1472	-1140
5000	-2130	-1646	-1724	-1832	-1444
6000	-2498	-2000	-2082	-2194	-1738
7000	-2904	-2344	-2440	-2558	-2014
8000	-3290	-2710	-----	-2928	-2280
9000	-3676	-3080	-----	-3304	-2548
10000	-3992	-3388	-----	-3612	-2792
10000	-3994	-3386	-----	-3598	-2754
10000	-3976	-3368	-----	-3578	-2740
10000	-3980	-3372	-----	-3582	-2744
10000	-3984	-3376	-----	-3582	-2750
10000	-3952	-3344	-----	-3546	-2728
10000	-3960	-3348	-----	-3552	-2732
9000	-3600	-3020	-----	-3206	-2444
8000	-3206	-2662	-----	-2840	-2148
7000	-2792	-2290	-----	-2460	-1854
6000	-2410	-1944	-----	-2102	-1572
5000	-2000	-1584	-----	-1730	-1286
4000	-1536	-1230	-----	-1372	-1002
3000	-954	-876	-----	-1010	-720
2000	-520	-520	-----	-644	-432
1000	-88	-188	-----	-320	-174
0	350	72	-----	60	54
0	400	90	-----	88	50

DISCUSSION

The alternate-model-scale AUSS Mod 2 cylinder wet wound from S2 glass also successfully withstood the proof test to 10,000 psi, and cyclic pressure tests to 9000 psi. The average of recorded strains on the interior surfaces of the cylinder during proof test to 10,000 psi was –7600 and –3700 microinches in hoop and axial directions at midbay, and –5500 and –3000 in hoop and axial directions at the ends. Based on these strains the moduli of elasticity in hoop and axial directions are estimated to be 8.2×10^6-psi and 6.6×10^6-psi, respectively (Appendix B).

Because the glass-fiber-reinforced cylinder has a lower modulus of elasticity in both hoop and axial orientations than the graphite-fiber-reinforced cylinder, the magnitude of radial support provided by the titanium end closures to the cylinder ends is much larger than for graphite-reinforced cylinder. Thus, the decrease in hoop strain at the end of the GRP cylinder, due to radial support provided by the end closure, is 28 percent, while in the GFRP, the decrease in hoop strain at the same location is only 9 percent.

When the GRP cylinder was equipped with flat plate bulkheads (Figure 28), an attempt was made to pressurize it to destruction. However, the GRP cylinder withstood 17,500 psi without implosion (Appendix B). When compared to the 12,600-psi implosion pressure of the GFRP cylinder, a postulate can be formulated that the GRP composite in dimensionally identical cylinders has approximately 40-percent higher compressive strength than the GFRP composite. Therefore, the GRP should be preferred for construction of external pressure hulls, providing that the 48-percent increase in weight-to-displacement ratio does not significantly degrade the operational performance of the vehicle (Table 3).

The tradeoff between the glass- and carbon-fiber-reinforced composites for external pressure-hull construction becomes further complicated when the cost of fabrication and material is included in the tradeoff process. The fabrication cost of a GRP cylinder was found to be approximately 10-percent less than that of a GFRP cylinder with the same payload capability.

Thus, it appears that if the vehicle can tolerate the 70-percent increase in the cylindrical-hull length needed to compensate for the 48-percent increase in weight-to-displacement ratio, the GRP construction is a better choice. The resulting hull with the same wall thickness will be 40-percent stronger, and 10-percent less expensive to fabricate.

Since the AUSS vehicle design cannot operationally tolerate a 70-percent increase in cylindrical-hull length in order to provide the GRP cylinder with the same payload capability as the AUSS Mod 2 GFRP cylinder, the GRP construction is considered unsuitable for fabrication of the AUSS vehicle pressure hull. The glass-reinforced plastic composite, although not chosen for the AUSS vehicle because of operational considerations, should be seriously considered for any other deep-submergence vehicle that does not require (for its operational scenarios) the dynamic agility that only can be achieved with the lighter and, therefore, shorter cylindrical GFRP hulls.

Table 3. Comparison of test results from model-scale AUSS Mod 2 cylinders.

	Models	
	Graphite-Fiber Epoxy Composite Model 1	Glass-Fiber Epoxy Composite Model 2
Material Systems	IM6/2258	S2/2258
Fiber Orientation	(90°/0°)	(90°/0°)
Fiber Distribution	2.4:1 inside 35 percent of thickness 1.9:1 outside	2.0:1
Fiber Content	67 percent	75 percent
Fabrication Process	wet winding	wet winding
No. of Cure Cycles	5	5
Dimensions: I.D.; Thickness; Length	5.30"; 0.52"; 13.4"	5.30"; 0.52"; 13.4"
Weight of the cylinder (lb)	7.0	10.4
W/D Ratio		
• Cylinder only	0.415	0.626
• With Ti End Rings	0.480	0.685
• With Ti End Rings and Hemiheads	0.529	0.695
Maximum Pressure, lb/in²	12,600	17,500
Maximum Stresses, lb/in²	85,000	116,214
Remarks	Model failed	Model is not broken yet.
Testing Configurations	Model was tested with hemiheads up to 9,000 psi and then tested to failure with flat-plate end closures.	Model was tested with hemiheads up to 9,000 psi and then tested to failure with flat-plate end closures.

CONCLUSION

The successful performance of the GFRP model-scale AUSS pressure-housing assembly during proof test to 10,000 psi, and subsequent cycling to design pressure of 9000 psi indicates that the design, materials, fiber layup schedule, and fabrication procedure proposed for the GFRP full-scale AUSS cylindrical hull resulted in a model-scale cylinder that, if scaled up properly, would meet the operational requirements of the full-size AUSS vehicle. Based on this finding, it was decided to proceed

with the fabrication of the AUSS Mod 2 full-scale GFRP cylindrical hull utilizing the design, materials, fiber layup schedule, and fabrication procedure that were experimentally evaluated on the model-scale cylinder.

FABRICATION OF FULL-SCALE AUSS MOD 2 HULL

LAYUP AND CONSTRUCTION

The AUSS pressure vessel is constructed entirely from wet-wound Hercules IM6G 12-k carbon fiber which has a nominal tensile modulus of 40×10^6 psi. The winding resin is ERL 2258 mixed with 25 phr (parts per hundred grams of resin) meta-phenylene diamine (MPDA) hardener.

The laminate stacking sequence of the cylinder is shown in Table 4. The layer thicknesses indicated in Table 4 are the values that were used in the design iteration and are based on measurements obtained in previous process trials. The hoop (90 degrees)-to-axial (0 degree) fiber ratio from the cylinder ID to approximately 40 percent (1 inch) of the wall thickness is nominally 2.5:1; a 2.0:1 hoop-to-axial fiber ratio is employed for remainder of the cylinder wall thickness. The overall hoop to axial (the fiber ratio for the composite cylinder) is 2.2:1.

TOOLING

The composite was filament wound on a 25.750-inch diameter, 95-inch long aluminum mandrel, which is shown chucked in the winding machine in Figure 35. A pin ring (Figure 36) was screwed to each end of the mandrel in order to keep the wet-wound axial fibers from slipping around the corners of the mandrel after being laid down, and as the mandrel rotated.

The pin rings resemble giant gears with nominally 0.35-inch deep teeth cut from around their circumferences. Their function is for the teeth to catch and hold the axial fibers after their laydown by the feedeye. Depending on their diameter, each pin ring contains from 550 to 640 teeth. To accommodate the increasing diameter of the AUSS vessel as it was wound, one set of pin rings was used for every 0.5-inch increase in the cylinder thickness. The nominal diameters of the pin rings used to build the AUSS (from tooth tip to tooth tip) were respectively 26.236, 27.278, 28.414, 29.220 and 30.119 inches.

Table 4. Laminate stacking schedule for AUSS Mod 2 composite cylinder.

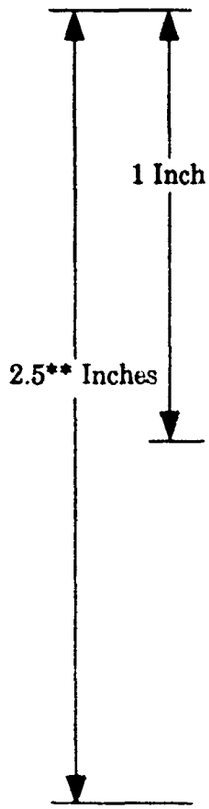

ORIENTATION (degrees)	LAYER THICKNESS (inches)	
90	0.0138	ID Layer
0	0.0136	
90	0.0345	} 2.5:1 Ratio
0	0.0136	
90	0.0345	
0	0.0136	
90	0.0345	
0	0.0136	
90	0.0345	
0	0.0136	
90	0.0276*	} 2.0:1 Ratio
0	0.0136	
90	0.0276	
0	0.0136	
90	0.0276	
0	0.0136	
90	0.0276	
0	0.0136	
90	0.0552	OD Layer

*Change in hoop-to-axial layer ratio occurs after 1 inch of wall thickness buildup.

**The overall hoop-to-axial layer ratio for the whole wall thickness is 2.211.

FABRICATION

The winding was performed using an EnTec programmable 4-axis winding machine. A schematic of the winding operation, identical to the one used in fabrication of model-scale GFRP cylinder, is shown in Figure 18. The nominal 6-pound spools of dry IM6G carbon fiber are unwound from the fiber creel and drawn through a wet-out pot. In the wet-out pot, the tows (bundles of fibers) pass under and over a series of bars through a heated (120° to 130°F) resin bath where they are impregnated with the winding resin. After leaving the wet-out pot, each tow is tensioned individually by running it through a pulley system connected to a magnetic brake (Figure 37). The tows are then guided via pulleys and rollers up to and through the feedeye of the winding machine and onto the mandrel.

Separate winding programs were written for the EnTec machine to lay down the hoop and axial layers. With respect to the axial layers, 20 tows were wound simultaneously in an approximately 1.80-inch-wide band that was then laid down the

length of the mandrel by the feedeye. A comb in the feedeye controlled the band width and the spacing of the tows within the band. The comb also kept the 20 tows from becoming entangled. After their laydown, the orientation and position of the bands was maintained by the teeth of the pin rings.

The laydown of the axial bands is illustrated in Figure 38; the feedeye rollers and the 20 tows are visible at the near end of the mandrel. After the feedeye completed the placement of one axial band down the length of the mandrel, and the band fibers were caught in the teeth of the pin rings, the mandrel was rotated to a position that placed the feeder directly adjacent to the last band's position. The feedeye then moved to anchor the band fibers firmly in the teeth of the pin rings and traveled down to the opposite end of the mandrel, laying a second band of axial fibers adjacent to the first band. This process continued until the mandrel circumference was covered with axial fibers (Figure 39).

During the process trials, the best axial layer coverage was achieved when the mandrel circumference was covered with two axial-band thicknesses laid one on top of the other, rather than one. Therefore, after the mandrel circumference was covered with one blanket of axial bands, the winding program continued to lay a second blanket of bands directly on top of these. The combined thickness of these two blankets was determined experimentally to average 0.0136 inch which, thereafter, was considered the fixed thickness for an axial layer.

Eight individual axial winding programs were employed to accommodate the increasing part diameter as the cylinder grew thicker – or one program for roughly each 0.135-inch increase in wall thickness. Since the band width was fixed at approximately 1.8 inch, the programs were based on fitting an integral number of bands two times around the circumference of the part. When the circumference grew to the point that another band of 1.8 inch could be fitted into the layer, the program was rewritten with an increase of one band width incorporated into the coverage. To prevent gaps between adjacent bands, the programs were contrived to start at the beginning of the winding cycle with a slight overlap of the bands which would decrease as the part grew thicker. Changeover to the next program was intended to occur after the point that the bands began laying adjacent to one another so that ideally there would never be noticeable gaps between the bands. Calculations based on the assumed layer thicknesses predicted that the overlaps and gaps between the bands would not be more than 0.010 inch.

Upon the completion of an axial layer, a separate program was loaded into the EnTec Winding Machine to lay down the hoop layer. A constant fiber advance of 0.090-inch-per-revolution was employed for the hoop tows. Thus, only one program was required to wind the hoop layers throughout the thickness of the cylinder. It has been determined experimentally that, at a 0.090-inch-per-revolution winding advance, the IM6G fiber layer thickness averages 0.0069 inch per tow. To achieve the 2.5:1 hoop-to-axial fiber ratio for the first inch of cylinder wall thickness, up to five tows were wound simultaneously in one pass down the mandrel to lay the targeted 0.0345-inch hoop layer thickness. For the remainder of the fabrication, up to four tows were wound simultaneously in one pass for the targeted 0.0276-inch hoop layer thickness necessary to yield the 2.0:1 hoop-to-axial fiber ratio. Figure 40 illustrates the laydown of a hoop layer over an axial layer.

During the winding of a hoop layer, a plastic wiper blade was used to lightly skim the composite surface and remove excess resin. The wiper traveled down the

mandrel directly after the feedeye and was visible in Figure 41. The excess resin was collected in either a bucket or a tray and later discarded.

The axial layers were wound with 3- to 4-lb tension per tow; 10- to 12-lb per tow were used to wind the hoop layers. The high-winding tension on the hoop layers was used to compact and spread the tows of the axial layer, driving out excess resin and entrapped air in the process. Ideally, the net effect would be an increase in the overall fiber content of the cylinder.

Some additional compaction of the hoop and axial layers was also achieved by using a compactor. The compactor consists of a set of stainless steel, dead-weight loaded rollers. The compactor travels behind the feedeye with its roller riding on top of the hoop tows immediately after laydown. It, too, is visible at the top of the mandrel (Figure 41). Its purpose is to apply additional pressure to consolidate the underlying layers and squeeze out excess resin. Approximately 10-lb per roller of compaction was used in the winding of the AUSS cylinder hoop layers.

The winding of the AUSS pressure vessel was initiated by preheating the mandrel surface to between 120 to 130°F by rotating the mandrel over radiant heaters. Two rows of IM6G fiber were hoop wound simultaneously on the mandrel in a single pass. No compaction or wiping was used on this first hoop layer. On top of this, an axial layer was then wound followed by a hoop layer of five tows wound simultaneously in a single pass. This hoop layer and the following hoop layers for the day were compacted and wiped. The layup continued according to Table 4. The last axial layer laid down for the day was followed by only three hoop tows wound simultaneously in a single pass. This partial hoop layer was also wiped and compacted.

At the end of a winding day, a fiberglass canopy or hood was placed over the mandrel to hold in as much heat as possible and the composite was allowed to turn overnight over radiant heaters to precure or gel the composite resin. The next morning, the hood was removed and the day's winding commenced with the laydown of two hoop tows wound simultaneously in a single pass. Again, no wiping or compaction was used on these first two tows. The remainder of the day's wind was done identically to the procedure mentioned above and according to Table 4.

The first two hoop tows laid down at the start of each winding day were not wiped or compacted so that they would not become too dry. The intent was that the excess resin would facilitate wetting the dry, rough surface of the previous day's composite so that voids would not be trapped when the axial layer was laid down. Only half of the tows of a full hoop layer were laid down at the end of the day so that the stopping and starting points of the fabrication would coincide with the middle of a hoop layer, rather than at the interface between a hoop and an axial layer.

During the first two days of winding, and because of ongoing process optimization, it was only possible to lay down two or three axial layers and their corresponding hoops per day. Later, the winding operation progressed to laying routinely between 4 to 6 axial layers per day. At the same time, an additional wiping step was introduced at the end of the day's fabrication. The mandrel was turned over radiant heaters for approximately 40 to 60 minutes to allow additional excess resin to bleed to the surface. This additional resin was then lightly skimmed in a single pass using the same wiper system described previously. This tended to leave a slightly dryer surface on the part so no resin band would remain in the middle of a hoop layer corresponding to the starting and stopping point of a day's fabrication.

The AUSS vessel was wound over a 5-week period with between 2 to 3 days per week actual winding time required to lay down approximately one-fifth of the cylinder wall thickness. At the end of the week, the mandrel was taken out of the EnTec winding machine and sent to a forced-air convection oven for a full cure of the composite. The cure cycle used was 2 hours each week at 185°F plus 4 hours at 300°F. Afterwards, the mandrel was reinstalled in the winding machine and set up for the coming week's fabrication.

Between the third and fourth week of fabrication, the cylinder was observed developing flat spots. These spots were approximately 3.5-inches wide, spaced evenly around the part circumference, and extended down the length of the part. Run out measurements taken after the fourth day of winding indicated that the cylinder roundness varied on the average between 0.040 and 0.050 inch from the center to the edge of the flat spots.

It is not known exactly how the out-of-roundness problem began. The compactor, no longer riding smoothly on the cylinder circumference, was bouncing up and down on the high spots. Because this accentuated the out-of-roundness problem, use of the compactor was discontinued for the last fifth of the cylinder wall thickness, subsequent to which the cylinder roundness appeared to improve. Runout measurements taken at random locations on the completed cylinder showed that the variation between the centers and the edges of the flat spots had been reduced and now averaged between 0.010 and 0.020 inch.

Table 4 shows the cylinder completed by winding eight hoop tows simultaneously in a single pass over the last axial layer. Thus, the final thickness of the cylinder was adjusted as closely as possible to within the tolerances provided by NOSC. After this last hoop layer, the cylinder was allowed to rotate approximately 20 minutes before being wiped again in a single pass by the plastic wiper blade. The cylinder was rotated overnight over heaters and sent for its final cure cycle the following morning.

CUTTING PART TO LENGTH

To minimize fixturing costs and the risk of inadvertently damaging the composite during handling, the AUSS cylinder was cut to length using the mandrel as the cutting arbor. After the composite's first full cure cycle, the cylinder became loose on the mandrel and would shift slightly when given sufficient momentum. This made it possible to make the initial rough cuts while the weight of the cylinder and scrap ends were supported fully by the mandrel. The scrap ends were then removed and the cylinder slid down until the cylinder end was overhanging the edge of the mandrel by three or four inches. A final cut was then made on the overhanging edge to remove just enough material to render it flat and perpendicular to the axis of the tube.

A diamond-grit cutting wheel was used to make the cuts. During the initial rough cuts, the operation was slowed during the last cutting revolutions near the ID to minimize overshooting the tube ID and going into the mandrel surface with the saw blade. As it turned out, some shallow scratches were made in the mandrel while the composite was cut all the way through. These were hand-sanded smooth after the scrap ends were removed and prior to sliding the cylinder to the end to make the final edge cut.

The force to slide the cylinder was provided by one edge of the lathe platform that travels the length of the machine and holds the saw blade. A wooden block padded with rubber was used between the cylinder edge and the platform to protect the composite surface as it was pushed by the machine. In this manner, it was very easy to slide the cylinder on the mandrel.

The sequence and details of the cutting operation are as follows. Initially, one rough cut was made in the cylinder, approximately 15 inches from one end of the mandrel. Liquid nitrogen was then pumped into the interior of the mandrel to further shrink the aluminum surface from the ID of the composite. Figure 42 illustrates one of the scrap ends being removed as the mandrel cools. After the scrap end was removed, the cylinder was slid down until the cut edge was overhanging the edge of the mandrel by 3 to 4 inches. The mandrel was then allowed to warm back to room temperature. To keep the cylinder from shifting while the final cut was made, toe clamps were used on the cylinder ID to secure the composite to the mandrel. Then, the final edge cut was made.

A second rough cut was made at the other end of the composite supported on the mandrel. This rough cut essentially fixed the final length of the cylinder. The other scrap end was removed, the mandrel was cooled with liquid nitrogen and the cylinder was slid back the other way so that the rough edge was overhanging the opposite end of the mandrel. After the mandrel had warmed back to room temperature, the cylinder was fixed in place with toe clamps and the final cut was made. The mandrel was then cooled one last time with liquid nitrogen and the cylinder was slid back onto the mandrel until its edge was flush with the mandrel end.

MANDREL REMOVAL

To remove the mandrel, the composite cylinder was strapped tightly in place to an uprighting skid. A rubber-padded wooden disk was placed between the skid support arms and the edge of the cylinder that was flush with the end of the mandrel. The uprighting skid was then lifted by one end to a vertical position and hung on a stand. In this position, the cylinder was held immobile by the straps with one end resting on the wooden disk.

Liquid nitrogen was poured into the open end of the mandrel in order to cool it down, thereby shrinking it away from the ID of the cylinder (Figure 43). When ready, the mandrel was lifted out of the cylinder, leaving the composite strapped to the skid (Figure 44). The skid was then lowered from the stand and placed back in a horizontal position.

Inspection of the cylinder revealed many light scratches on the ID running longitudinally 3 to 6 inches from the cylinder edge into the interior. The scratches were all around the circumference and estimates are that they were 0.002- to 0.005-inch deep. It is speculated that they were caused in the cutting operation by sliding the composite over surface cuts in the mandrel that had not been adequately sanded. Several longitudinal scratches were also found on the ID at the center of the body of the cylinder. The majority of the scratches were patched with a room-temperature curing epoxy which was applied, cured, and then lightly sanded back down to the surface.

Table 5. Thickness measurements of hoop and axial layers in material coupon from the end of AUSS MOD 2 composite cylinder.

(From ID to 1 inch of wall thickness)

	[Layer Thickness]	
	Hoop	Axial
ID Layer	4.42	
		10.86
	33.50	
		12.52
	34.18	
		13.56
	35.30	
		13.24
	33.24	
		12.36
	32.84	
		11.94
	35.68	
		11.72
	31.54	
		12.18
	31.22	
		12.48
	31.30	
		11.24
	31.94	
		14.54
	33.72	
		10.60
	35.76	
		9.90
	32.34	
		12.76

(From 1 inch of wall thickness to OD)

	[Layer Thickness]	
	Hoop	Axial
		11.28
	26.00	
		13.68
	24.06	
		15.42
	25.66	
		14.72
	26.16	
		13.04
	26.72	
		12.30
	25.38	
		8.20

Table 5 (continued). Thickness measurements of hoop and axial layers in material coupon from the end of AUSS MOD 2 composite cylinder.

	[Layer Thickness]	
	Hoop	Axial
	26.96	
		9.12
	26.86	
		19.42
	26.62	
		12.50
	26.84	
		14.48
	24.28	
		13.38
	24.54	
		14.30
	24.80	
		15.02
	25.74	
		11.36
	26.70	
		14.90
	27.42	
		13.68
	27.06	
		12.88
	27.60	
		14.56
	27.74	
		15.18
	28.74	
		12.94
	26.68	
		11.30
	27.82	
		12.70
	28.46	
		13.68
	26.52	
		13.20
	26.64	
		12.18
	26.60	
		12.88
OD Layer	47.60	

Average measured layer thicknesses: (excluding ID and OD layers)

Axial: 12.9 mils
Hoop (ID to 1 inch of wall thickness): 33.3 mils
Hoop (1 inch of wall thickness to OD): 26.5 mils

Note: Measurements were made on random layers throughout the sample wall thickness.

PART COMPOSITION

Samples were taken from the scrap composite ends (Figure 45) removed in the cutting operation and submitted for analysis to determine the cylinder's composition and layer thicknesses (Table 5). The density of specimens taken from both scrap ends of the cylinder is nominally 1.58 g/cc (0.0567 lb in^3). Based on a rule-of-mixtures calculation, this density corresponds to an average fiber content of 70-volume percent.

The average composition also appears to be uniform through the thickness of the cylinder. During cutting apart of the ring (Figure 46), its ends would separate wider than the width of the saw blade indicating the presence of residual compressive hoop stresses on the interior of the cylinder. The total width of separation was measured to be 0.20 inch at the interior surface of the ring. Straingages mounted on the interior of the ring measured +165 microinches/inch in the hoop and +5 microinches/inch in the axial direction after cutting apart of the ring. The magnitude of the residual stress on the interior surface of the ring prior to cutting was calculated from these strains to be -2900 psi.

A wedge driven between the ends of the ring split the ring into two concentric rings when the space between the ends reached 0.375 inch. The split occurred approximately 1.5 inches from the interior surface of the ring, the stopping point of fiber winding for the third cure cycle.

The reason for the separation at the stopping point for the third cure cycle is not known. By comparison, the interface bonds at the other cure stopping points were significantly stronger. It is speculated that the fast spots of the cylinder may have contributed to this by presenting high and low areas which were difficult to contact uniformly for the first critical hoop layer laid down the following week. Two suggestions for improving the interface bond are eliminating the flat spots and lightly sanding the composite following a cure cycle to "rough up" the surface prior to winding.

Samples of one scrap end were also mounted and polished for examination under a microscope. Photomicrographs taken from various locations through the sample wall thickness are shown in Figures 47 to 51. Generally, the photomicrographs indicate good fiber consolidation in both the hoop and axial layers, and few voids (Figures 47 and 48).

Some flaws were observed. Figure 49 shows some voids between a hoop layer and the axial layer which was wound over it. Apparently air became entrapped between the two layers and the winding pressure from the successive hoop layer laid over the axial was unable to drive it out. Figure 50 also shows a resin band in the middle of a hoop layer. This corresponds to one of the stopping points at the end of a day's fabrication in which excess resin bled out to the surface. These bands become less frequent as one moves toward the OD of the cylinder due to the development of better surface-wiping techniques by fabrication personnel.

Because of the flat spots generated on the surface of the cylinder during winding of the hoop layers in the upper thickness of the cylinder, pockets of resin-rich material (Figure 52) that are prone to contain excessive porosity have been created. This porosity was detected by a C scan performed on the whole cylinder (Figures 53 and 54). The acoustic signals were generated by a transducer on the exterior surface of the cylinder and, subsequently, received by a transducer located

on the interior surface directly under the transmitter. Streams of water served as coupling agents between the transducers and the rough surfaces of the GFRP cylinder.

With the acoustic system delivering acoustic energy at 2.25 MHz frequency and 49-dB power setting, narrow bands of porosity oriented along the axis of the cylinder were detected at approximately 4-inch intervals around the circumference of the cylinder (Figure 55). At this power setting, the 0.010-inch thick lead-tape witness discs bonded to the exterior surface of the cylinder at 2-inch intervals were barely visible on the recording paper. When the power setting was increased to 55 dB, the white bands disappeared from the recording. At this power setting, the 0.010-inch thick lead-tape witness discs were not discernible on the recording. Only after 0.005-inch thick lead-tape discs were placed over the existing 0.010-inch thick discs did the witness discs again become visible on the recording.

Based on the above observations (detectable at 49-dB, but not 55-dB power settings), it can be concluded that the periodically occurring longitudinal imperfections around the circumference of the cylinder are not delaminations but resin-rich areas with minor gas-bubble porosity that do not threaten the structural integrity of the cylinder under hydrostatic loading. It is thought that these longitudinal interior resin-rich areas with gas-bubble porosity coincide with the flat spots on the cylinder observed during winding.

Table 5 is a summary of the average hoop- and axial-layer thicknesses measured from ring cross section. The average hoop-layer thickness from the cylinder ID to 40 percent of the wall thickness (excluding the hoop layer at the ID to 40 percent of the wall thickness (excluding the hoop layer at the ID) is 33.3 mils; the average hoop-layer thickness for the remainder of the sample (excluding the OD hoop layer) is 26.5 mils. The average axial-layer thickness is 12.9 mils. Based on the individual readings, there was more variation between the axial-layer thicknesses than with the hoop layers (Figure 48).

The average hoop-to-axial layer ratio from the cylinder ID to 40 percent of the wall thickness is

$$\frac{33.3 \text{ mils}}{12.9 \text{ mils}} = 2.58 \quad \text{(Figure 47)}$$

or 2.58:1. The average hoop-to-axial layer ratio for the remainder of the cylinder wall thickness is

$$\frac{26.5 \text{ mils}}{12.9 \text{ mils}} = 2.05 \quad \text{(Figure 48)}$$

or 2.05:1. These values compare well with the intended design ratios of 2.5:1 and 2.0:1 specified in Table 5. The hoop layer on the outside surface of the cylinder has been made twice as thick as the hoop layers just below (Figure 51). Based on the measured layer ratios and the average 70-volume percent fiber content, the elastic properties of the cylinder calculated to be as follows:

Circumferential Modulus = 17.3×10^6 psi
Longitudinal Modulus = 8.7×10^6 psi
Shear Modulus = 1.0×10^6 psi
Major Poisson's Ratio (nu0Z)* = 0.056

* 0 refers to the hoop direction of the cylinder; Z refers to the cylinder longitudinal axis.

MATERIAL PROPERTIES

The properties of the composite in the cylinder were established by testing of material coupons machined from rings remaining after cutting the 96-inch cylinder to a 65-inch length. Two kinds of specimens were prepared. The specimens used in determination of compressive strength were 1.0-inch OD × 3.0-inch OL cylinders cut along axial and hoop orientations of the fibers in the cylinder (Figures 57 and 58). After potting in of the cylinder ends in steel cups and instrumentation with strain-gages, the cylinders were axially loaded to failure (Figure 59).

Three cylindrical specimens cut along the axis of the cylinder (i.e., axial specimens) failed at an average nominal (load divided by bearing area) stress level of 67,800 psi (Figure 60). The specimens failed by delamination of fibers. When an axial specimen was cyclically loaded to only 51,000 psi, delamination did not take place even after 60 load cycles. Since the number of acoustic events recorded during each cycle decreased after the first cycle, and remained so for the balance of the 60 cycles, it can be postulated that the cyclic fatigue life of composite in axial direction of the AUSS Mod 2 cylinder at 29,000-psi design stress level generated by 9000-psi design pressure probably exceeds 1000 cycles.

Three specimens cut along the circumference of the cylinder (i.e., hoop specimens) failed at an nominal stress level of 77,500 psi. When a hoop specimen was cyclically loaded to a nominal stress level of 76,5000 psi, delamination was initiated after 10 cycles. At the cyclically applied 76,500 psi nominal compressive stress level, the maximum compressive stress on the surface of the cylindrical specimens facing the interior of the AUSS cylinder was 107,000 psi while the minimum compressive stress on the surface facing the exterior of the cylinder was only 46,000 psi. The differences between the maximum and minimum compressive stresses on the surface of the cylindrical specimen and the nominal compressive stress are due to the fact that the hoop fibers are not parallel to the axis of the cylindrical test specimen.

The measured compressive strains indicate that the tangent modulus, and Poisson's ratio of the composite along axial fibers are 8,030,000 psi and 0.25, respectively. Along hoop fibers, the composite has a 17,600,000-psi tangent modulus of elasticity and 0.27 Poisson's ratio. These values compare very favorably to the calculated values of 8,700,000 psi and 17,300,000 psi for tangent moduli of elasticity in axial and hoop directions.

Different material specimens were prepared for determination of composite properties in flexure. The square, oblong specimens cut along axial- and hoop-fiber orientations (Figure 57) were 0.25 × 0.25 × 3 inches in size (Figure 63). When tested to destruction they failed along axial and hoop orientations at maximum flexure stress of 61,000 and 81,000 psi, respectively (Figure 64). Based on the magnitudes of deflection measured during flexure testing, the tangent moduli of elasticity were calculated to be 9,000,000 psi along axial fibers, and 18,000,000 psi along hoop fibers.

Based on these measurements, one can conclude that the compressive strengths and moduli of elasticity in the as-fabricated composite cylinder are adequate to withstand the (1) 60,750-psi and 26,100-psi design hoop and axial stresses at 9,000-psi design depth, and (2) buckling in the 0- to 18,000-psi pressure range. Furthermore, the ratio between the ultimate material strengths of 67,800 psi in axial and 108,500 psi in hoop directions and design stresses provide safety factors of 2.5 in

the axial and 1.8 in the hoop directions of the fiber in the composite. These safety factors are less than the specified value of 2, yet close enough to make the cylinder acceptable for a ROV application with limited cyclic fatigue life.

EVALUATION OF FULL-SCALE AUSS MOD 2 HULL

BONDING OF COUPLING RINGS TO GFRP CYLINDER

The Test Assembly consisted of a Mod 2 cylinder, two coupling rings, two end bells, two adapter rings, and two split clamp bands. Before the components of the pressure hull could be assembled for pressure testing, the GFRP cylinder had to be (1) bonded to the titanium coupling rings, and (2) instrumented with electric resistance straingages and acoustic-emission transducers. The bonding of the coupling rings P/N 55910-0114521 (Figures 10, 65, and 66) to the GFRP cylinder (Figure 67) demands great care in the selection of the adhesive, thorough cleaning of surfaces to be bonded, and meticulous attention to procedure for application of adhesive to the cou pling ring. The epoxy adhesive, for bonding of coupling rings to the GFRP cylinder was chosen on its ability to withstand high-bearing stress without extruding from the joint, or debonding from the mating components.

The evaluation of adhesive proposed for this application consisted of testing specimens assembled from two 1.0-inch OD × 1.0-inch L steel plugs bonded by a 0.01-inch thick layer of epoxy. Each of the specimens were subjected to cyclic axial compressive loads that generated 30,000-psi nominal bearing stress in the bond. After 10 cyclic load applications, the specimen was inspected for extrusion, or debonding of epoxy from metal plugs. Epoxies that extruded or debonded were excluded from further consideration.

The remaining specimens were subjected to a bearing stress of 60,000 psi for one hour. After this test, the specimens were again inspected for debonding, or extrusion of epoxy. Epoxies that failed this test were removed from further consideration. Only one adhesive passed this severe test and was chosen for bonding of the coupling rings to GFRP cylinder. The adhesive chosen for bonding of the coupling rings to GFRP cylinder. The adhesive chosen for this application was CIBA epoxy resin 6010 and CIBA 283 hardener mixed in 100 to 70 ratio.

The surface of the titanium coupling ring seat and the ends of the GFRP cylinder were prepared for bonding by sanding first with 240-grit sandpaper, followed by thorough cleaning with methyl ethyl ketone solvent. The titanium surface was subsequently passivated by brushing on Pasa Gell® 107 (Semco, a Division of Products Research and Chemical Corporation, Glendale, CA), rinsing with tap water after 20 minutes of soaking, and drying with a forced-air heater.

The thickness of the adhesive joint was controlled by placement on the horizontally placed plane titanium bearing surface of 1 × 1 × 0.01-inch-thick cardboard spacers on approximately 4-inch intervals. After placement of the spacers, premixed epoxy adhesive was poured into the seat cavity. Sufficient epoxy was poured into the cavity to cover it to a depth of 0.25 inch. At this time, the GFRP cylinder was rotated to vertical position, raised above ground, and gently lowered into the seat on the coupling ring until it came to rest on the cardboard spacers. This action squeezed out

excess epoxy through the annular spaces between the GFRP cylinder and the titanium seat. After a 72-hour cure at room temperature, the ends of the cylinder were reversed and the bonding process repeated with a coupling ring on the other end of the cylinder. After curing the adhesive, the exterior of the coupling rings was cleaned thoroughly to insure good fit with the titanium end closures and split clamps (Figure 68).

INSTRUMENTATION OF THE GFRP CYLINDER

The full-scale AUSS Mod 2 cylinder was instrumented on its interior surface with 25 rectangular 0.25-inch straingage rosettes and 8 acoustic-emission sensors. The straingages were bonded to the interior of the cylindrical pressure hull with Eastman 910 contact cement at the following three locations: (1) midbay; (2) 2.5 inches from the end of cylinder; and (3) on the coupling ring itself (Figure 69). The objective of the straingage instrumentation was to detect incipient buckling at midbay, to compare the radial contraction of the GFRP cylinder to that of the titanium end closure, and to measure the magnitude of bending in the cylinder at the titanium coupling rings. The titanium end closures were not instrumented with straingages as their performance under hydrostatic loading was already established during prior prooftesting of AUSS Mod 1 pressure hull (Reference 2).

The 8 acoustic-emission 150-kHZ resonant frequency sensors were bonded with polyurethane elastomeric cement to the interior surface of the GFRP cylinder 21 inches from its ends (Figure 70). The objective of the acoustic-emission instrumentation was to detect and record acoustic stress waves generated inside the GFRP cylinder during pressure cycling by microcracking of the plastic matrix and breakage of fibers during hydrostatic pressurization of the AUSS Mod 2 pressure hull. These data would be used to predict impending material failure.

TEST ASSEMBLY

The AUSS Mod 2 pressure hull was assembled by mating the two titanium end closures (Figure 71) to the titanium coupling rings, placing test clamps (Figure 72) over the equatorial flanges on the end closures, and clamping the titanium end closures to the titanium coupling rings with aluminum split clamps (Figure 13). The completed test assembly (Figure 73) was then placed inside the test cage (Figure 74) for insertion into the deep-ocean test simulation vessel (Figure 75).

The caged test assembly was placed inside the deep-ocean test simulator located at the NOSC Arctic Laboratory, followed by the instrumentation cables being connected to bulkhead penetrators in the vessel walls and the hydraulic tube to the vessel end closure. After placement and locking in place of the vessel end closure, the interior of the test assembly, as well as the vessel itself, were filled with tap water and purged of trapped air. Next, the hydraulic tubing used for filling the interior of the test assembly with water was connected to the manometer for measuring the volume of water displaced from the interior of the test assembly during pressurization.

TEST SCHEDULE

The test schedule encompassed 20 consecutive pressure cycles. The magnitude of peak pressure in each cycle was to increase in 1000-psi steps during the first ten

cycles until, in the tenth cycle, the proof pressure of 10,000 psi would be attained. If the test assembly successfully withstood the proof test without any detectable deformation or cracking, it would be subjected to ten more pressure cycles with 9000-psi peak pressure. During these 10 pressure cycles to design pressure, the acoustic emission would be monitored continuously to determine whether there is any increase in acoustic activity during cycling. If the acoustic activity remained constant from one cycle to another it would be an indication that there is no crack propagation or initiation during pressurization to design pressure.

TEST PROCEDURE

The test procedure followed during each pressure cycle consisted of pressurization to peak pressure at approximately 1000-psi/minute rate, sustained loading of 30-minute duration at peak pressure, depressurization at 1000-psi/minute rate, and relaxation at 0 psi for 30 minutes. The strain readings were recorded at 1000-psi intervals during pressurization, at start and end of sustained loading, and at start and end of relaxation. The acoustic emission was monitored and recorded continuously from the beginning to the end of each pressure cycle (Figure 76). The volume of water displaced from the interior of the test assembly was measured and recorded at 1000- psi steps during pressurization, at the start and end of sustained loading, at 1000-psi steps during depressurization, and at the start and end of relaxation.

TEST RESULTS

STRAINS ON CYLINDER

The strains increased linearly with pressure during all pressure cycles (Figures 77 to 81). The maximum strains were recorded on the interior surface at midbay in hoop direction. The average magnitude of hoop strains at midbay under 9000-psi design pressure was –3383 microinches/inch (Figure 77). The average axial strain at the same location was –3086 microinches/inch (Figure 78).

The magnitude of hoop strains on the interior surface of the cylinder near the ends was about the same (Figure 79), and of axial strains significantly more (Figure 80) than at midbay (Figures 77 and 78). Still, the magnitude of axial strains on the interior surface at the end of the cylinder did not exceed the magnitude of hoop strains at midbay.

The average magnitude of hoop strains on the interior of the titanium coupling ring (Figure 81) was –3015 microinches/inch, significantly less than the –3383 microinches/inch hoop strain at midbay. The axial strains on the same location were less than –1000 microinches/inch (Figure 82). The strains at the base of the tie-rod lugs on the coupling ring were also less than –1900 microinches/inch (Figure 83).

VOLUMETRIC CHANGE OF THE PRESSURE-HULL ASSEMBLY

The overall contraction of the AUSS Mod 2 pressure-hull assembly (GFRP cylinder capped with titanium hemispheres) varied linearly with external pressure loading (Figure 84). The overall loss of displacement was 0.67 milliliter per psi of external pressure loading (1.5 milliliters per foot of depth). The slight nonlinearities

in the volume versus pressure plot are due to problems associated with the volume-displacement measurement arrangement. The magnitude of time dependent volume displacement under 9000-psi design depth was found to be negligible (i.e., less than 35 milliliters during 30 minutes of sustained loading).

ACOUSTIC EMISSIONS OF THE PRESSURE-HULL ASSEMBLY

The total number of acoustic events (i.e., hits) per pressure cycle did not vary significantly from one pressure cycle to another. The significant variation was in the number of events during sustained pressure loading in each cycle that decreased with each pressurization to higher pressure. For example, the number of recorded events during sustained pressurizations to 3000, 4000, 5000, 6000, 7000, 8000, 9000, and 10,000 psi was 300, 305, 328, 427, 69, 35, and 33. During the subsequent pressure cycles (11 through 20) to 9000 psi, the number of events during each sustained loading was less than 20.

During the first ten pressure cycles, where the maximum pressure in each cycle was increased stepwise by 1000 psi, particular attention was paid to the number of events generated during the last 1000-psi pressure increment. It was assumed that the acoustic activity during this pressure interval could be utilized as a predictor of material failure. If the number of acoustic events during the last 1000-psi pressurization step did not increase significantly from one pressure cycle to another, the catastrophic failure of the composite was not considered to be imminent. This was accomplished by graphically adding the number of acoustic events generated in each pressure cycle during the last 1000-psi increment (Figure 85).

Inspection of the graph on Figure 4 shows that the number of acoustic emissions during the last 1000-psi increment in pressure cycles 1 through 10 increased very little. During the first five pressure cycles, the acoustic activity during the last 1000-psi increment was, on the average, 2300 events while during pressure cycles 9 through 10 it had increased to 4000 events per increment. This increase is substantial, but not yet exponential.

The total number of acoustic events during each of the ten cycles to 9000 psi (cycles 11 through 20) was approximately the same (Figure 86). These events were generated at identical pressures during pressurization and depressurization phases of each cycle. Because these events took place every time at the same pressure level, it can be assumed that they were generated by sliding contacts between components of the pressure hull assembly and not crack propagation in the composite (Figures 87 and 88). Very few (less than 20), or no events were recorded during the sustained loading phases of these cycles.

MATERIAL PROPERTIES OF THE GFRP COMPOSITE

Testing of the coupons cut from the ends of the Mod 2 cylinder (Figures 57 to 64) has shown that the composite is elastic at the design stresses generated in the cylinder by the 9000-psi pressure. As expected, the properties of the composite differed between hoop and axial orientations in the cylinder.

The moduli of elasticity in compression were measured to be 17,600,000 psi along hoop fibers and 8,030,000 psi along axial fibers (Figures 61 and 62). The

Poisson's ratios along the hoop and axial orientations were 0.27 and 0.25, respectively. The ultimate strength of the composite in compression and in flexure varied with the orientation of the fibers in the cylinder. Along hoop fibers, the nominal compressive and flexure strengths were 77,500 and 81,000 psi. Along the axial fibers, the compressive and flexure strengths were 67,800 and 61,000 psi. The failure in all cases was due to delamination (i.e., matrix failure).

The ratio of material strength along hoop fibers to material strength along axial fibers (1.6 for compressive strengths), did not follow closely the 2:1 ratio of hoop to axial fibers in the composite. There is no simple explanation for this discrepancy.

VISUAL INSPECTION OF PRESSURE-HULL ASSEMELY

Visual inspection of the exterior and interior surfaces on the AUSS Mod 2 pressure-house assembly after completion of 21 pressure cycles did not detect any (1) deterioration of the GFRP composite, (2) extrusion of epoxy adhesive from the annular spaces between the cylinder and cylinder seat in the titanium coupling ring, or (3) permanent deformation of the titanium coupling ring or end closures.

DISCUSSION OF TEST RESULTS

STRUCTURAL PERFORMANCE

1. The structural perfo. .nance of the full-scale AUSS Mod 2 pressure-hull assembly is almost identical to the structural performance of the model-scale pressure-hull AUSS Mod 2 pressure cycled 100 times to 9000 psi prior to implosion testing. This observation is based on the fact that the strains (microinches per inch) recorded during pressure testing on both pressure hulls at the same geometrical locations are approximately the same as shown below (Table 6).

Table 6. Strains recorded during pressure testing.

	Hoop Orientation		Axial Orientation	
	Model	Full Size	Model	Full Size
Strains				
Midbay	3,579	3,383	3,097	3,086
End	3,150	3,304	—	3,573
Ring	—	3,015	—	674
Elastic Constants				
Modulus of Elasticity	16,600,000	17,600,000	8,700,000	8,030,000
Poisson's Ratio	—	0.27	—	0.25

2. The structural performance of the AUSS Mod 2 pressure hull is adequate for the design depth of 9000 psi. This observation is based on the fact that the strains on the GFRP cylinder and titanium components were elastic during pressurization to 10,000-psi proof pressure and that they returned to zero after depressurization.

3. The elastic stability of the AUSS Mod 2 pressure hull is adequate for the design pressure of 9000 psi. This observation is based on the linearity of (1) hoop

strains at midbay of the model-scale and full-scale GFRP cylinders, and of the (2) strains on the interior surface of titanium end closures during pressurization to 10,000 psi (Reference 2).

4. The structural performance of the Mod 2 cylinder is superior to Mod 1 cylinder fabricated previously by Hercules, Inc. Aerospace Division (Reference 2). This statement is based on the comparison of strains on the interior surface at midbay of full scale Mod 1 and Mod 2 cylinders (Figures 89 to 92). Since both GFRP cylinders have the same internal diameter and wall thickness, the difference in strains at mid-bay reflects the difference in elastic properties of the two composites. The difference in strain magnitude is substantial, as shown below:

	Hoop Orientation	Axial Orientation	Units
Mod 1 Cylinder	0.570	0.466	microinches/inch/psi
Mod 2 Cylinder	0.377	0.342	microinches/inch/psi

From the above comparison, it appears that the wet fiber wound GFRP cylinder is 51-percent stiffer in hoop and 36-percent stiffer in axial orientations than the prepregged broadgoods wound GFRP cylinder. The moduli of elasticity measured experimentally on test specimens cut out from Mod 1 and Mod 2 cylinders confirm this finding.

	Hoop Orientation	Axial Orientation	Units
Mod 1 Cylinder	12,100,000	6,500,000	psi
Mod 2 Cylinder	17,600,000	8,700,000	psi

Because of increased stiffness, Mod 2 cylinder has a higher safety margin against catastrophic failure by elastic instability at design depth of 9,000-psi (20,000 feet).

5. The residual strains inside the Mod 2 cylinder generated by the fabrication process measured prior to hydrostatic testing were significantly less than those inside Mod 0 cylinder (i.e., -165 vs. -780 microinches/inch). This would seem to indicate that the wet-winding procedure and associated curing process incorporates smaller residual strains into the cylinder than winding of prepregged broadgoods. As a result, the magnitude of compressive residual hoop stresses on the interior surface of Mod 2 cylinder is only -2900 psi, while on the interior of Mod 0 cylinder it was measured to be -9500 psi. Because of the smaller residual stress there is less tendency for the Mod 2 cylinder to delaminate due to static fatigue while in storage.

MATERIAL PROPERTIES

The strength of the GFRP composite material in the cylinder appears to be adequate for the stresses to which it is subjected at design pressure of 9000 psi. This observation is based on the fact that the maximum hoop stress of 60,750 psi on the interior surface of GFRP cylinder at midbay, and the axial stress of 34,900 psi at the end of the cylinder are approximately 44 to 48 percent less than the ultimate compressive strength of the GFRP material in hoop (108,500 psi), and axial (67,800 psi) directions established by testing of material coupons cut from the ends of the

cylinder. This observation is further supported by the fact that crack propagation and/or delamination of the composite in the cylinders was neither detected by acoustic-emission instrumentation nor noticed during post-test inspection after repeated pressure cycling of the model-scale and full-scale AUSS Mod 2 pressure housings.

The compressive yield strength of cast titanium end closures (120,000 psi) and of wrought Ti-6AL-4Va titanium coupling rings (130,000 psi) is adequate for the stresses to which these components are subjected at design pressure of 9000 psi. This observation is supported by the fact that the maximum recorded compressive stress of 98,670 psi on the interior surface of the hemispherical end closure (Reference 2) and 54,800 psi on the inside of the coupling ring are at least 18-percent less than the yield strength of these materials in compression.

The compressive strength and creep resistance of epoxy adhesive bonding and sealing the titanium coupling rings to the ends of the GFRP cylinder are adequate for the axial and radial bearing stresses generated between the ends of the cylinder and the coupling ring under 9000-psi design pressure. This observation is supported by the fact that (1) steel compressive test specimens with 0.010-inch-thick simulated epoxy joint did not debond under repeatedly applied 76,500-psi compressive bearing stress, and (2) the adhesive did not extrude, debond, or fail to maintain a seal between the GFRP cylinder and the titanium coupling ring under 10,000-psi external proof pressure.

CYCLIC FATIGUE LIFE EXPECTANCY

The cyclic fatigue life of the AUSS Mod 2 pressure hull is predicted to exceed 1000 pressurizations to design pressure of 9000 psi. This prediction is based on the fact that (1) the model-scale AUSS Mod 2 composite cylinder successfully withstood 100 pressure cycles to 9000-psi design pressure, and (2) the full-scale AUSS Mod 2 composite cylinder successfully withstood 12 pressure cycles to 9000 psi without any increase in acoustic activity during pressure cycling. In addition, the model-scale cylinder did not exhibit any unusual acoustic activity at 12500-psi overpressure, indicating absence of cracking or delamination even at 38-percent overpressure. This margin of strength remaining after 100 pressurizations to design pressure indicates that the cyclic fatigue life of the GFRP composite utilized in the construction of the AUSS model-scale and full-scale cylinders significantly exceeds 100 loadings to design stress levels.

CONCLUSIONS

The AUSS Mod 2 pressure-hull assembly, consisting of a wet-wound graphite-fiber epoxy composite cylinder, capped with adhesive-bonded titanium coupling rings, and closed off with titanium hemispherical bulkheads appears to satisfy the operational requirements of the autonomous, deep-submergence AUSS vehicle.

The 0.58 weight-to-displacement ratio of this pressure-hull assembly represents the lowest ratio achieved to date by any unmanned full-size pressure hull for a remotely operated or autonomous unmanned vehicle with a payload of 950 lb and predicted cyclic fatigue life in excess of 100 dives to 20,000-foot design depth.

The wet winding of hoop and axial fibers appears to produce thick GFRP cylinders with higher fiber content (> 70 percent), fewer internal wrinkles, smaller residual stresses, and less resin-rich areas than winding of prepegged broadgoods. The wet-winding technique, unlike winding of broadgoods, poses no limitation on the length of cylinder. Construction of AUSS Mod 2 composite cylinder by wet winding has shown that GFRP cylinders with $t/D_o < 0.1$ can be successfully fabricated by this technique, providing that the winding is cured at wall thickness intervals less than 0.2t.

RECOMMENDATIONS

1. The GFRP composite AUSS Mod 2 cylindrical-hull assembly should be incorporated into the pressure housing of the AUSS vehicle for service to a 20,000-foot depth.

2. The design, materials, and fabrication procedure used in the AUSS Mod 2 cylindrical hull should be applied without further development to the construction of deep-submergence cylindrical hulls for remotely operated or autonomous vehicles, providing that their external diameter is less than 3 feet.

3. An R&D program should be initiated immediately to investigate the feasibility of applying the AUSS Mod 2 pressure-hull design, materials, and fabrication procedures to construction of GFRP pressure hulls with external diameter in the 7- to 10- foot range and 10- to 20-foot length for potential service as pressure hulls in manned noncombatant submersibles.

REFERENCES

1. Stachiw, J.D. 1964. *Solid Glass and Ceramic External Pressure Vessels*, Pennsylvania State University Ordnance Research Laboratory Report No. 63-0209-C-2.

2. Stachiw, J.D. 1968. "Hulls for Deep Submergence Capsules," American Ceramic Society, *Ceramic Bulletin*, Vol. 47, No. 2.

3. Stachiw, J.D. and J. Held. September 1987. *Exploratory Evaluation of Alumina Ceramic Cylindrical Housings for Deep Submergence Service; The Second Generation NOSC Ceramic Housings*, NOSC Technical Report 1176.

4. Myers, M.C., G.D. Lee, F.C. Wright, and J.V. Daines. January 1984. *Investigation of Structural Problems with Filament-Wound Deep Submersibles*, H.I. Thompson Fiber Glass Co., Final Report, Bureau of Ships.

5. Hom, K. and W.P. Couch. September 1963. *Hydrostatic Pressure Tests of Unstiffened and Ring-Stiffened Cylindrical Shells Fabricated of Glass-Filament Plastics for Deep-Submergence Application*, David Taylor Model Basin Report 1745.

6. Hom, K. and W.P Couch. November 1966. *Investigation of Filament-Reinforced Plastic Pressure Hull Models to External Hydrostatic and Short-Term and Long-Term Cyclic Pressure Loadings*, NSRDC Report 3560.

7. Couch, W.P. December 1967. *Structural Response of Identical Glass-Reinforced Plastic Pressure Hull Models to External Hydrostatic and Short-Term and Long-Term Cyclic Pressure Loadings*, NSRDC Report 3560.

8. Couch, W.P., G.D.Ward, and W.F. Blumenburg. June 1969. *Investigation of Filament Reinforced Plastic Deep Submergence Pressure Hulls, July 1966 to March 1969*, David Taylor Model Basin Report 3071.

9. Tinley, T.N. and G. Ward. September 1970. *Investigation of Filament Reinforced Plastic Deep Submergence Pressure Hulls, April 1969 to May 1970*, NSRDC Report 3440.

10. Tinley, T.N. and V.A. Morrison. July 1971. *Investigation of Fiber Reinforced Plastic Deep-Submergence Pressure Hulls, June 1970-April 1971*, David Taylor Model Basin Report 3670.

11. Tinley, T.N. June 1973. *Investigation of Fiber-Reinforced Plastic Deep Submergence Hulls*, David Taylor Model Basin Report 4126.

12. Garala, H.J. 1987. "Experimental Evaluation of Graphite-Epoxy Composite Cylinders Subjected to External Hydrostatic Compressive Loading," *Proceedings of the Society of Experimental Mechanics*, Spring Conference.

13. Stachiw, J.D. October 1984. *Graphite Reinforced Plastic Pressure Hull For The Advanced Unmanned Search System*, NOSC Technical Report 999.

14. Stachiw, J.D. December 1986. *Graphite Reinforced Plastic Pressure Hull Mod 1 for the Advanced Unmanned Search System (AUSS)*, NOSC Technical Report 1182.

15. W. Blake. July 1988. "AUSS Cylinder Design Analysis," DARPA/ONT/ORNL *Second Annual Workshop On Thick Composites in Compression*, Oak Ridge, TN.

16. Couch, W.P. September 1965. *Hydrostatic Creep and Cyclic Tests of Radially Oriented Glass Fiber Reinforced Plastic Spheres*, David Taylor Model Basin Report 2089.

GLOSSARY

GFRP	Graphite-fiber-reinforced plastic
GRP	Glass-fiber reinforced plastic
ID	Inside diameter
L	Length
OD	Outside diameter
ROV	Remotely operated vehicle

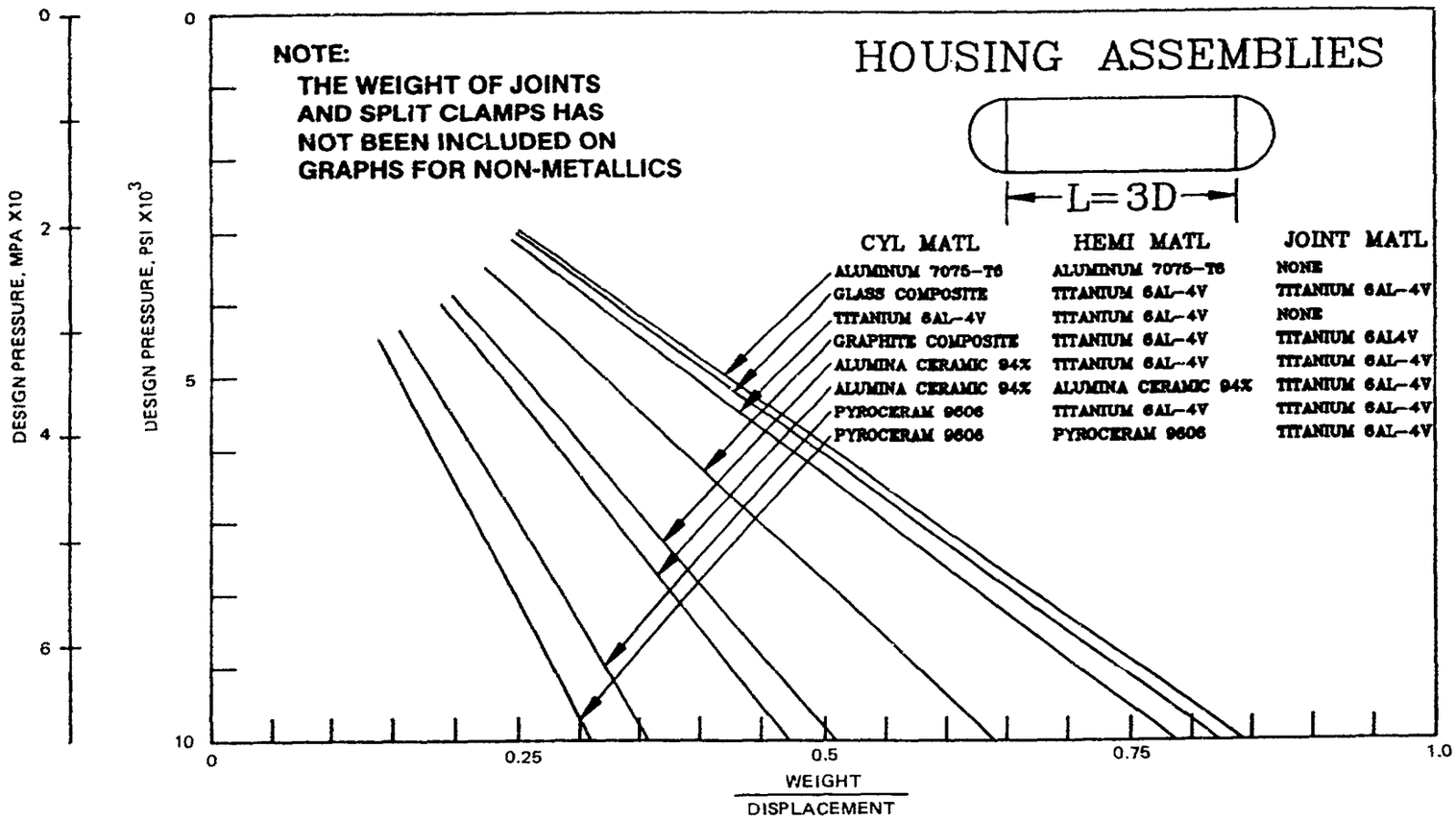

Figure 1. Weight-to-displacement of cylindrical pressure housings with hemispherical end closures fabricated from different structural materials. Note that Pyroceram 9606® provides the lowest weight-to-displacement ratio. In calculation of weight-to-displacement ratios, the design stresses were based on the ultimate compressive strengths and safety factors shown in Table 1. The weight of joints was not included in above calculations.

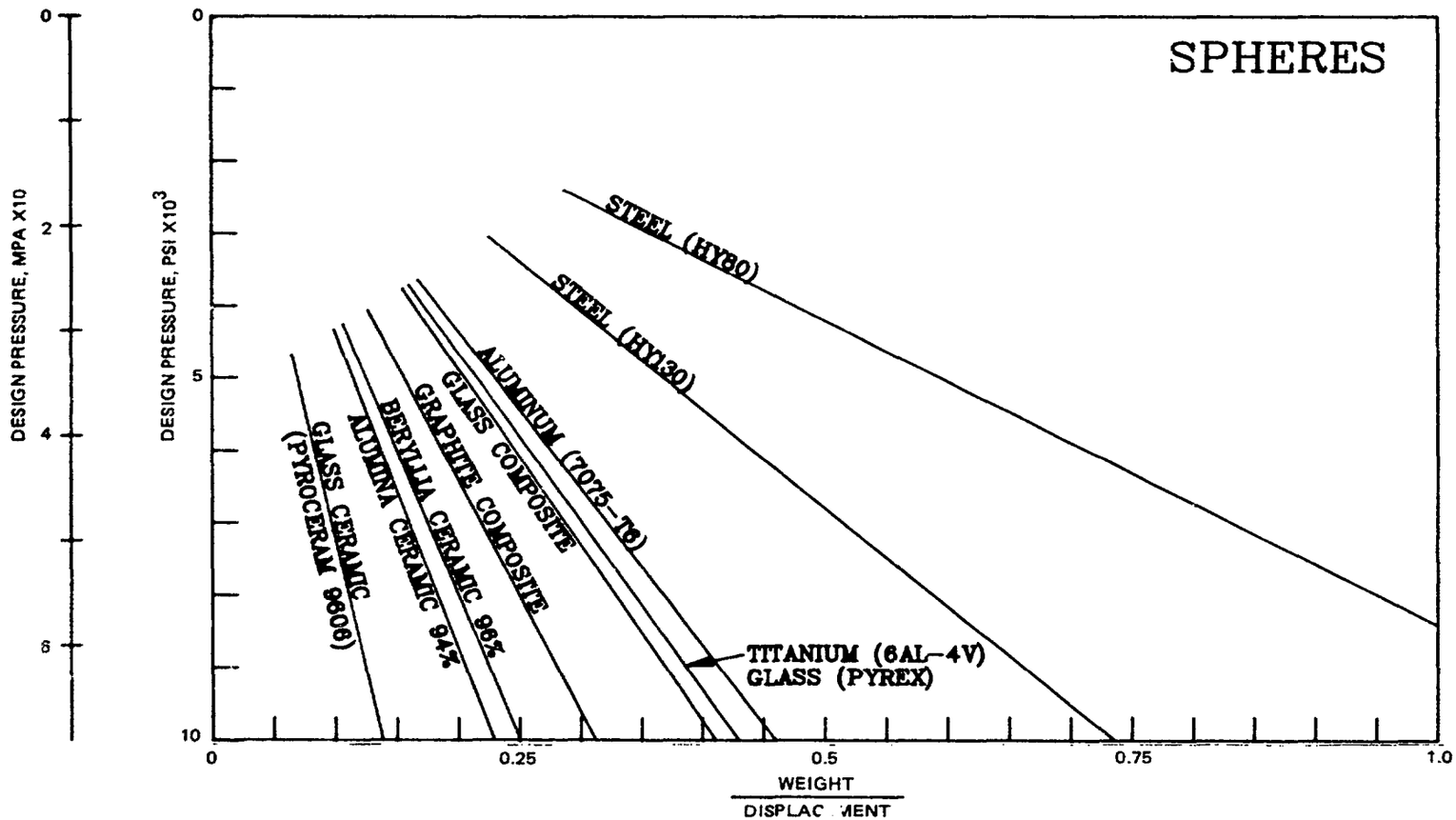

Figure 2. Weight-to-displacement ratios of *spherical pressure housings*. Design stresses are based on ultimate compressive strengths and safety factors shown on Table 1.

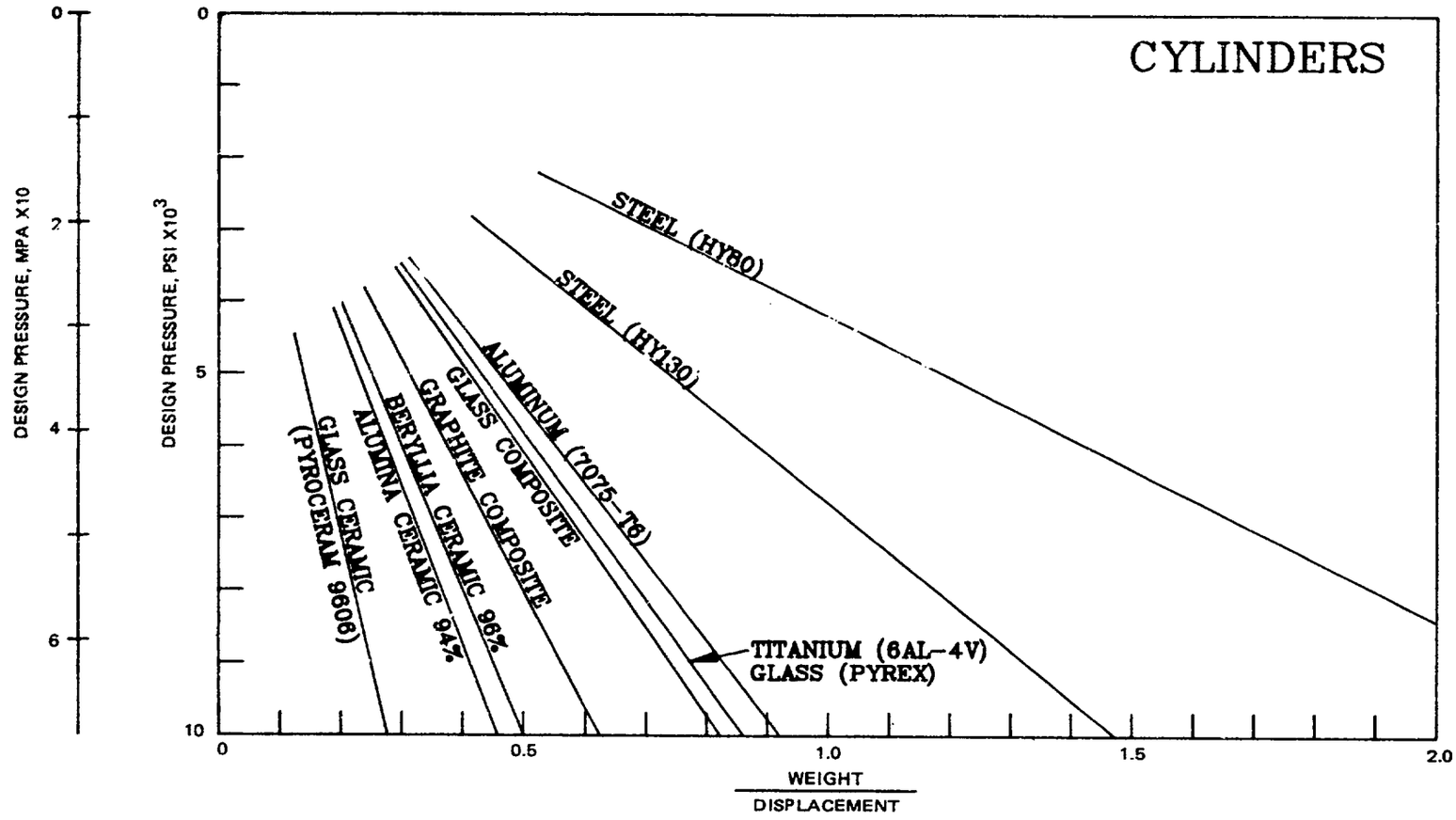

Figure 3. Weight-to-displacement ratios of *cylindrical pressure housings*. Design stresses are based on ultimate compressive strengths and safety factors shown on Table 1.

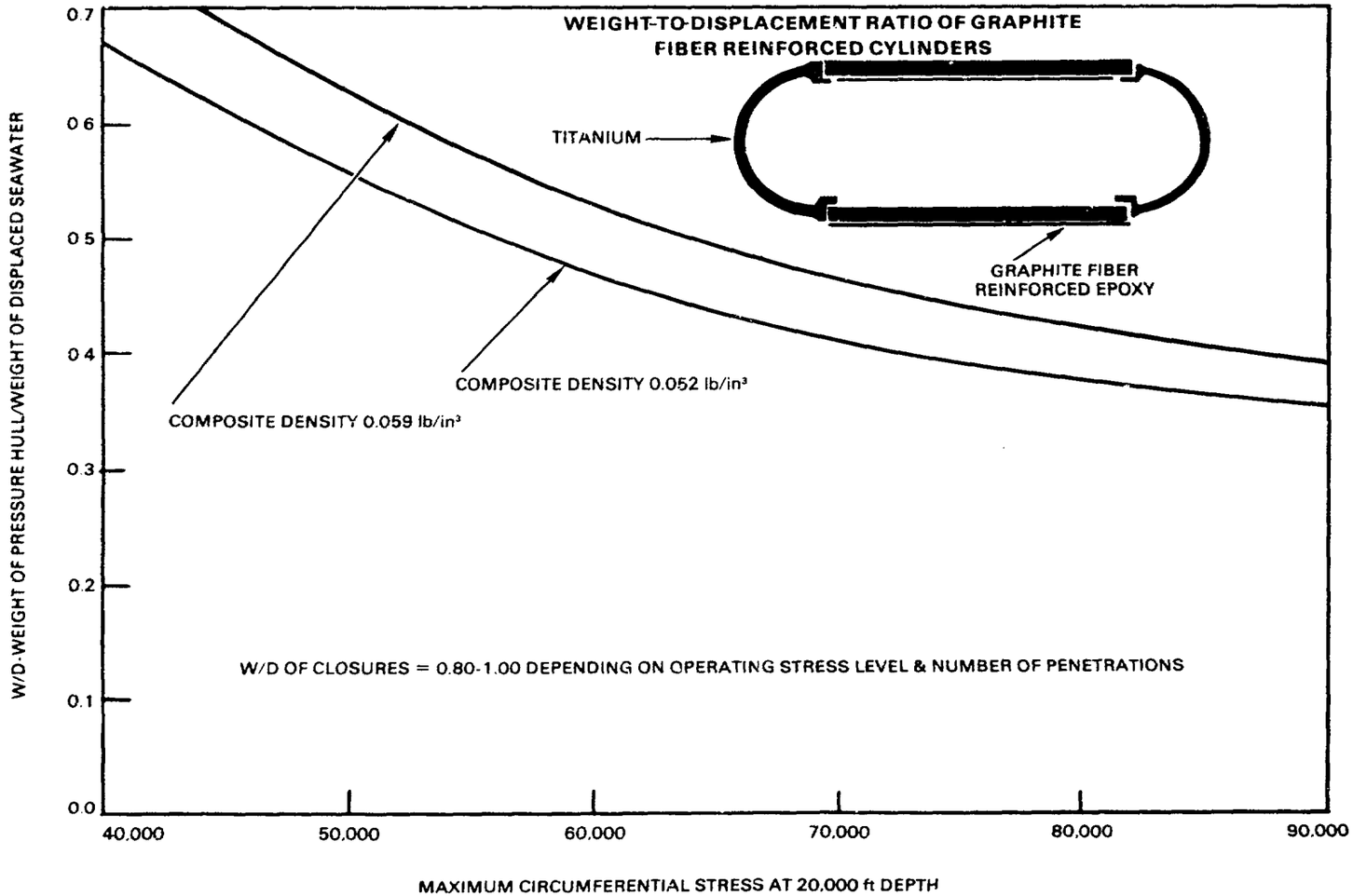

Figure 4. Weight-to-displacement ratio of *cylindrical graphite fiber reinforced* plastic (GFRP) housings supported radially by optimized titanium end closures. The weight-to-displacement ratio is plotted as a function of design stress selected for the 20,000-foot design depth.

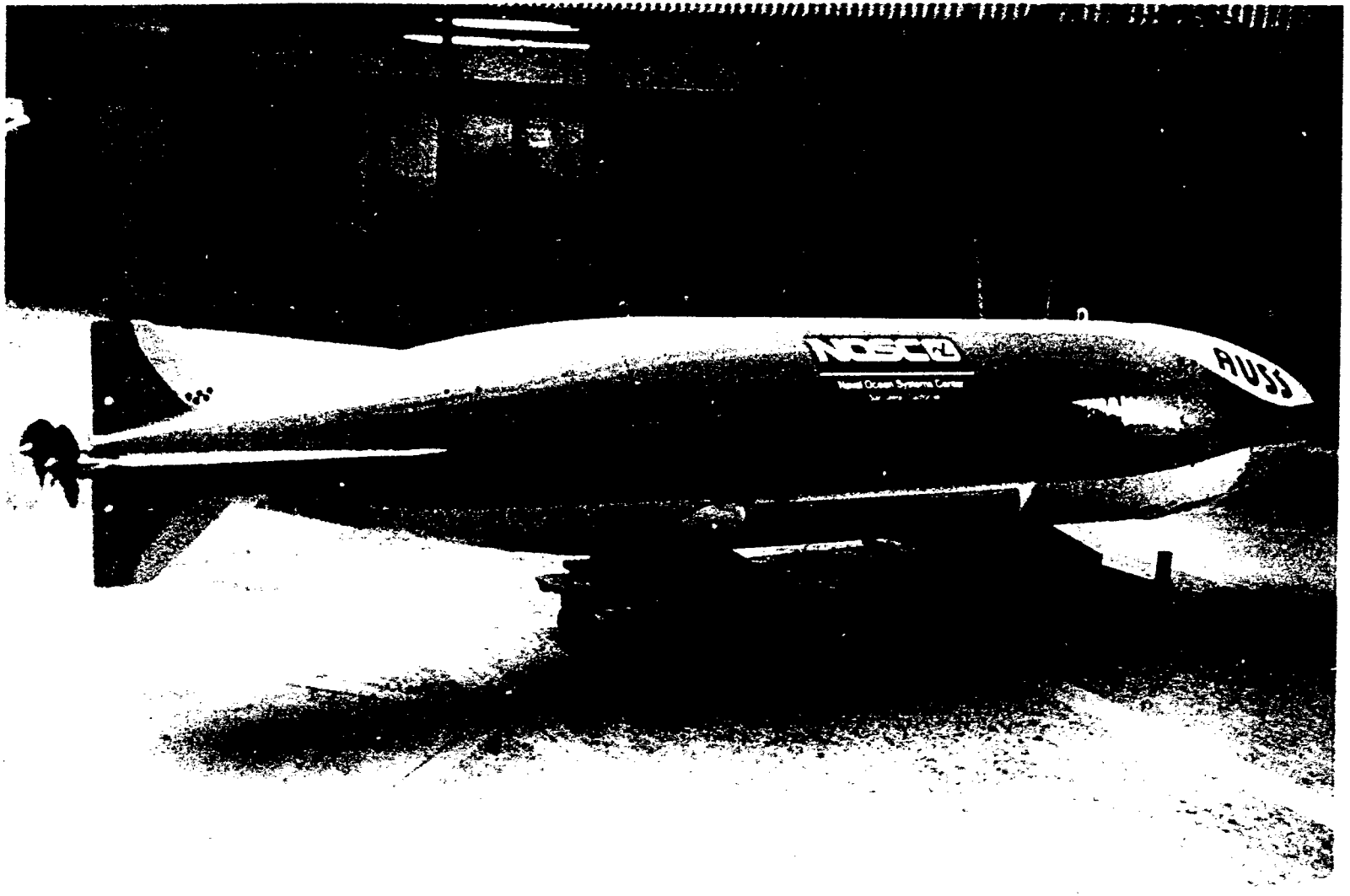

Figure 5. The Advanced Unmanned Search System (AUSS) vehicle with 20,000 foot operational depth capability.

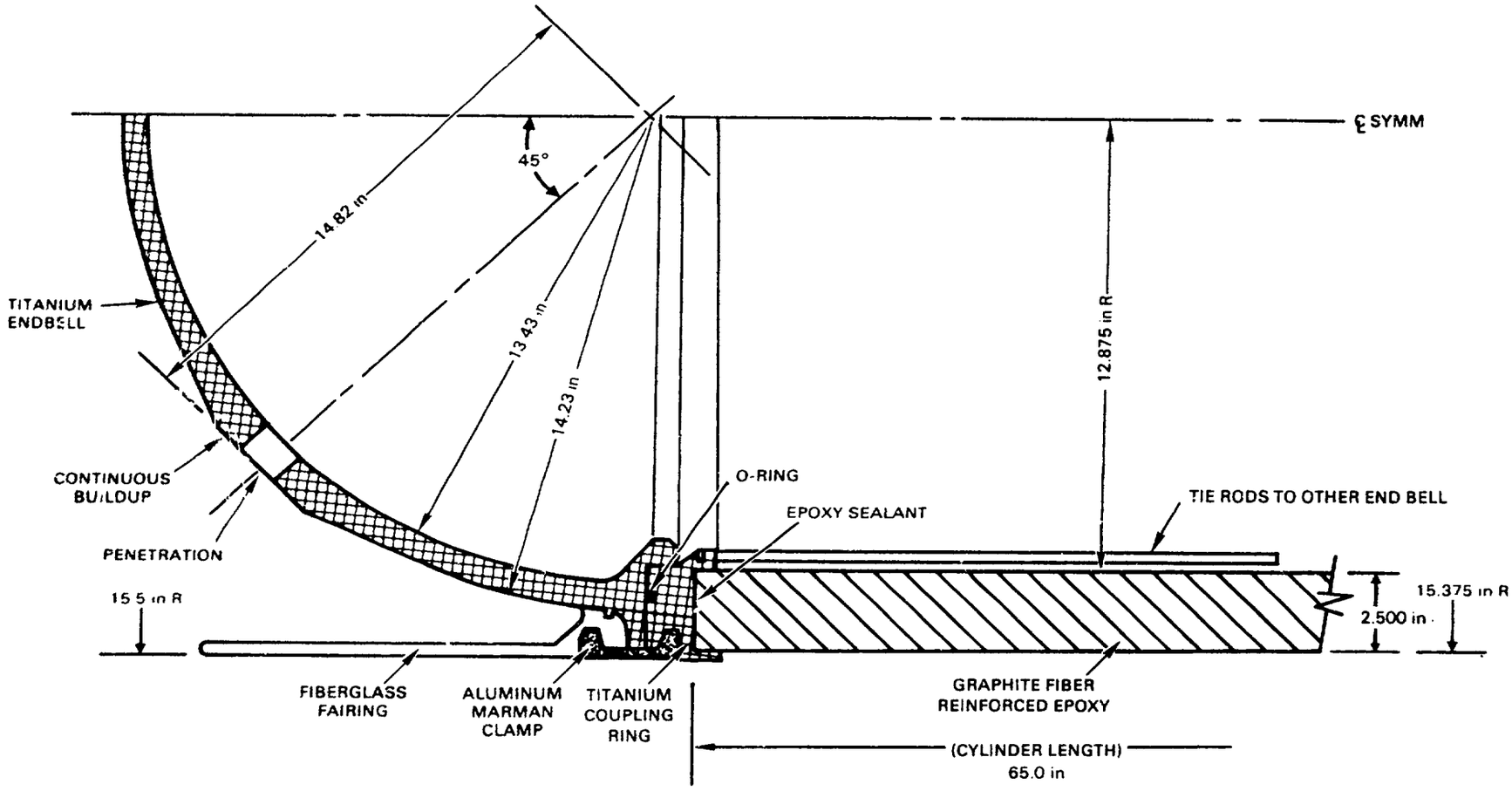

Figure 6. Components of the *AUSS Mod 2* pressure housing assembly. It differs from the Mod 1 (Figure 7) assembly only in the shape of the coupling ring. The Mod 2 coupling ring provides radial restraint *to both the external and internal cylindrical surfaces* at the ends of the GFRP cylinder.

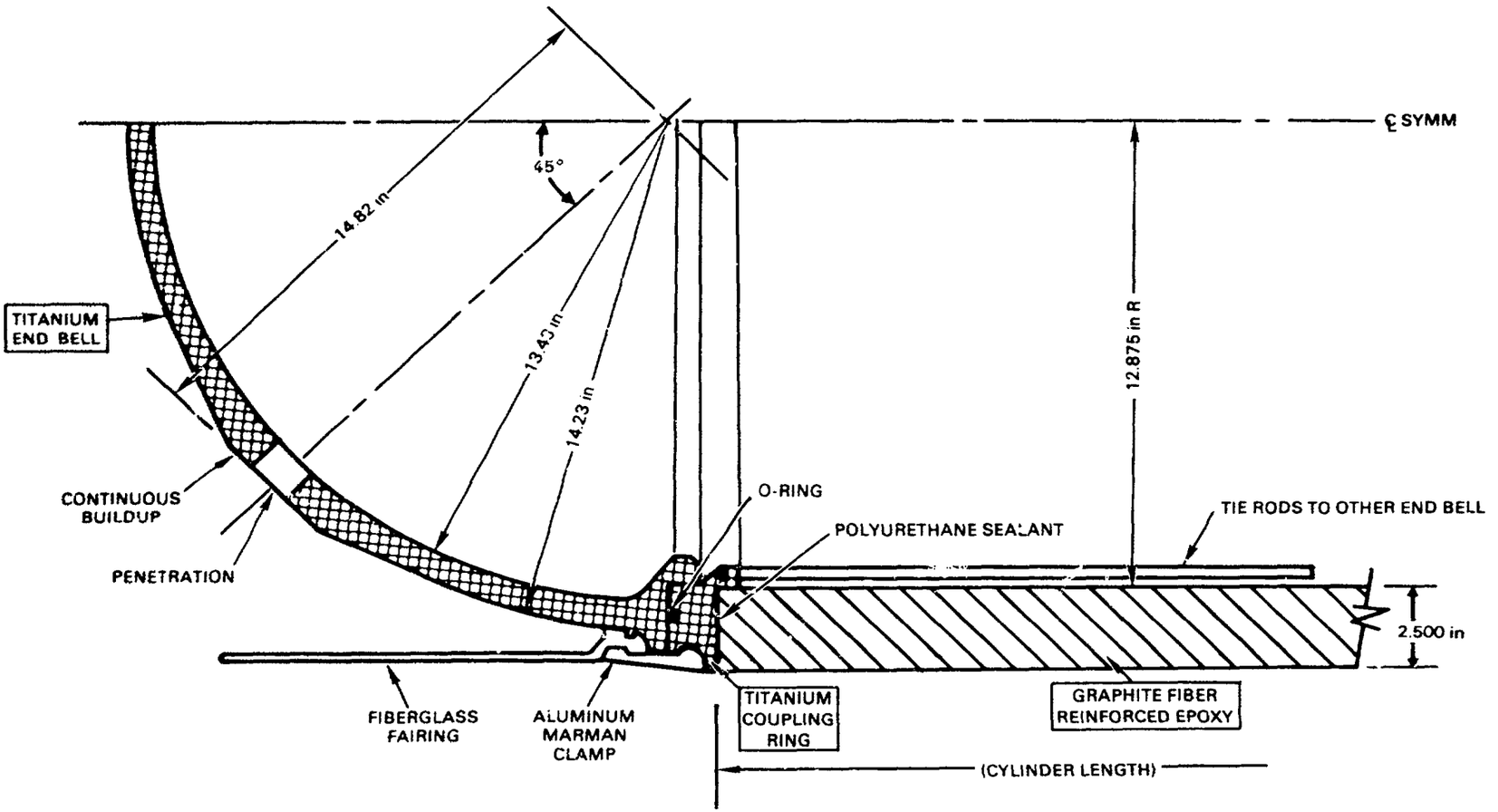

Figure 7. Components of the *AUSS Mod 1* pressure housing assembly. Note the shape of the coupling ring. The Mod 1 rings provide radial restraint *only to the interior cylindrical* surfaces at the ends of the GFRP cylinder.

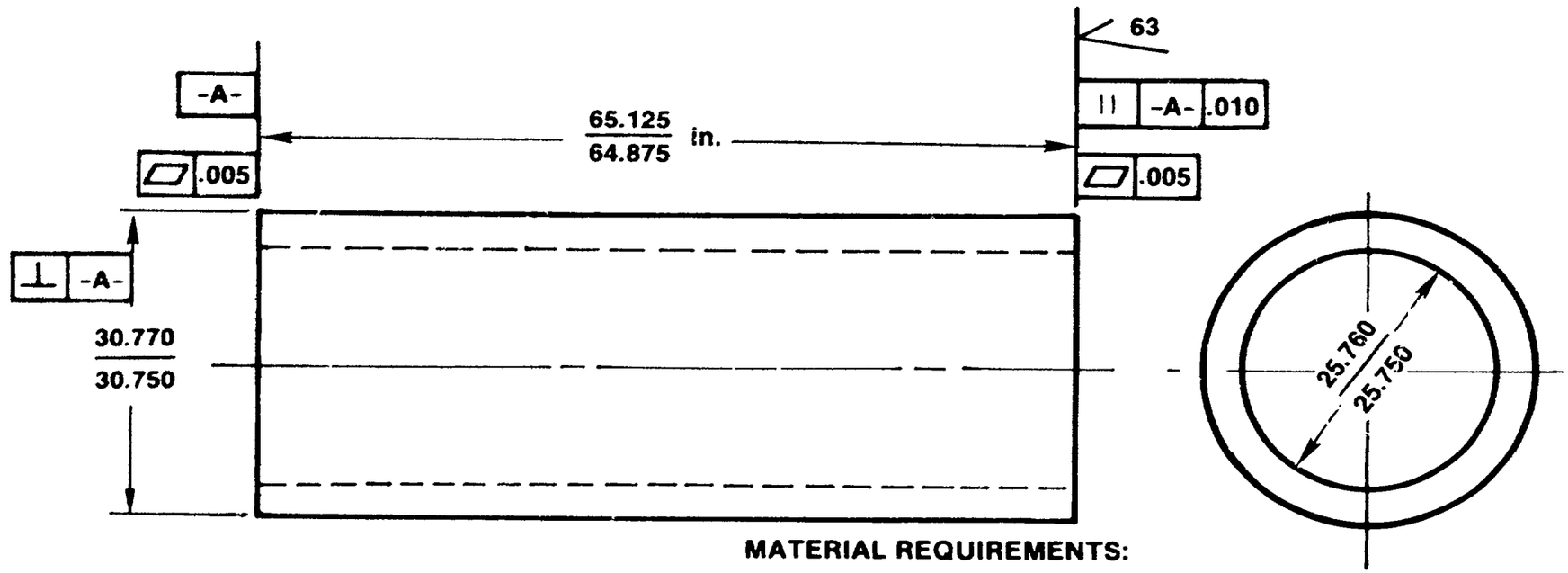

CONSTRUCTION:

GRAPHITE FIBER
EPOXY COMPOSITE
2:1 BIDIRECTIONAL
FIBER LAYUP

STRUCTURAL PERFORMANCE:

DESIGN PRESSURE	9000 psi
IMPLOSION PRESSURE	> 13,500 psi

MATERIAL REQUIREMENTS:

COMPRESSIVE PROPERTIES

HOOP	> 100,000 psi
AXIAL	> 75,000 psi
RADIAL	> 120,000 psi
E-HOOP	> 12.5 x10^6 psi

FLEXURAL PROPERTIES

HOOP	> 160,000 psi
E-HOOP	> 12.5 x10^6 psi

PHYSICAL PROPERTIES

FIBER CONTENT	> 68.5%
VOID CONTENT	< 0.5%

Figure 8. Full-scale *AUSS Mod 2* pressure hull for 20,000-foot design depth.

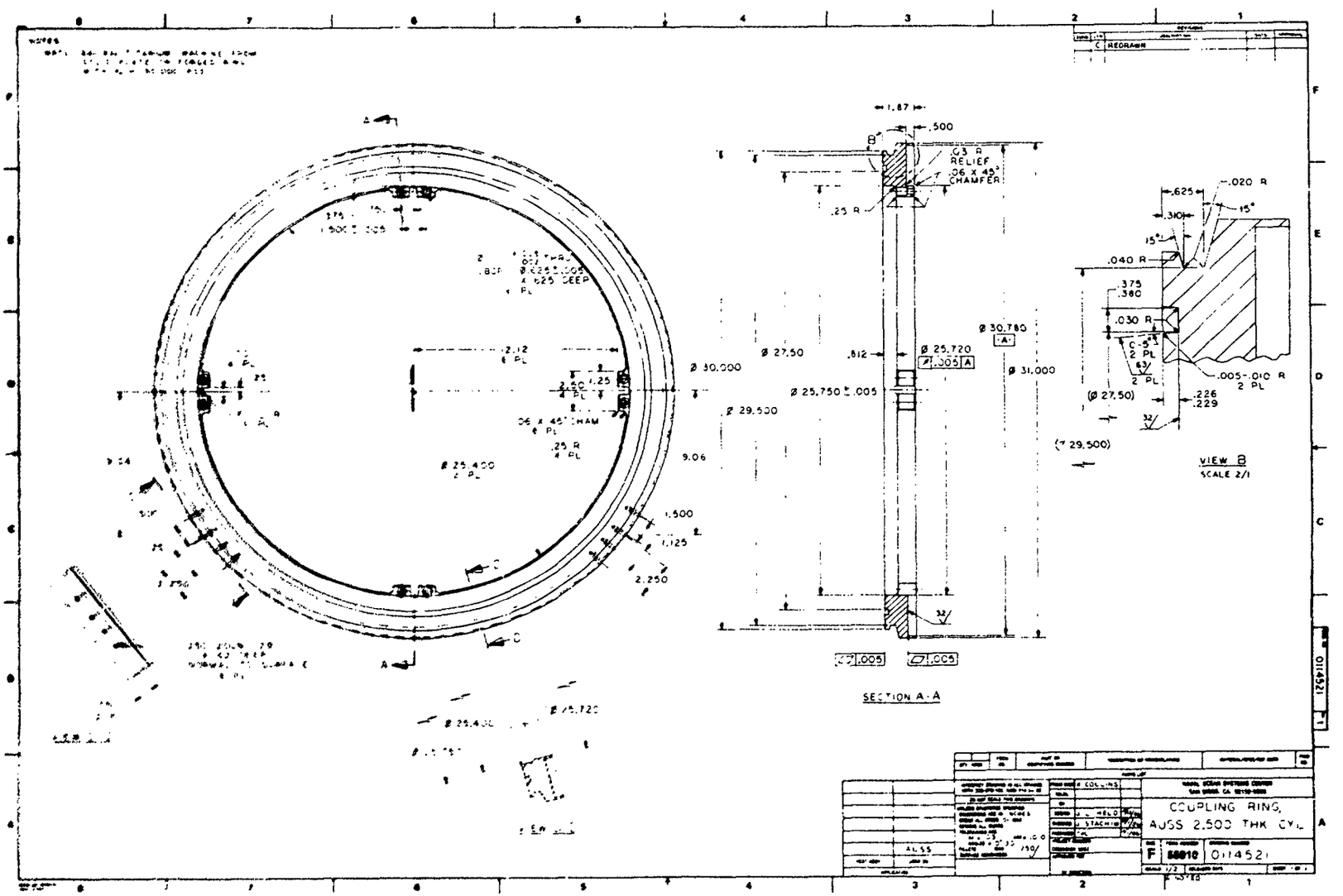

Figure 9. Coupling ring for the *AUSS Mod 2* pressure hull.

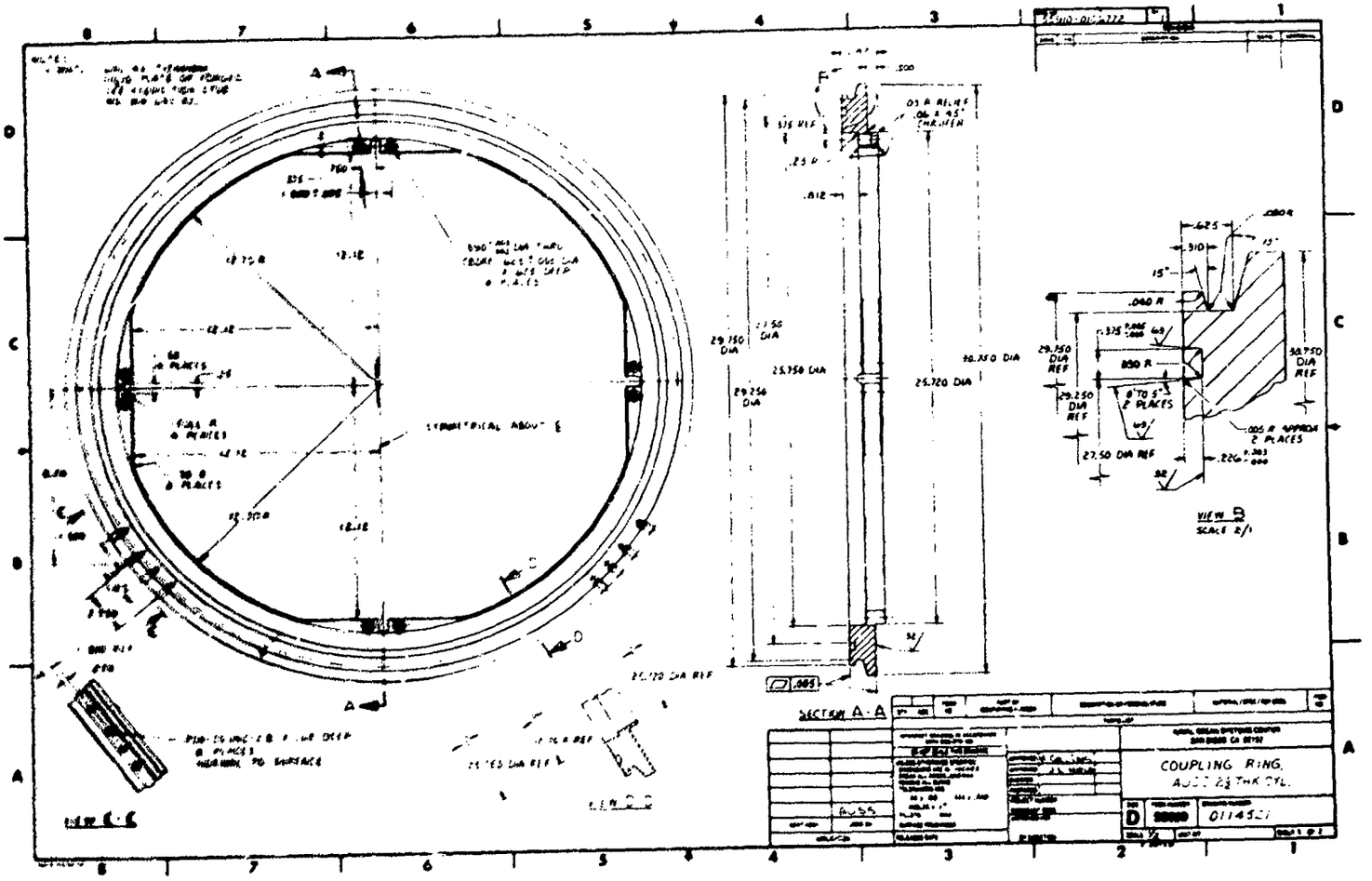

Figure 10. Coupling ring for the *AUSS Mod 1* pressure hull. Note the absence of radial restraint to the exterior surface of the GFRP hull found on the Mod 2 coupling ring (Figure 9).

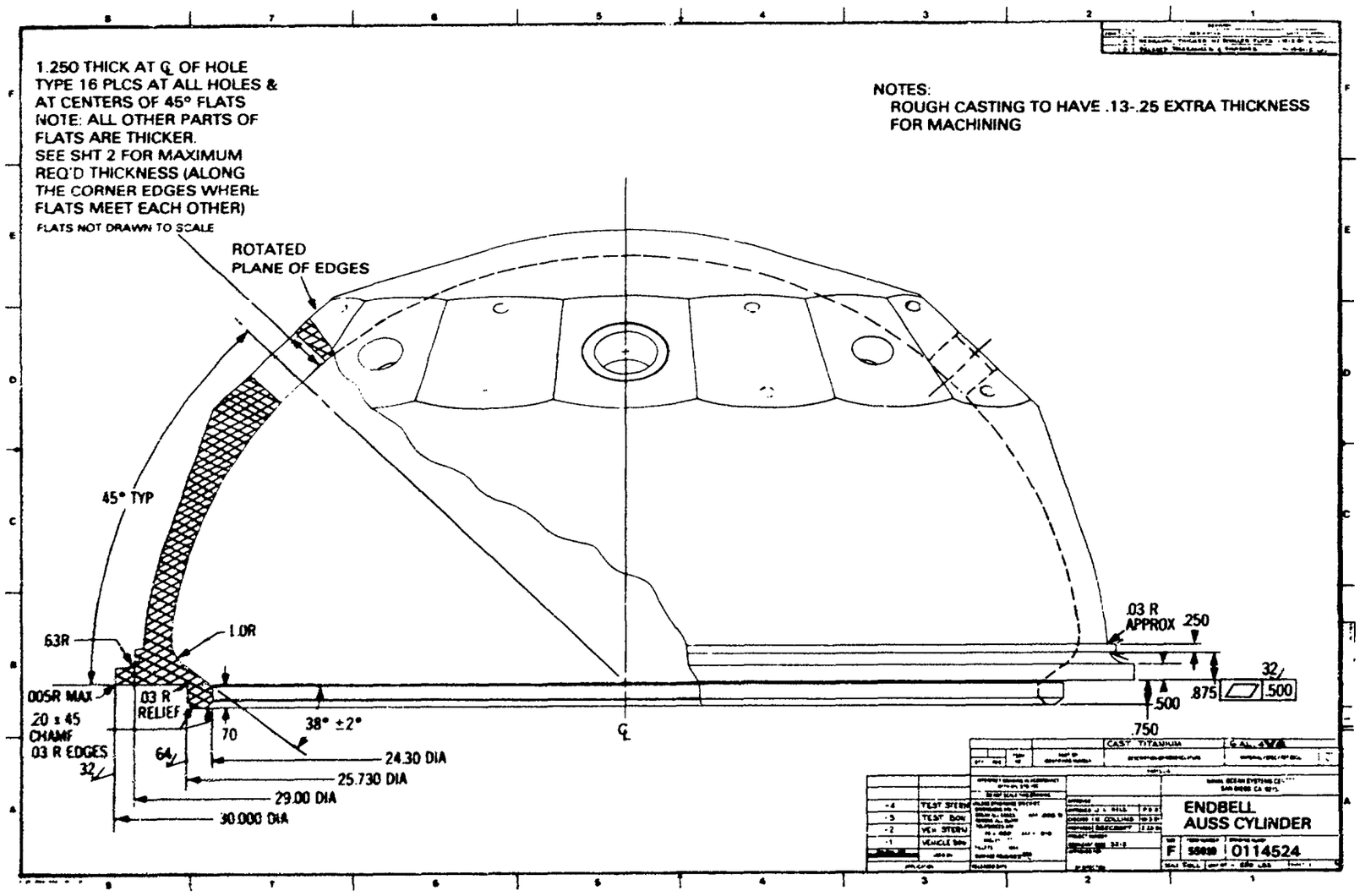

Figure 11. Titanium end closures for AUSS pressure hulls. These end closures fit both the Mod 1 and Mod 2 coupling rings.

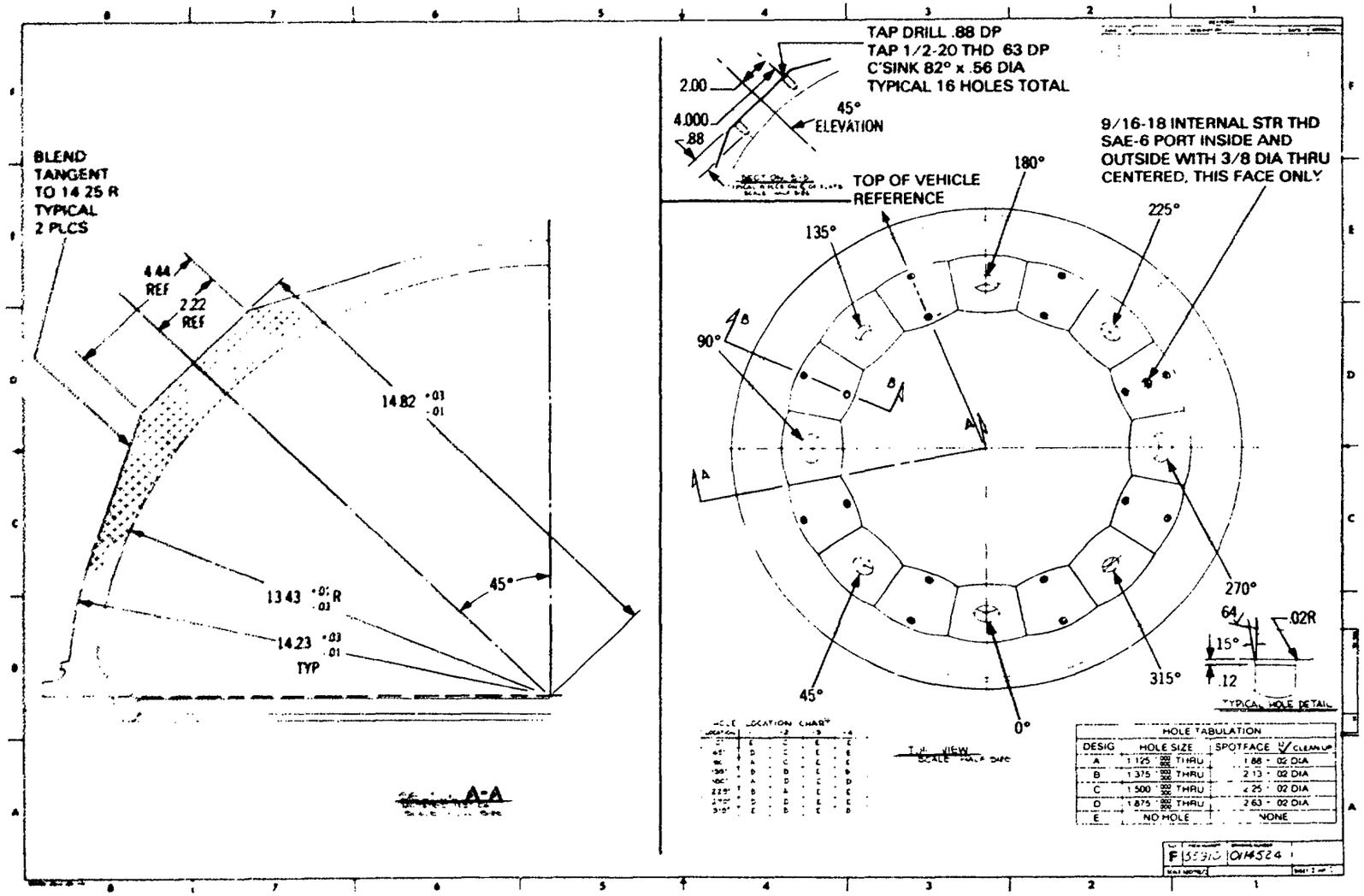

Figure 12. Note the number and size of penetrations in the end closures of Figure 11.

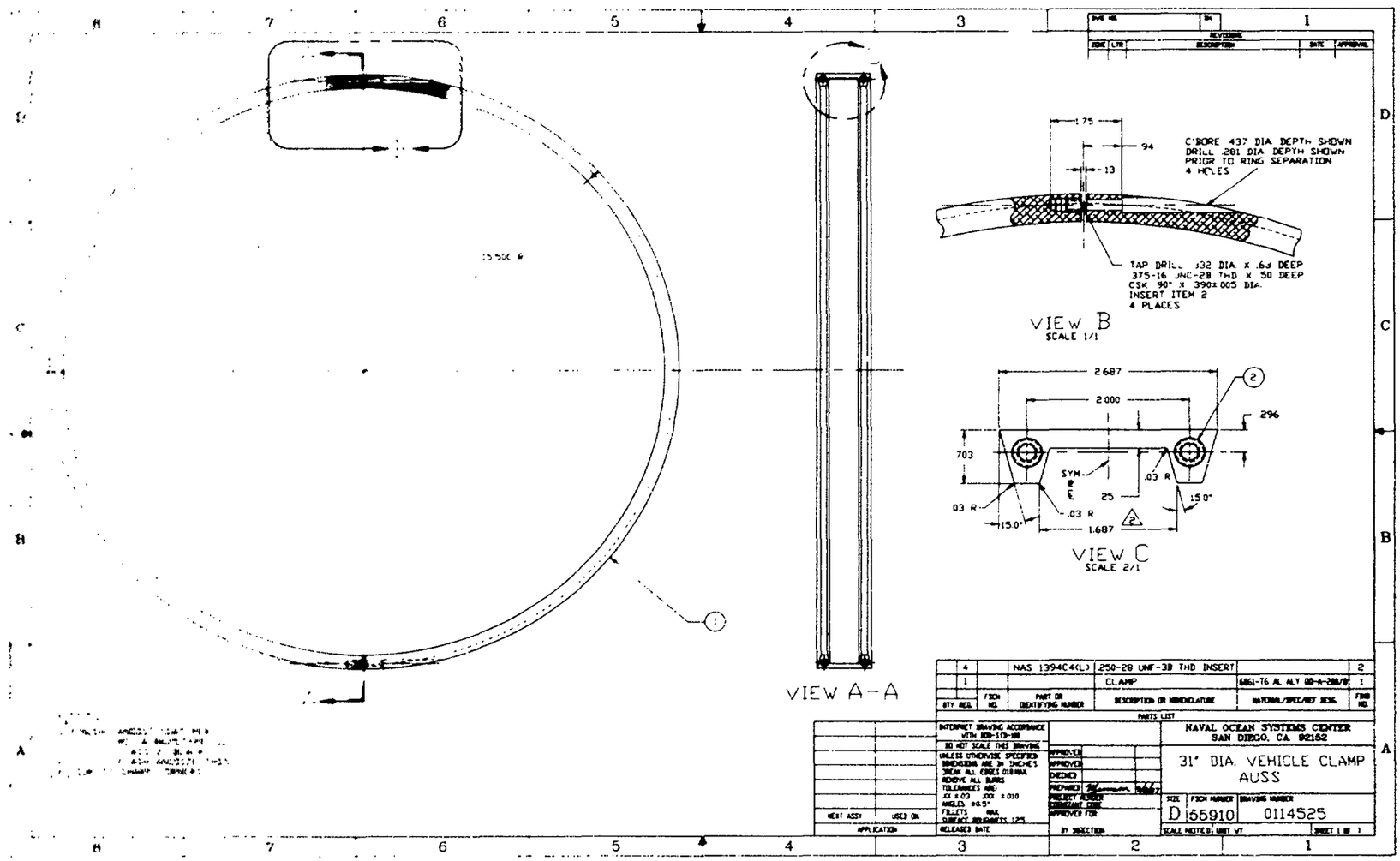

Figure 13. Clamps for attaching the cylindrical hull to the end closure as shown on Figure 7.

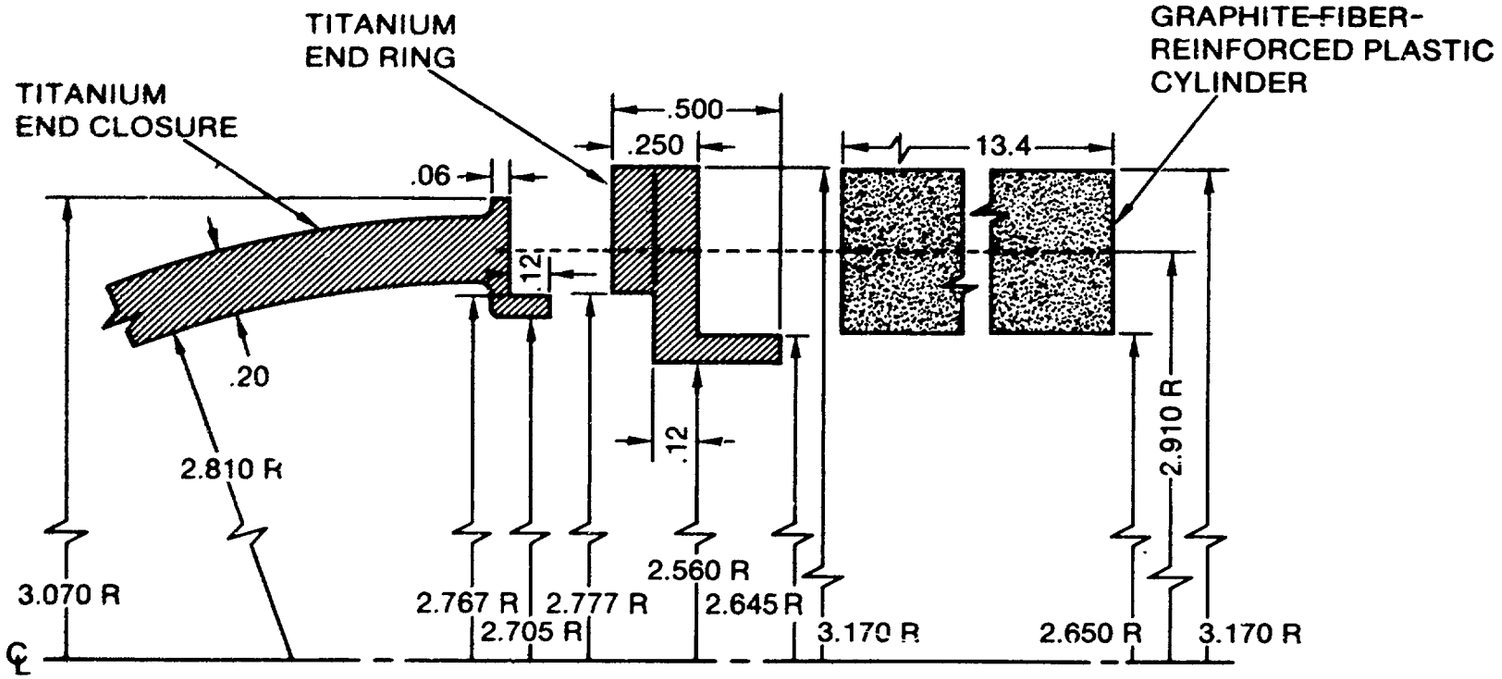

Figure 14. Components of test fixture for proof testing model-scale Mod 2 cylindrical GFRP pressure hull to 10,000 psi.

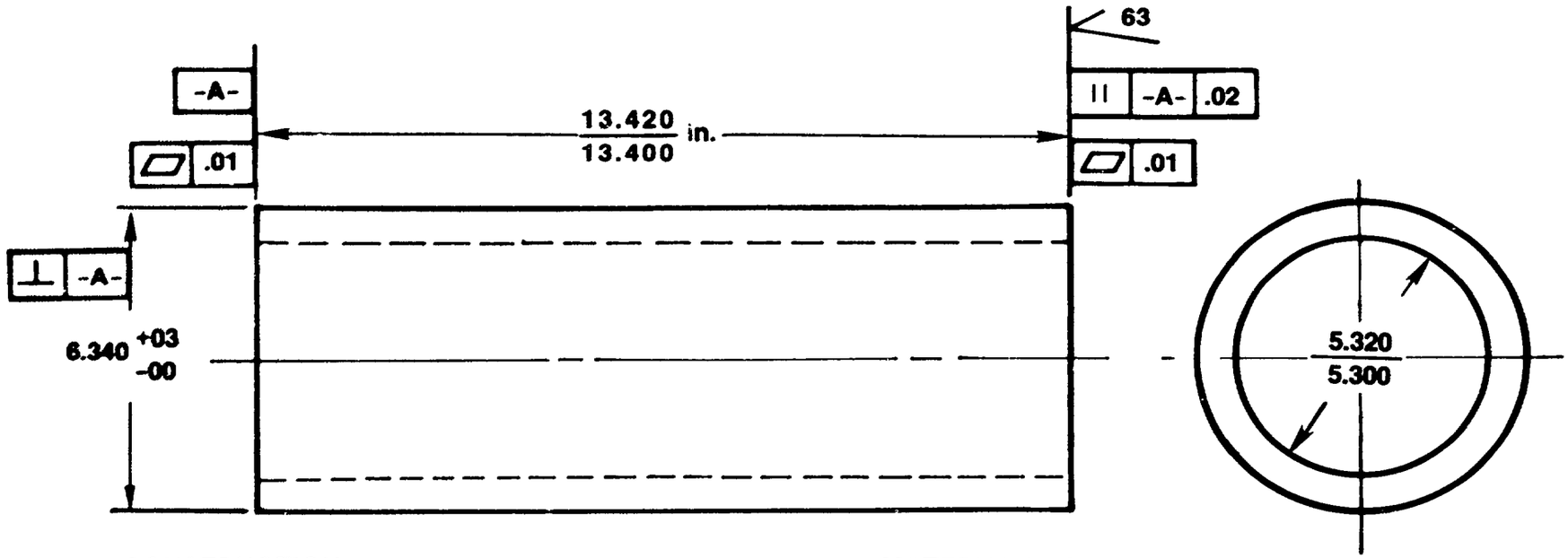

CONSTRUCTION:

GRAPHITE FIBER EPOXY COMPOSITE
2:1 BIDIRECTIONAL FIBER ORIENTATION

STRUCTURAL PERFORMANCE REQUIREMENTS:

DESIGN PRESSURE	9000 psi
IMPLOSION PRESSURE (WITH RADIAL END SUPPORTS)	> 13,500 psi

MATERIAL REQUIREMENTS:

COMPRESSIVE PROPERTIES

HOOP	> 100,000 psi
AXIAL	> 50,000 psi
RADIAL	> 120,000 psi
E-HOOP	> 12.5×10^6 psi

FLEXURAL PROPERTIES

HOOP	> 160,000 psi
AXIAL	> 80,000 psi

Figure 15. Dimensions of the model-scale AUSS Mod 2 cylindrical GFRP pressure hull.

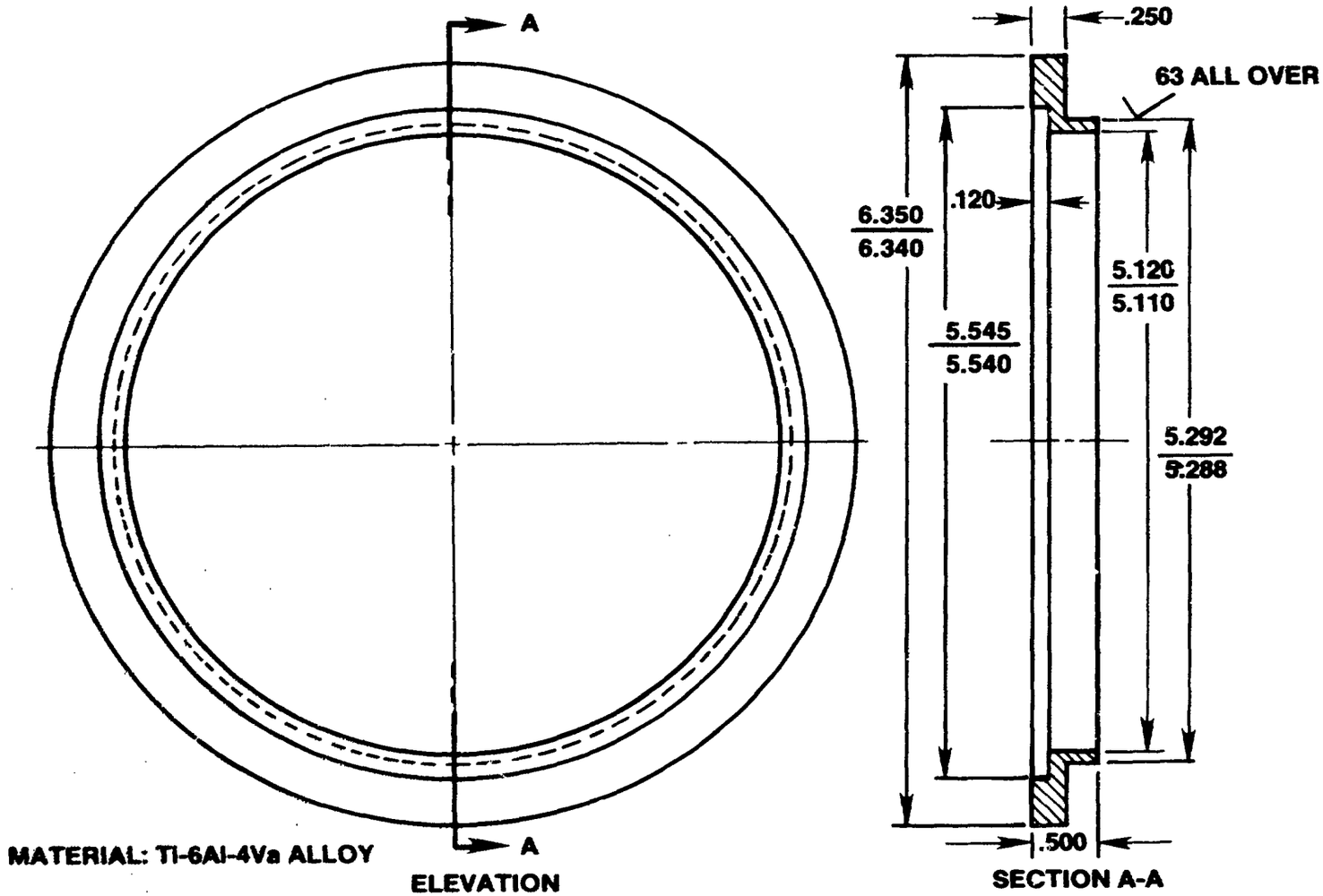

Figure 16. End rings for mating the GFRP model-scale cylinder to the end closures shown on Figure 17.

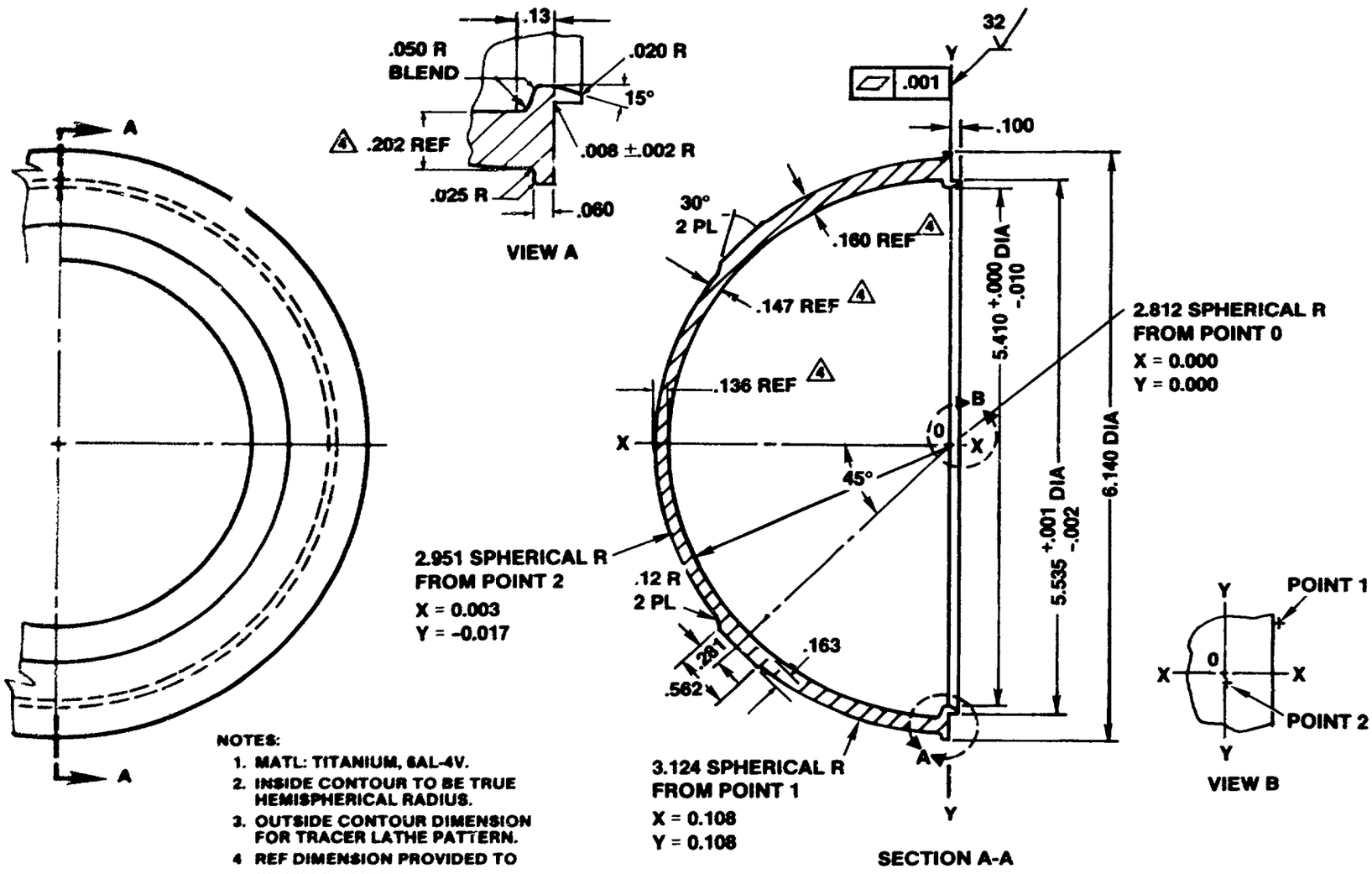

Figure 17. End closures for GFRP model-scale cylinder. These end closures represent optimized design for 9000-psi design depth with a safety factor of 1.25.

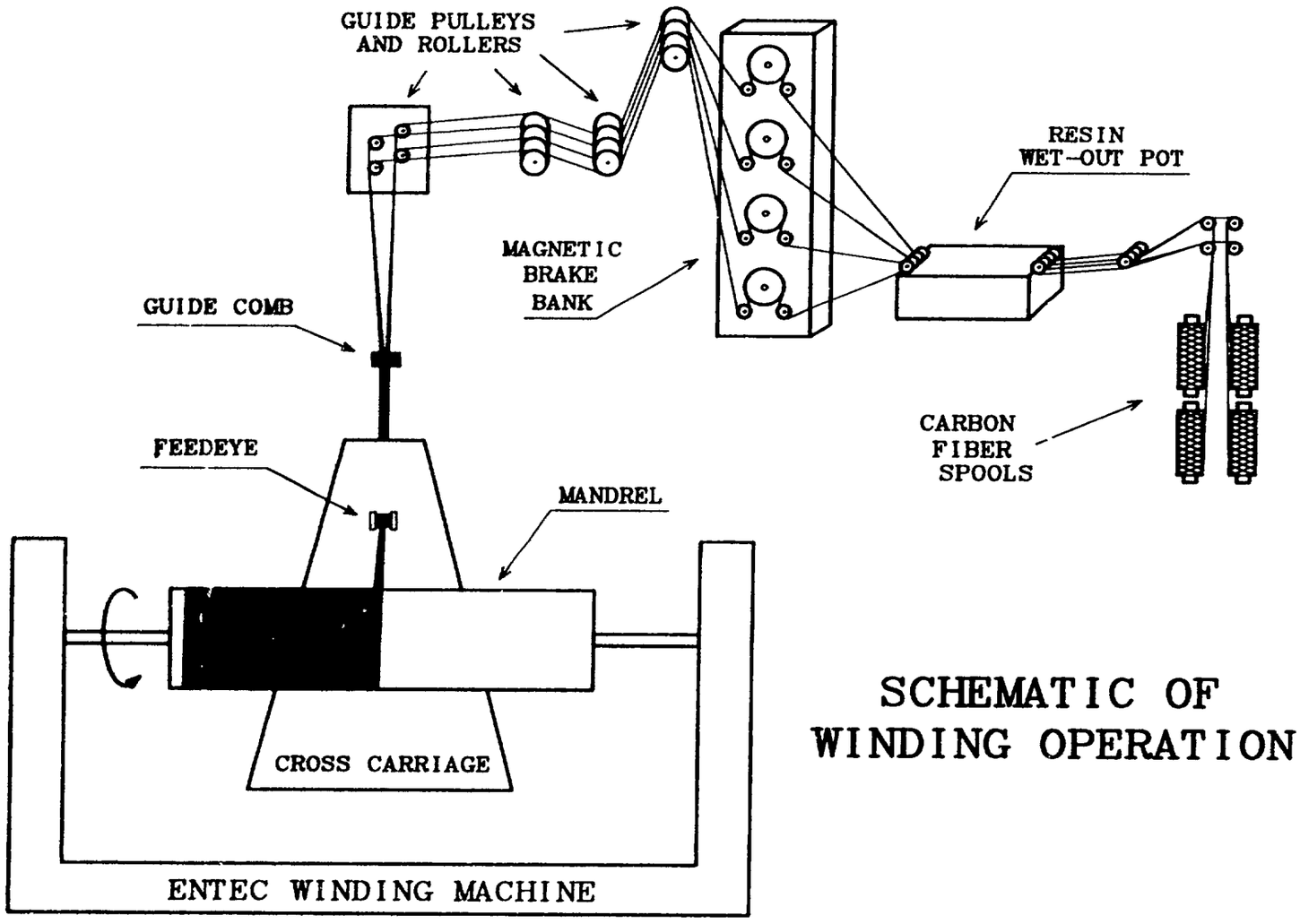

Figure 18. Schematic of winding procedure for composite AUSS Mod 2 cylindrical hulls. The same procedure and equipment was used in winding of both model- and full-scale AUSS Mod 2 cylinders.

Figure 19. Winding of model-scale AUSS Mod 2 cylinder by computer controlled EnTec 4 axis machine. In this photograph, the feedeye is stringing tows axially between pinwheels attached to the ends of the mandrel

AUSS MODEL-SCALE PRESSURE HULL
CYLINDER FABRICATION INSTRUCTION

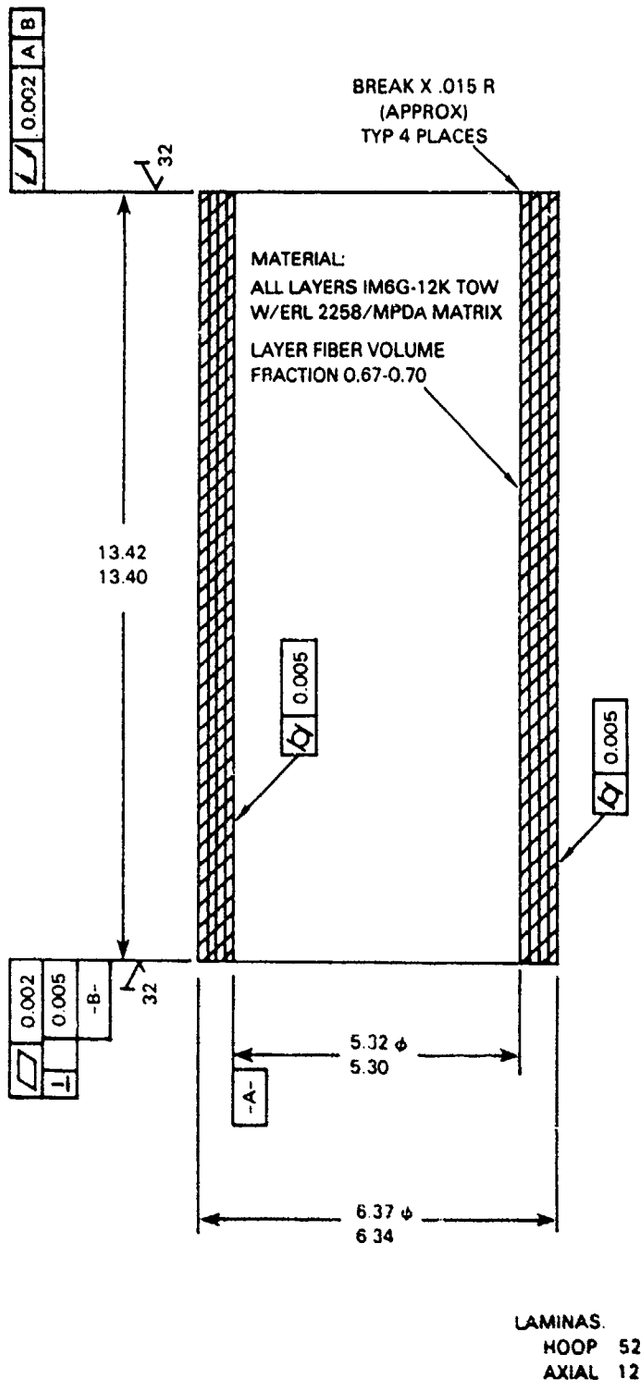

LAMINATE STACKING SEQUENCE

	Layer No.	Orientation (deg)	Tension (lbs)	Thickness (in.)	Cumulative Thickness (in.)
1st LAYER	1	90	8	0.0069	0.0069
	2	90		0.0069	0.0138
	3	0		0.0136	0.0274
	4	90	12	0.0069	0.0343
	5	90		0.0069	0.0412
	6	90		0.0069	0.0481
	7	90		0.0069	0.0550
	8	90		0.0069	0.0619
	9	0		0.0136	0.0755
	10	90	12	0.0069	0.0824
	11	90		0.0069	0.0893
	12	90		0.0069	0.0962
	13	90		0.0069	0.1031
	14	90		0.0069	0.1100
	15	0		0.0136	0.1236
	16	90	12	0.0069	0.1303
	17	90		0.0069	0.1374
	18	90		0.0069	0.1443
	19	90		0.0069	0.1512
	20	90		0.0069	0.1581
	21	0		0.0136	0.1717
	22	90	16	0.0069	0.1786
	23	90		0.0069	0.1855
2nd LAYER	24	90	8	0.0069	0.1924
	25	90		0.0069	0.1993
	26	0		0.0136	0.2129
	27	90	12	0.0069	0.2198
	28	90		0.0069	0.2267
	29	90		0.0069	0.2336
	30	90		0.0069	0.2405
	31	0		0.0136	0.2541
	32	90	12	0.0069	0.2610
	33	90		0.0069	0.2679
	34	90		0.0069	0.2748
	35	90		0.0069	0.2817
	36	0		0.0136	0.2953
	37	90	12	0.0069	0.3022
	38	90		0.0069	0.3091
	39	90		0.0069	0.3160
	40	90		0.0069	0.3229
	41	0		0.0136	0.3365
	42	90	16	0.0069	0.3434
	43	90		0.0069	0.3503
3rd LAYER	44	90	8	0.0069	0.3572
	45	90		0.0069	0.3641
	46	0		0.0136	0.3777
	47	90	12	0.0069	0.3846
	48	90		0.0069	0.3915
	49	90		0.0069	0.3984
	50	90		0.0069	0.4053
	51	0		0.0136	0.4189
	52	90	12	0.0069	0.4258
	53	90		0.0069	0.4327
	54	90		0.0069	0.4396
	55	90		0.0069	0.4465
	56	0		0.0136	0.4601
	57	90	12	0.0069	0.4670
	58	90		0.0069	0.4739
	59	90		0.0069	0.4808
	60	90		0.0069	0.4877
	61	0		0.0136	0.5013
	62	90	16	0.0069	0.5082
	63	90		0.0069	0.5151
	64	90		0.0069	0.5220

Figure 20. Laminate stacking sequence for the model-scale AUSS-Mod 2 cylinder. Note that in the first layer, the ratio of hoop to axial fibers is 2.5:1. In the second and third layers, the ratio decreases to 2:1.

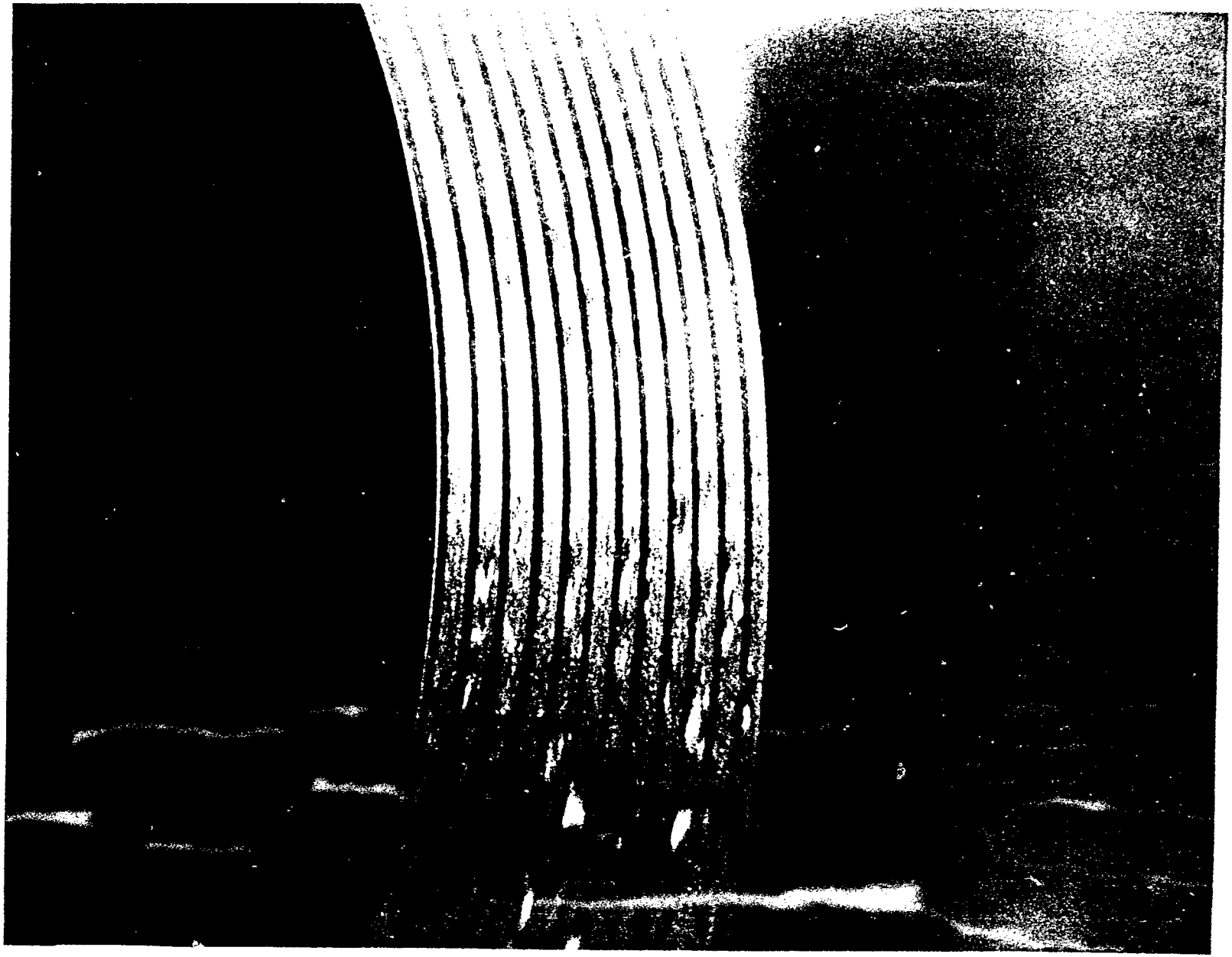

Figure 21. Cross-section of wall thickness in model-scale AUSS Mod 2 cylinder

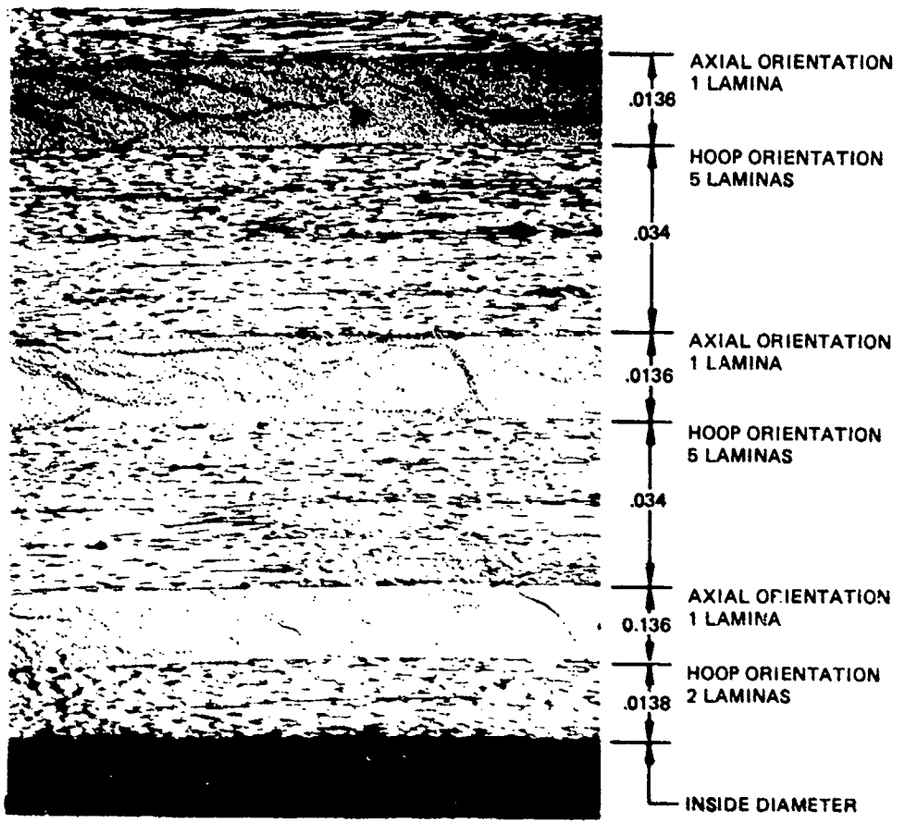

MAGNIFICATION 30

Figure 22. Cross-section of wall thickness in model-scale AUSS Mod 2 cylinder shown in figure 21 magnified 30 times. Note the uniformity of lamina thicknesses and their circularity, attesting to the high quality of winding process utilized by Martin Marietta Energy Systems for fabrication of the model-scale GFRP cylinder.

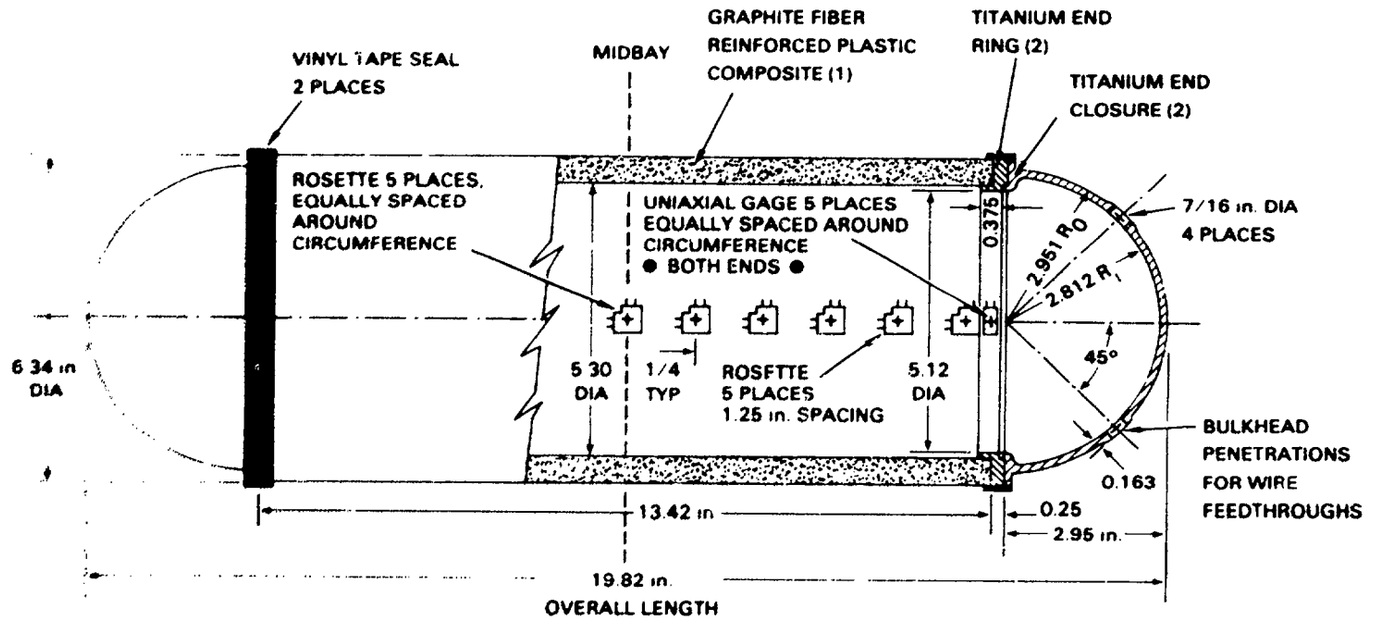

Figure 23. Location of straingages on the GFRP model-scale AUSS Mod 2 pressure housing.

Figure 24. Components of the GFRP model-scale AUSS Mod 2 pressure housing prior to assembly

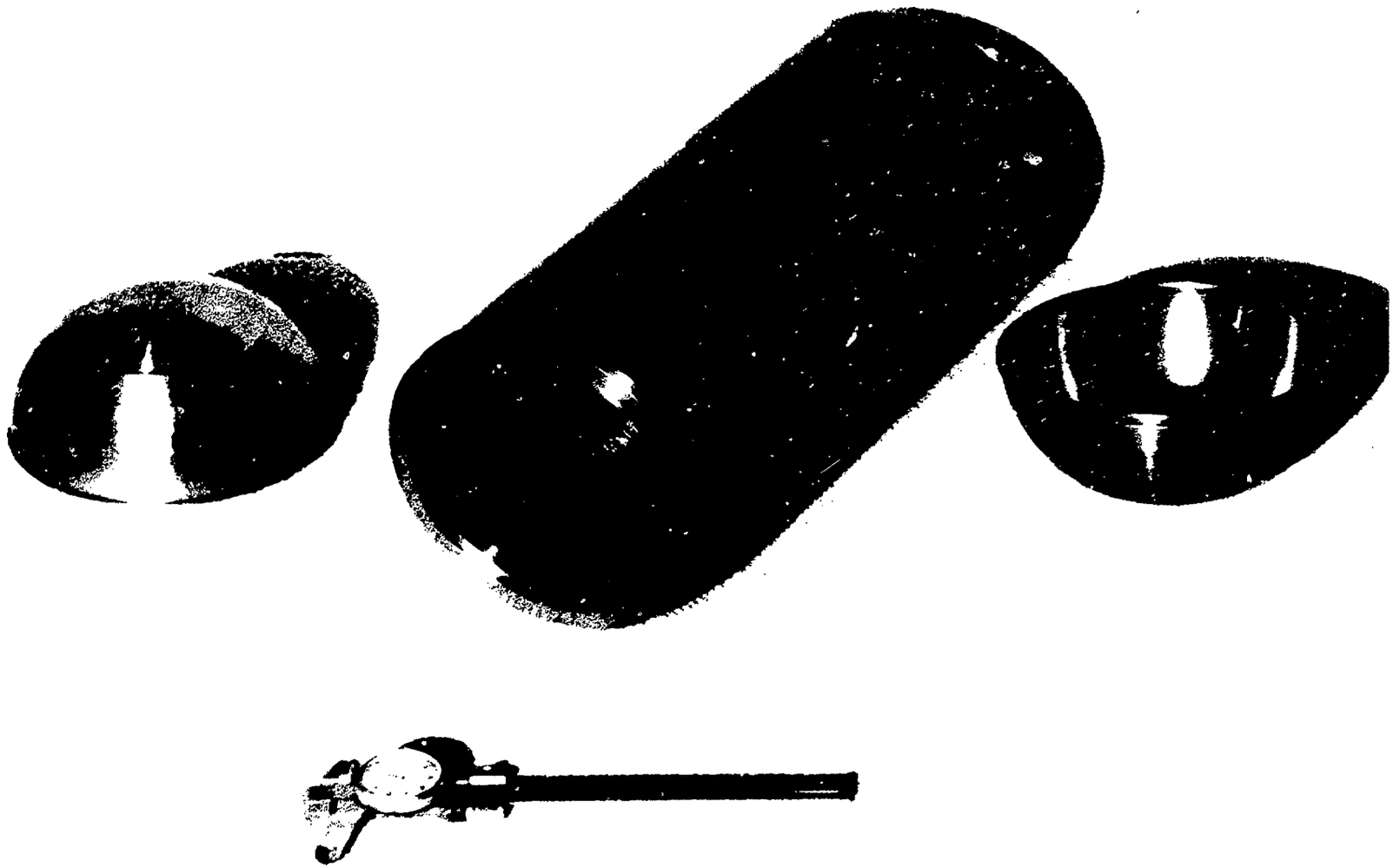

Figure 25. Model-scale AUSS Mod 2 pressure housing. Note that the titanium end rings have been already bonded to the GFRP cylinder.

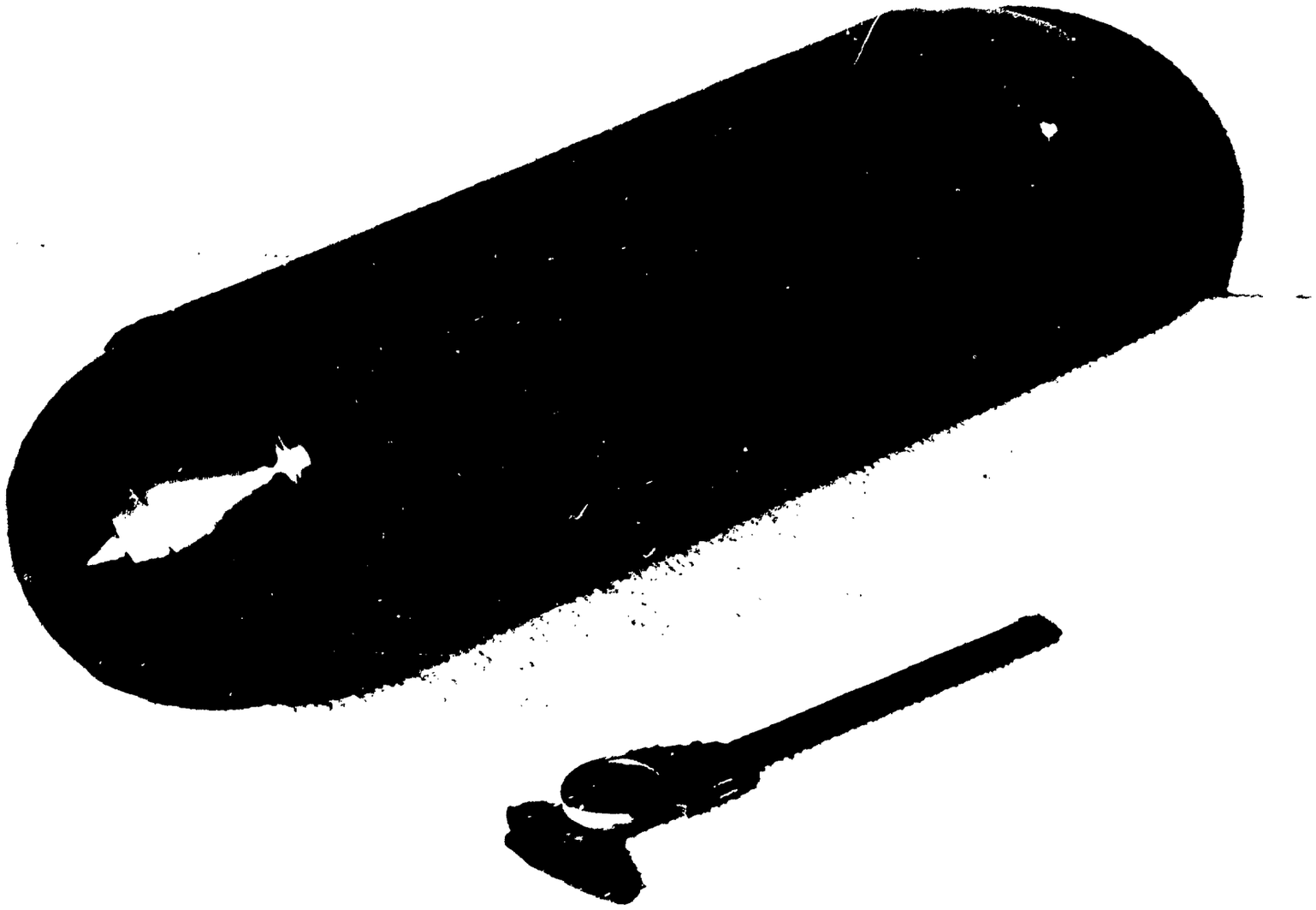

Figure 26. Assembled model-scale AUSS pressure housing.

Figure 27. Assembled and instrumented model-scale AUSS Mod 2 pressure housing prior to placement into a deep-ocean simulator vessel for proof testing to 10,000 psi and pressure cycling to 9000-psi design pressure

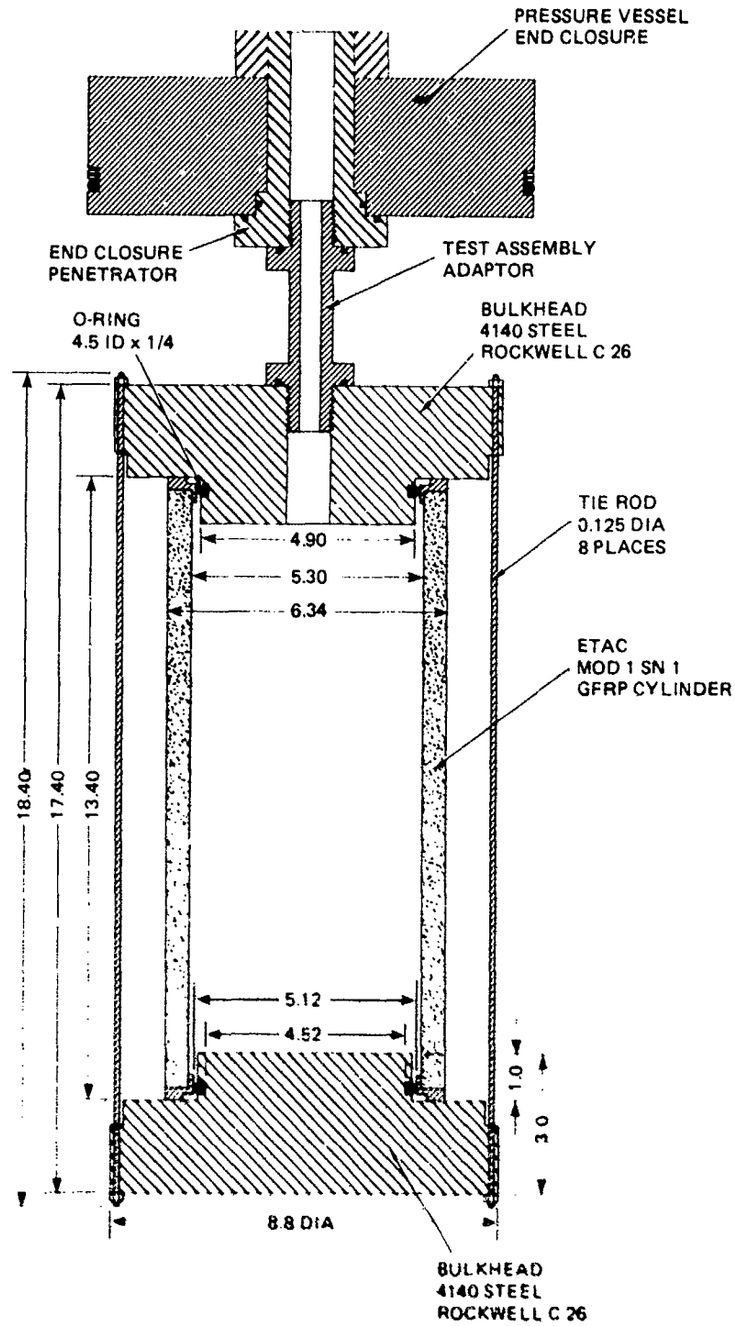

Figure 28. Test setup for testing of model-scale AUSS Mod 2 pressure housing to implosion Note that in this test arrangement, the titanium hemispherical end closures have been replaced by flat steel bulkheads that do not provide any radial support to the cylinder ends during pressure testing of the cylinder. The oversized O-rings in the bulkheads are not intended to seal the ends of the cylinder but to provide a uniform radial clearance between the steel bulkhead and the cylinder. The hemispherical end closures could not be used for the implosion test as they have been optimized for the 9000-psi design pressure with only a 1.25 safety factor and would probably implode prior to the cylinder designed with a safety factor of 2.

Figure 29. Test assembly prior to placement into the deep-ocean simulation vessel.

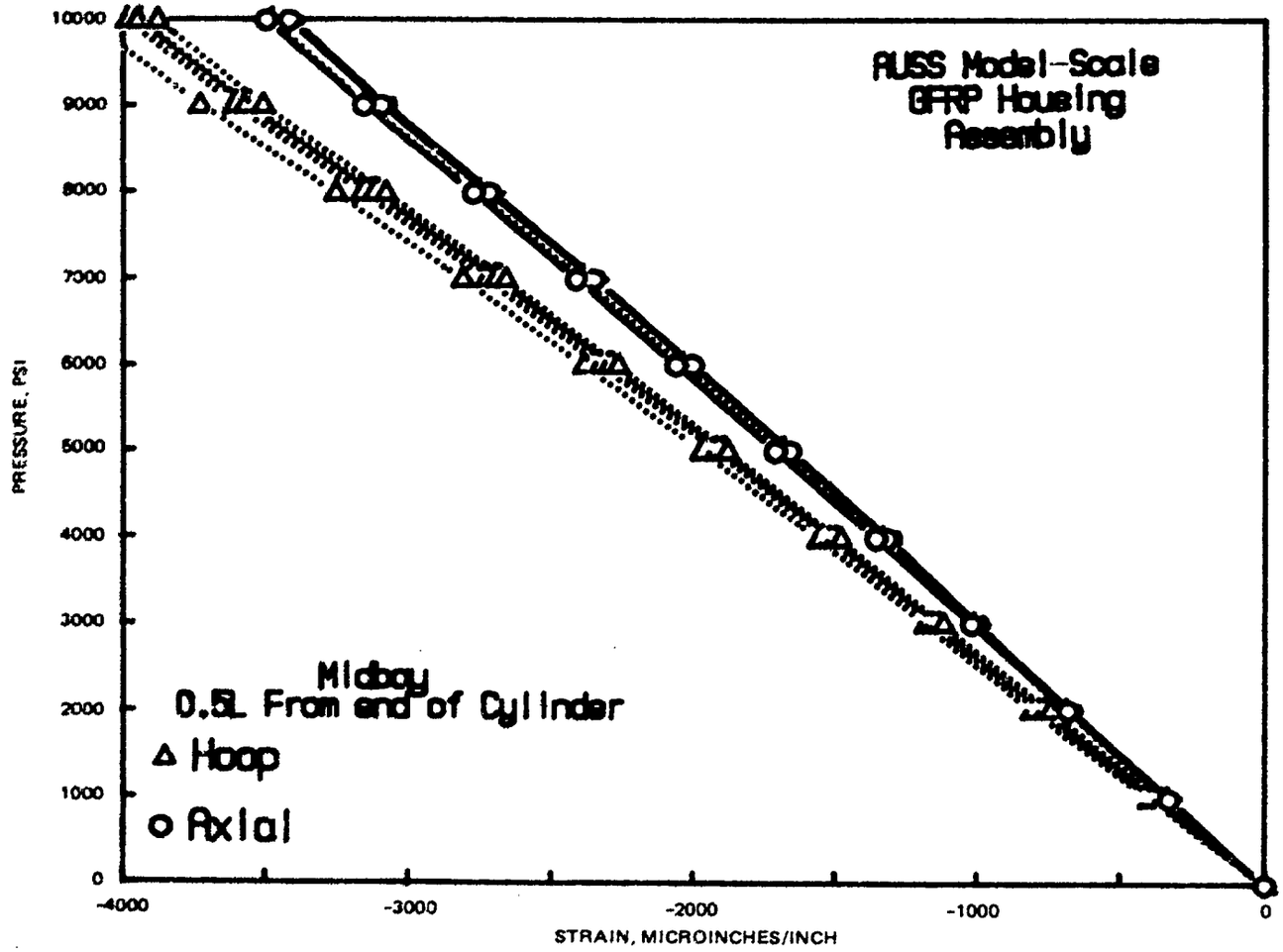

Figure 30. Strains at midbay of the GFRP model-scale AUSS Mod 2 cylinder supported radially end the ends by hemispherical end closures. Note that there is very little divergence between hoop strains measured by individual straingages, indicating absence of incipient elastic instability.

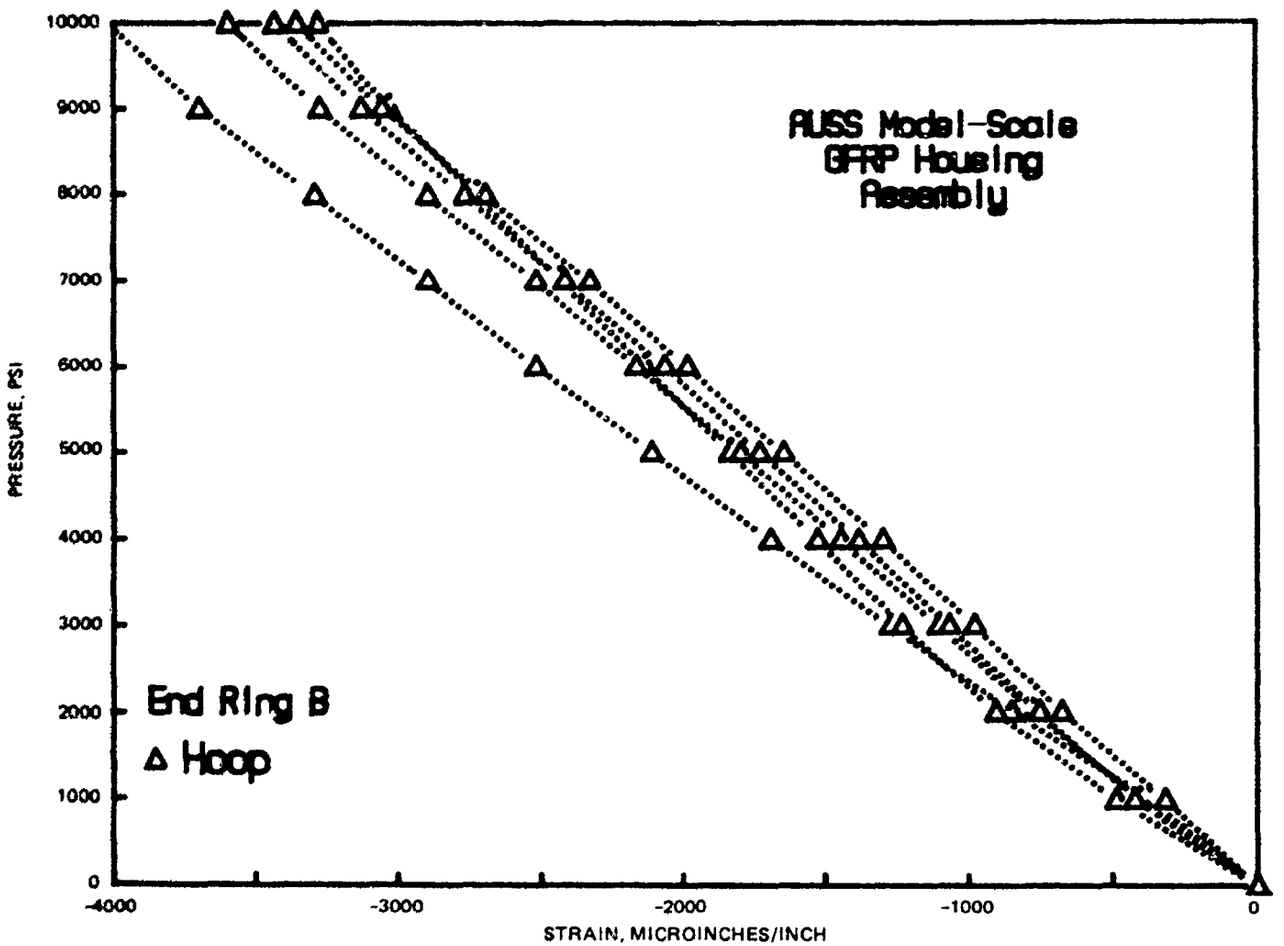

Figure 31. Hoop strains at the end of the GFRP model-scale AUSS cylinder supported by hemispherical end closures, approximately 10 percent less than at midbay (Figure 30). The *small decrease* in magnitude of hoop strains at the end indicates that the radial compliance of titanium hemispherical end closures is well matched to the radial compliance of the GFRP cylinder and, therefore, provides only minor radial support to the ends of the cylinder, thus minimizing shear stresses at these locations.

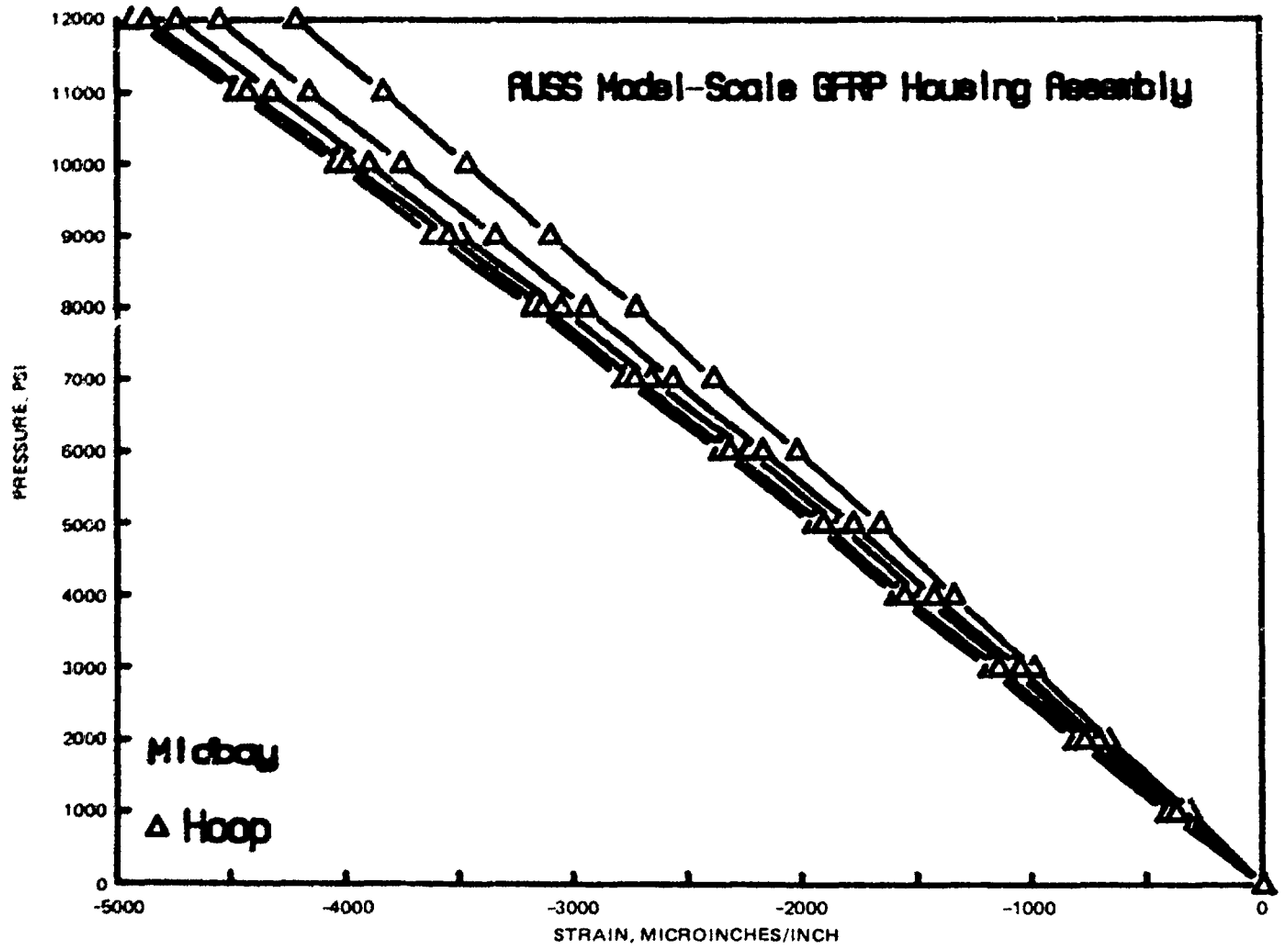

Figure 32. *Hoop strains* at midbay of GFRP model-scale cylinder closed off with flat steel bulkheads. Note that the magnitude of hoop strains at midbay of the cylinder supported by flat bulkheads is the same at 10,000 psi as it was when the cylinder was supported by hemispherical end closures (Figure 30).

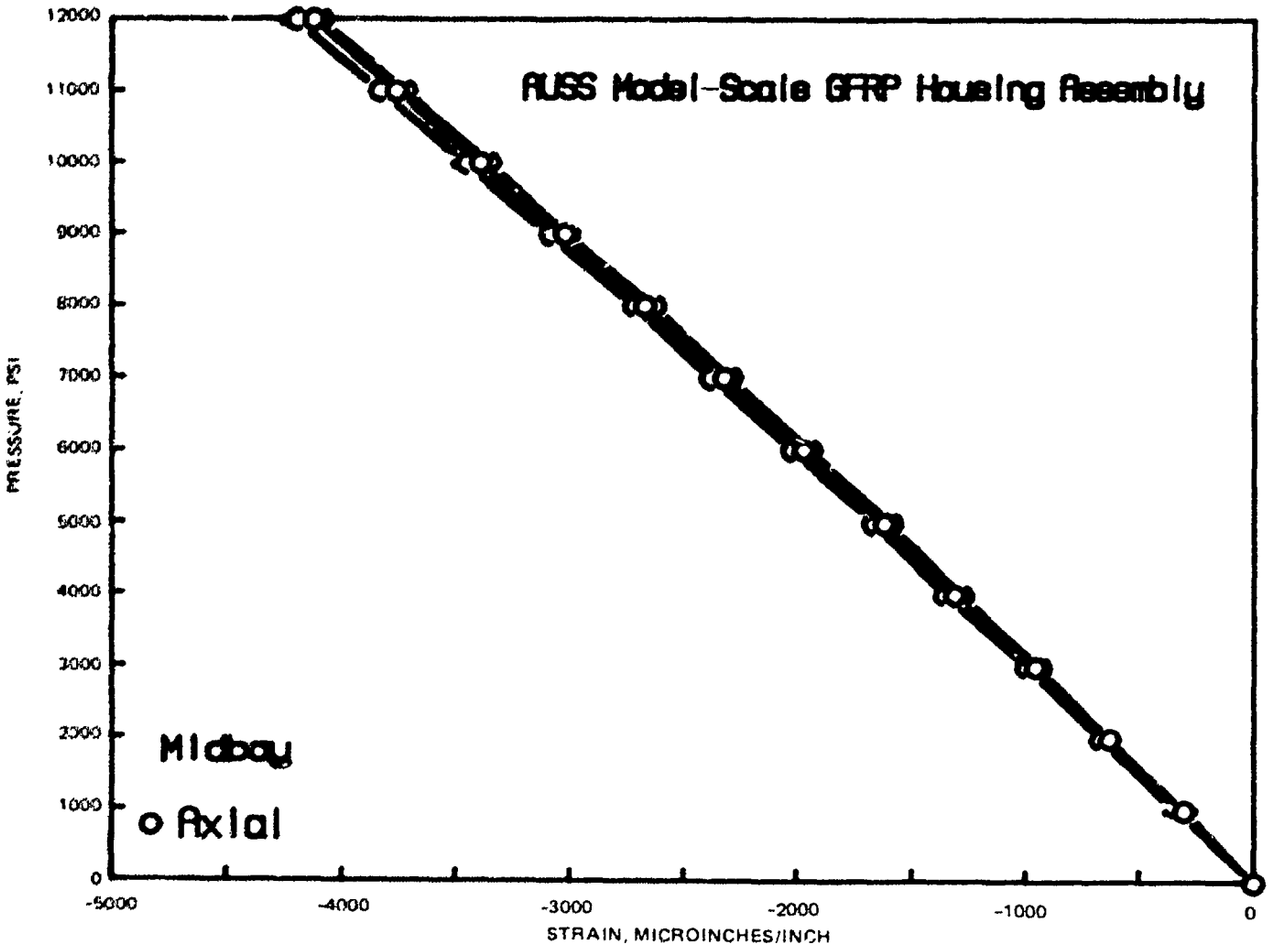

Figure 33. Axial strains at midbay of GFRP model-scale cylinder closed off with flat steel bulkheads. Note that their magnitude also is the same as in the test arrangement utilizing hemispherical end closures (Figure 30).

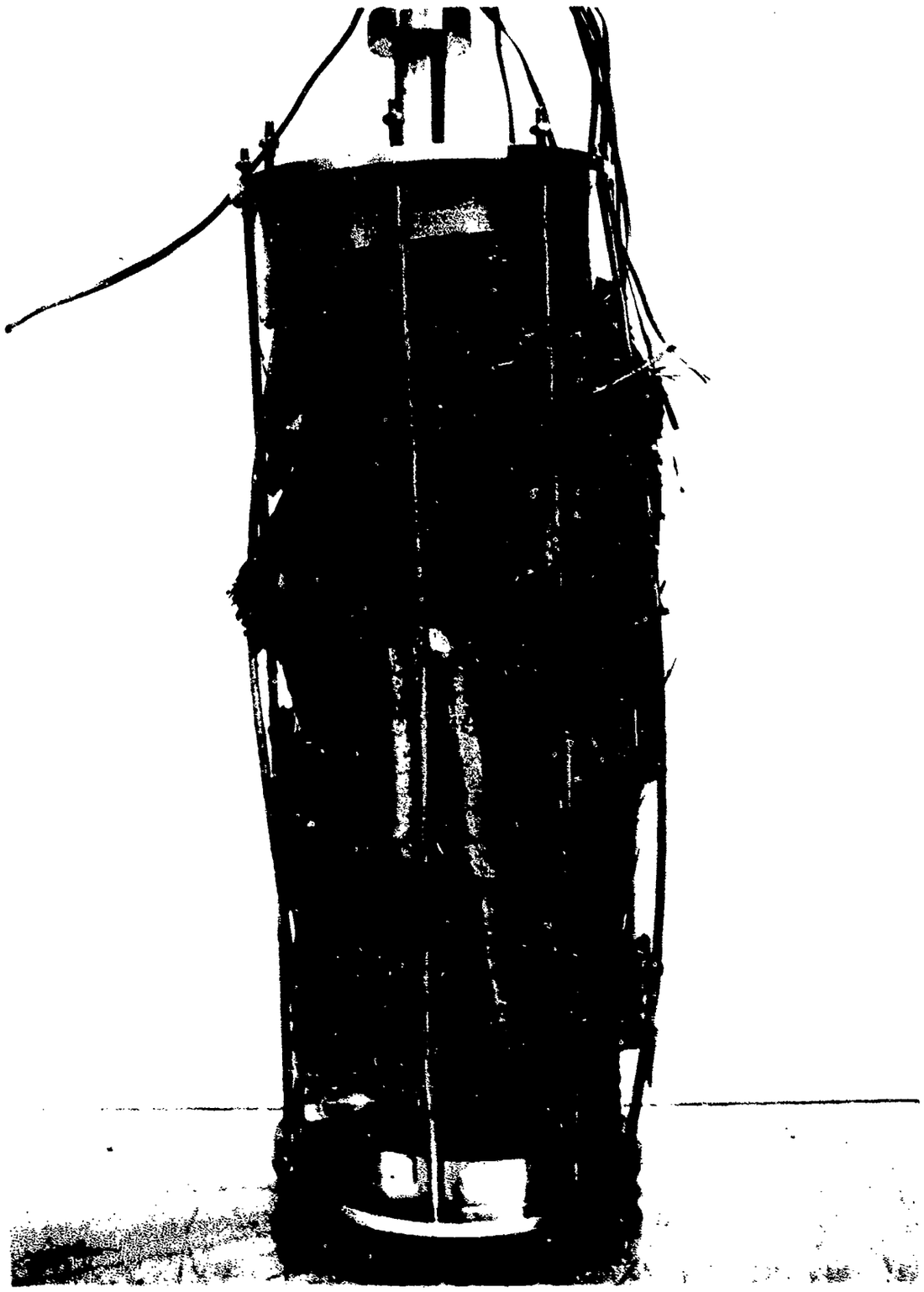

Figure 34. GFRP model-scale cylinder after implosion at 12,600 psi of external hydrostatic pressure

71/72

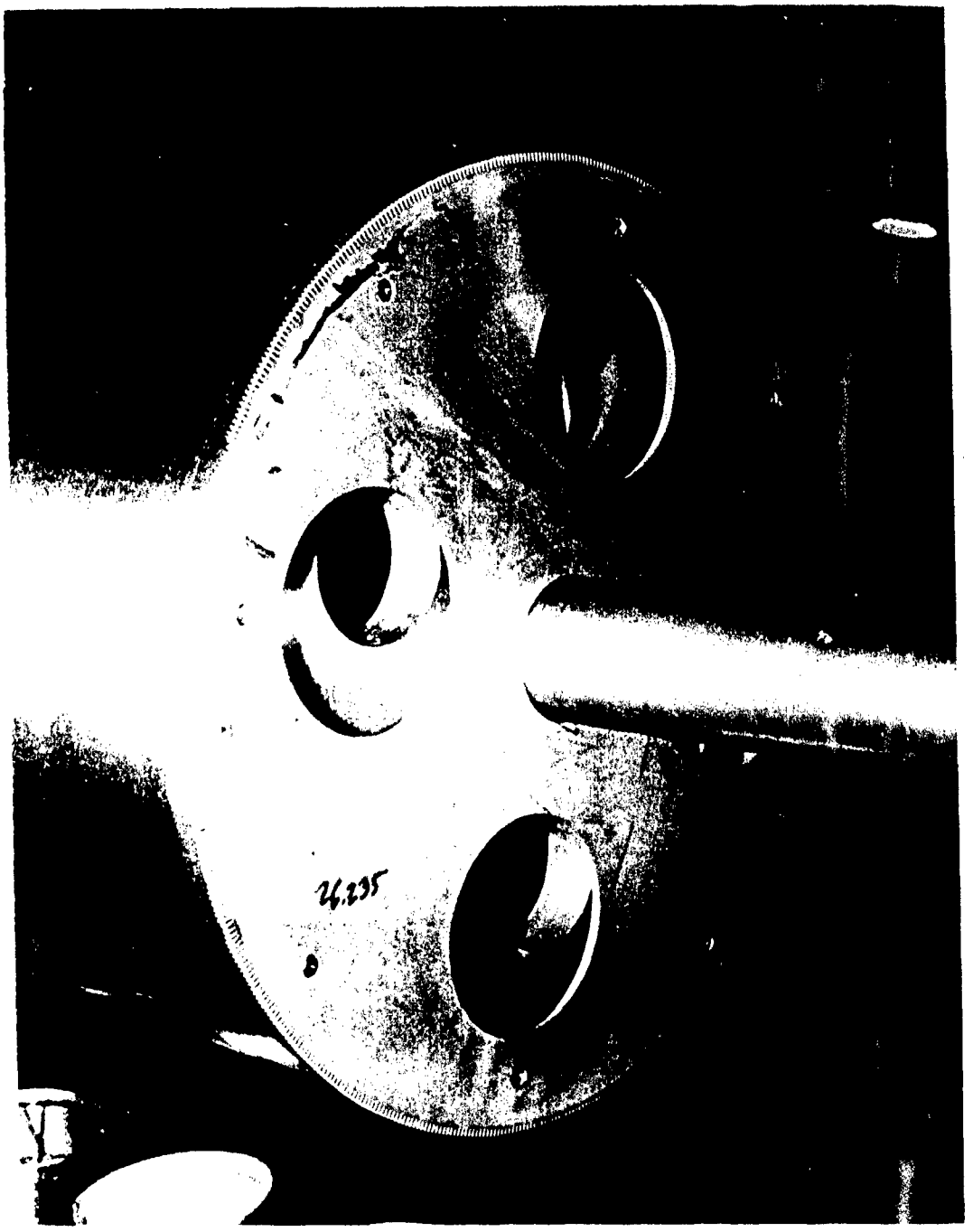

Figure 36 - [illegible] pinwheels at the ends of a cylindrical mandrel serve as attachment points for the [illegible] Several sets of pinwheels with different diameters are employed during the [illegible] as the thickness of the wound layer increases, pinwheels with larger [illegible] pinwheels with smaller diameter.

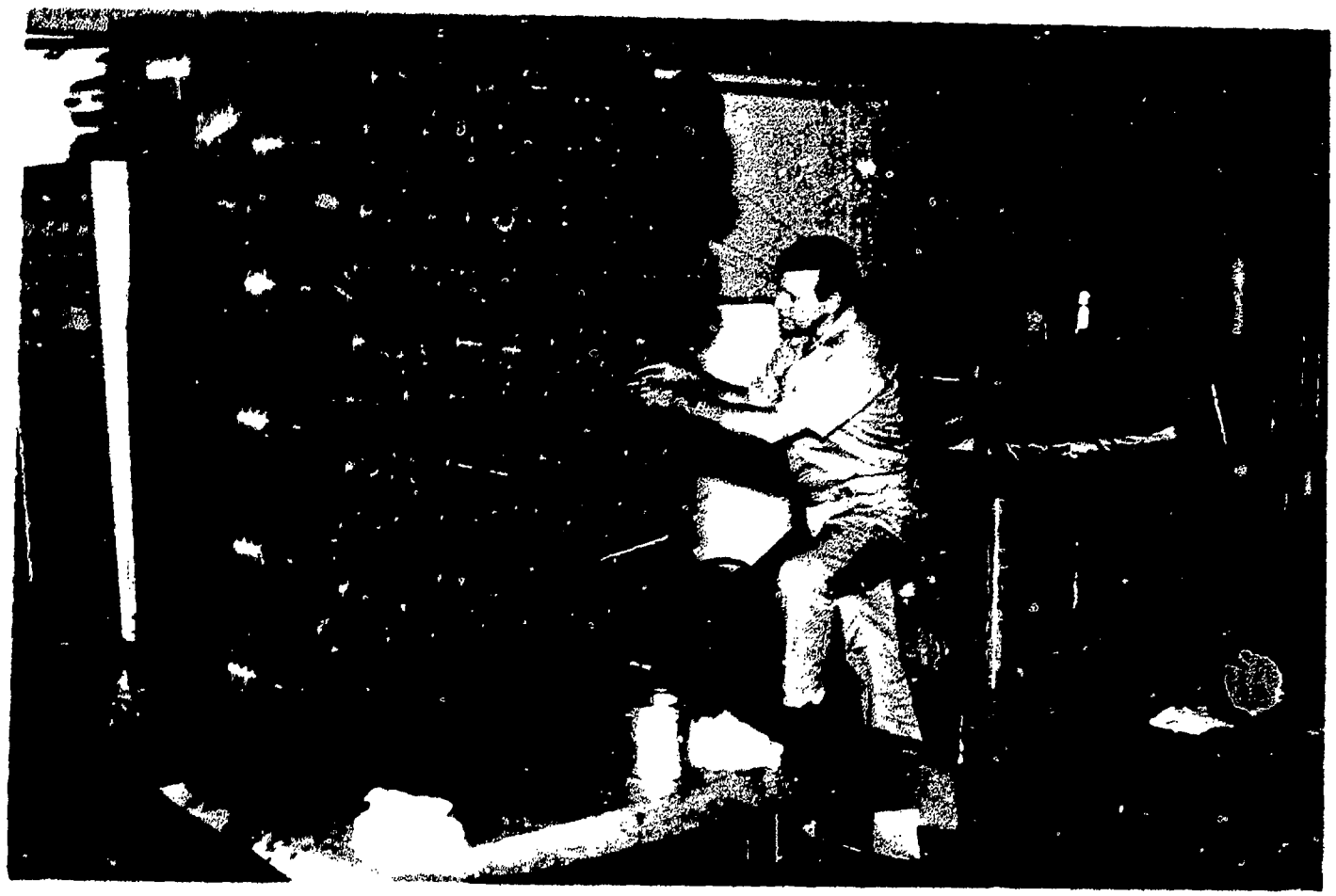

Figure 37. Array of spools from which the tows are unwound under preset tension

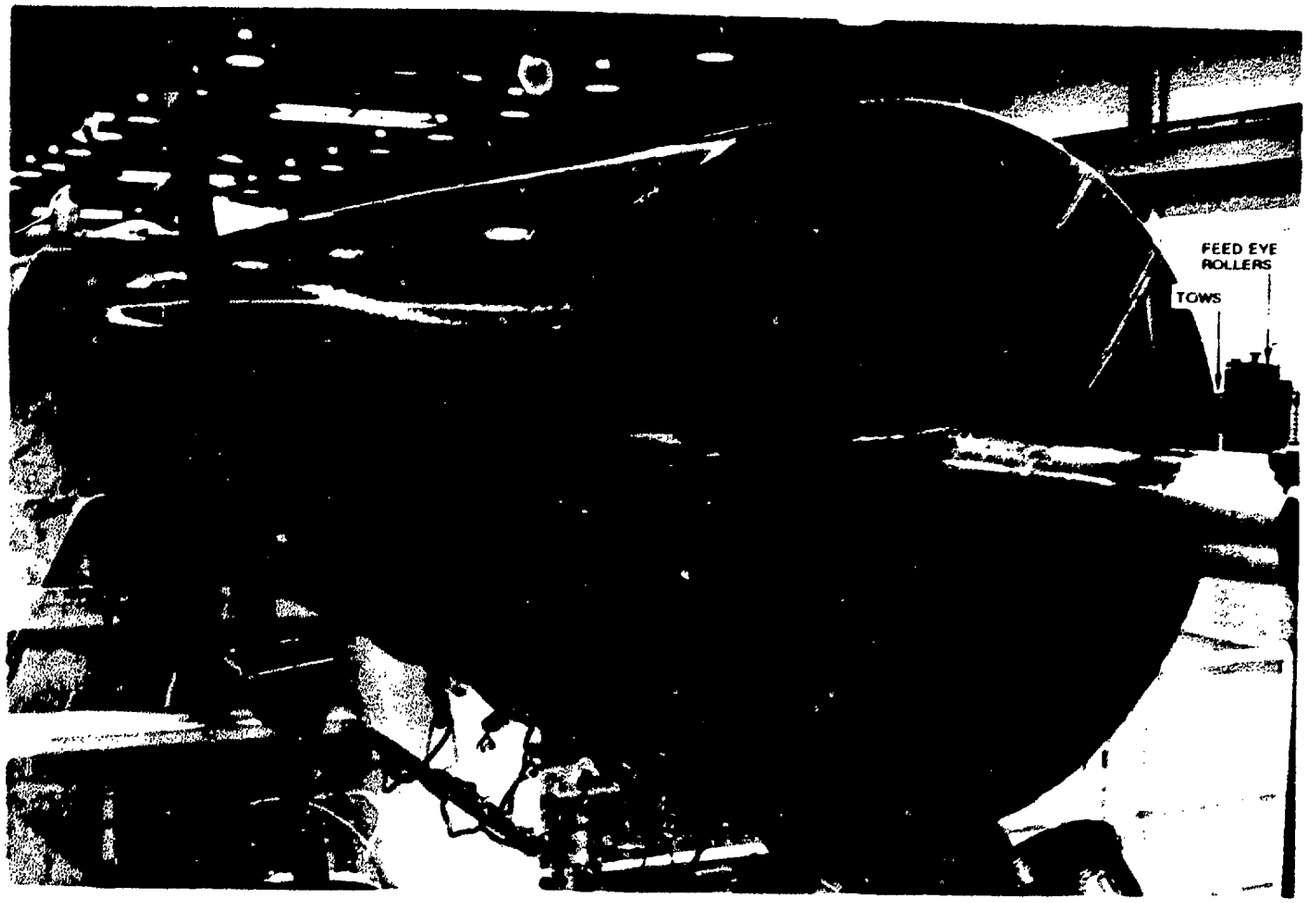

Figure 38. Winding of axial oriented tows over the hoop lamina.

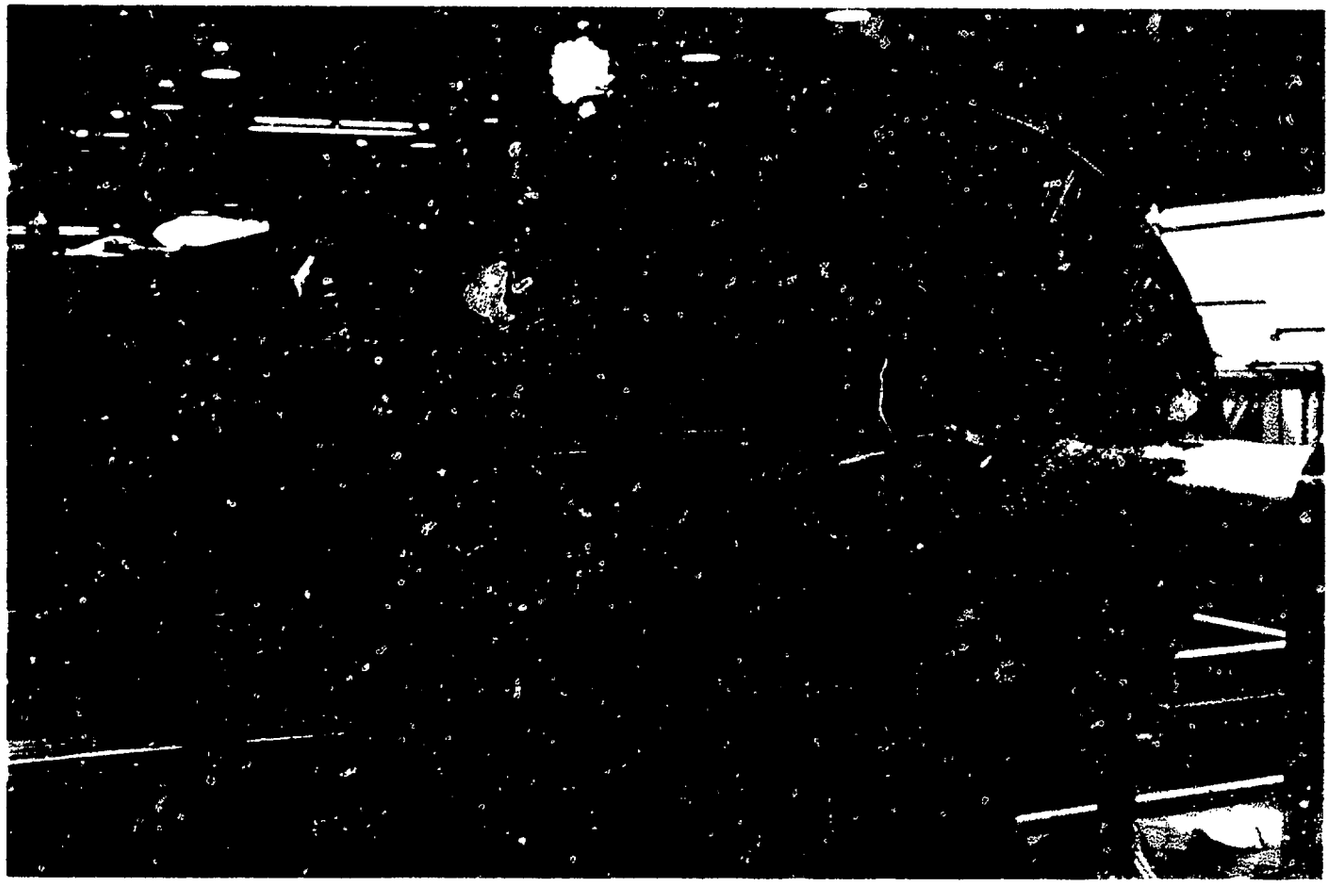

Figure 39. Completed lamina of axial oriented tows.

Figure 40. Winding of the hoop lamina over a completed axial lamina. Note the scoop for removal of excess resin from the winding.

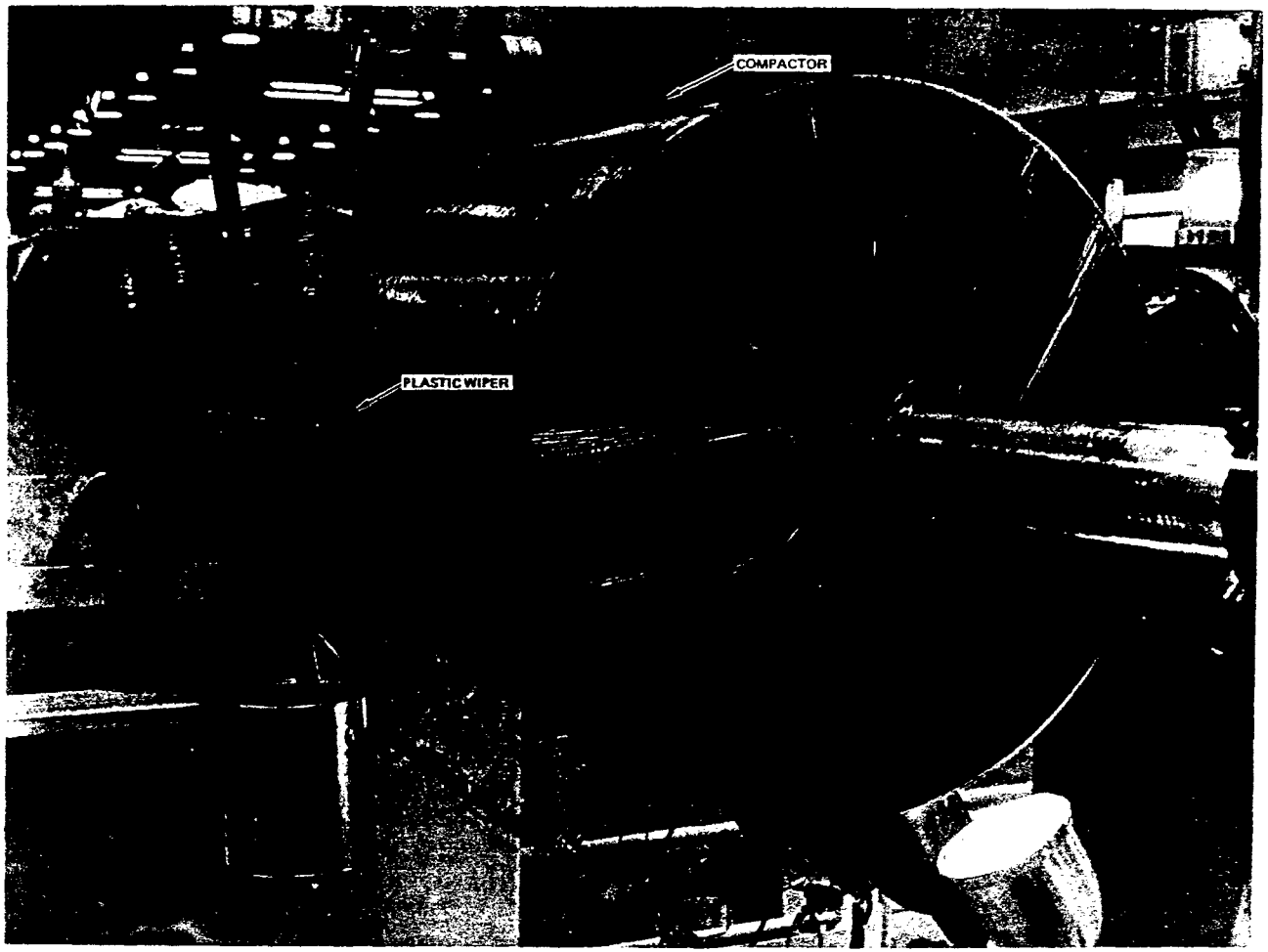

Figure 41. Partially completed hoop lamina.

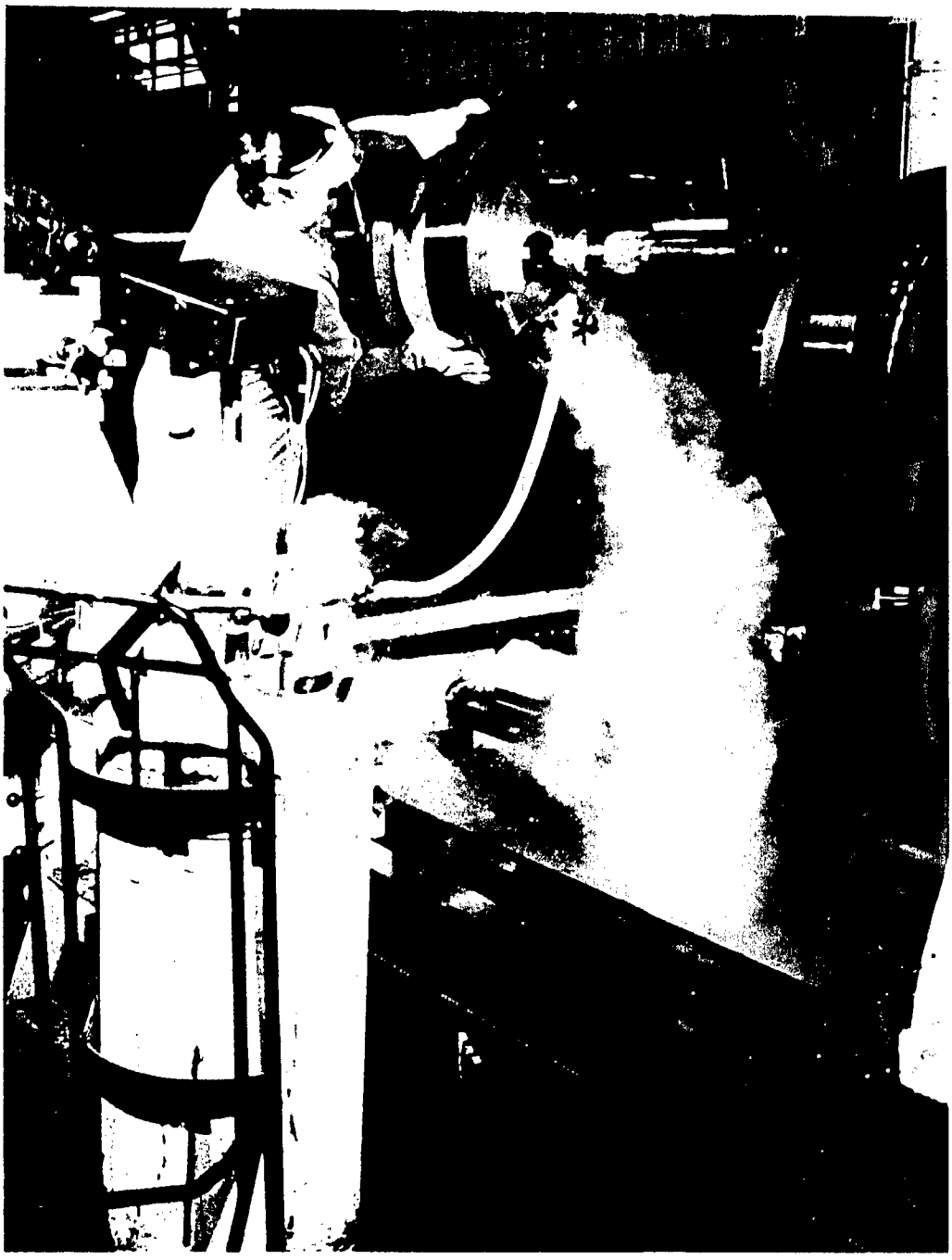

Figure 42. Trimming the polymerized cylinder to the specified length of 65 inches. Liquid nitrogen is used to shrink the aluminum mandrel for making the removal of rings easier

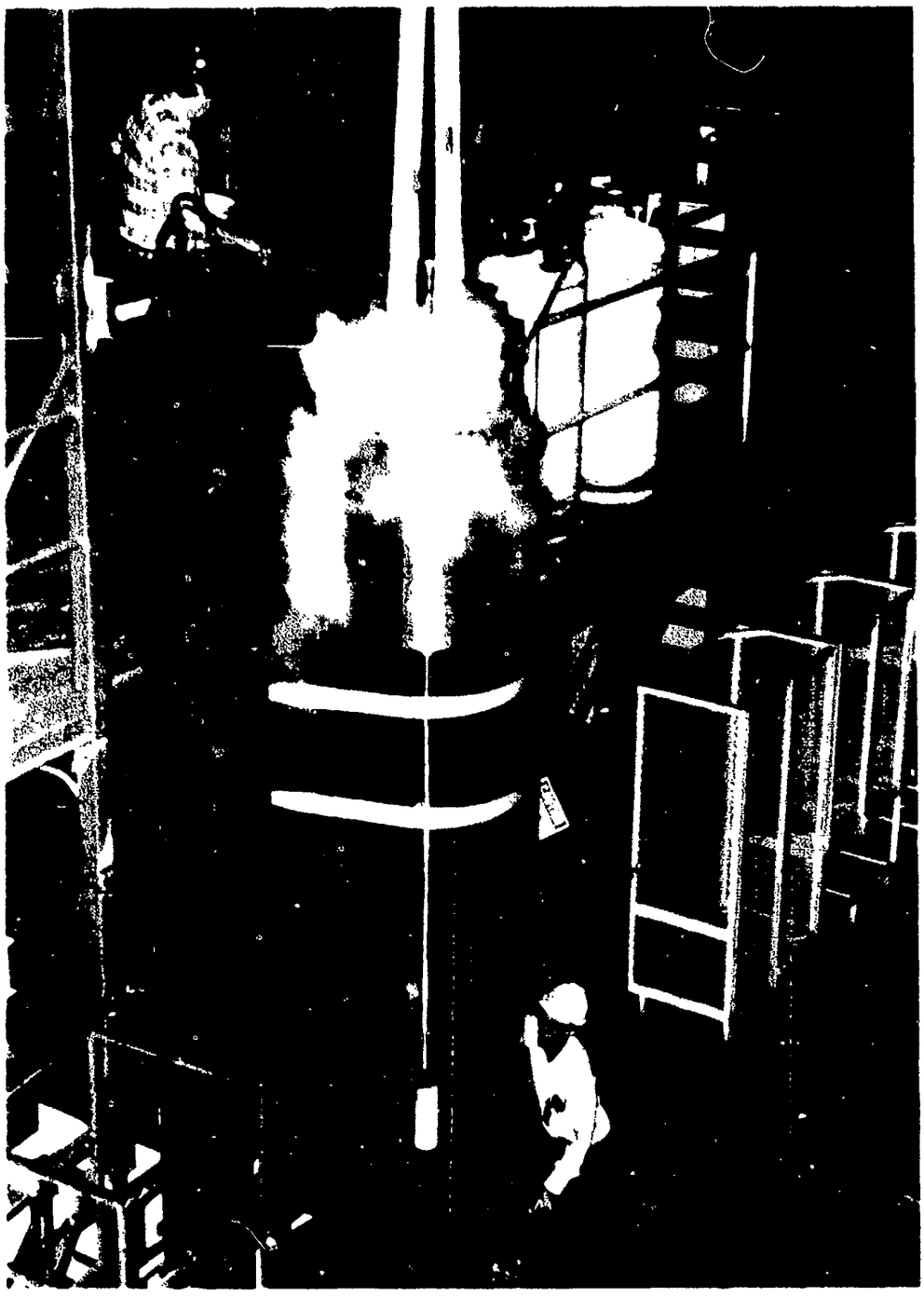

Figure 44 Full scale AUSS Mod 2 [illegible]

Figure 45. Inspection of the rings trimmed off from the ends of the GFRP full-scale AUSS Mod 2 cylinder

Figure 46. Making a radial saw cut through the GFRP ring instrumented with electrical resistance

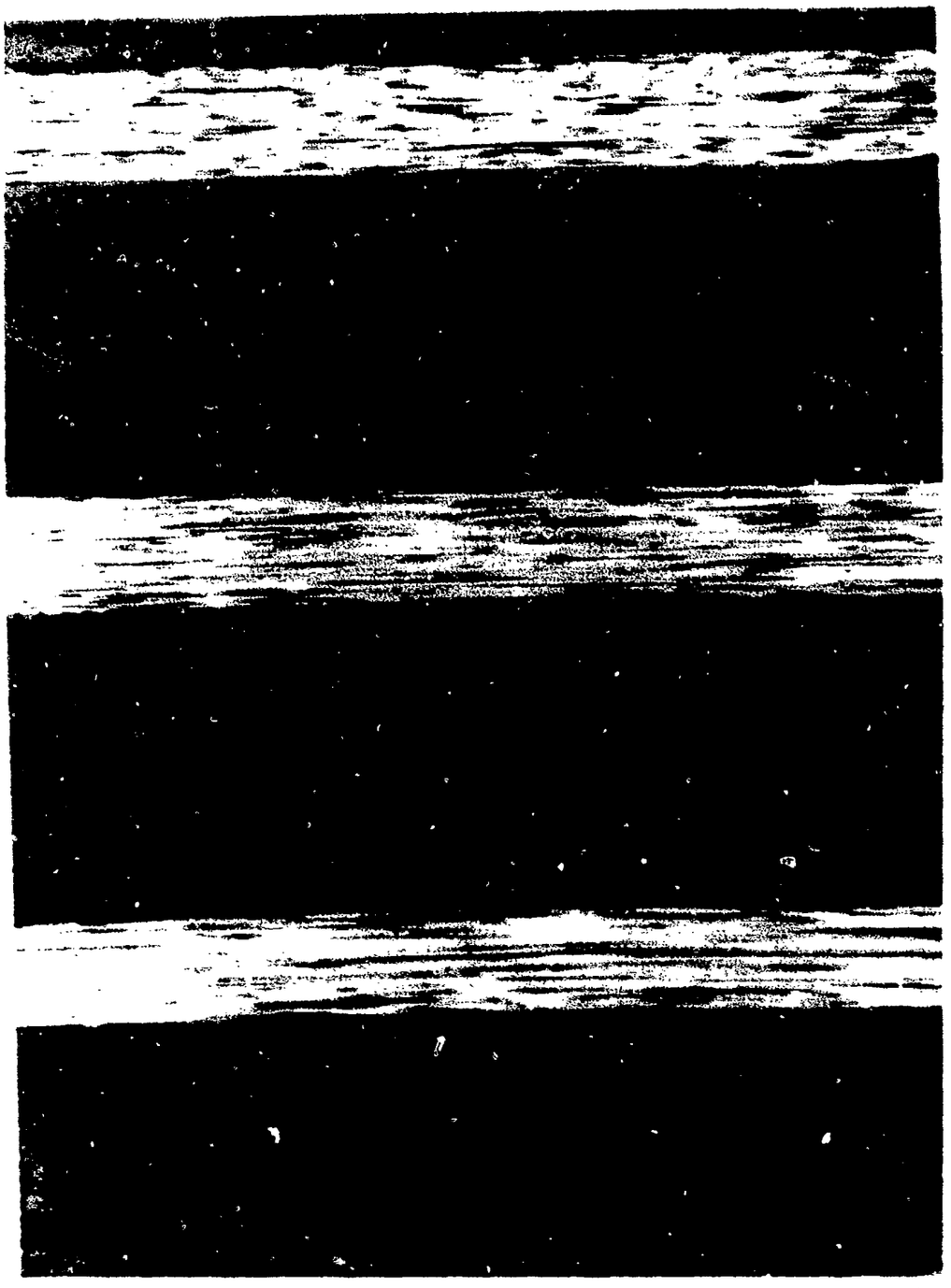

Figure 47. Typical quality of the composite in the AUSS Mod 2 hull, the construction of the composite in *the first inch of wall thickness* displays a 2.5:1 ratio of hoop- to axial-oriented fibers. The alternating hoop- and axial-oriented laminas are 0.0345" and 0.0136 inch thick, respectively.

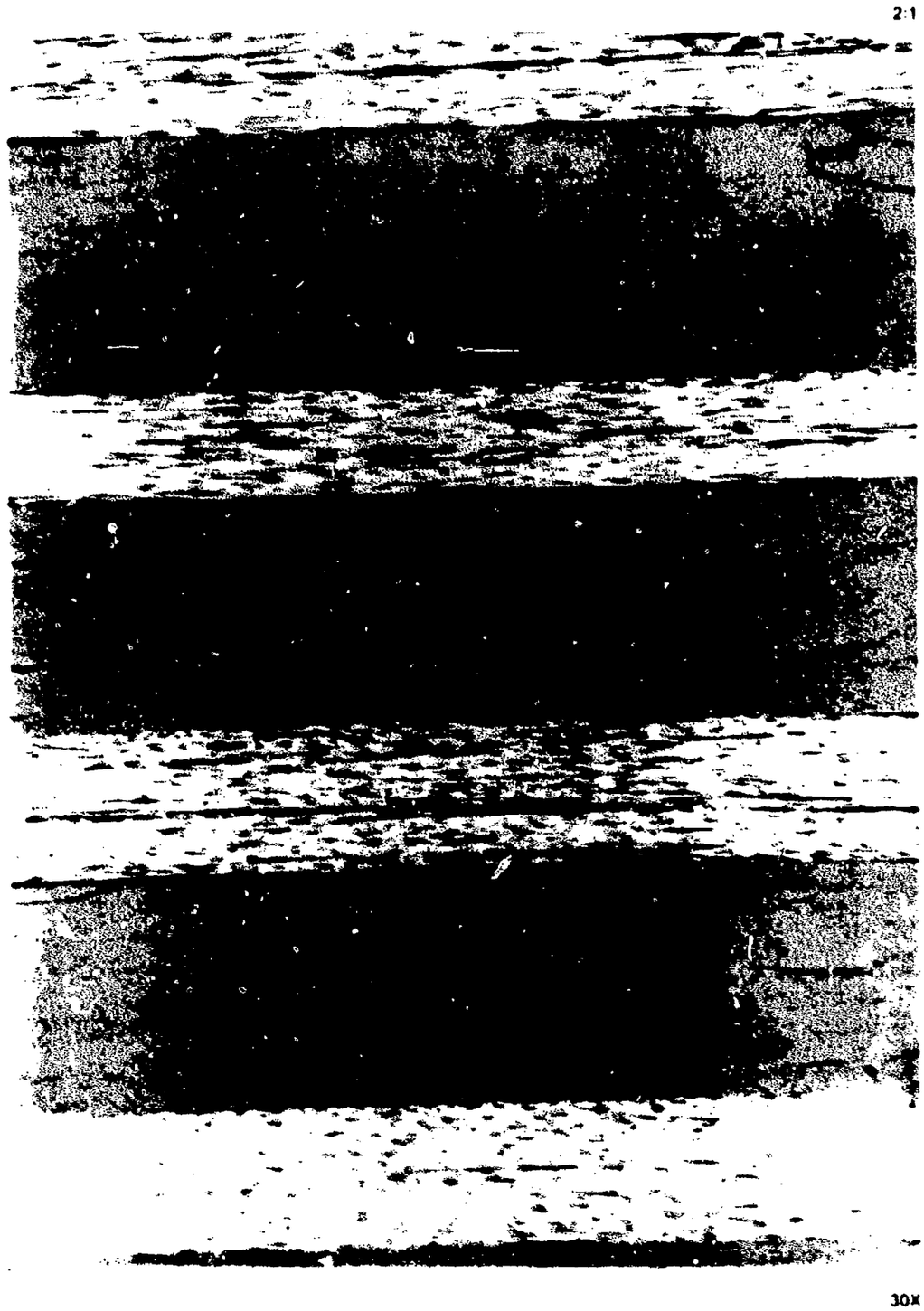

Figure 48. Typical quality of the composite in the AUSS Mod 2 hull, the construction of the composite in the *1 to 2 5 inch thickness interval* displays a 2 1 ratio of hoop to axial-oriented fibers The alternating hoop-and axial oriented laminas are 0 027 and 0 0136 inch thick respectively

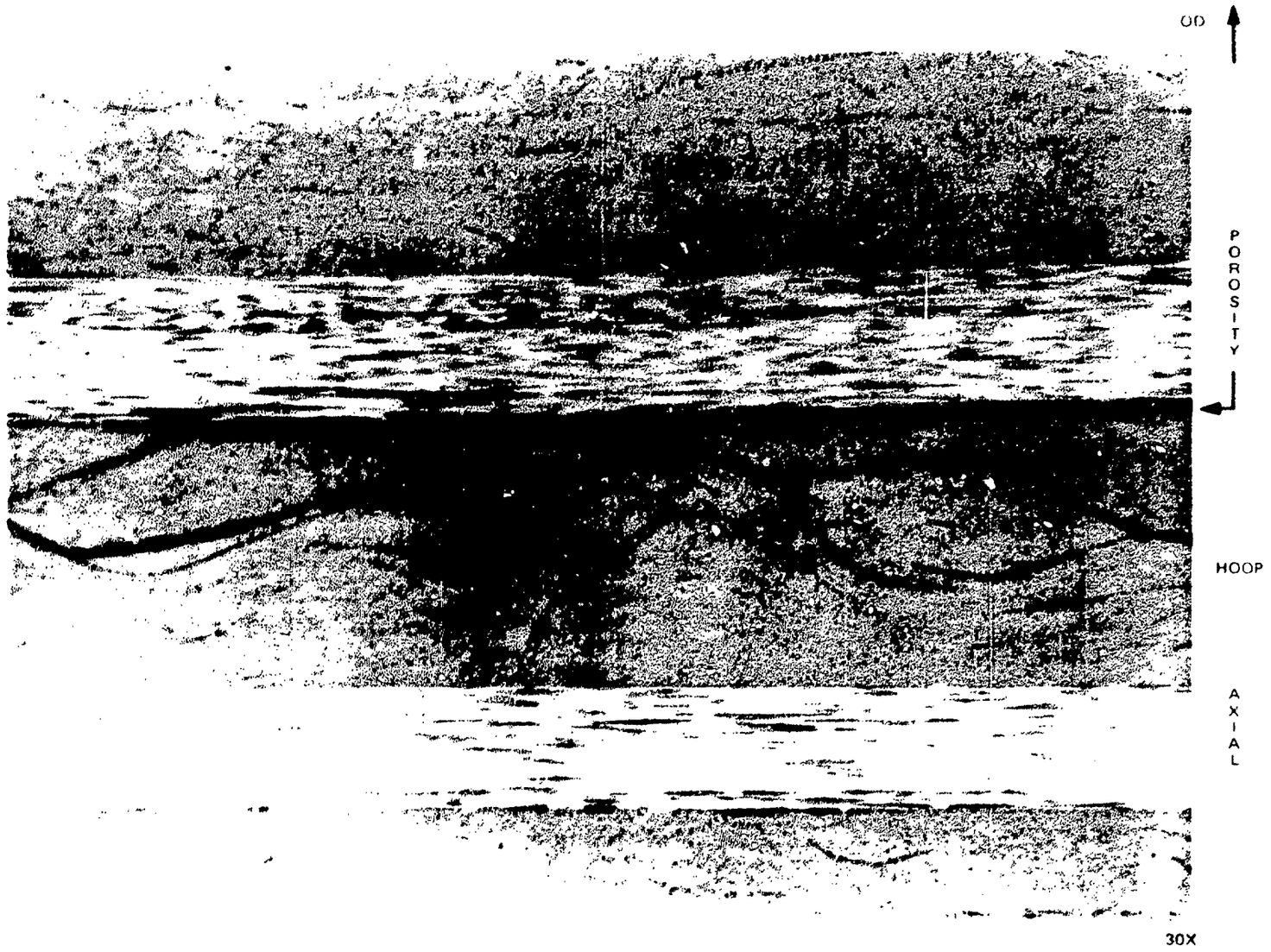

Figure 49. Typical example of entrapped air porosity between hoop fibers at several locations in the AUSS Mod 2 hull

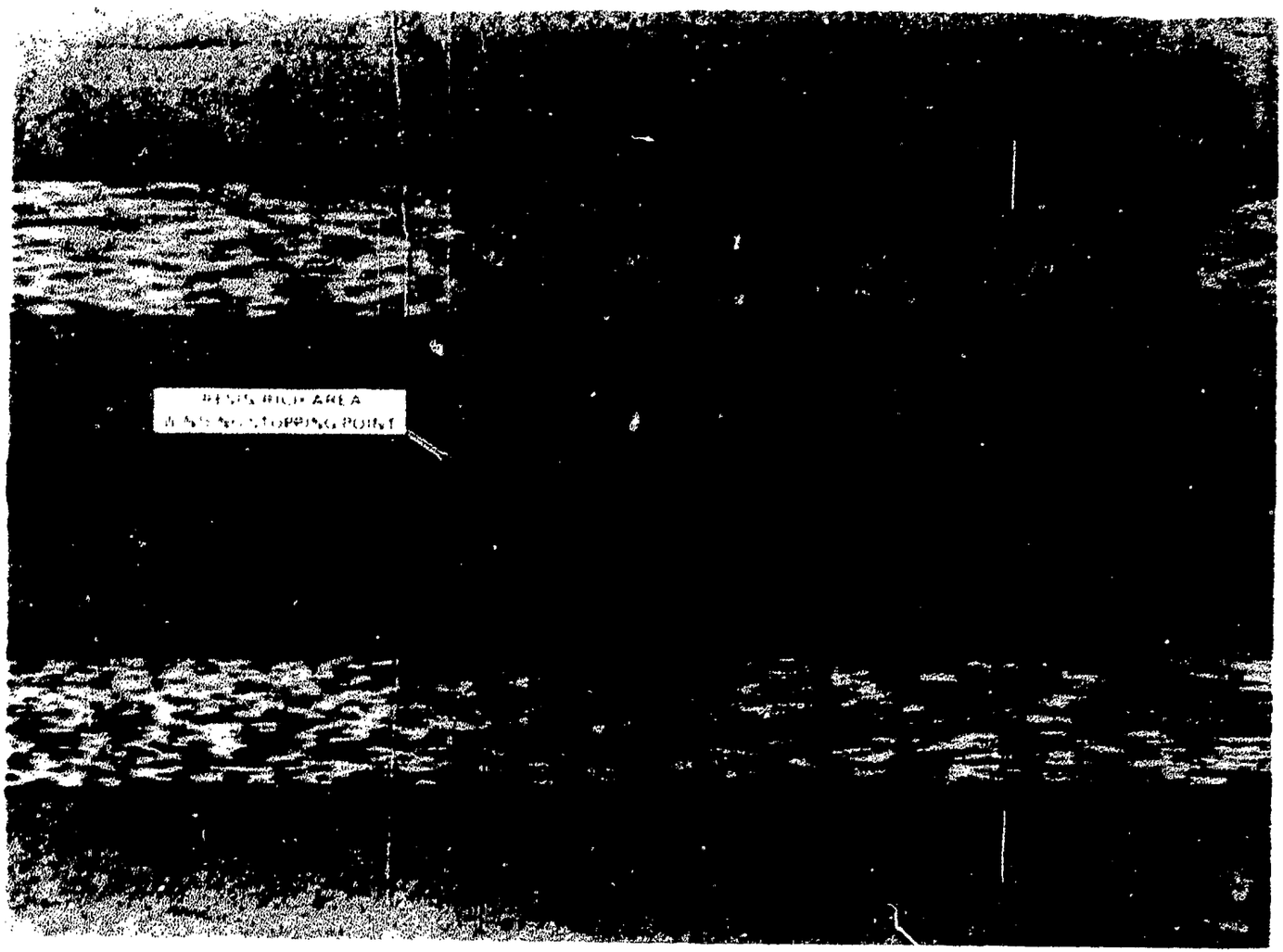

Figure 50. Typical example of resin-rich layers between hoop fibers in laminas where the winding of AUSS Mod 2 hull terminated at the end of the day.

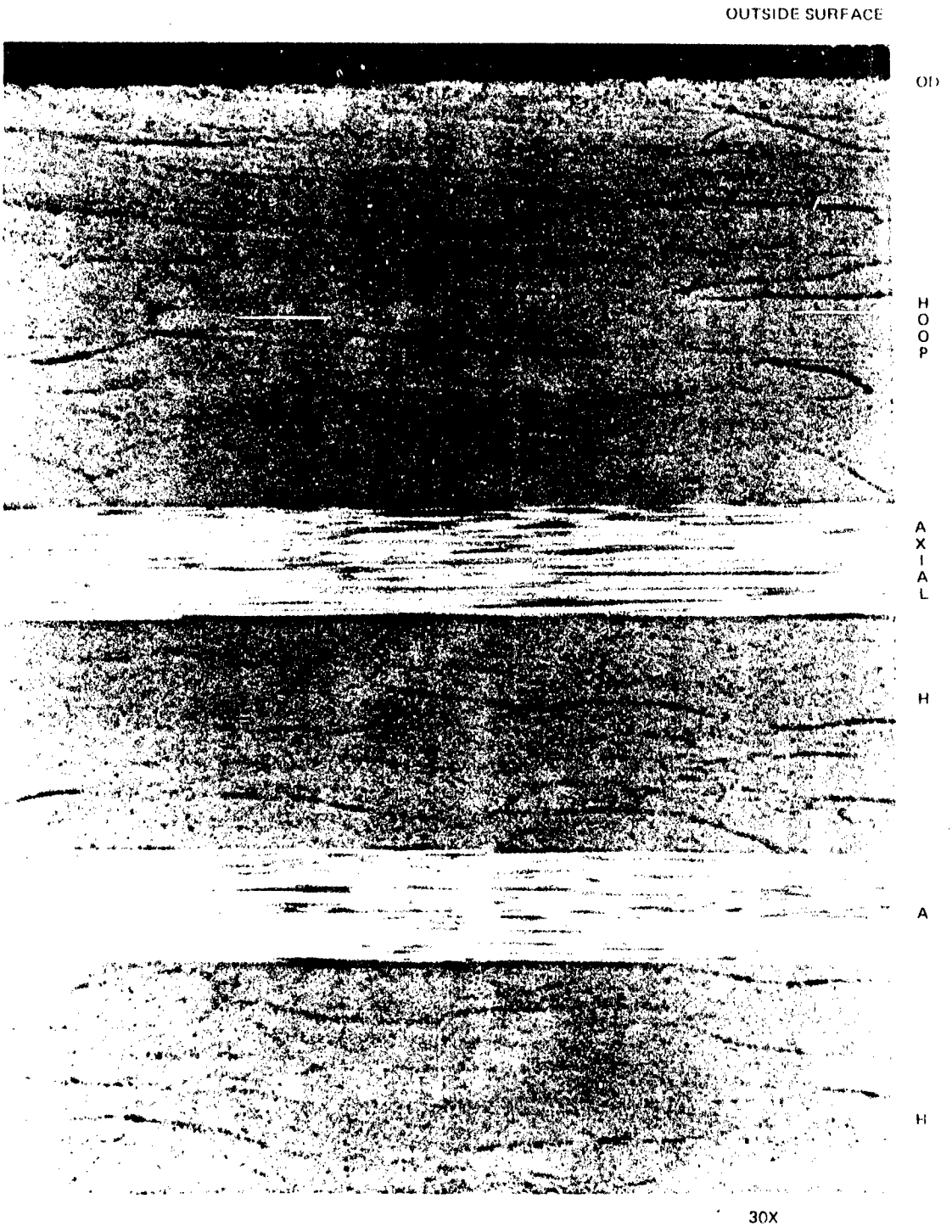

Figure 51. Typical quality of the composite in the last five laminas under the exterior surface of the composite in the AUSS Mod 2 hull; the hoop winding on the exterior surface is 0.048-inch thick.

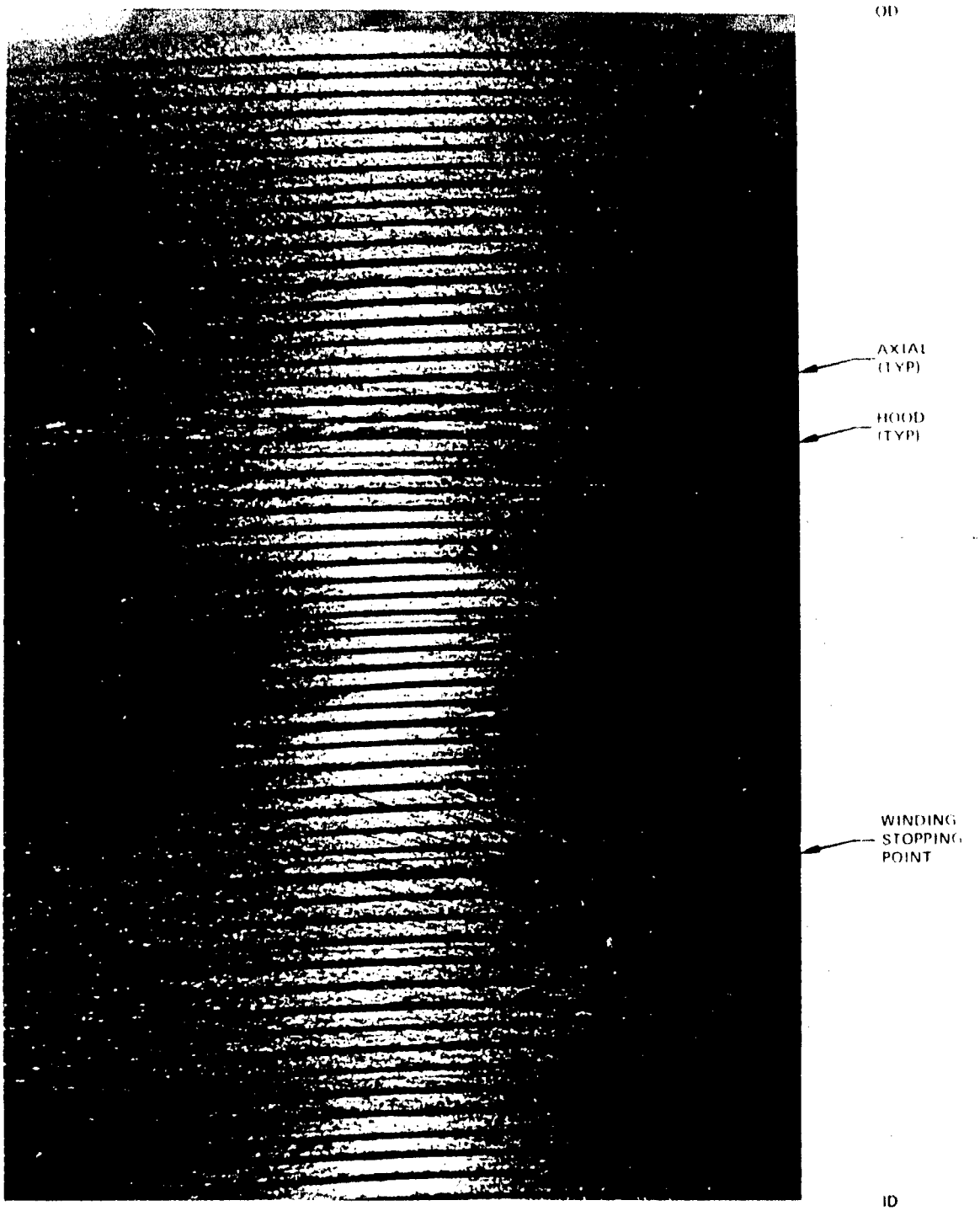

Figure 52. Overall view of the wall cross-section in AUSS Mod 2 hull. Note the uniformity and circularity of the individual hoop laminas in the composite indicating the high quality of fiber winding procedure employed by Martin Marietta Energy Systems to fabricate the cylinder.

Figure 53. Set up for sonic scanning of the full-scale AUSS cylinder by transmitted acoustic energy. Jets of water are used to couple the acoustic signal with the surfaces of the cylinder

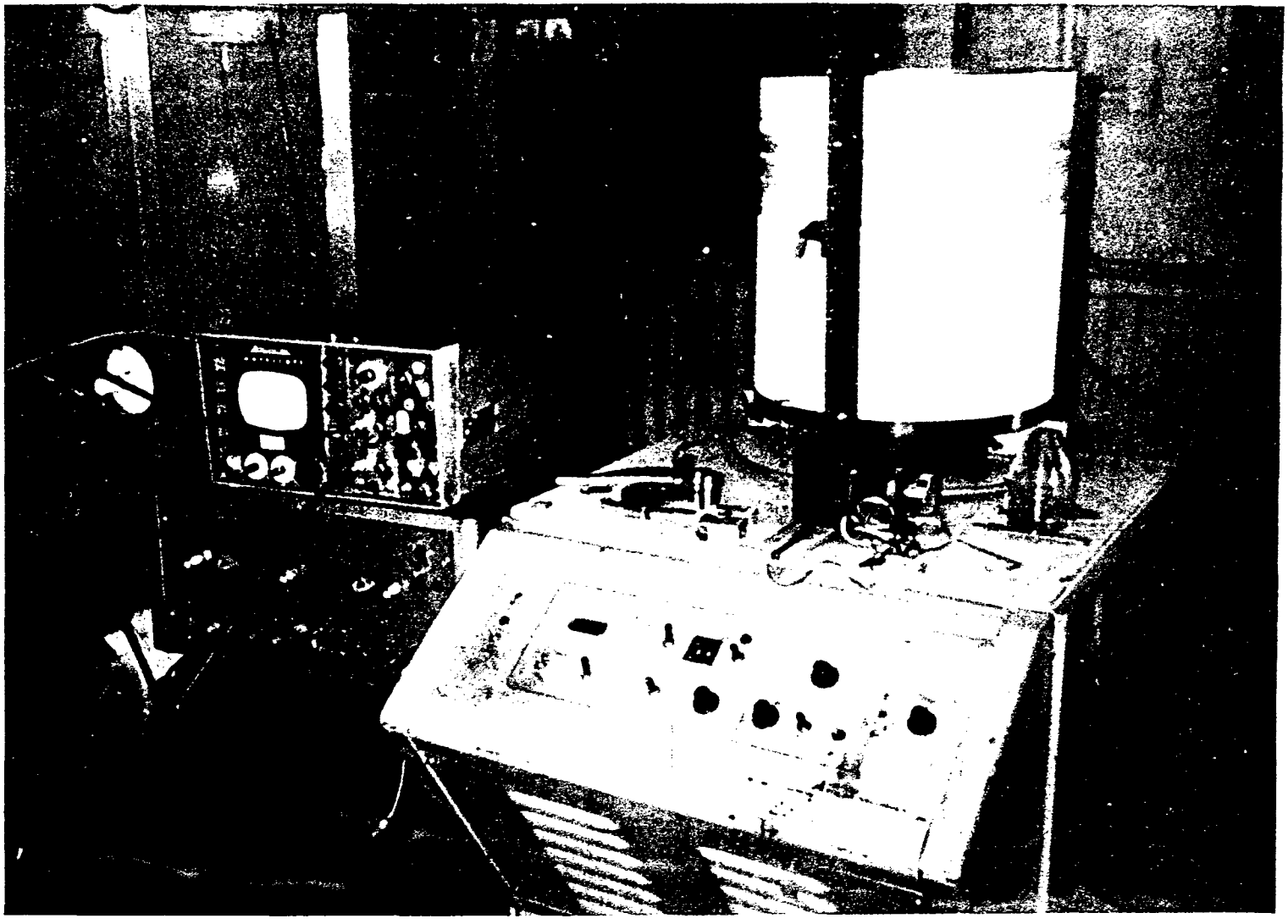

Figure 54. The transmitted acoustic signal is continuously plotted on a sheet of paper wrapped around a revolving drum

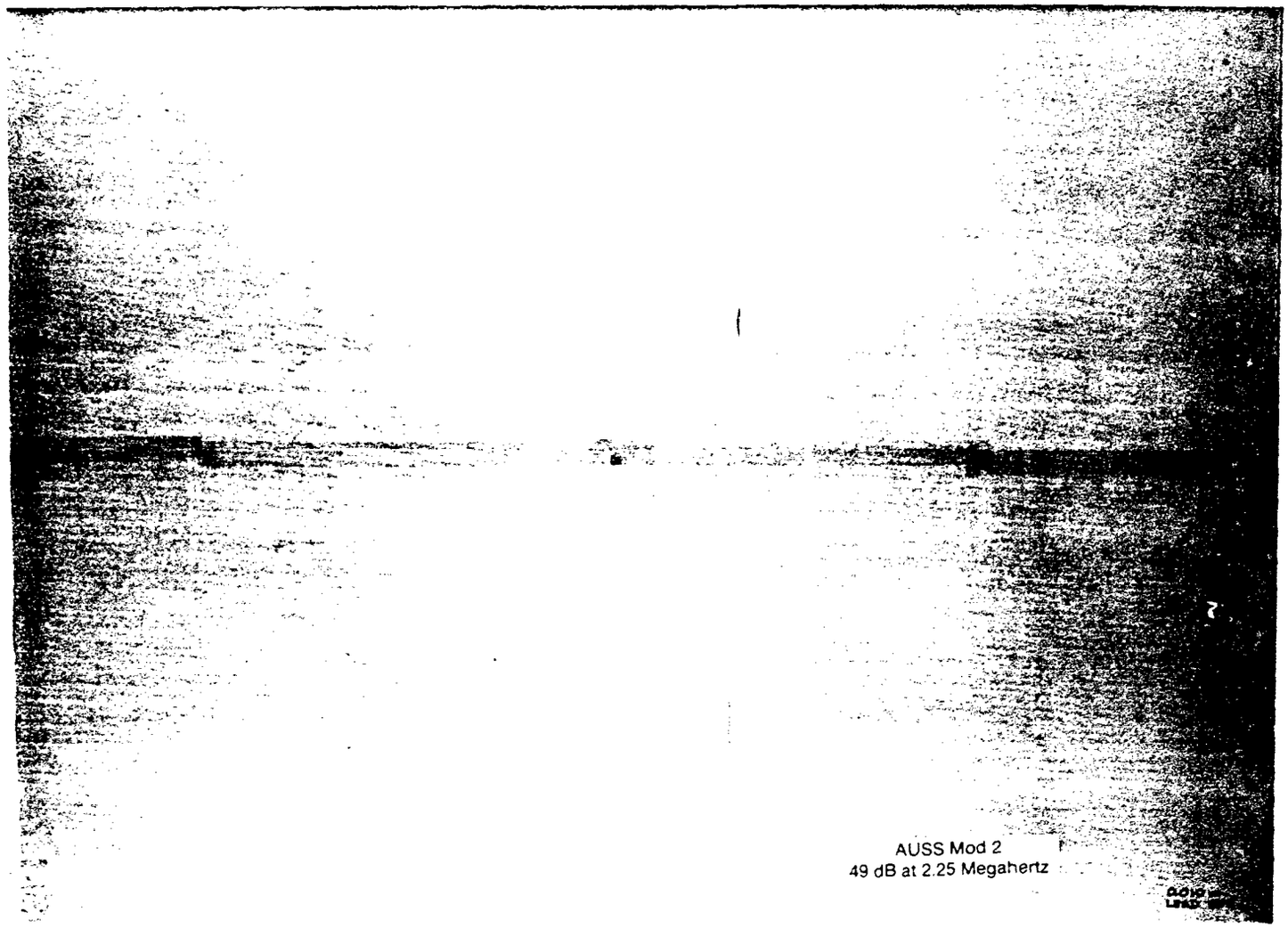

Figure 55. Record of sonic scan at 2.25-MHz frequency and 49-db signal strength setting. Note the white longitudinal streaks appearing at regular intervals around the circumference of the cylinder. These streaks indicate locations of minor porosity along the axis of flat spots generated during winding along the axis of the cylinder.

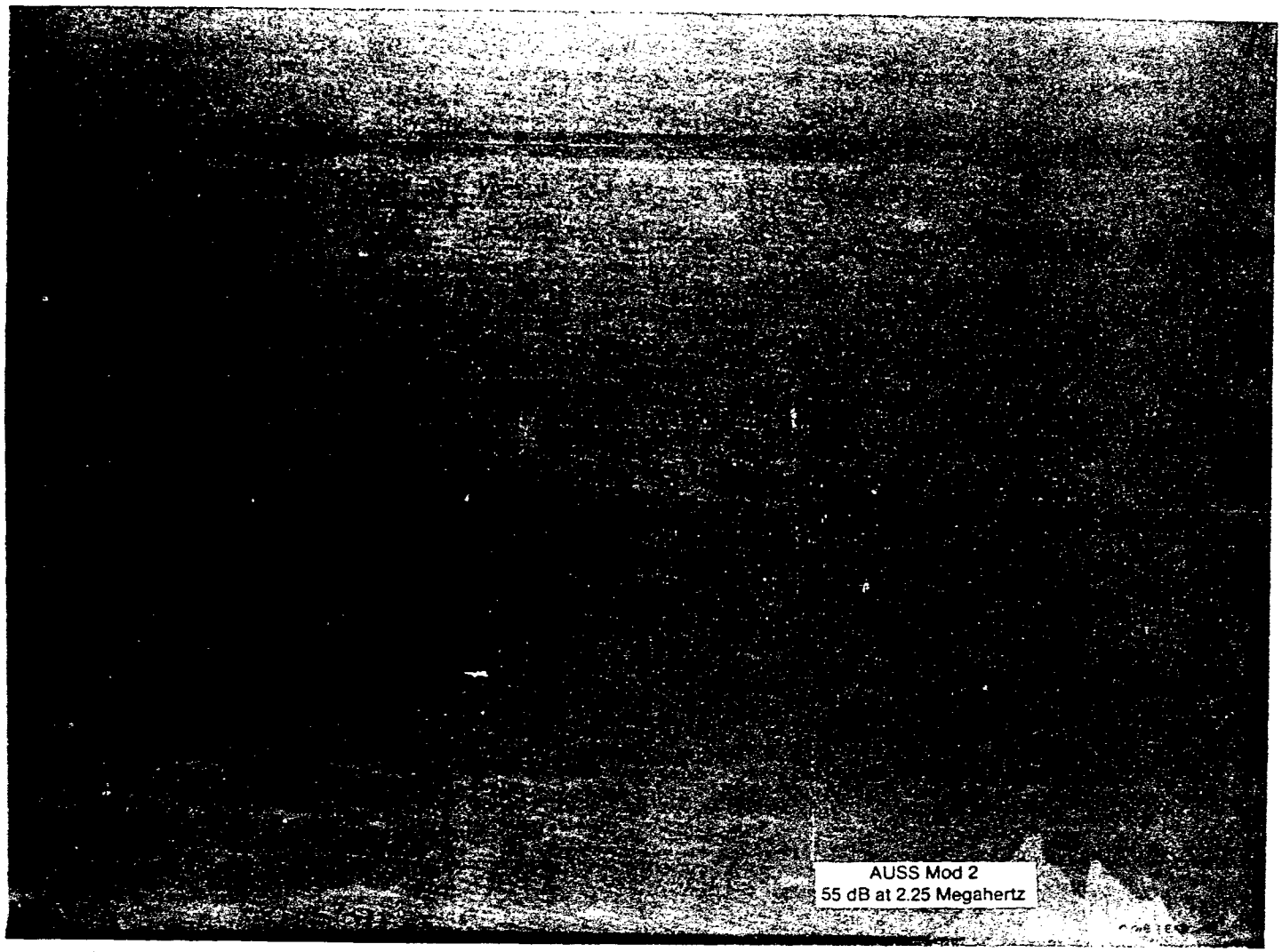

Figure 56. Record of sonic scan at 2.25 MHz frequency and 55-dB signal strength setting [illegible] that most of the white spots have disappeared in this recording because of the [illegible] strength setting during the test.

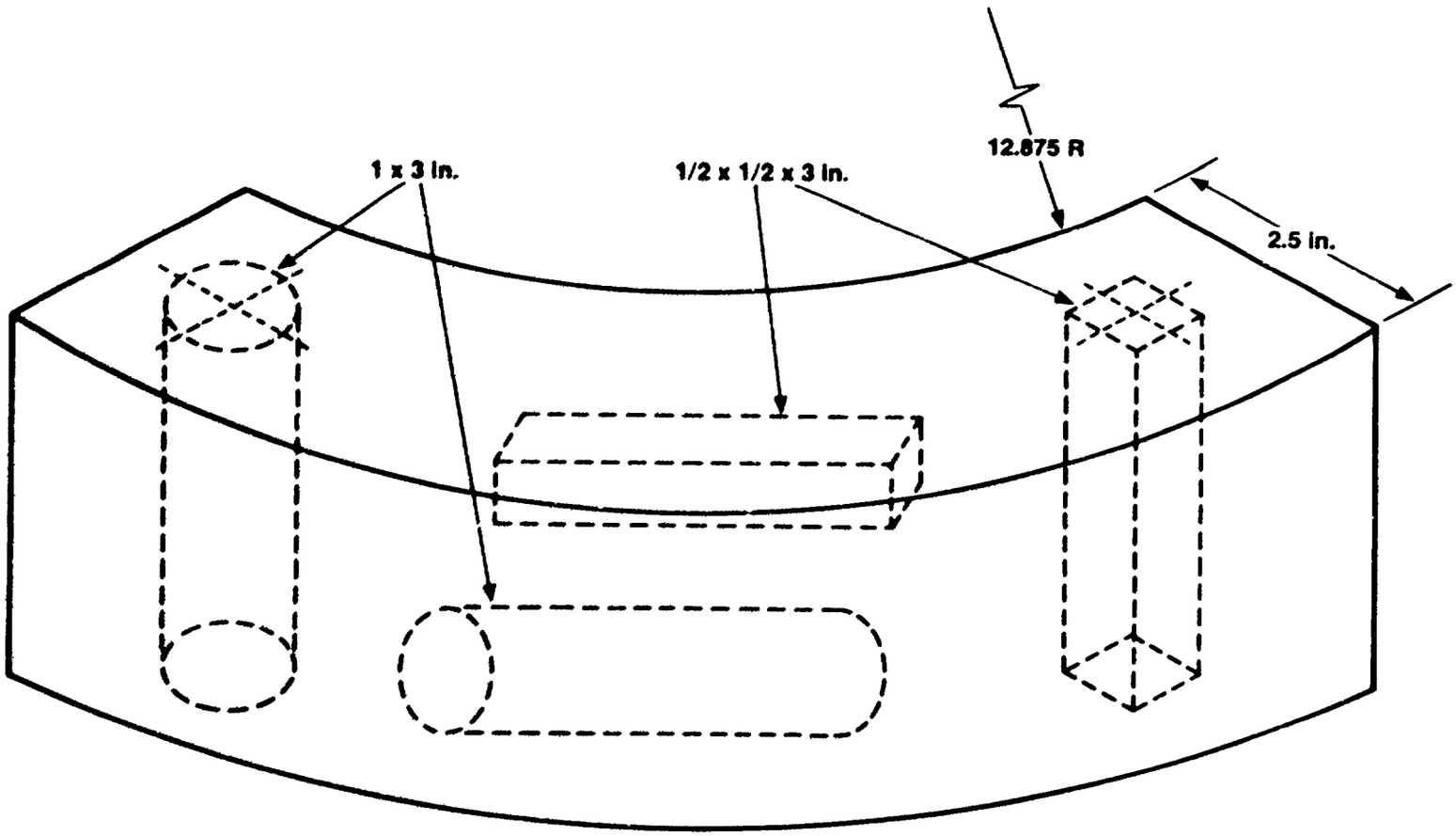

Note: All surfaces to have 32 rms finish

Figure 57. Locations inside the cylinder wall from which material coupons were removed.

Figure 58. Compressive test specimens machined from material coupons. Note that one test specimen was machined from axial-oriented material coupon while the other one was machined from a hoop-oriented material coupon.

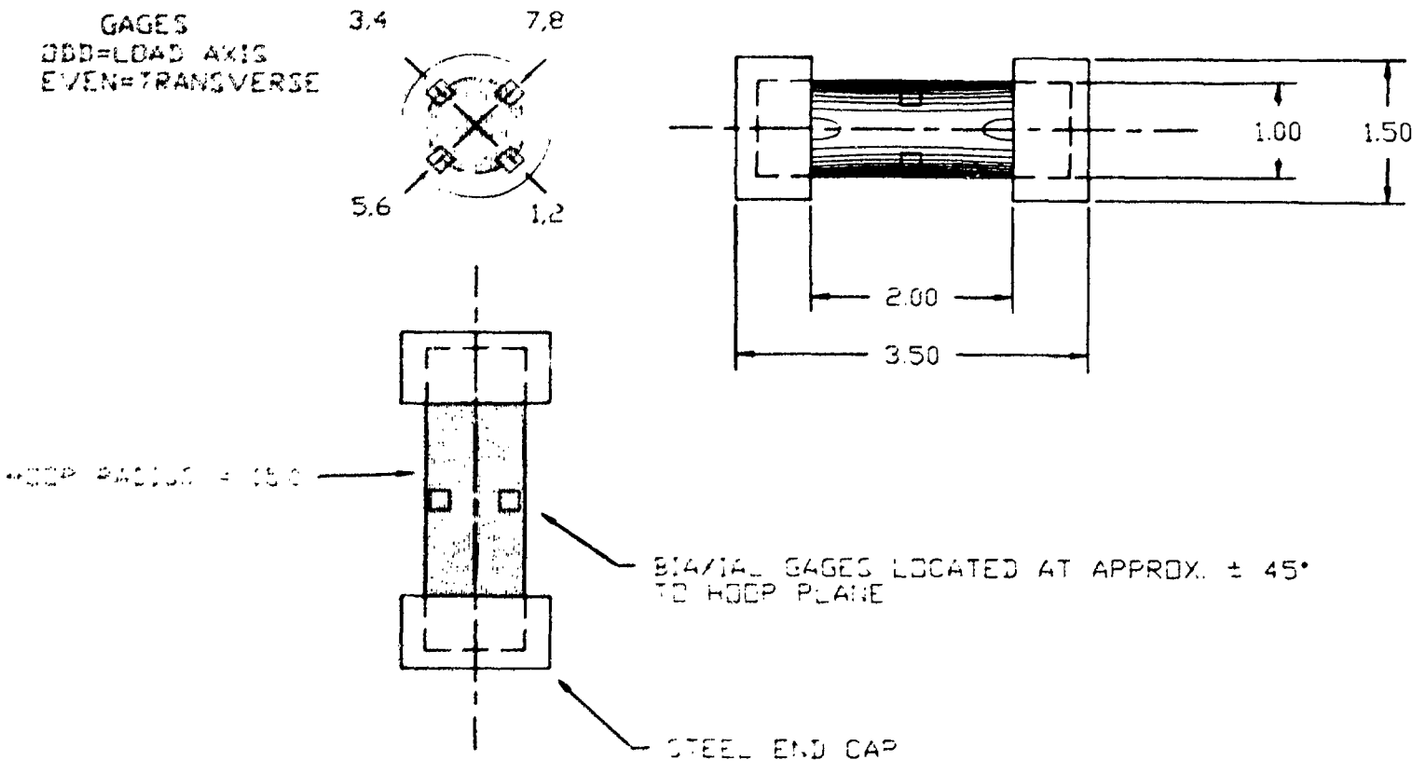

Figure 59. Dimensions of hoop-compression specimen and location of straingages. The dimensions of axial-compression specimen and location of gages is identical.

Figure 60. Failed axial-compression specimen. The average compressive stress at failure was 67,600 psi.

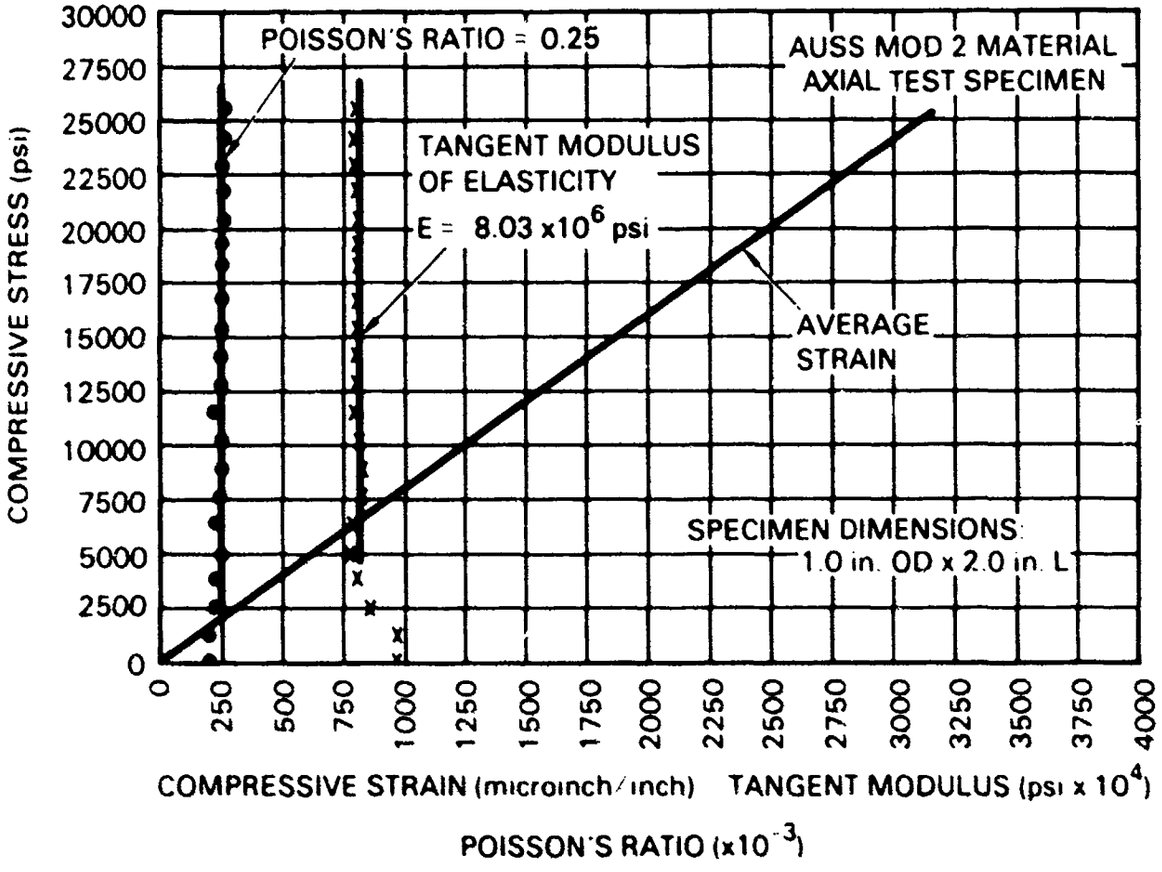

Figure 61. Strains recorded during compression testing of the *axial-oriented* test specimen. Based on these strains, the tangent modulus of elasticity was calculated to be 8.06 x 10^6 psi.

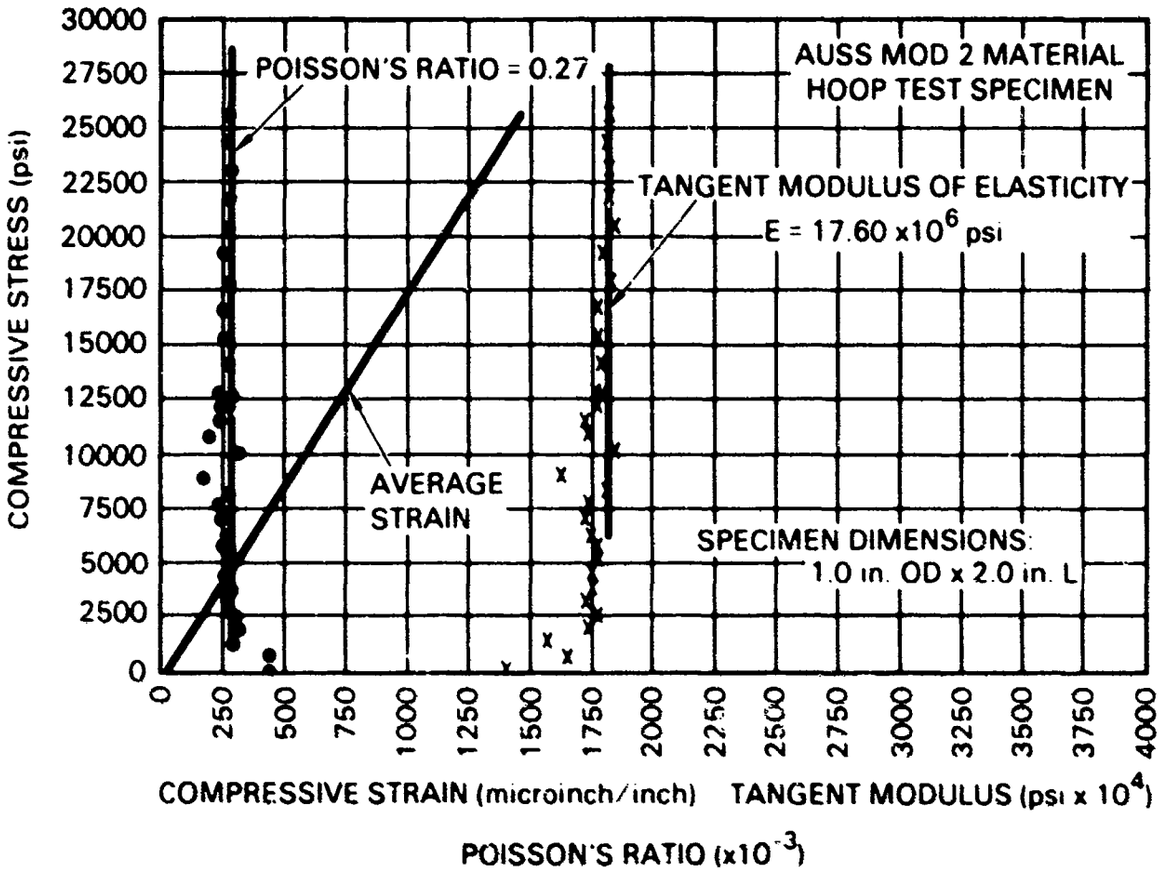

Figure 62. Strains recorded during compression testing of the *hoop-oriented* test specimen. Based on these strains, the tangent modulus of elasticity was calculated to be 17.6 x 10 psi.

Figure 63. Flexure test specimens machined from material coupons. Note that one test specimen was machined from axial-oriented and the other one from hoop-oriented material coupons.

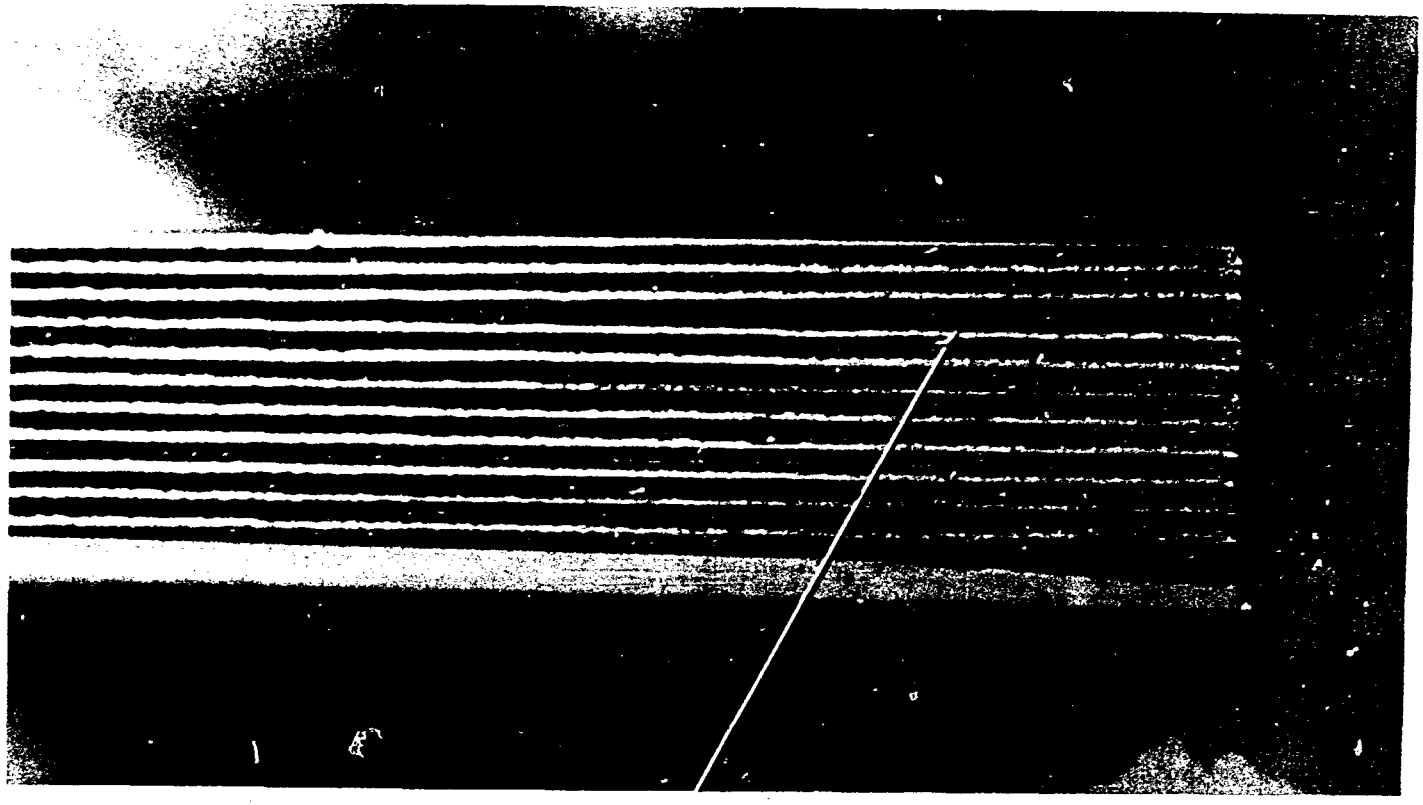

SHEAR FAILURE IN LAYER WITH FIBERS AT RIGHT ANGLE TO FLEXURE STRESS.

Figure 64. Failed flexure specimens. The maximum tensile stresses were 61,000 psi in axial- and 81,000 psi in hoop-oriented specimens.

Figure 65. Titanium coupling ring; interior view. Note the bosses for attachment of guide rails used to support payload components inside the cylinder.

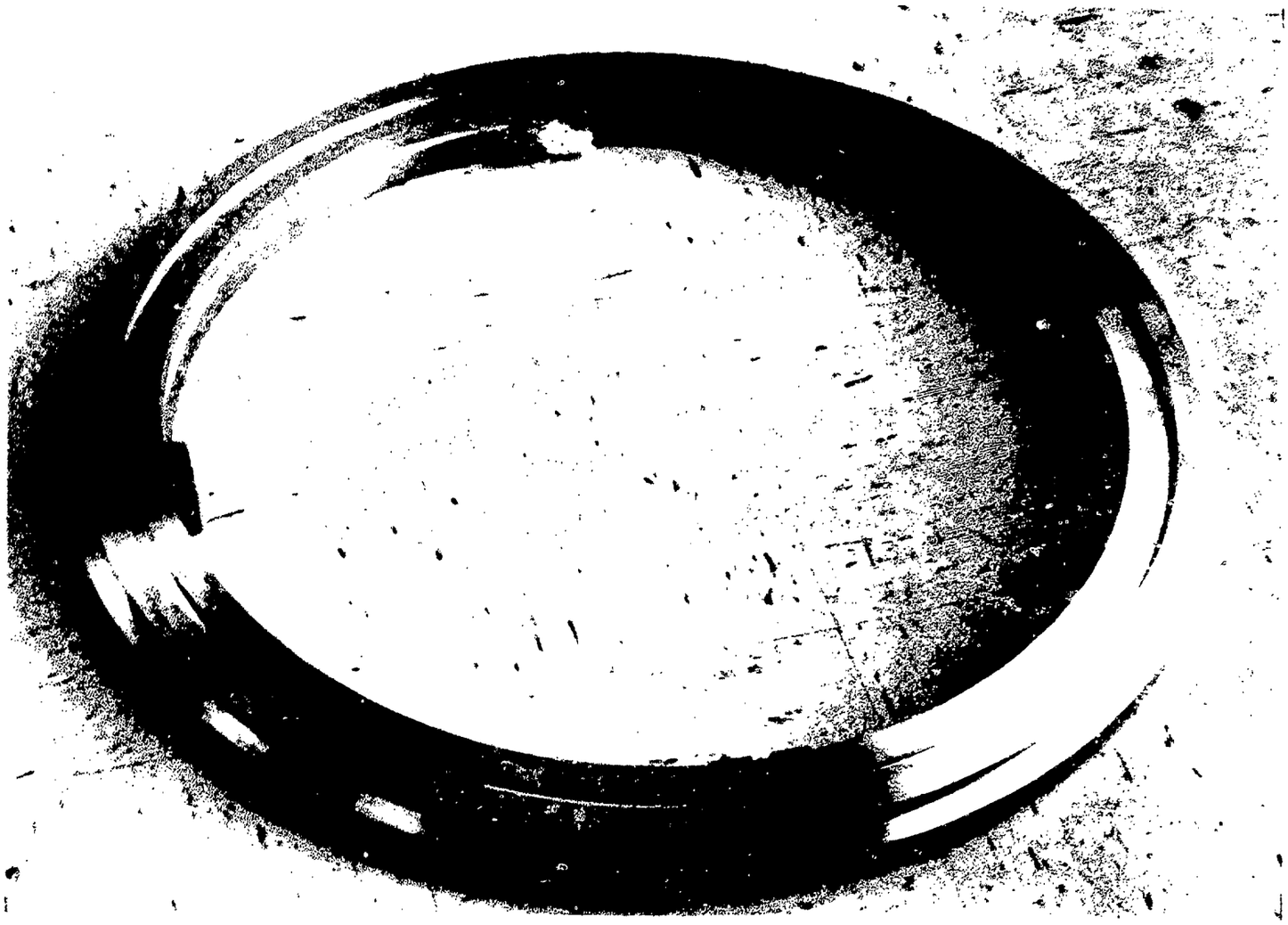

Figure 66. Titanium coupling ring; exterior view. Note the groove for containment of O-ring seal between the end of the cylinder and the end closure.

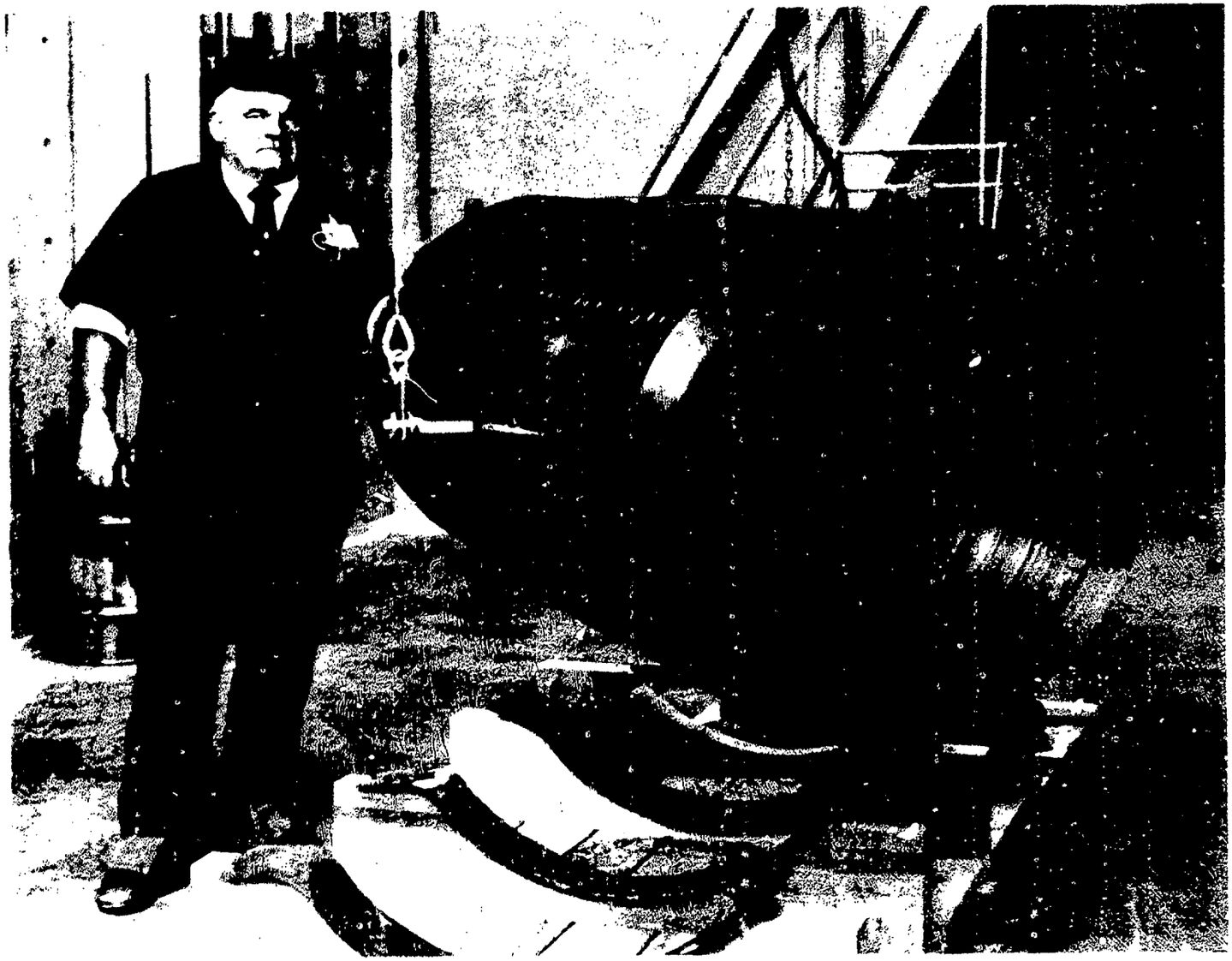

Figure 67. The 30 785-inch OD x 25 75-inch ID x 65-inch L AUSS Mod 2 cylindrical pressure hull being prepared for bonding of titanium coupling rings.

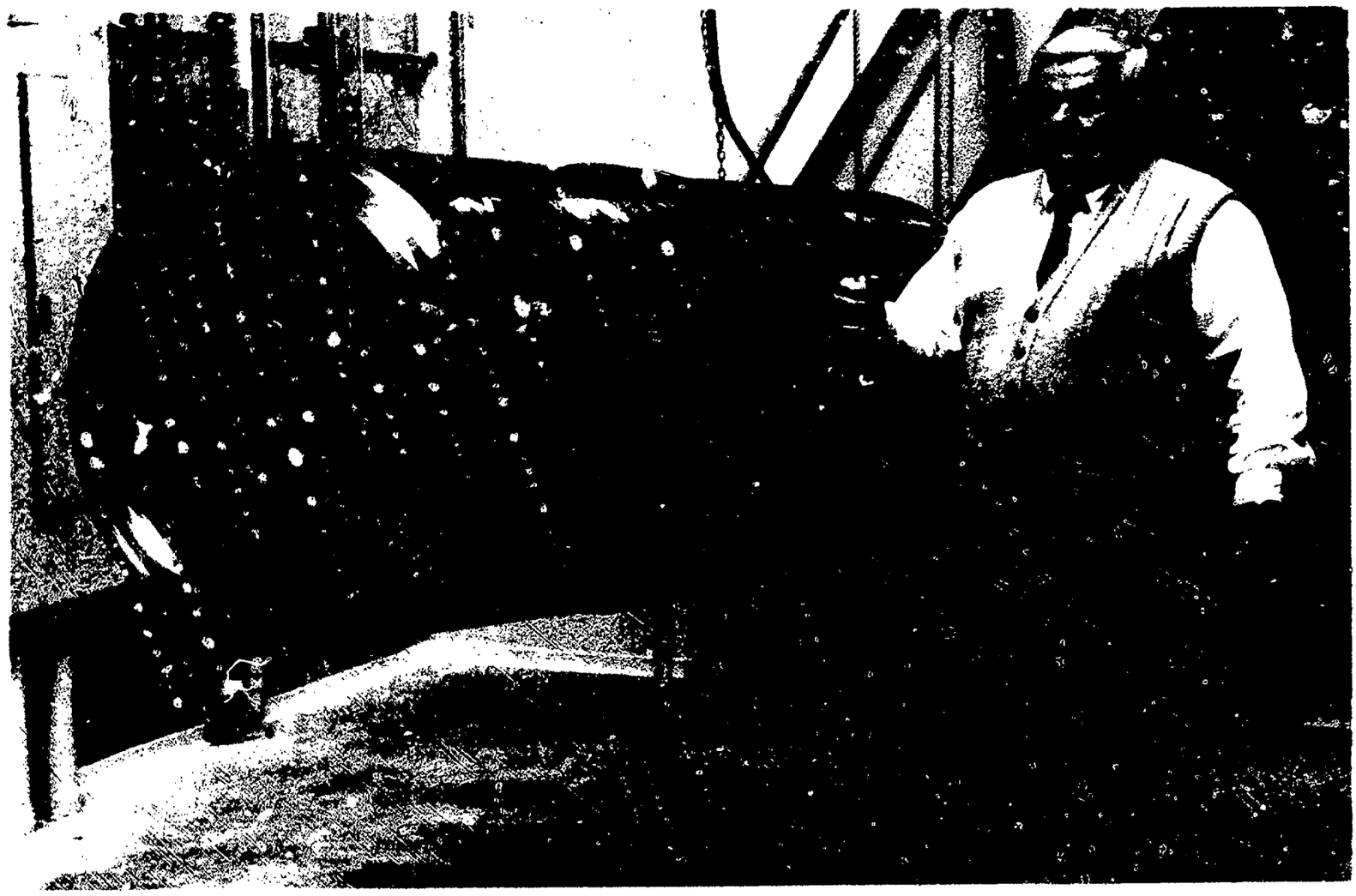

Figure 68. AUSS Mod 2 cylindrical pressure hull after bonding of titanium coupling rings.

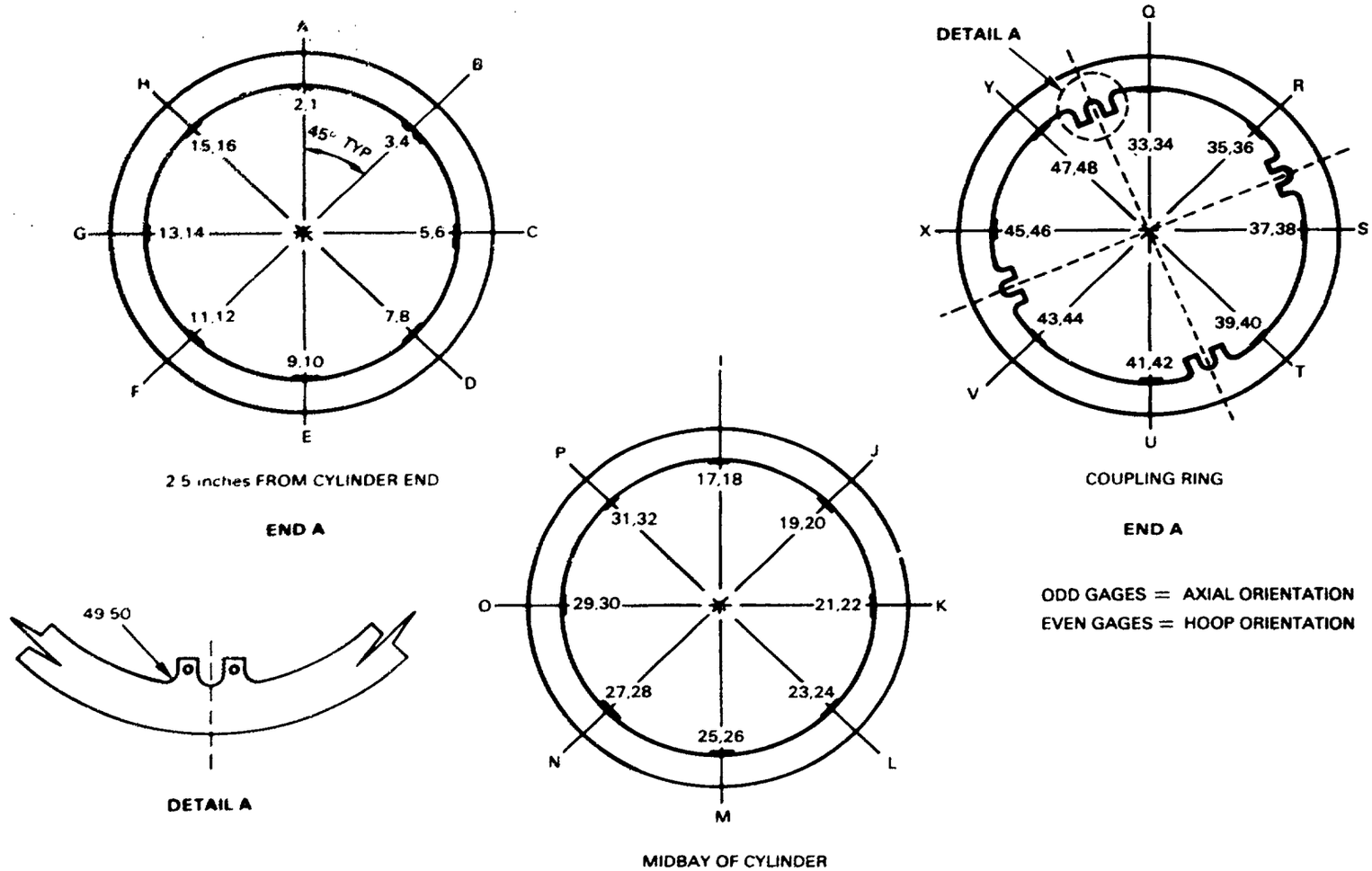

Figure 69. Location of the electric resistance straingages on the interior surface of the AUSS Mod 2 cylindrical hull.

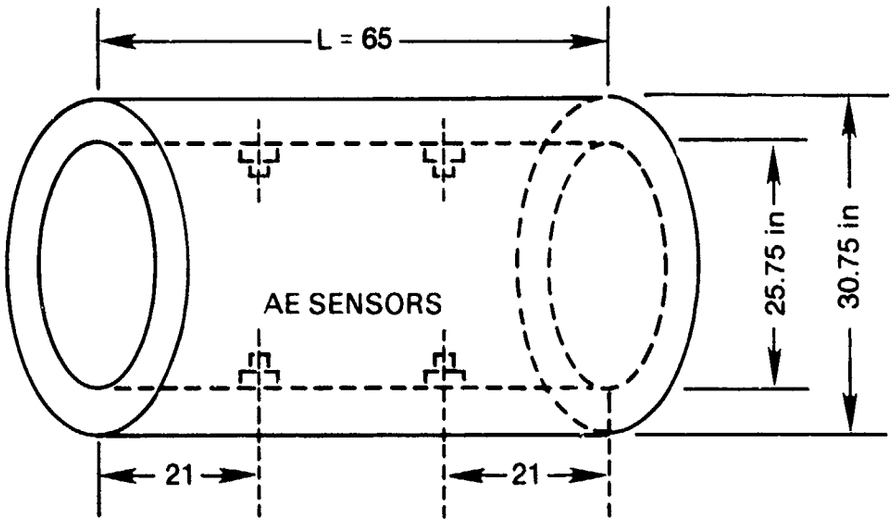

LOCATIONS OF AE SENSOR IN THE CYLINDER

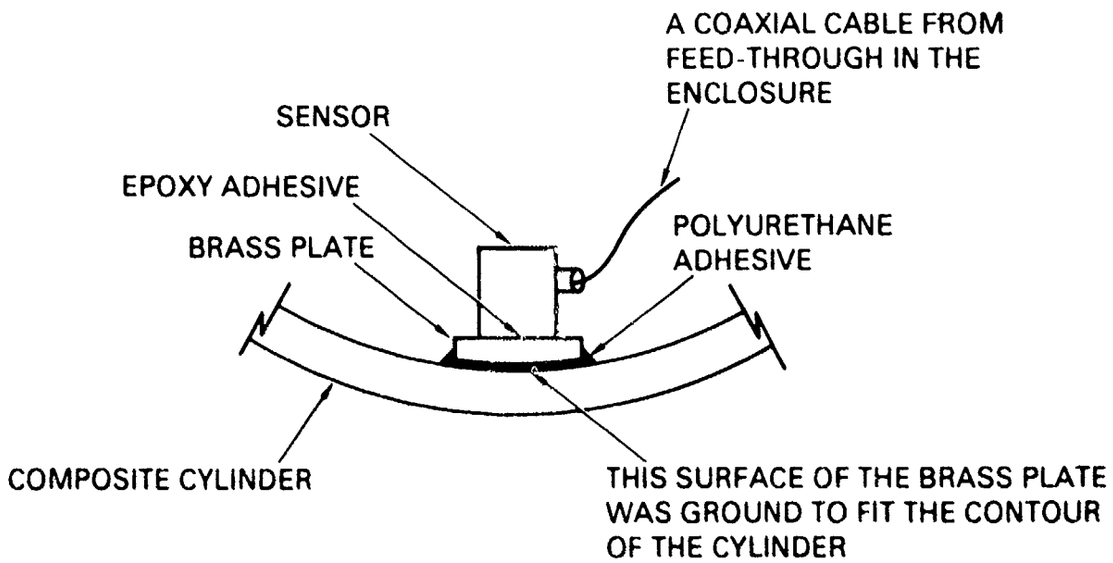

Figure 70. Location of the acoustic-emission sensors on the interior surface of the AUSS Mod 2 cylindrical hull.

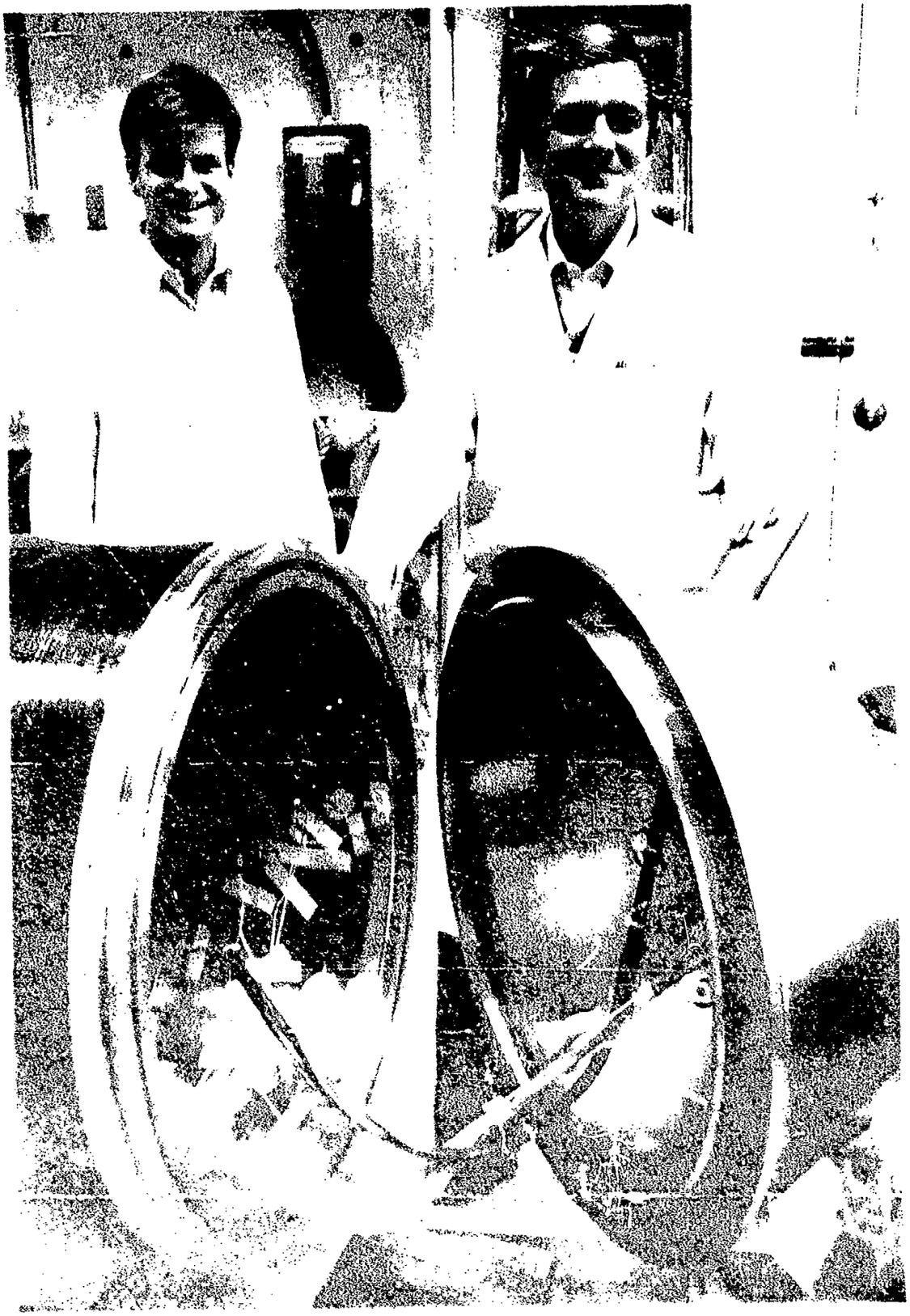

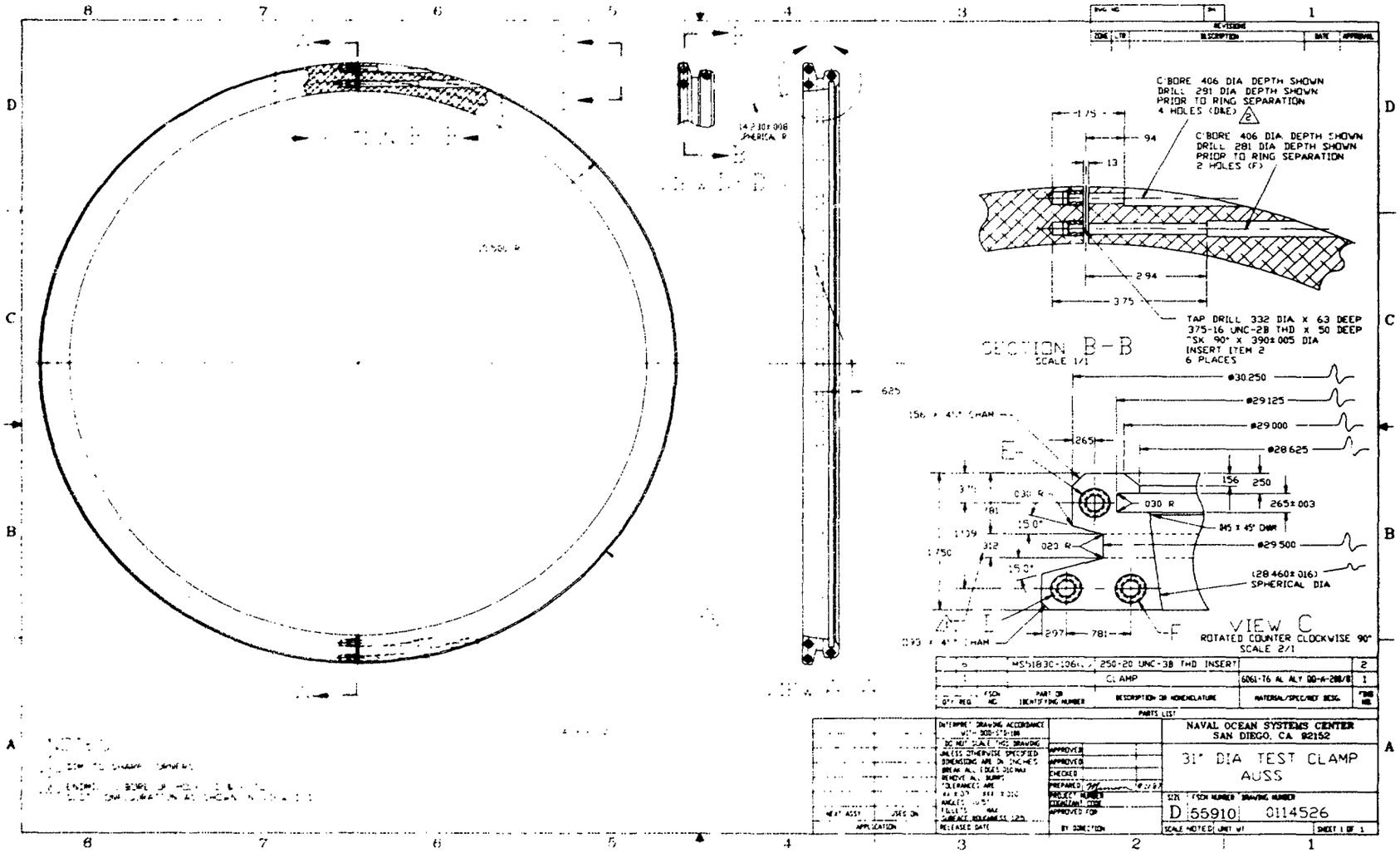

Figure 72. An aluminum test clamp was clamped to the ridge on the equatorial flange of the hemisphere to provide the bearing surface for the wedge clamp during assembly of the AUSS Mod 2 hull for pressure testing (see Figure 13).

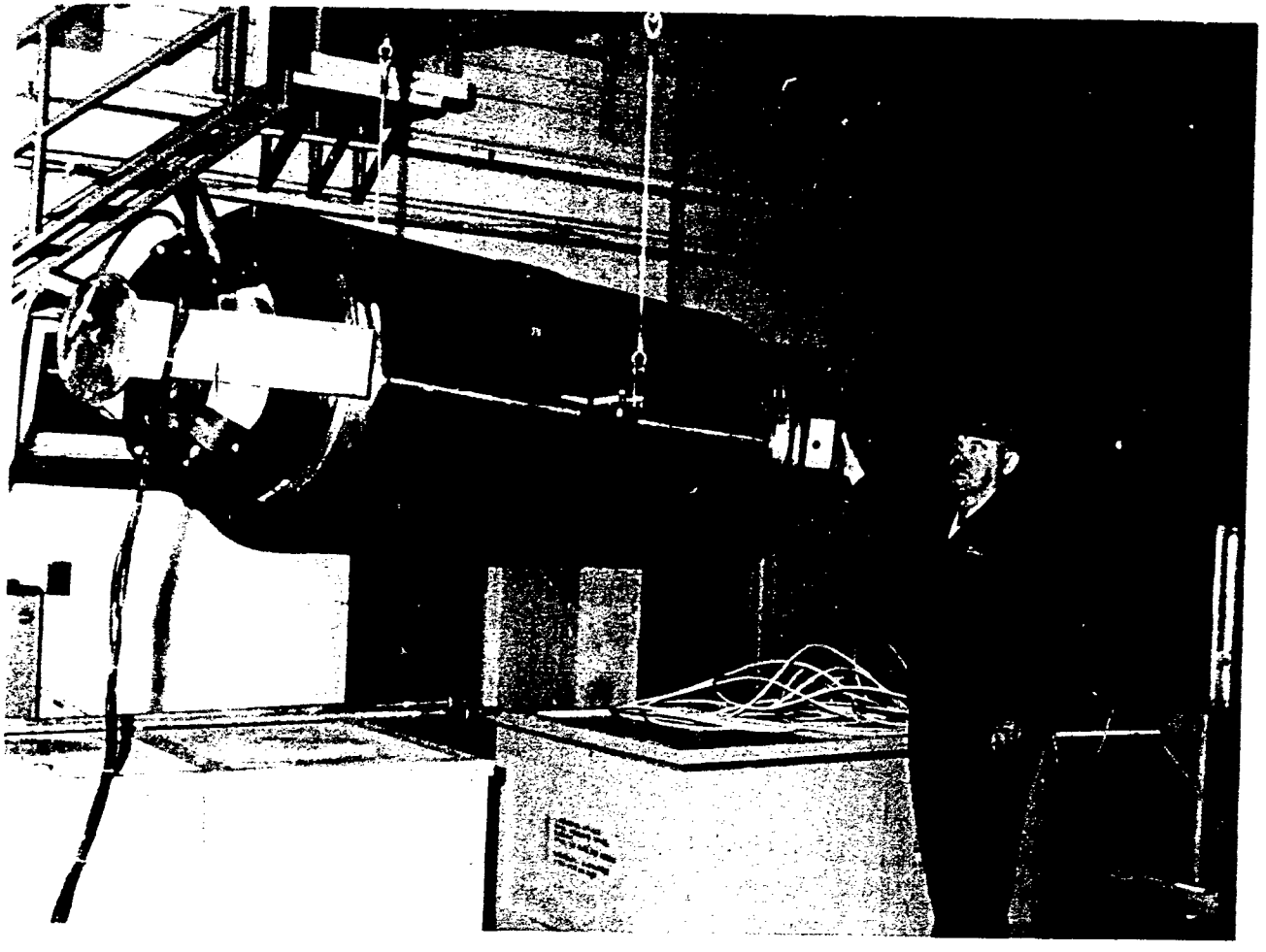

Figure 73. AUSS Mod 2 hull assembly. Note the fixtures on the end closures for securing the hull assembly to the test cage

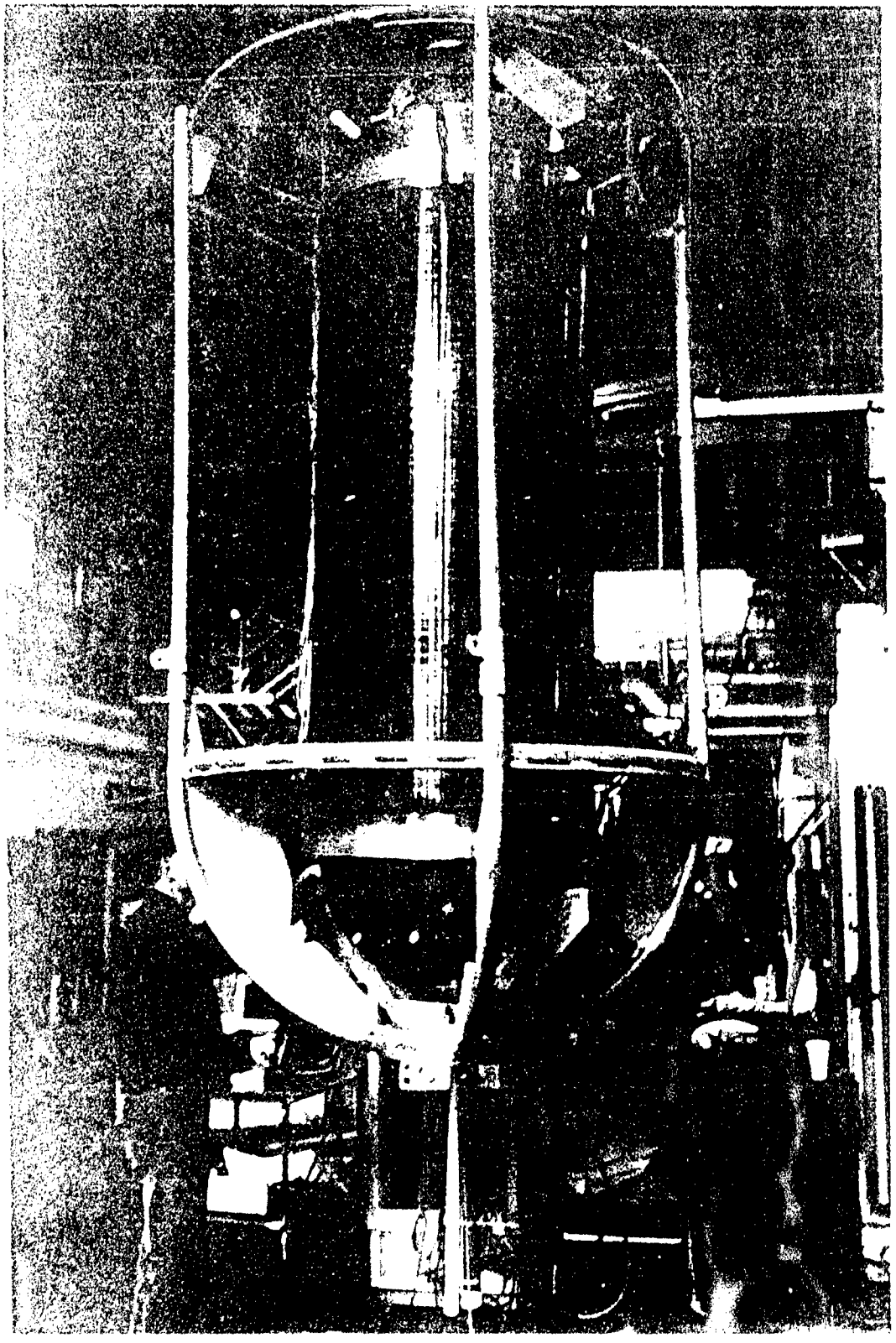

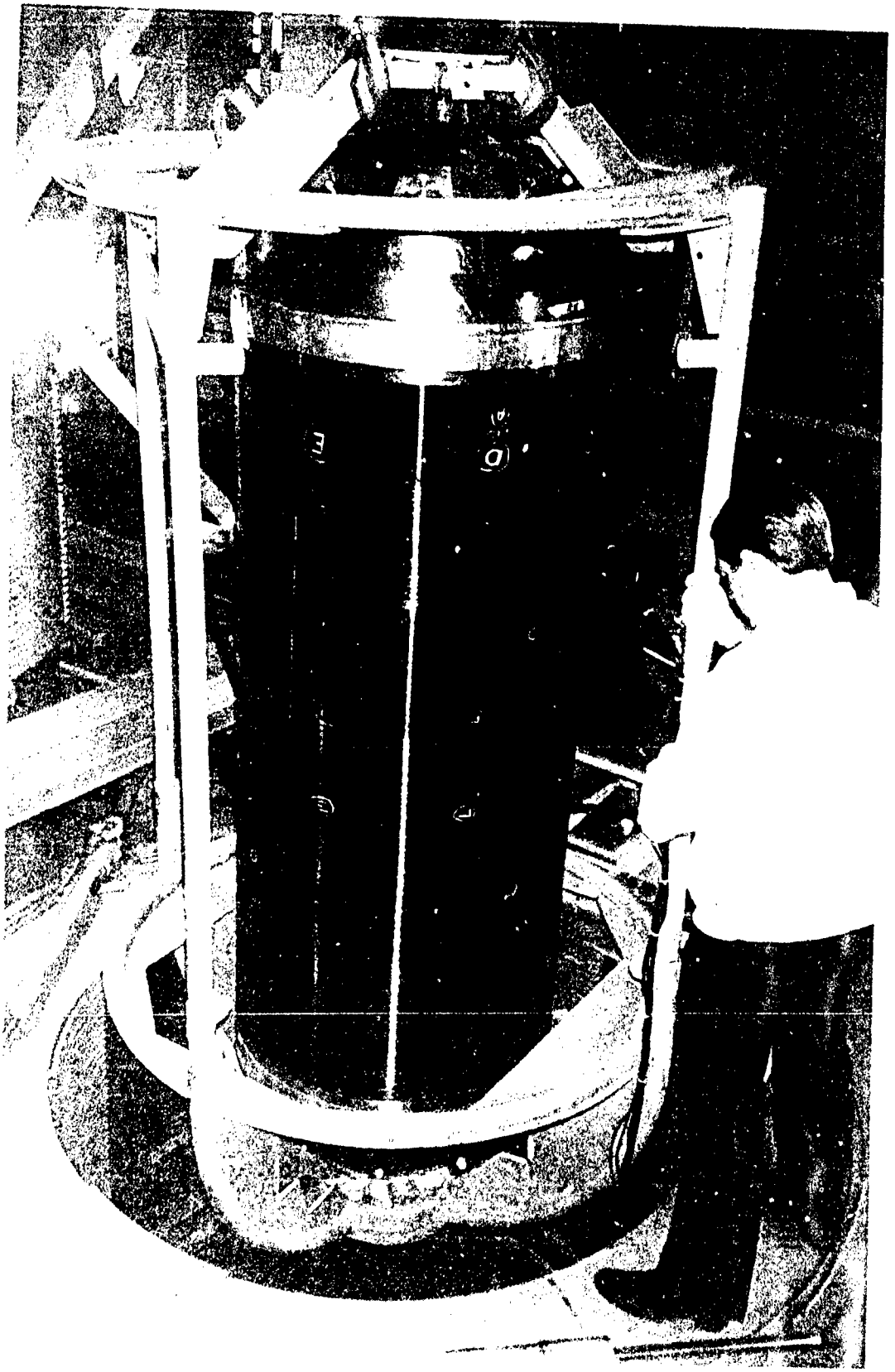

Figure 75. [illegible] at NUSC, Arctic Laboratory

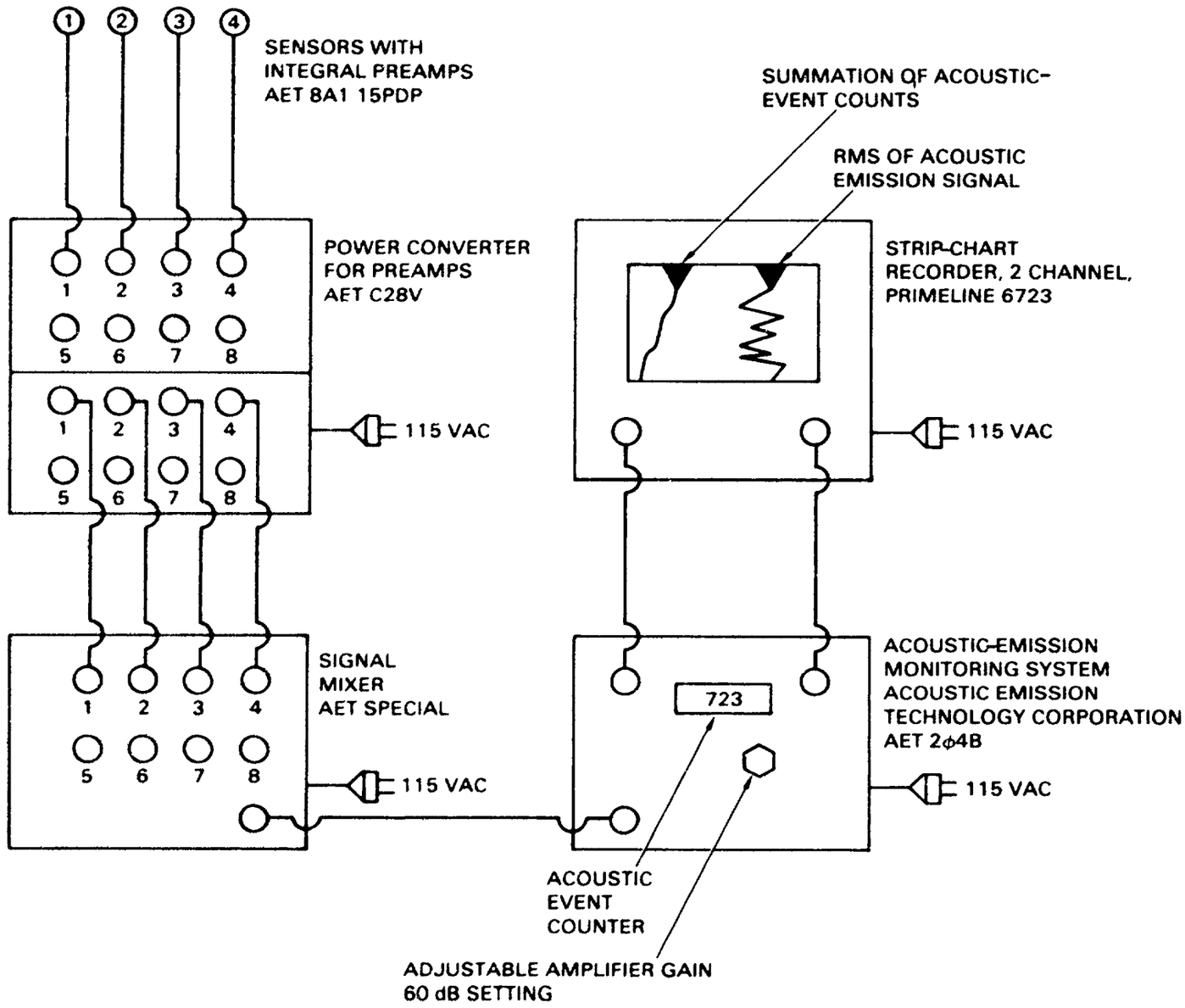

Figure 76. Instrumentation setup for monitoring and recording of acoustic-emission signals.

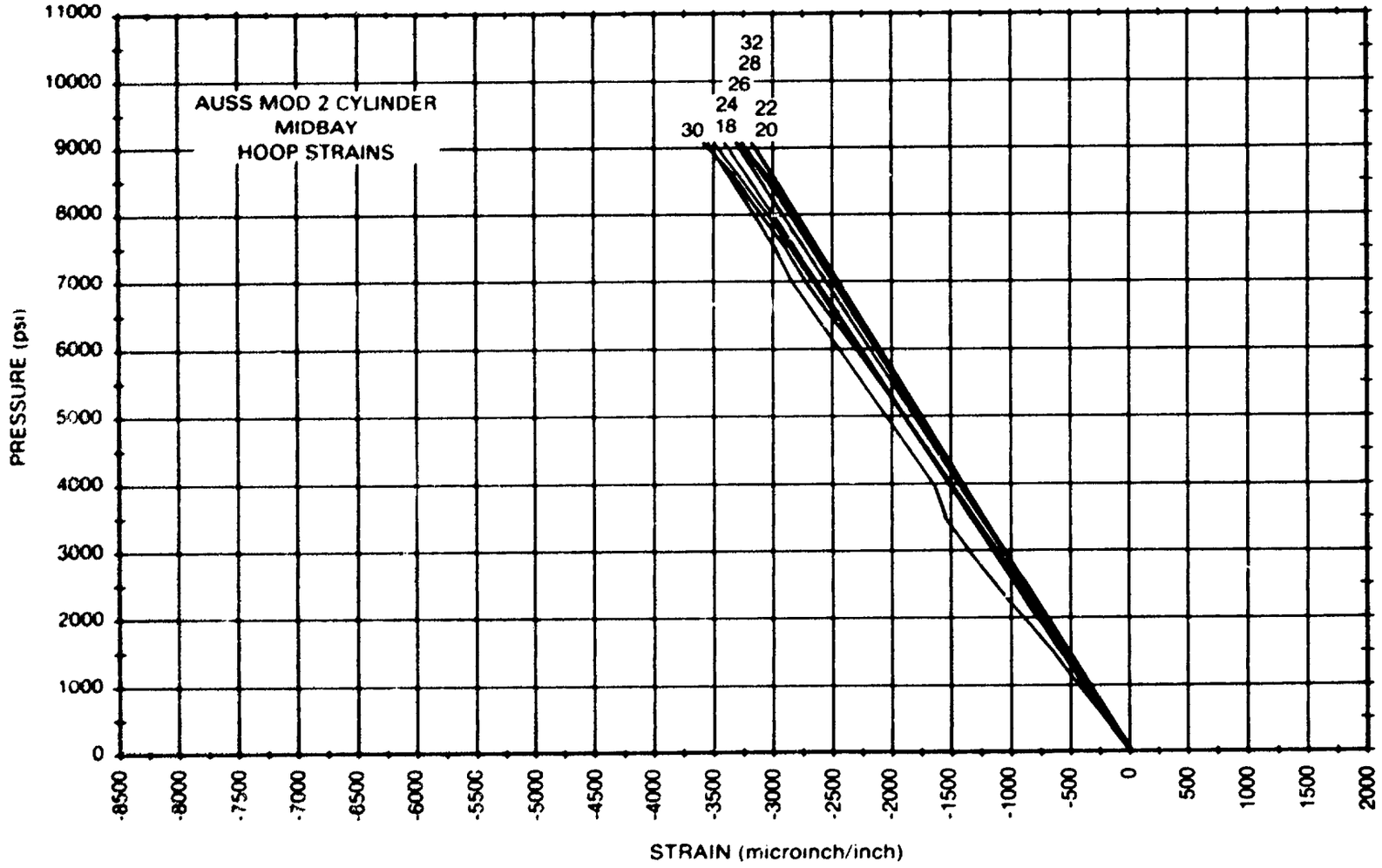

Figure 77. *Hoop strains* measured on the interior surface of AUSS Mod 2 cylindrical hull *at midbay*. These strains are identical to those on GFRP model scale AUSS cylinder (Figure 30).

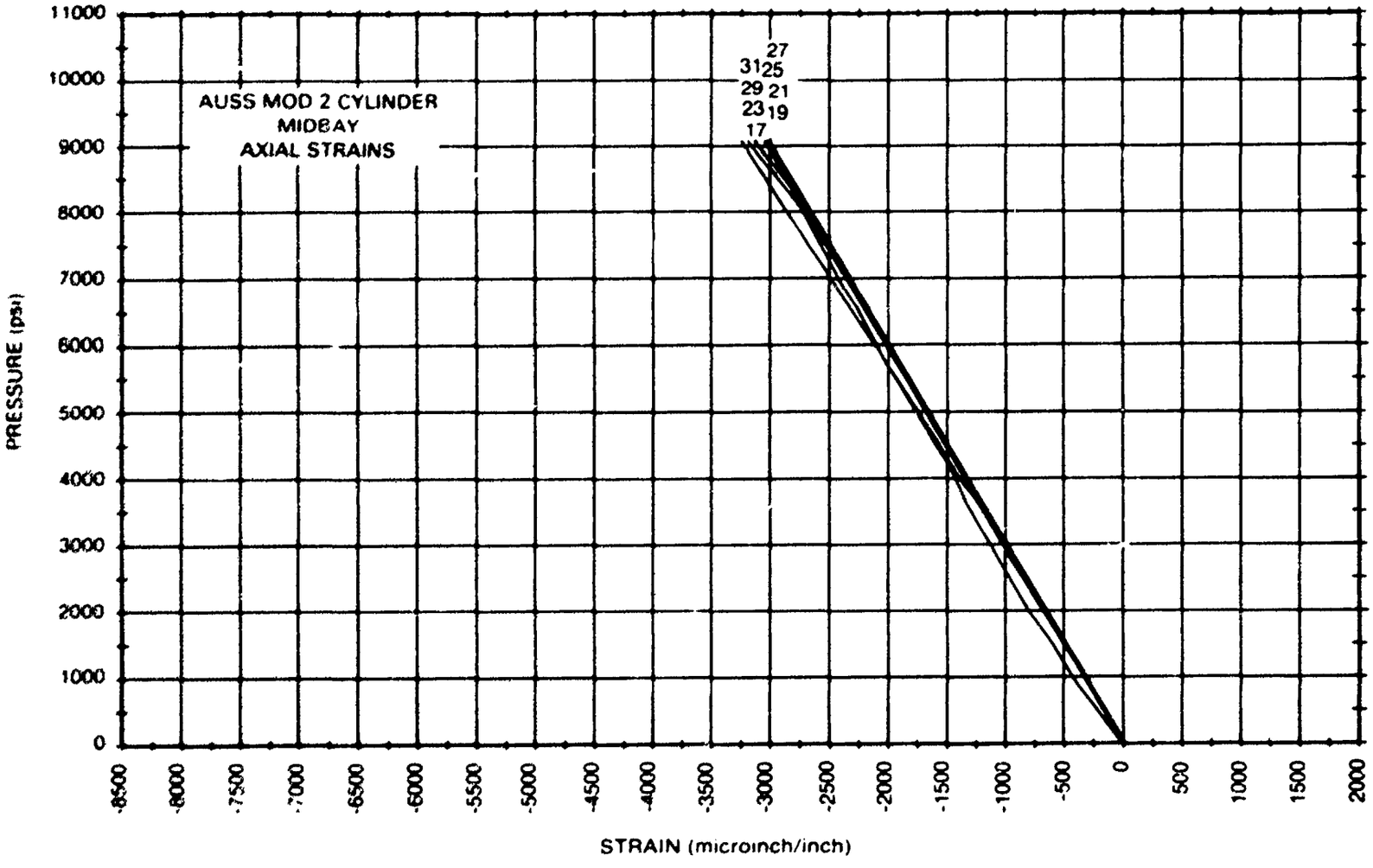

Figure 78. *Axial strains* measured on the interior surface of AUSS Mod 2 cylindrical hull *at midbay*. These strains are identical to those on GFRP model-scale AUSS cylinder (Figure 30).

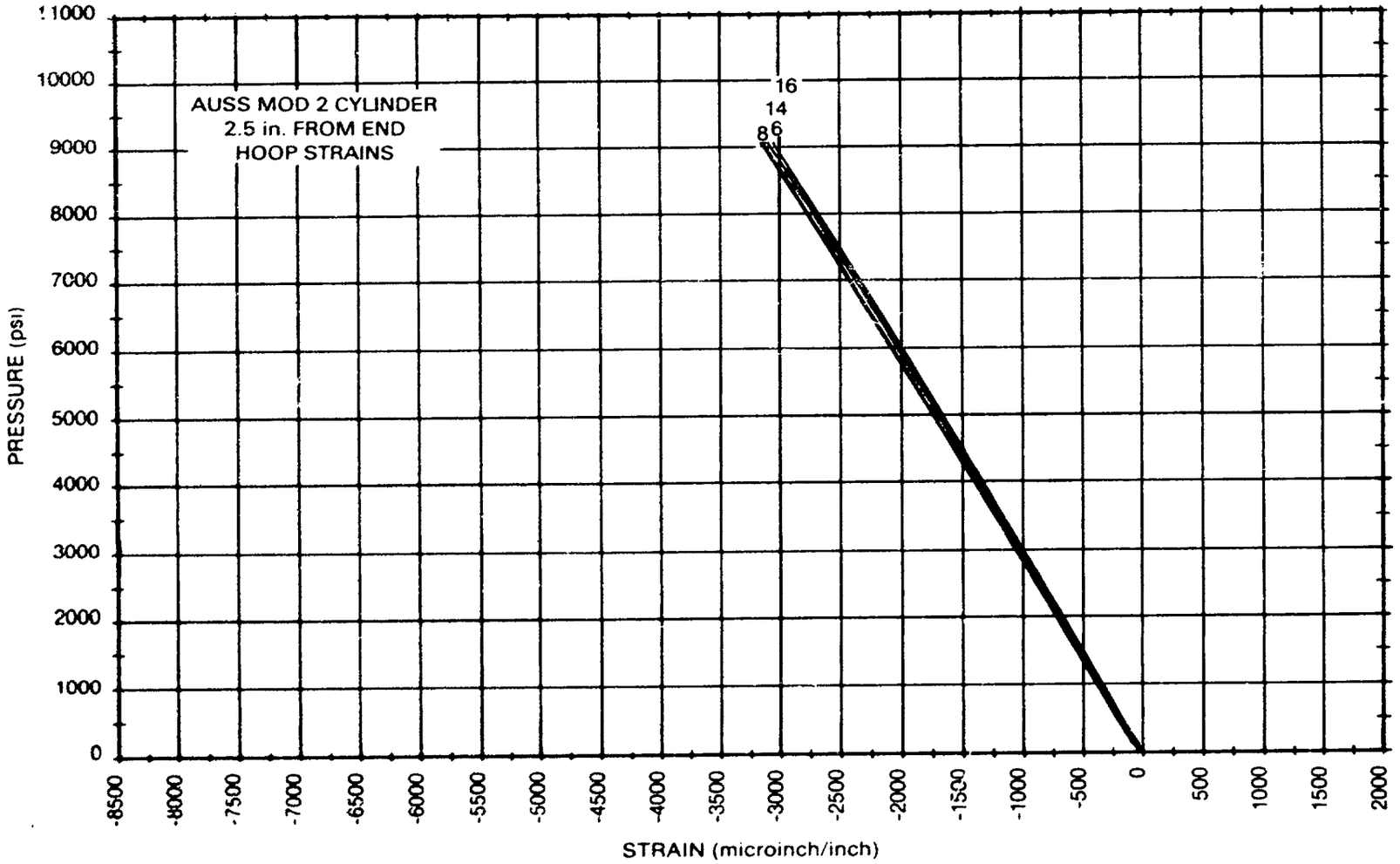

Figure 79. *Hoop strains* measured on the interior surface of AUSS Mod 2 cylindrical hull *at the end*. The strains are identical to those on GFRP model-scale AUSS cylinder (Figure 31). The magnitude of strains is approximately 10-percent *less* than at midbay (Figure 77) indicating that the titanium hemispherical end closures provide only minor radial support to the ends of the GFRP cylinder.

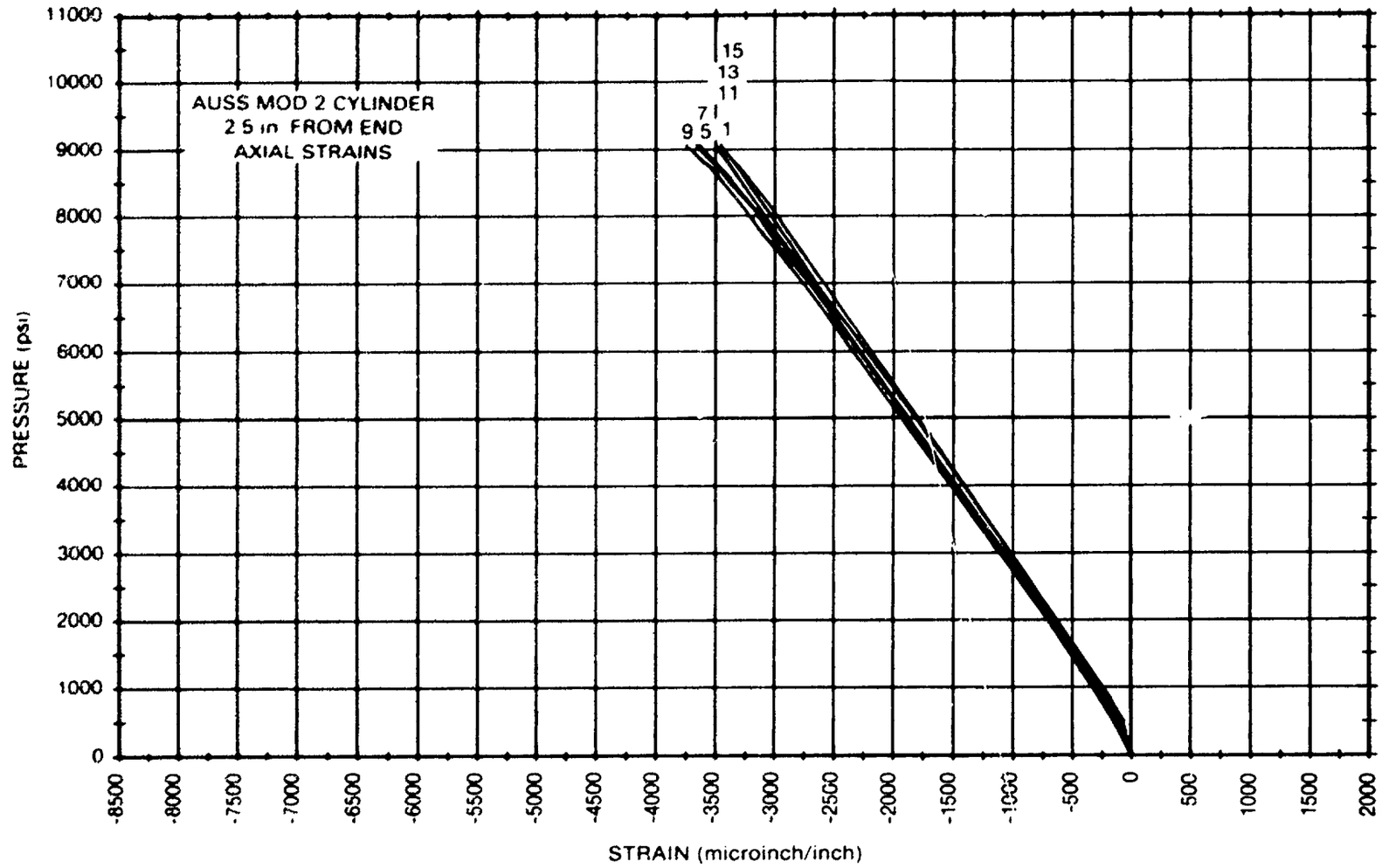

Figure 80. *Axial strains* measured on the interior surface of AUSS Mod 2 cylindrical hull at the end. The magnitude of strains is approximately 10-percent *greater* than at midbay (Figure 78) indicating minor bending of the cylinder wall due to radial support of its ends by the titanium end closures.

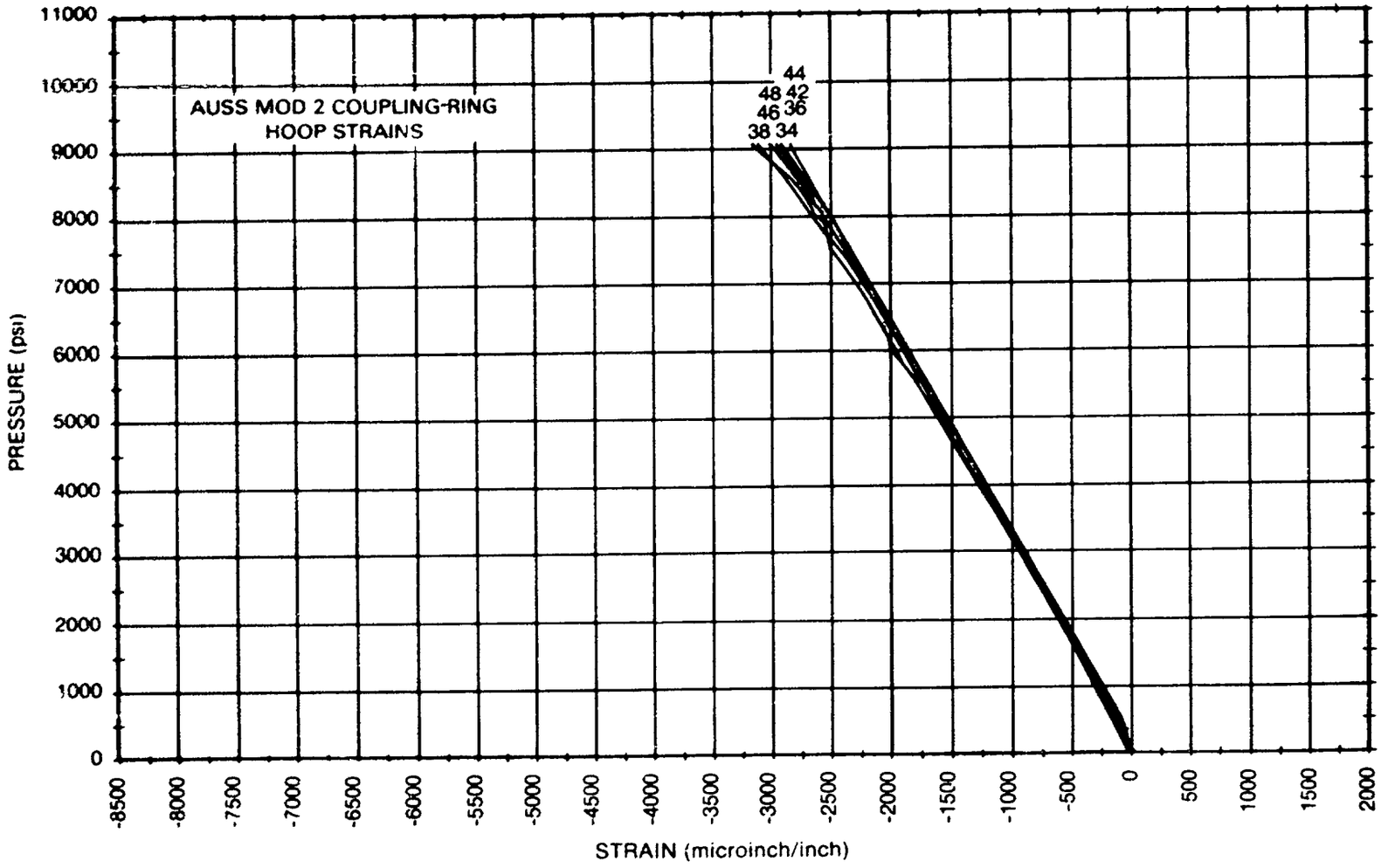

Figure 81. *Hoop strains* on the interior surface of the titanium coupling ring supported radially by the end closure. Note that the hoop strains are approximately 10 percent less than at midbay, indicating that the mismatch in radial compliance between the GFRP cylinder and titanium hemisphere is only 10 percent.

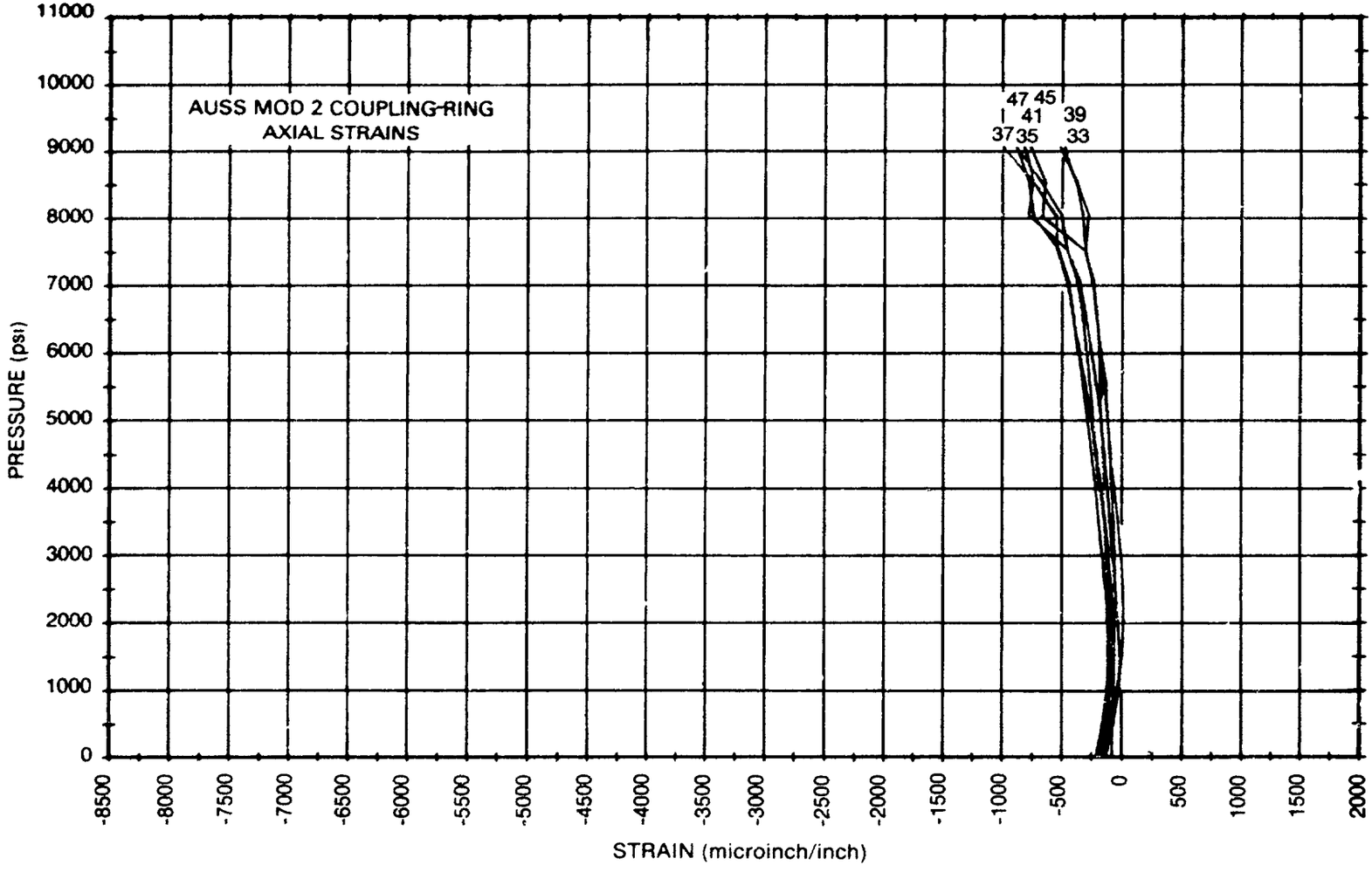

Figure 82. *Axial strains* on the interior surface of the coupling ring on AUSS Mod 2 cylinder.

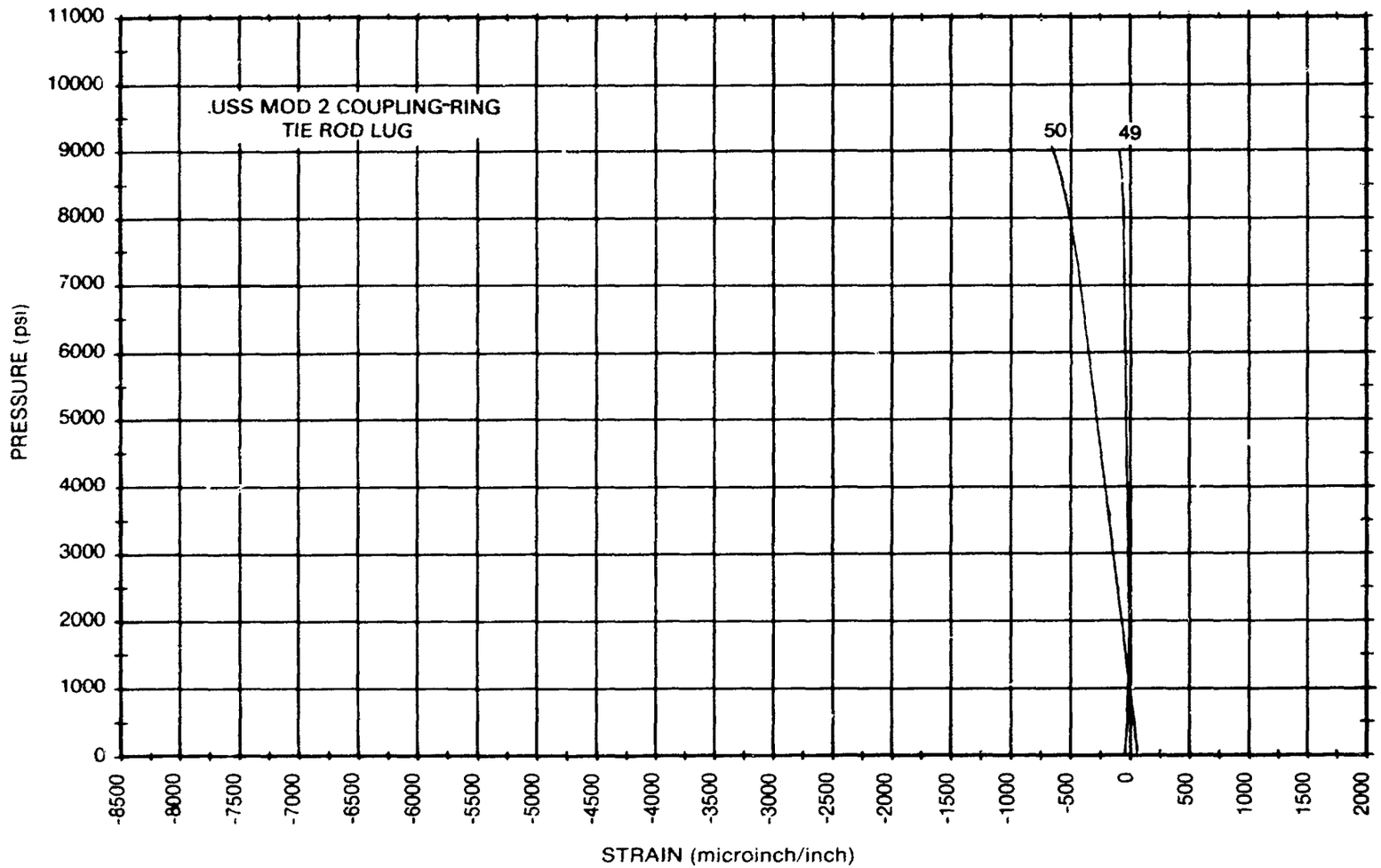

Figure 83. Strains at the base of the bosses on the coupling ring.

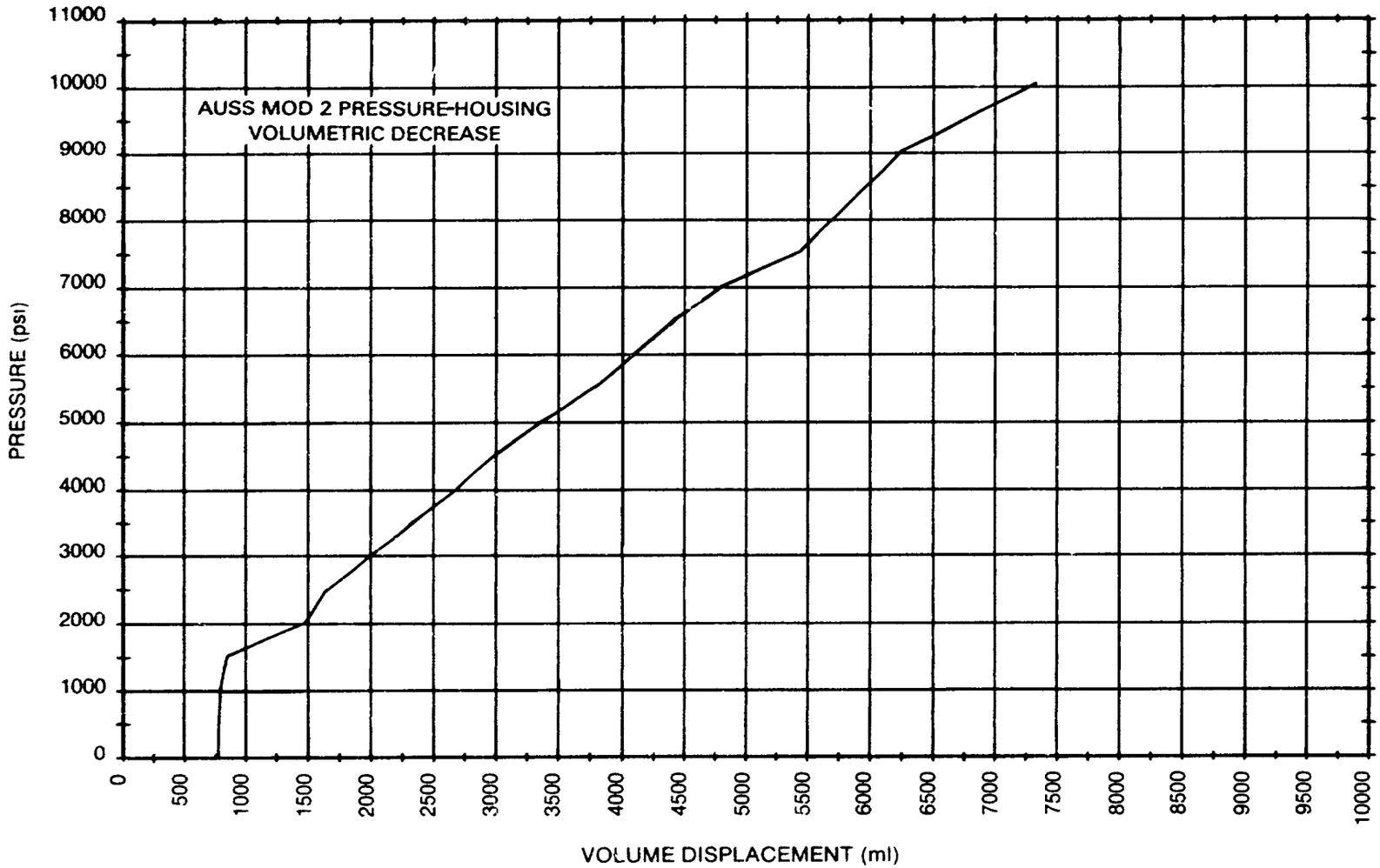

Figure 84. Volumetric decrease of the AUSS Mod 2 pressure-hull assembly during proof testing. The displacement of the hull assembly decreases by 6250 ml (0.6 percent) at operational pressure of 9000 psi. Since the density of seawater has increased at that pressure by 2.66 percent, the overall result is an increase in buoyancy of 48 lb for the whole AUSS Mod 2 hull assembly.

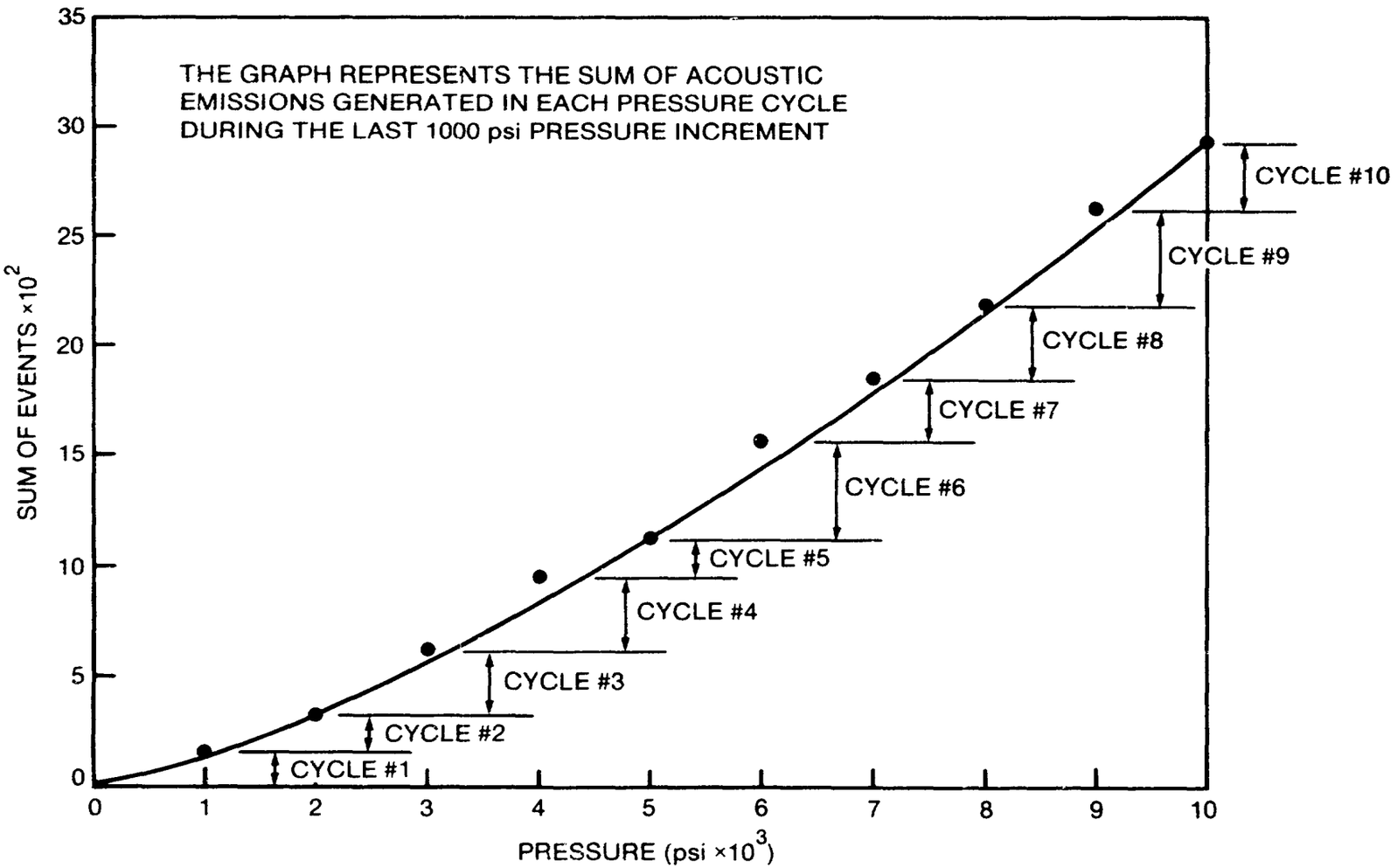

Figure 85. Acoustic events recorded during the first ten pressure cycles where the maximum pressure increased in each cycle by 1000 psi. Note that the number of acoustic events generated during the last 1000-psi pressure interval in each cycle was constant indicating material failure was not imminent in the 10,000-to 12,000-psi pressure range.

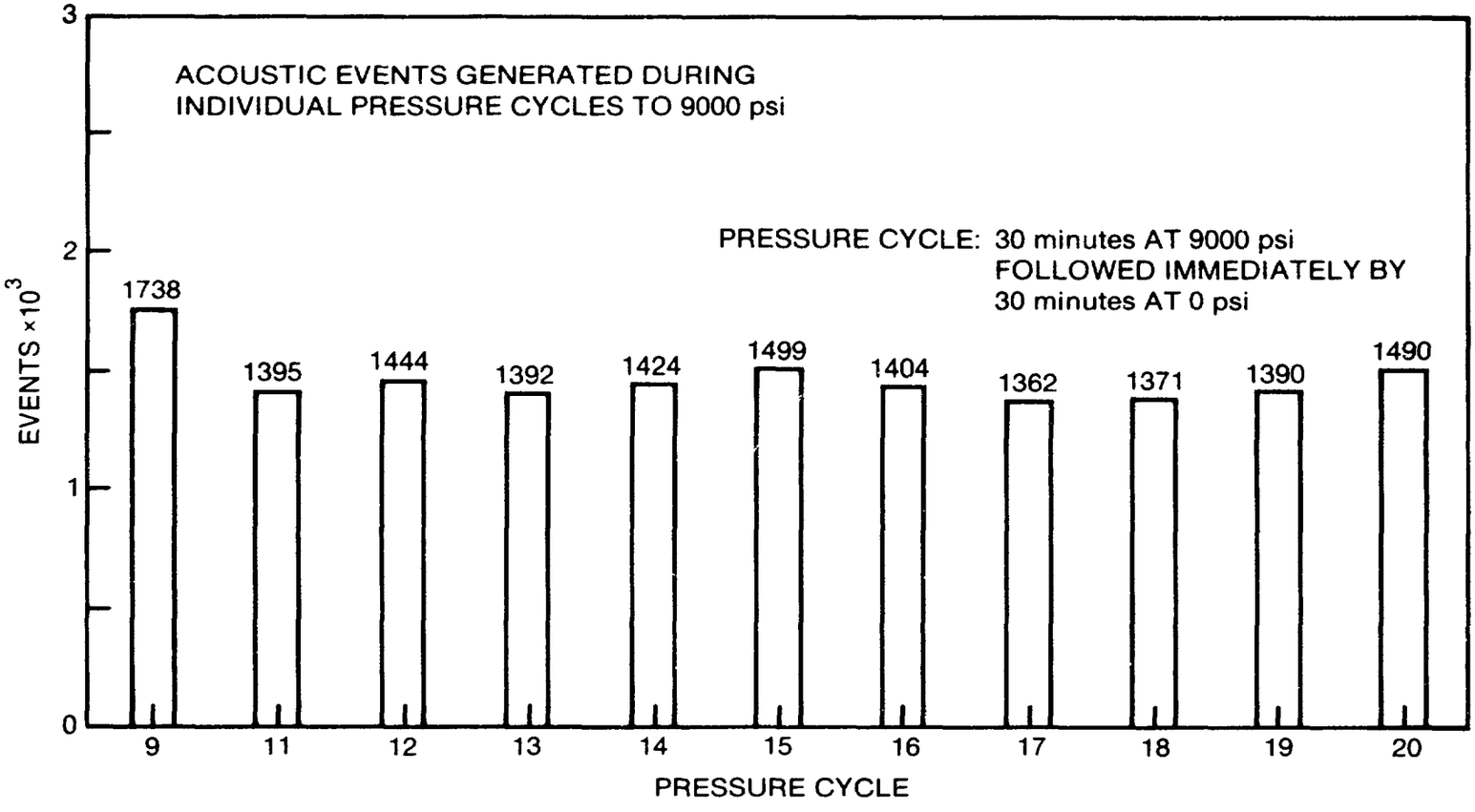

Figure 86. Acoustic events recorded during pressure cycling from 0 to 9000 psi. Note that the sum of events recorded during each cycle was approximately constant except for cycle No. 9 that preceded the proof test cycle No. 10 to 10,000 psi, indicating that no progressive material deterioration took place during pressure cycling.

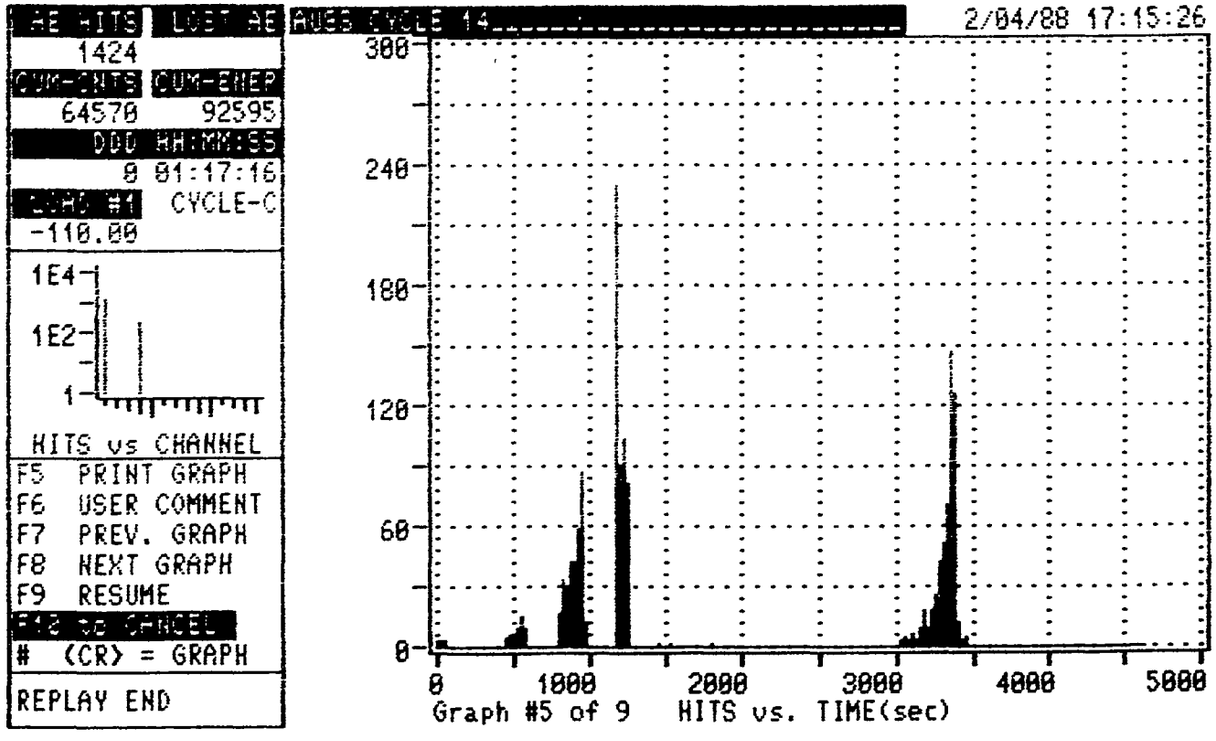

Figure 87. Distribution of acoustic events during pressure cycle No. 14 to 9000 psi.

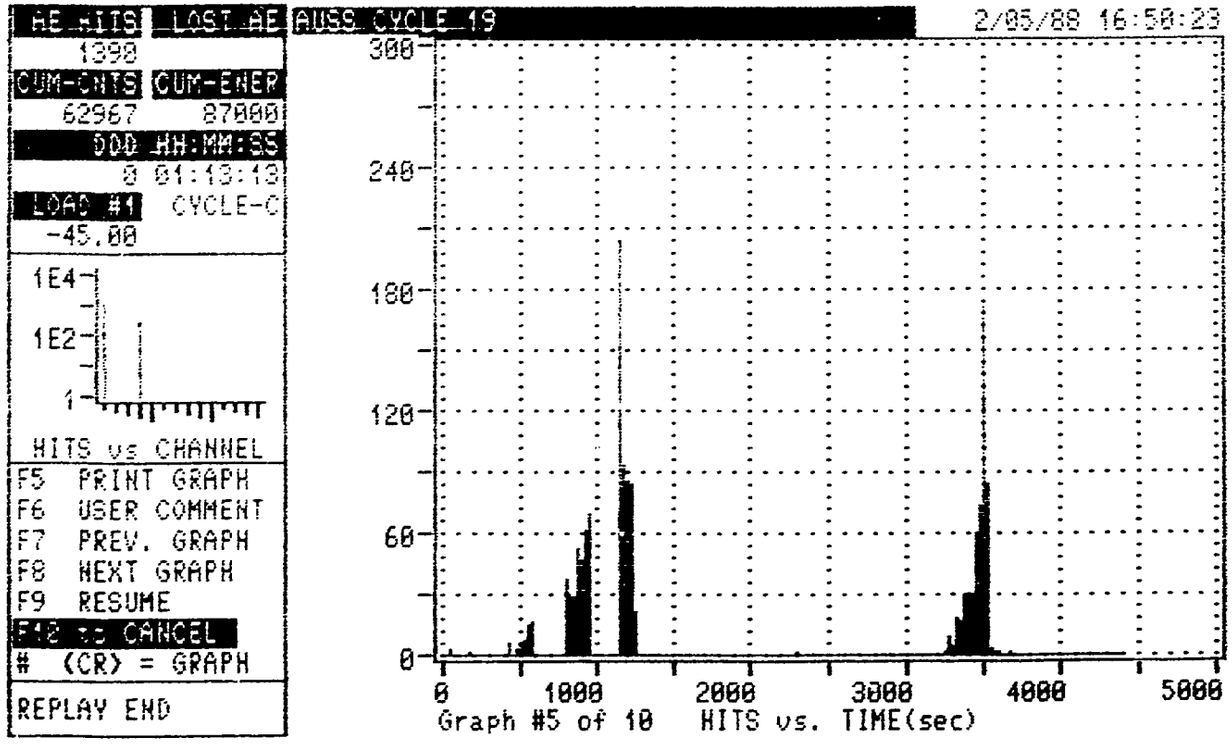

Figure 88. Distribution of acoustic events during pressure cycle No. 19 to 9000 psi. Note that the distribution is almost identical to cycle No. 14, indicating that these events are probably caused by relative movements between components of the pressure-hull assembly, rather than cracking of epoxy matrix or fibers inside the cylinder.

MOD2 02/03/87 9:51:50 AM START OF SUSTAINED LOADING

CHAN	0	1	2	3	4	5	6	7	8	9
	$$$$$$$ $$$$$$$	$$$$$$$ $$$$$$$	$$$$$$$ $$$$$$$	$$$$$$$ $$$$$$$	$$$$$$$ $$$$$$$	$$$$$$$ $$$$$$$	$$$$$$$ $$$$$$$	$$$$$$$ $$$$$$$	$$$$$$$ $$$$$$$	$$$$$$$ $$$$$$$
0	7044psi	-2618 ue	-2441 ue	-2854 ue	-2276 ue	-2717 ue	-2389 ue	-2685 ue	-2364 ue	-2752 ue
10	-2596 ue	-2704 ue	-2354 ue	-2714 ue	-2448 ue	-2643 ue	-2330 ue	-2347 ue	-2661 ue	-2350 ue
20	-2490 ue	-2324 ue	-2458 ue	-2345 ue	-2629 ue	-2331 ue	-2620 ue	-2335 ue	-2559 ue	-2325 ue
30	-2617 ue	-2321 ue	-3969 ue	-218 ue	-2201 ue	-336 ue	-9024 ue	-321 ue	-2204 ue	-127 ue
40	-2229 ue	-362 ue	-2215 ue	-132 ue	-2238 ue	-104 ue	-2213 ue	-209 ue	-2194 ue	-45 ue
50	-419 ue	7062psi	4803ml	$$$$$$$	$$$$$$$	$$$$$$$				

MOD2 02/03/87 10:23:43 AM END OF SUSTAINED LOADING

CHAN	0	1	2	3	4	5	6	7	8	9
	$$$$$$$ $$$$$$$	$$$$$$$ $$$$$$$	$$$$$$$ $$$$$$$	$$$$$$$ $$$$$$$	$$$$$$$ $$$$$$$	$$$$$$$ $$$$$$$	$$$$$$$ $$$$$$$	$$$$$$$ $$$$$$$	$$$$$$$ $$$$$$$	$$$$$$$ $$$$$$$
0	7008psi	-2578 ue	-2425 ue	-2832 ue	-2264 ue	-2695 ue	-2374 ue	-2665 ue	-2344 ue	-2735 ue
10	-2585 ue	-2672 ue	-2346 ue	-2689 ue	-2431 ue	-2613 ue	-2318 ue	-2329 ue	-2641 ue	-2333 ue
20	-2472 ue	-2309 ue	-2441 ue	-2327 ue	-2621 ue	-2312 ue	-2601 ue	-2319 ue	-2541 ue	-2308 ue
30	-2616 ue	-2306 ue	-3935 ue	-210 ue	-2174 ue	-309 ue	-8943 ue	-295 ue	-2182 ue	-110 ue
40	-2214 ue	-366 ue	-2195 ue	-130 ue	-2217 ue	-82 ue	-2184 ue	-215 ue	-2171 ue	-38 ue
50	-389 ue	7024psi	5369ml	$$$$$$$	$$$$$$$	$$$$$$$				

Figure 89. Strains and water displacement during sustained loading of AUSS Mod 2 pressure-hull assembly in Cycle No. 7 to 7000 psi.

MOD2 02/03/87 10:30:42 AM START OF RELAXATION

CHAN	0	1	2	3	4	5	6	7	8	9
	$$$$$$$ $$$$$$$	$$$$$$$ $$$$$$$	$$$$$$$ $$$$$$$	$$$$$$$ $$$$$$$	$$$$$$$ $$$$$$$	$$$$$$$ $$$$$$$	$$$$$$$ $$$$$$$	$$$$$$$ $$$$$$$	$$$$$$$ $$$$$$$	$$$$$$$ $$$$$$$
0	11psi	-17 ue	14 ue	21 ue	2 ue	13 ue	-27 ue	12 ue	1 ue	2 ue
10	26 ue	-6 ue	1 ue	-26 ue	-44 ue	7 ue	-11 ue	26 ue	29 ue	18 ue
20	22 ue	14 ue	12 ue	16 ue	0 ue	19 ue	16 ue	17 ue	22 ue	18 ue
30	-30 ue	19 ue	53 ue	-53 ue	24 ue	-144 ue	120 ue	-174 ue	10 ue	-64 ue
40	-1 ue	-198 ue	11 ue	-157 ue	15 ue	-32 ue	30 ue	-62 ue	36 ue	-46 ue
50	81 ue	20psi	1909ml	$$$$$$$	$$$$$$$	$$$$$$$				

MOD2 02/03/87 11:01:26 AM END OF RELAXATION

CHAN	0	1	2	3	4	5	6	7	8	9
	$$$$$$$ $$$$$$$	$$$$$$$ $$$$$$$	$$$$$$$ $$$$$$$	$$$$$$$ $$$$$$$	$$$$$$$ $$$$$$$	$$$$$$$ $$$$$$$	$$$$$$$ $$$$$$$	$$$$$$$ $$$$$$$	$$$$$$$ $$$$$$$	$$$$$$$ $$$$$$$
0	13psi	-9 ue	23 ue	24 ue	7 ue	18 ue	-17 ue	17 ue	6 ue	9 ue
10	35 ue	0 ue	9 ue	-5 ue	-28 ue	13 ue	-6 ue	29 ue	32 ue	20 ue
20	27 ue	19 ue	17 ue	20 ue	0 ue	22 ue	20 ue	21 ue	26 ue	21 ue
30	-22 ue	22 ue	58 ue	-46 ue	26 ue	-147 ue	112 ue	-162 ue	13 ue	-70 ue
40	7 ue	-194 ue	16 ue	-152 ue	19 ue	-31 ue	31 ue	-55 ue	38 ue	-42 ue
50	79 ue	20psi	800ml	$$$$$$$	$$$$$$$	$$$$$$$				

Figure 90. Strains and water displacement during relaxation of AUSS Mod 2 pressure hull assembly after sustained pressure loading in Cycle No. 7.

MOD1 CYCLE 7 03/06/86 11:47:56 AM START OF SUSTAINED LOADING

CHAN	0	1	2	3	4	5	6	7	8	9
0	7079psi	-3229ue	-3565ue	-3428ue	-3538ue	-3289ue	-3491ue	-3251ue	-3442ue	-3133ue
10	-3725ue	-3408ue	-3550ue	-3326ue	-3504ue	-3330ue	-3524ue	-3241ue	-4036ue	-3299ue
20	-3840ue	-3280ue	-3871ue	-3284ue	-3918ue	-3263ue	-4280ue	-3294ue	-4029ue	-3196ue
30	-3980ue	-3247ue	-4021ue	-3311ue	-3512ue	-3306ue	-3462ue	-3227ue	-3460ue	-3395ue
40	-3402ue	-3535ue	-3786ue	-3586ue	-3540ue	-3357ue	-3476ue	-3281ue	-3627ue	-148ue
50	-5346ue	476ue	-2916ue	-3417ue	-3179ue	-3377ue	-3367ue	-3762ue	-3039ue	-3209ue
60	-3746ue	-3099ue	-3792ue	-3132ue	-3875ue	977ue	-2923ue	1169ue	-2855ue	-6665ue
70	-2420ue	-2609ue	-2707ue	-1628ue	-2759ue	-2450ue	-2150ue	-2809ue	-1361ue	-2755ue
80	-1329ue	-2030ue	-2750ue	-3051ue	-3195ue	6ue	-4473ue	-1044ue	-2855ue	-249ue
90	-4386ue	-250ue	-4343ue	-912ue	-2867ue	81ue	-4410ue	281ue	-4350ue	-722ue
100	-2871ue	343ue	-4466ue	291ue	-4301ue	-522ue	-2879ue	274ue	-4470ue	7085psi
110	-5361cc	0$$$	0$$$	0$$$	0$$$	0$$$	0$$$	0$$$	0$$$	0$$$

MOD1 CYCLE 7 03/06/86 12:21:15 PM END OF SUSTAINED LOADING

CHAN	0	1	2	3	4	5	6	7	8	9
0	7039psi	-3207ue	-3547ue	-3409ue	-3521ue	-3270ue	-3474ue	-3231ue	-3426ue	-3114ue
10	-3707ue	-3389ue	-3536ue	-3309ue	-3490ue	-3314ue	-3510ue	-3227ue	-4015ue	-3281ue
20	-3818ue	-3265ue	-3850ue	-3268ue	-3897ue	-3252ue	-4261ue	-3279ue	-4010ue	-3170ue
30	-3961ue	-3229ue	-4001ue	-3293ue	-3496ue	-3291ue	-3447ue	-3215ue	-3446ue	-3386ue
40	-3395ue	-3515ue	-3771ue	-3571ue	-3528ue	-3340ue	-3459ue	-3276ue	-3608ue	-79ue
50	-4612ue	468ue	-2859ue	-3344ue	-3162ue	-3354ue	-3353ue	-3743ue	-3025ue	-3194ue
60	-3729ue	-3085ue	-3775ue	-3122ue	-3856ue	969ue	-2904ue	1163ue	-2838ue	-5733ue
70	-2405ue	-2593ue	-2535ue	-1619ue	-2746ue	-2437ue	-2139ue	-2794ue	-1356ue	-2740ue
80	-1325ue	-2020ue	-2736ue	-3035ue	-3180ue	-32ue	-4438ue	-1093ue	-2836ue	-265ue
90	-4352ue	-286ue	-4312ue	-953ue	-2847ue	57ue	-4375ue	266ue	-4315ue	-738ue
100	-2851ue	341ue	-4425ue	303ue	-4258ue	-634ue	-2859ue	249ue	-4431ue	7047psi
110	-5777cc	0$$$	0$$$	0$$$	0$$$	0$$$	0$$$	0$$$	0$$$	0$$$

Figure 91. Strains and water displacement during sustained loading of AUSS Mod 1 pressure-hull assembly in Cycle No. 7 to 7000 psi. Note that the strains in Mod 1 cylinder were 32.9 percent greater, indicating that Mod 2 pressure hull is approximately 33-percent stiffer; i.e., has a 33-percent higher resistance to buckling.

MOD1 CYCLE 7 03/06/86 12:38:57 PM START OF RELAXATION

CHAN	0	1	2	3	4	5	6	7	8	9
0	[illegible]	-1ue	-24ue	-16ue	-24ue	-18ue	-24ue	-18ue	-14ue	-27ue
10	27ue	-16ue	12ue	-10ue	-14ue	-15ue	-16ue	-3ue	1ue	-25ue
20	-3ue	-5ue	-2ue	-1ue	-3ue	10ue	-10ue	2ue	-4ue	6ue
30	-7ue	-30ue	10ue	-30ue	-14ue	30ue	-17ue	5ue	-19ue	-11ue
40	-1ue	-22ue	16ue	-23ue	-10ue	40ue	17ue	102ue	-93ue	310ue
50	-540ue	-34ue	0ue	14ue	-15ue	14ue	-18ue	-17ue	-17ue	22ue
60	-12ue	-5ue	-12ue	-16ue	-13ue	-17ue	-3ue	-3ue	-7ue	-2243ue
70	-16ue	-5ue	-15ue	-17ue	-19ue	-15ue	-17ue	-14ue	-16ue	-2ue
80	-22ue	-16ue	-20ue	-16ue	-16ue	-32ue	-27ue	-181ue	0ue	-71ue
90	3ue	-32ue	-5ue	-206ue	3ue	-39ue	15ue	2ue	7ue	-54ue
100	11ue	13ue	-1ue	13ue	3ue	-15ue	16ue	-32ue	50ue	10ps1
110	-55cc	0SSS	0SSS	0SSS	0SSS	0SSS	0SSS	0SSS	0SSS	0SSS

MOD1 CYCLE 7 03/06/86 1:28:38 PM END OF RELAXATION

CHAN	0	1	2	3	4	5	6	7	8	9
0	[illegible]	-9ue	-13ue	-20ue	30ue	15ue	-20ue	-14ue	-9ue	-25ue
10	-23ue	-3ue	-5ue	-1ue	-7ue	-4ue	-9ue	1ue	3ue	-24ue
20	-3ue	-1ue	3ue	2ue	-7ue	19ue	-5ue	7ue	1ue	2ue
30	-3ue	-27ue	-7ue	-21ue	-11ue	-23ue	-12ue	12ue	-14ue	-2ue
40	3ue	-13ue	-12ue	-13ue	-3ue	-31ue	-12ue	154ue	-118ue	266ue
50	-538ue	-24ue	3ue	0ue	-13ue	-10ue	-15ue	-13ue	-14ue	-16ue
60	-3ue	5ue	-5ue	-3ue	-9ue	-15ue	1ue	-10ue	-4ue	-2582ue
70	-14ue	-7ue	-13ue	-16ue	-15ue	-14ue	-16ue	-11ue	-13ue	2ue
80	-18ue	-13ue	-17ue	-13ue	-14ue	-29ue	-29ue	-125ue	-3ue	-59ue
90	1ue	57ue	-5ue	-147ue	1ue	-49ue	12ue	-17ue	4ue	-57ue
100	3ue	6ue	3ue	-10ue	0ue	-31ue	15ue	-40ue	42ue	8ps1
110	-2cc	0SSS	0SSS	0SSS	0SSS	0SSS	0SSS	0SSS	0SSS	0SSS

Figure 92. Strains and water displacement during relaxation of AUUS Mod 1 pressure-hull assembly in Cycle No. 7.

APPENDIX A

AUSS CYLINDER DESIGN ANALYSIS

WAYLAND BLAKE

OAK RIDGE NATIONAL LABORATORY
ENRICHMENT TECHNOLOGY APPLICATIONS CENTER

SECOND ANNUAL
"THICK COMPOSITES IN COMPRESSION" WORKSHOP

JULY 12-13, 1988

OAK RIDGE, TENNESSEE

PART I

CONCEPTUAL CASE

AUSS MODEL SUBSCALE CYLINDER DESIGN APPROACH

MATERIAL SCREENING AND SELECTION

UTILIZE 0/90 LAYUP TO MAXIMIZE STIFFNESS FOR BUCKLING RESISTANCE

FINITE ELEMENT STRESS ANALYSIS OF CYLINDER (2:1 PLY RATIO)

FINITE ELEMENT STRESS ANALYSIS OF TEST ASSEMBLY (CYLINDER+RINGS+END DOMES)

APPLY 2-D FAILURE CRITERIA AT INNER AND OUTER RADII SEPARATELY TO DETERMINE OPTIMUM PLY RATIOS USING FINITE ELEMENT DERIVED STRESSES

OPTIMUM RATIO CORRESPONDS TO TRANSITION FROM HOOP TO AXIAL FIRST PLY FAILURE

SUBDIVIDE WALL THICKNESS INTO TWO LAYERS WITH DIFFERENT PLY RATIOS

SET POSITION OF INTERFACE BETWEEN TWO DIFFERENT PLY RATIOS BASED ON CYLINDER EDGE AND MIDPLANE AXIAL STRESS DISTRIBUTIONS

REPEAT FINITE ELEMENT STRESS ANALYSES FOR TWO-LAYER DESIGN

RING COMPRESSION SPECIMEN

DENSITY AND FIBER FRACTION

MATERIAL	DENSITY, lb/in3	VF
IM6/ERL2258/MPDA	0.0569	.70
T40/ERL2258/MPDA	0.0594	.71
IM6/ERX4903/MPDA	0.571	.68
T40/ERX4903/MPDA	0.597	.70

RING COMPRESSION TEST

ULTIMATE STRAIN DATA

MATERIAL	ϵ_{ULT}, %	C.V. %
IM6/ERL2258/MPDA	1.02	5.8
T40/ERL2258/MPDA	0.91	10.0
IM6/ERX4903/MPDA	1.09	3.5
T40/ERX4903/MPDA	1.02	16.8

CONCEPTUAL CASE

FINITE ELEMENT STRESS ANALYSIS OF CYLINDER

A8

IM6/ERL2258 0/90 2:1 LAYUP

1/2 CYLINDER MODEL (SYMMETRY BOUNDARY CONDITION AT MIDBAY

10,000 PSI EXTERNAL PRESSURE

UNIFORM END PRESSURE - (10,000 PSI) X AREA RATIO

INCREMENTAL LOADING - FINITE DEFORMATION - INFINITESIMAL STRAINS

CONCEPTUAL CASE

1. Layup ratio for fiber layers 2.0:1.0 with 90/0 degree orientations.

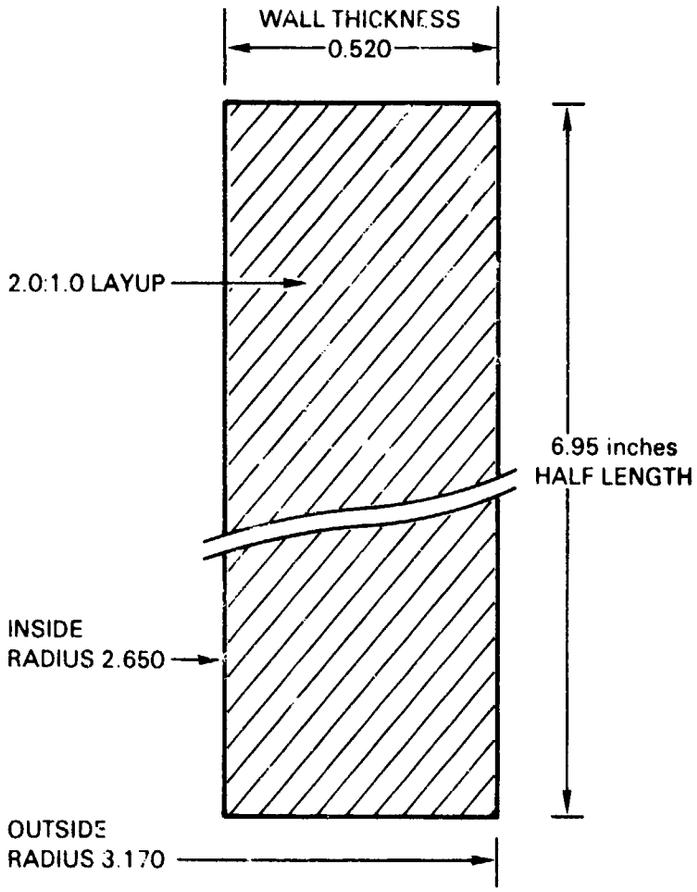

CONCEPTUAL CASE

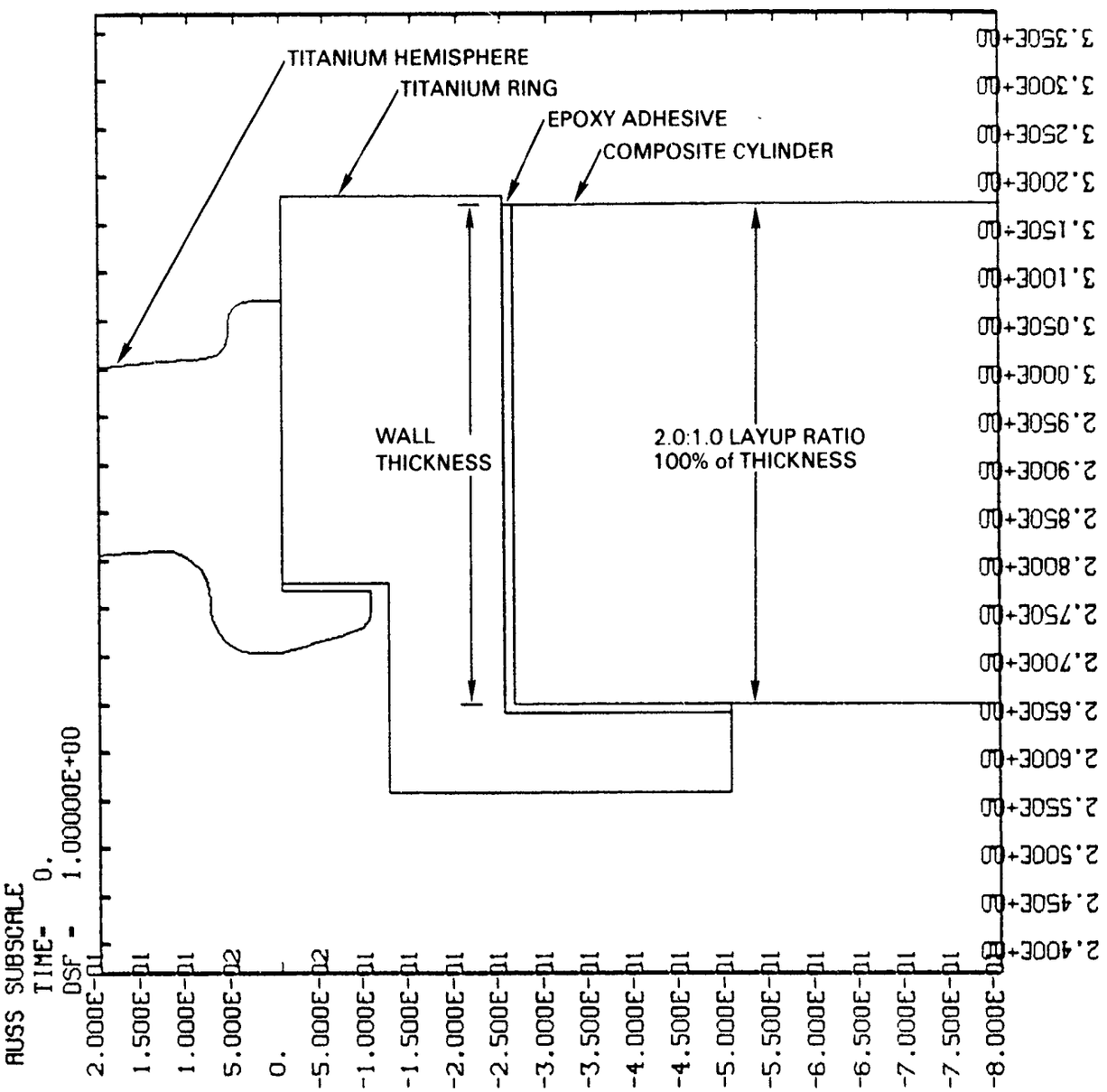

CONCEPTUAL CASE

2-D LAYER PROPERTIES USED AS BASIS FOR 2-D LAMINATE ANALYSIS

IM6/ERL2258/MPDA $V_F = 0.7$

$E_L = 24.67$ Msi	$(\sigma_L)_{Tu} = 460$ Ksi
$E_T = 1.55$ Msi	$(\sigma_L)_{Cu} = 250$ Ksi
$G_{LT} = 0.935$ Msi	$(\sigma_T)_{Tu} = 6$ Ksi
$\nu_{LT} = 0.311$	$(\sigma_T)_{Cu} = 30$ Ksi
$\nu_{TT} = 0.374$	$(\tau_{LT})_u = 7$ Ksi

CONCEPTUAL CASE

PLY RATIO OPTIMIZATION RESULTS
IM6/ERL2258

	FAILURE RATIO*			
	I.D.		O.D.	
PLY RATIO	RATIO	MODE	RATIO	MODE
2:1	2.67**	H	2.79	A
2.4:1	2.80	H/A	2.51	A
1.9:1	2.63	H	2.87	H/A

*HASHIN PLANE STRESS INTERACTION CRITERIA
**ALL FAILURE RATIOS REFERRED TO 10000 PSIG

CONCEPTUAL CASE

3-D Orthotropic Elastic Constants
0/90 2:1 Layup (volume averaged)

E_R = 1.75 Msi	ν_{RO} = 0.040
E_O = 17.04 Msi	ν_{OR} = 0.393
E_Z = 9.30 Msi	ν_{OZ} = 0.052
G_{RO} = 0.811 Msi	ν_{ZO} = 0.028
G_{OZ} = 0.935 Msi	ν_{ZR} = 0.386
G_{RZ} = 0.688 Msi	ν_{RZ} = 0.072
ρ = 0.577 lb/in^3	

fiber volume = 0.7

ORNL/ETAC
H.W. Blake
7/11/88

CONCEPTUAL CASE

AUSS SUBSCALE ASSEMBLY

COMPONENT RADIAL DISPLACEMENT
P = 10,000 PSIG

COMPONENT	U_r
HEMISHELL	0.0075 IN.
RING	0.009 IN.
CYLINDER	0.010 IN.

CONCLUSION: RADIAL DISPLACEMENT MISMATCH CAUSES SHEAR STRESS ON END OF TUBE

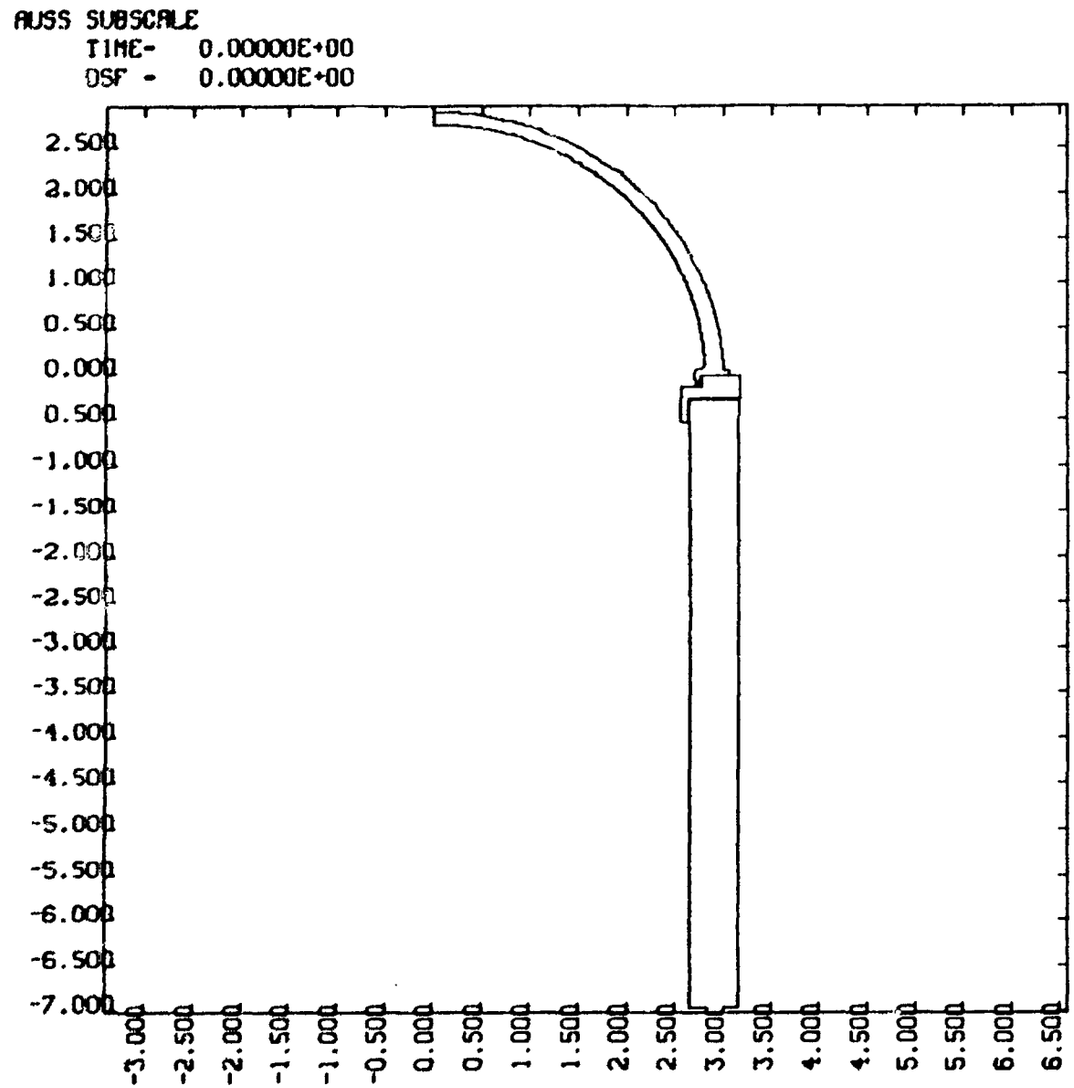

CONCEPTUAL CASE

Stress Analysis

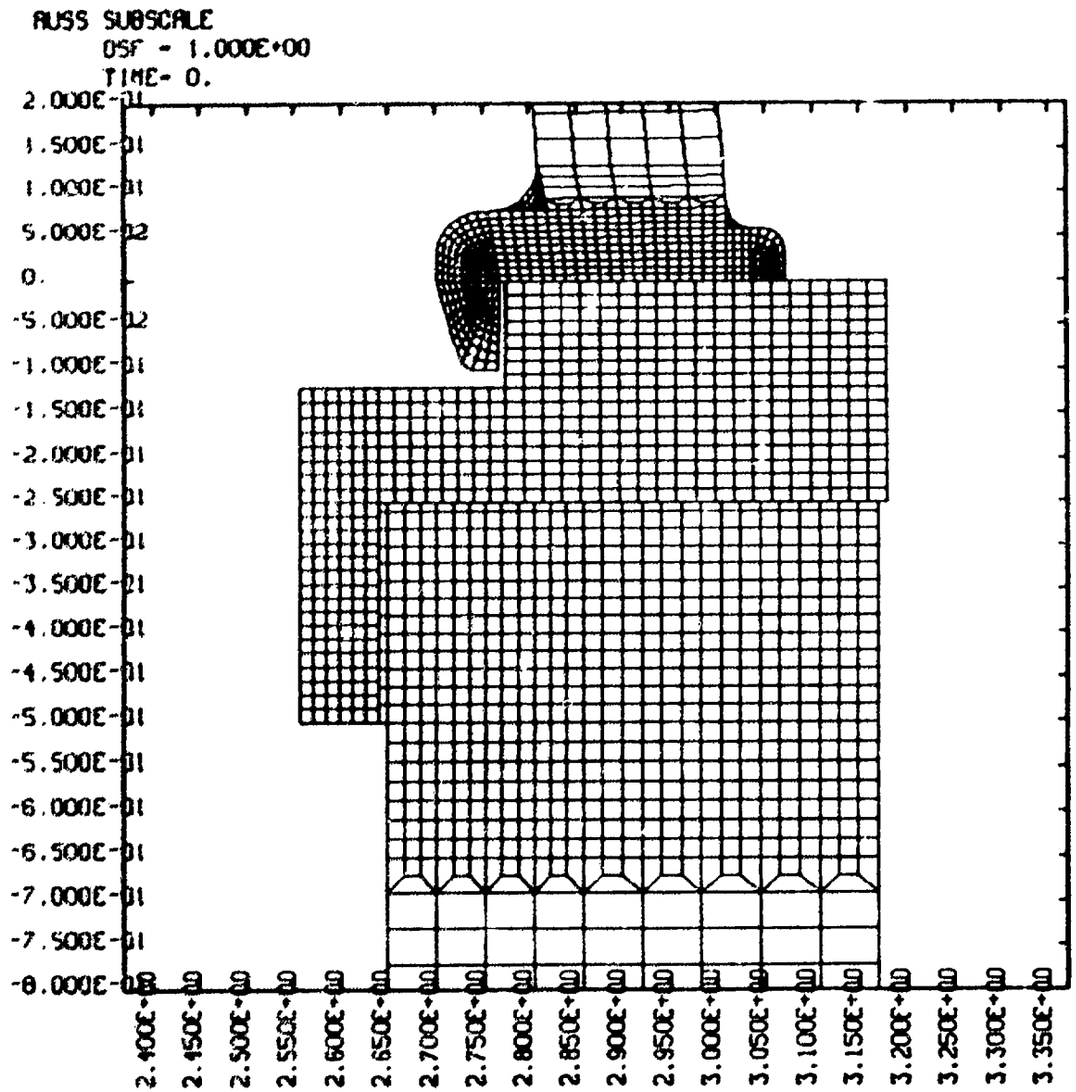

CONCEPTUAL CASE

Stress Analysis

CONCEPTUAL CASE

Stress Values* at Cylinder Midbay

Radius	Hoop Stress (psi)	Axial Stress (psi)	H/A Ratio
Inside	-64,950	-31,300	2.075
Outside	-59,500	-34,700	1.715

Layup ratio between hoop and axial fibers for the whole thickness 2.0:1.0

Stress ratio is lower at outside radius than at inside radius. Optimum ply ratio should be different for inside and outside.

*All stress values referred to 10,000 psig pressure

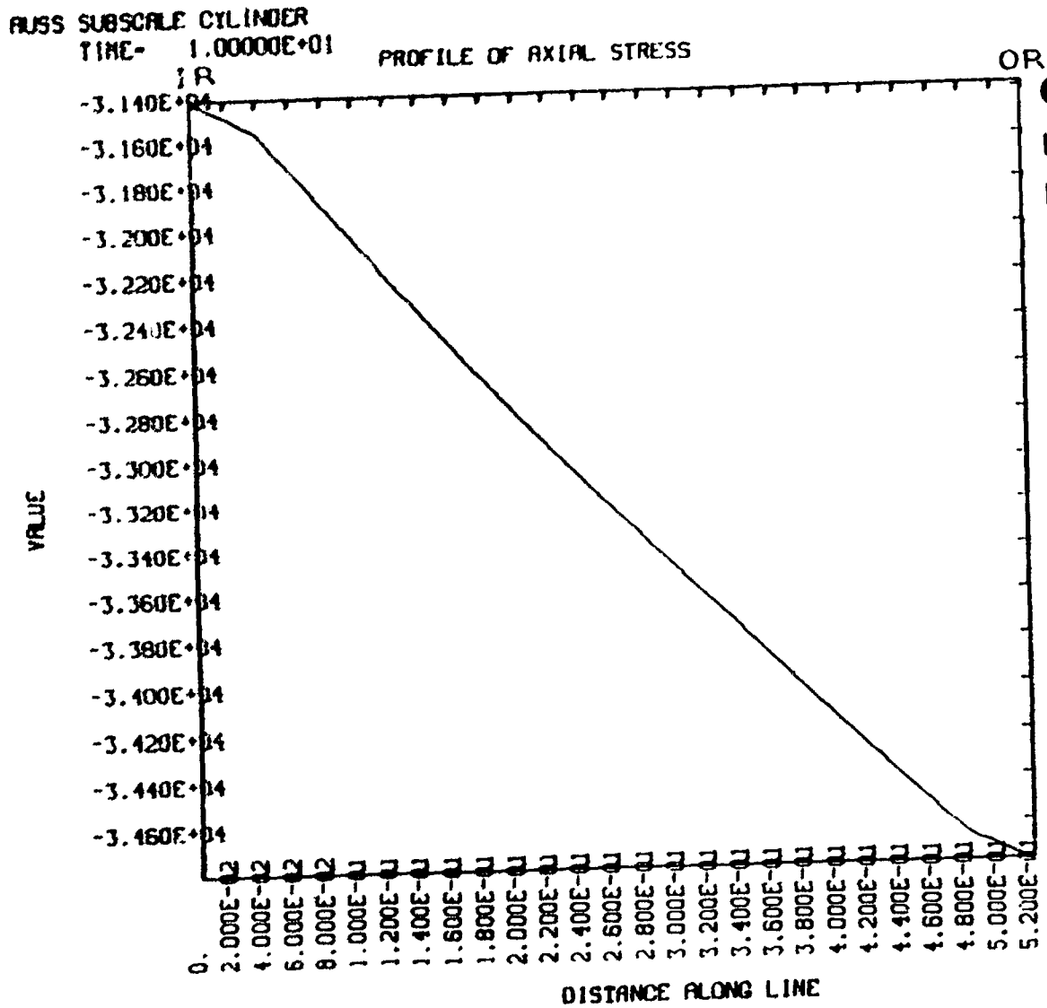

CONCEPTUAL CASE

Location: Cylinder, midbay

Presure: 10,000 psi

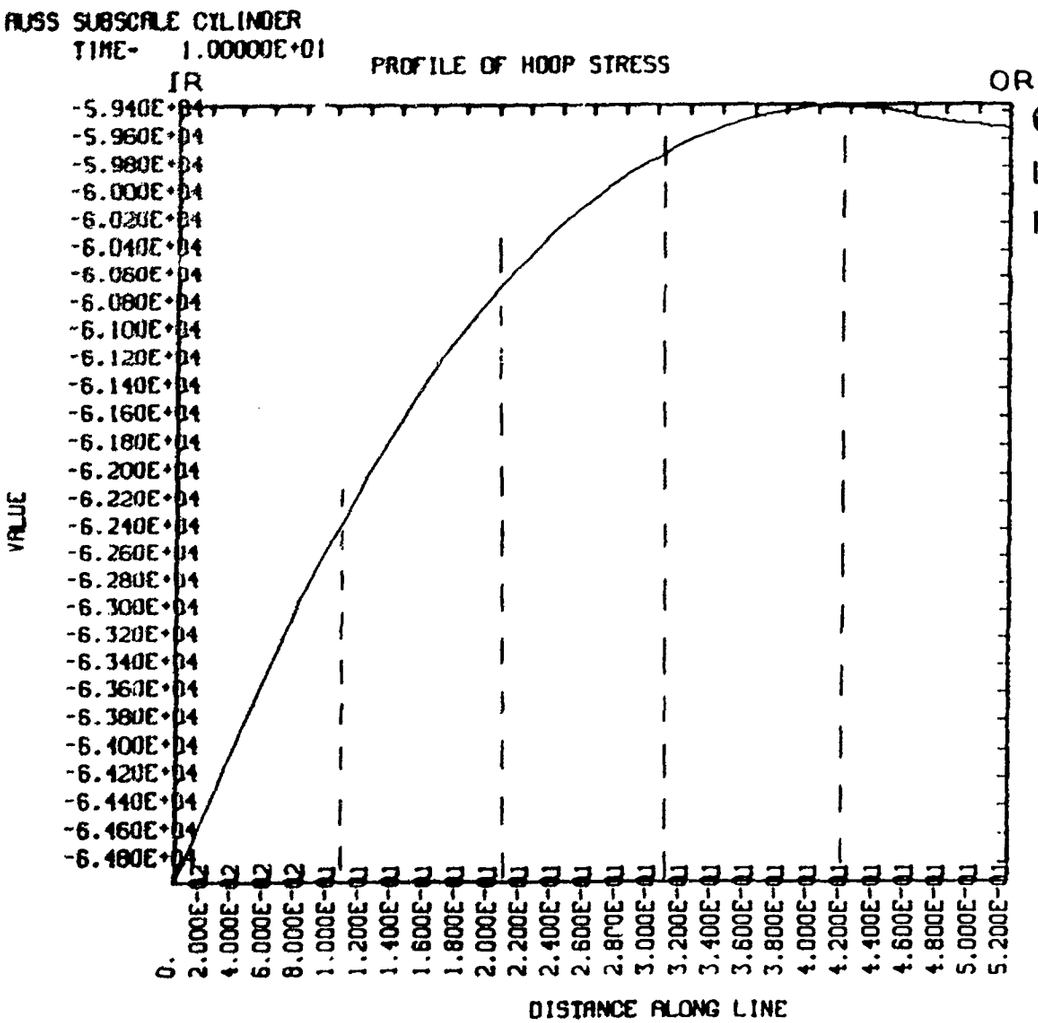

CONCEPTUAL CASE

Location: Cylinder, midbay

Presure: 10,000 psi

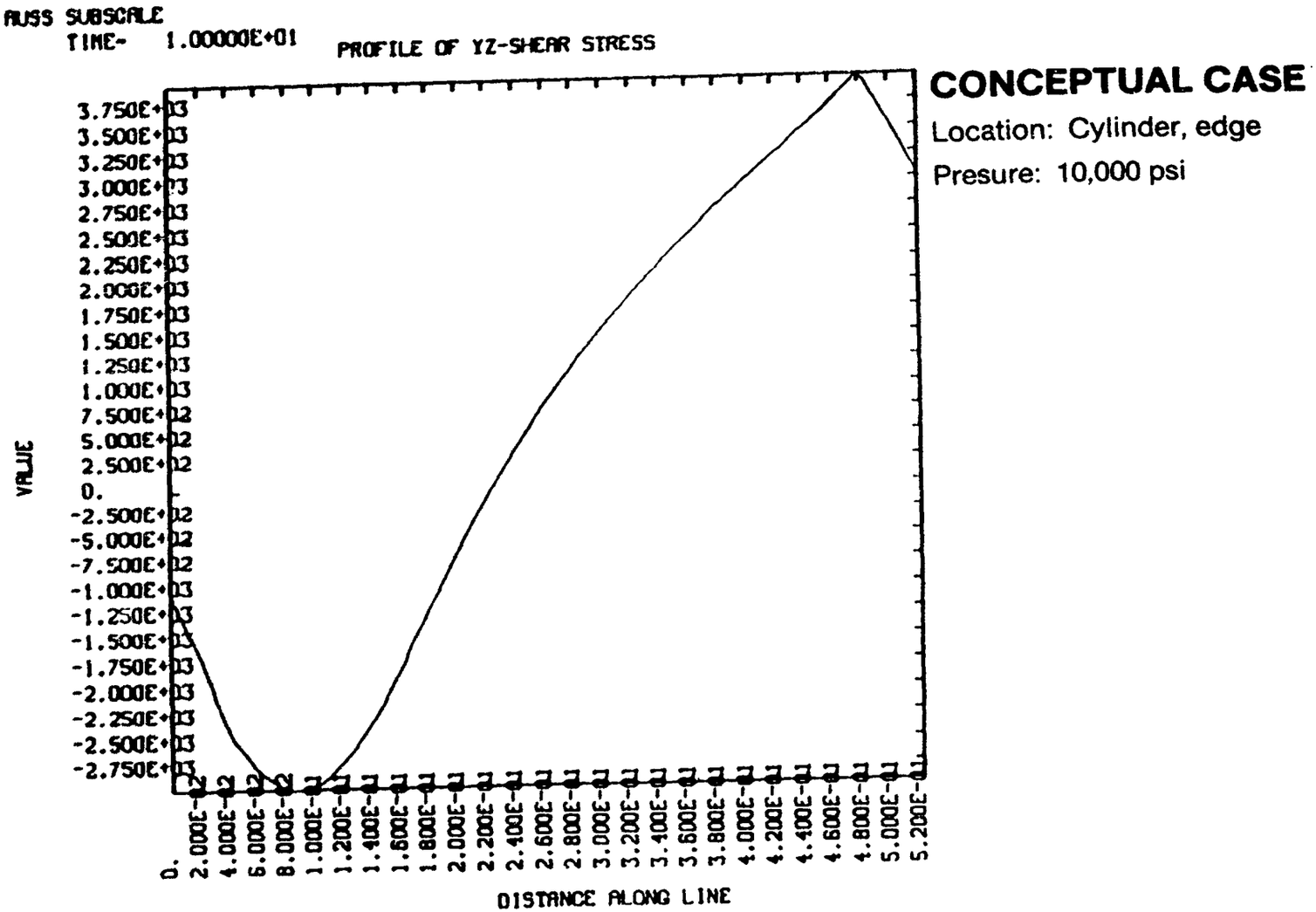

CONCEPTUAL CASE

Location: Cylinder, edge

Presure: 10,000 psi

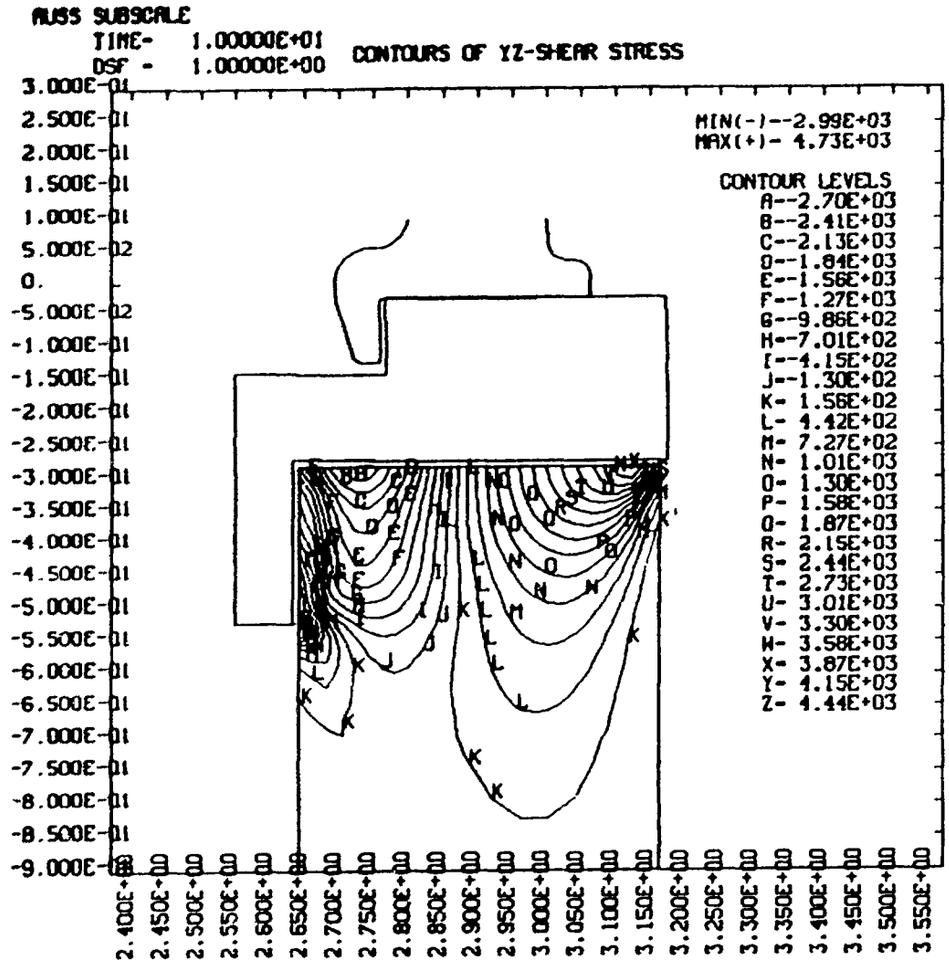

CONCEPTUAL CASE

Location: Cylinder, end

Presure: 10,000 psi

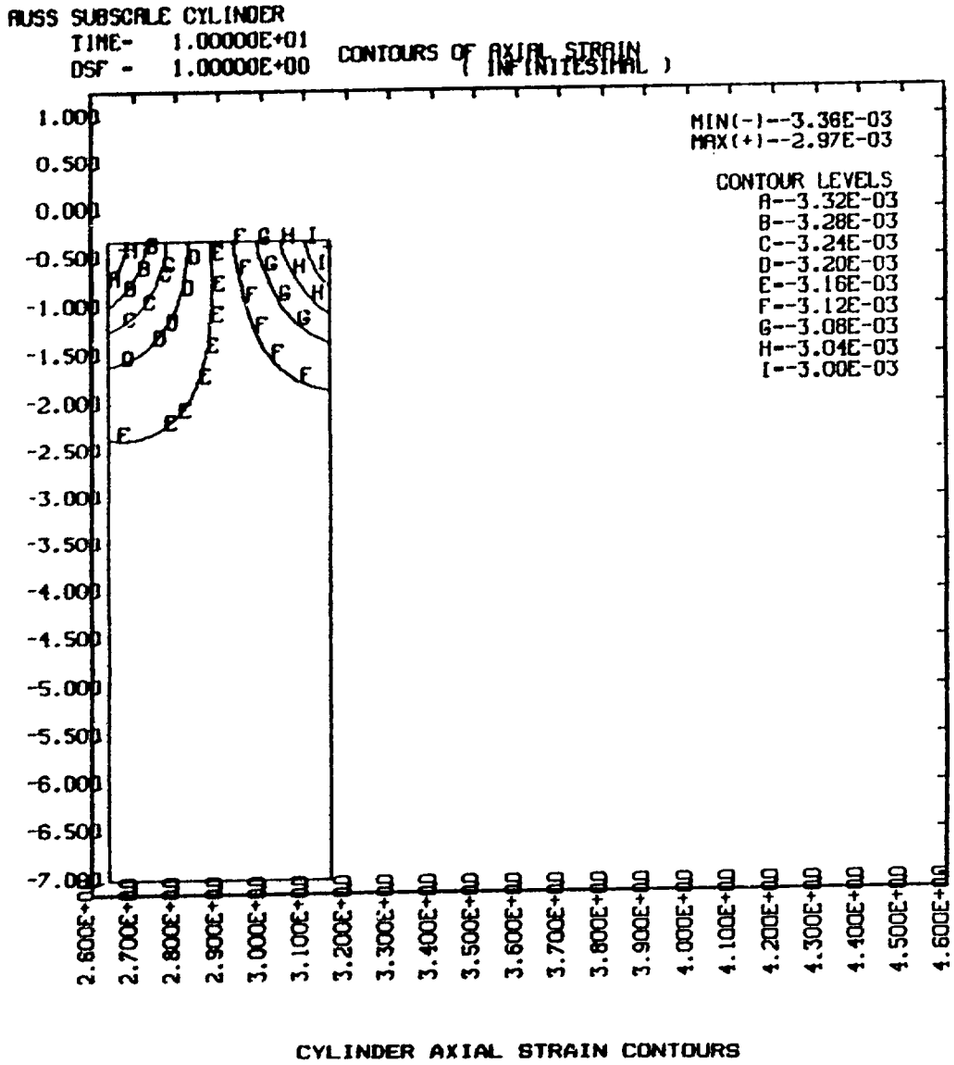

CYLINDER AXIAL STRAIN CONTOURS

CONCEPTUAL CASE

Location: Cylinder, end

Presure: 10,000 psi

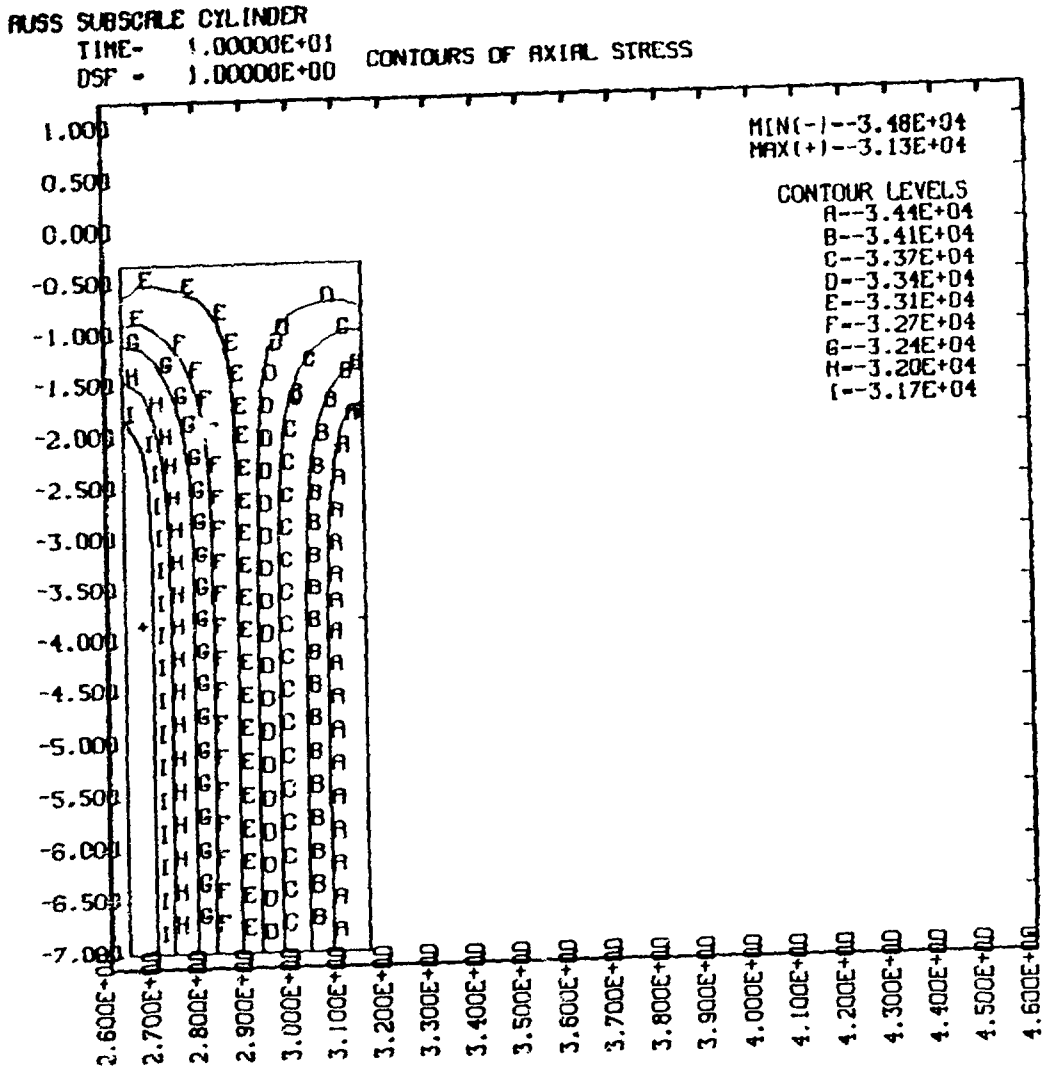

CYLINDER AXIAL STRESS CONTOURS

CONCEPTUAL CASE

Location: Cylinder, end

Presure: 10,000 psi

PART II

DESIGN CASE

DESIGN CASE

1. Layup ratios for fiber layers 2.4:1.0/1.9:1.0 with 90/0 degree orientations.
2. Thickness ratio of layup layers — 40:60.

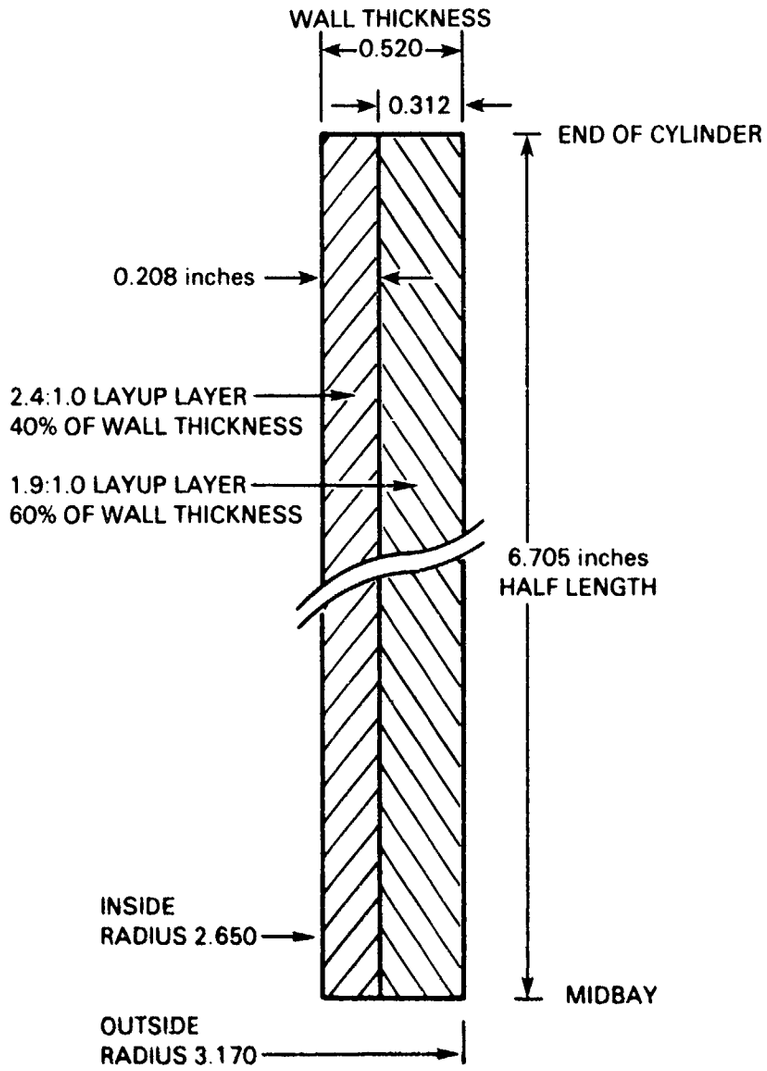

DESIGN CASE

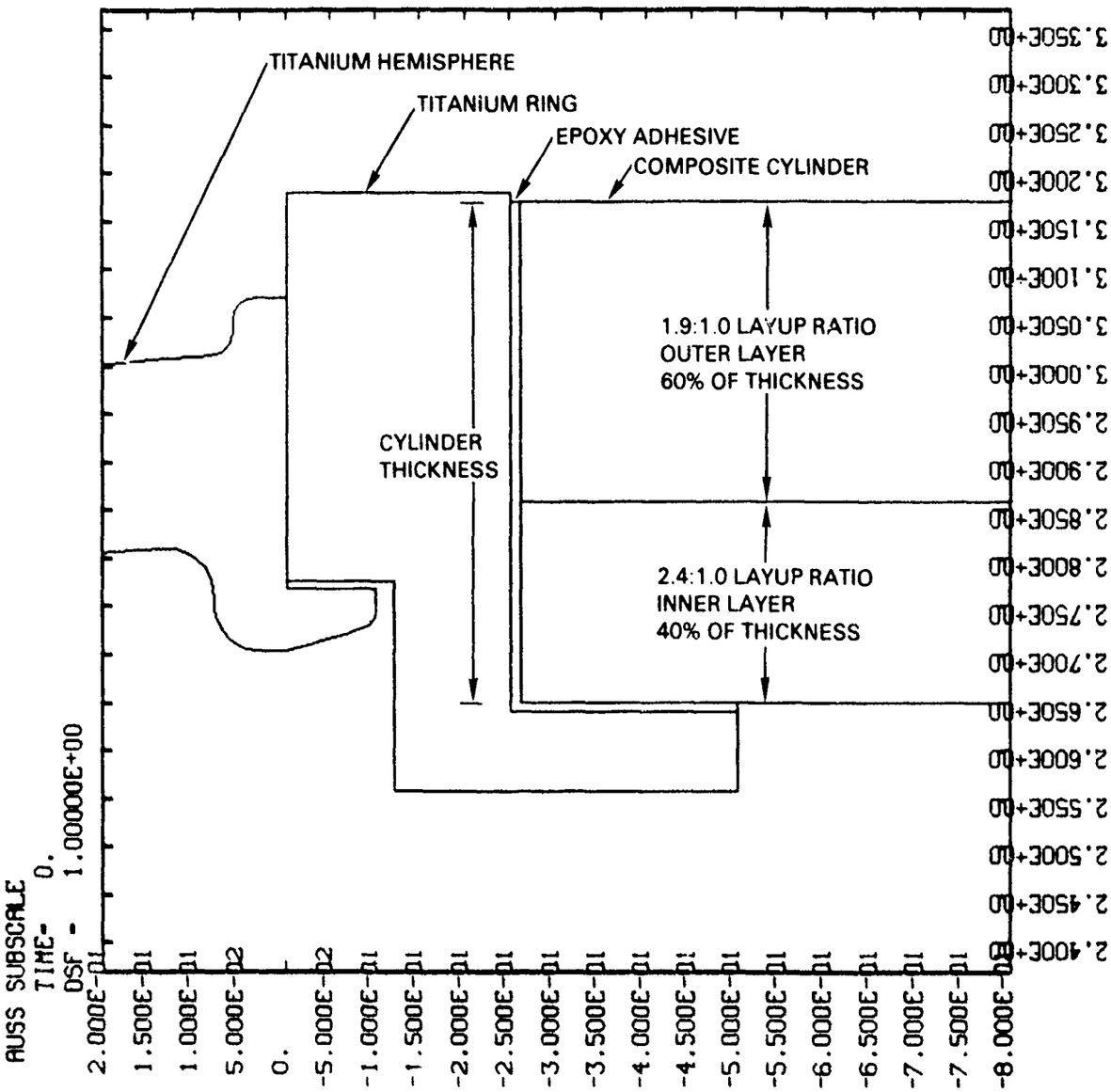
TITANIUM HEMISPHERE
TITANIUM RING
EPOXY ADHESIVE
COMPOSITE CYLINDER
CYLINDER THICKNESS
1.9:1.0 LAYUP RATIO
OUTER LAYER
60% OF THICKNESS
2.4:1.0 LAYUP RATIO
INNER LAYER
40% OF THICKNESS
AUSS SUBSCALE
TIME= 0.
DSF = 1.000000E+00

DESIGN CASE

3-D Orthotropic Elastic Constants
0/90 2.4:1.0 Layup (volume averaged)

E_R	= 1.74 Msi	ν_{RO}	= 0.038
E_0	= 17.95 Msi	ν_{OR}	= 0.393
E_Z	= 8.39 Msi	ν_{OZ}	= 0.058
G_{RO}	= 0.826 Msi	ν_{ZO}	= 0.027
G_{OZ}	= 0.935 Msi	ν_{ZR}	= 0.385
G_{RZ}	= 0.673 Msi	ν_{RZ}	= 0.080

ρ = 0.0577 lb/in^3

fiber volume = 0.7

DESIGN CASE

3-D Orthotropic Elastic Constants
0/90 1.9:1.0 Layup (volume averaged)

E_R = 1.75 Msi	ν_{RO} = 0.041
E_O = 16.78 Msi	ν_{OR} = 0.393
E_Z = 9.57 Msi	ν_{OZ} = 0.050
G_{RO} = 0.807 Msi	ν_{ZO} = 0.029
G_{OZ} = 0.935 Msi	ν_{ZR} = 0.387
G_{RZ} = 0.692 Msi	ν_{RZ} = 0.071

ρ = 0.0577 lb/in^3

fiber volume = 0.7

DESIGN CASE

Stress Values* at Cylinder Midbay

Radius	*Hoop Stress (psi)	Axial Stress (psi)	H/A Ratio
Inside	-67,500	-29,000	2.32
Outside	-58,000	-36,000	1.61

Layup ratios between hoop and axial fibers

Inner Layer	2.4:1.0
Outer Layer	1.9:1.0

Thickness ratio of inner and outer layers 40:60

*All stress values referred to 10,000 psig pressure

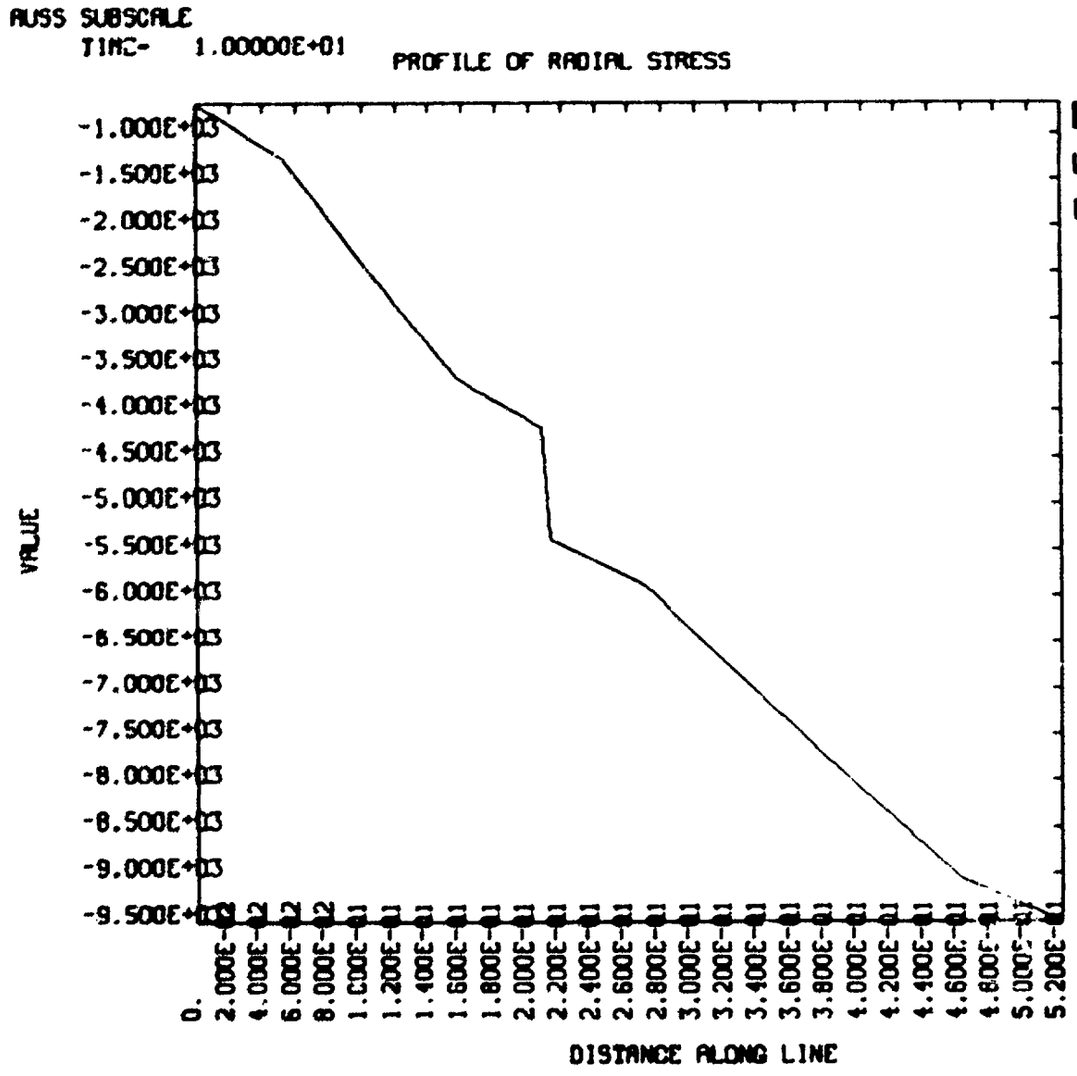

DESIGN CASE

Location: Cylinder, midbay

Pressure: 10,000 psi

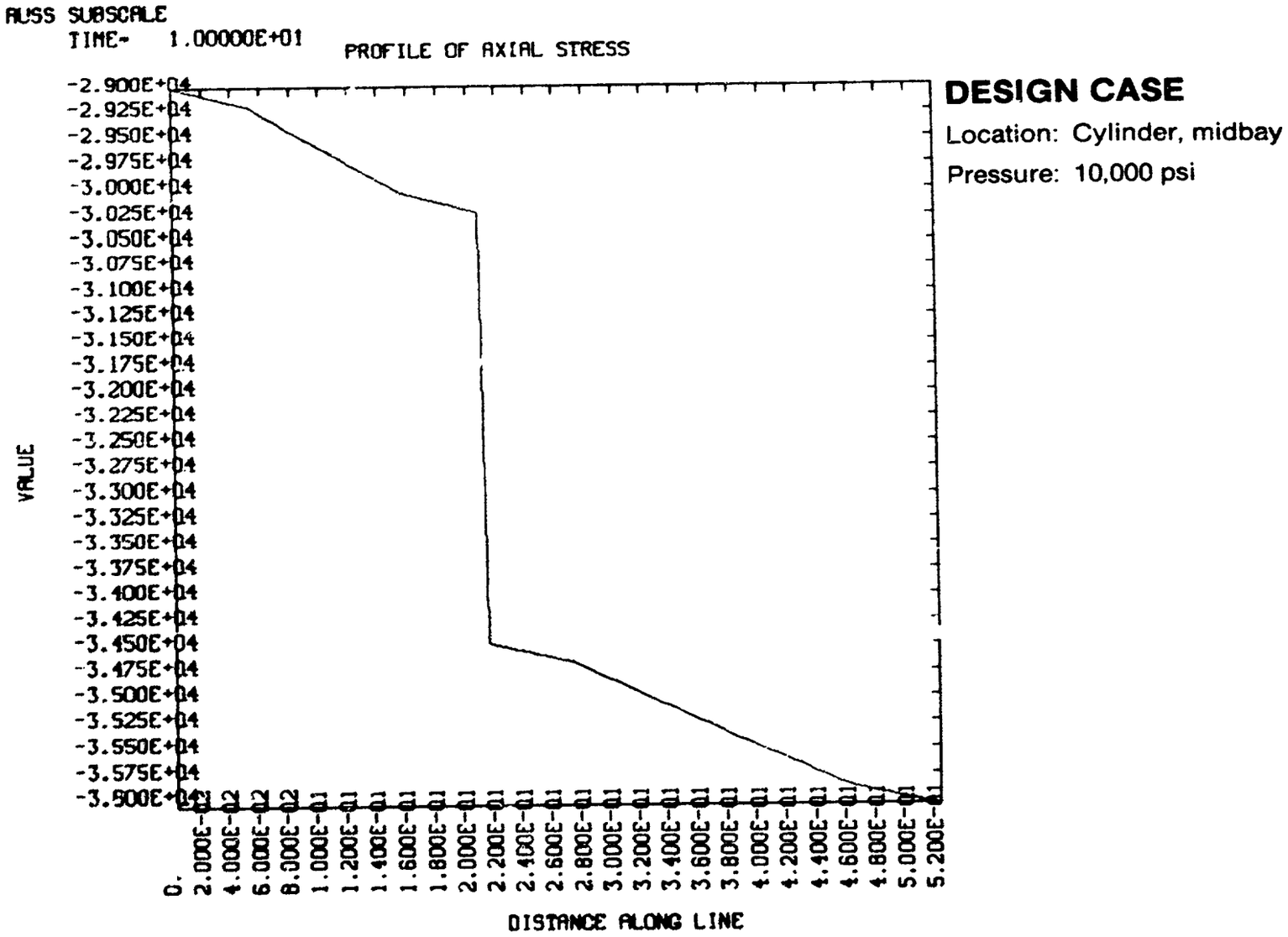

DESIGN CASE

Location: Cylinder, midbay

Pressure: 10,000 psi

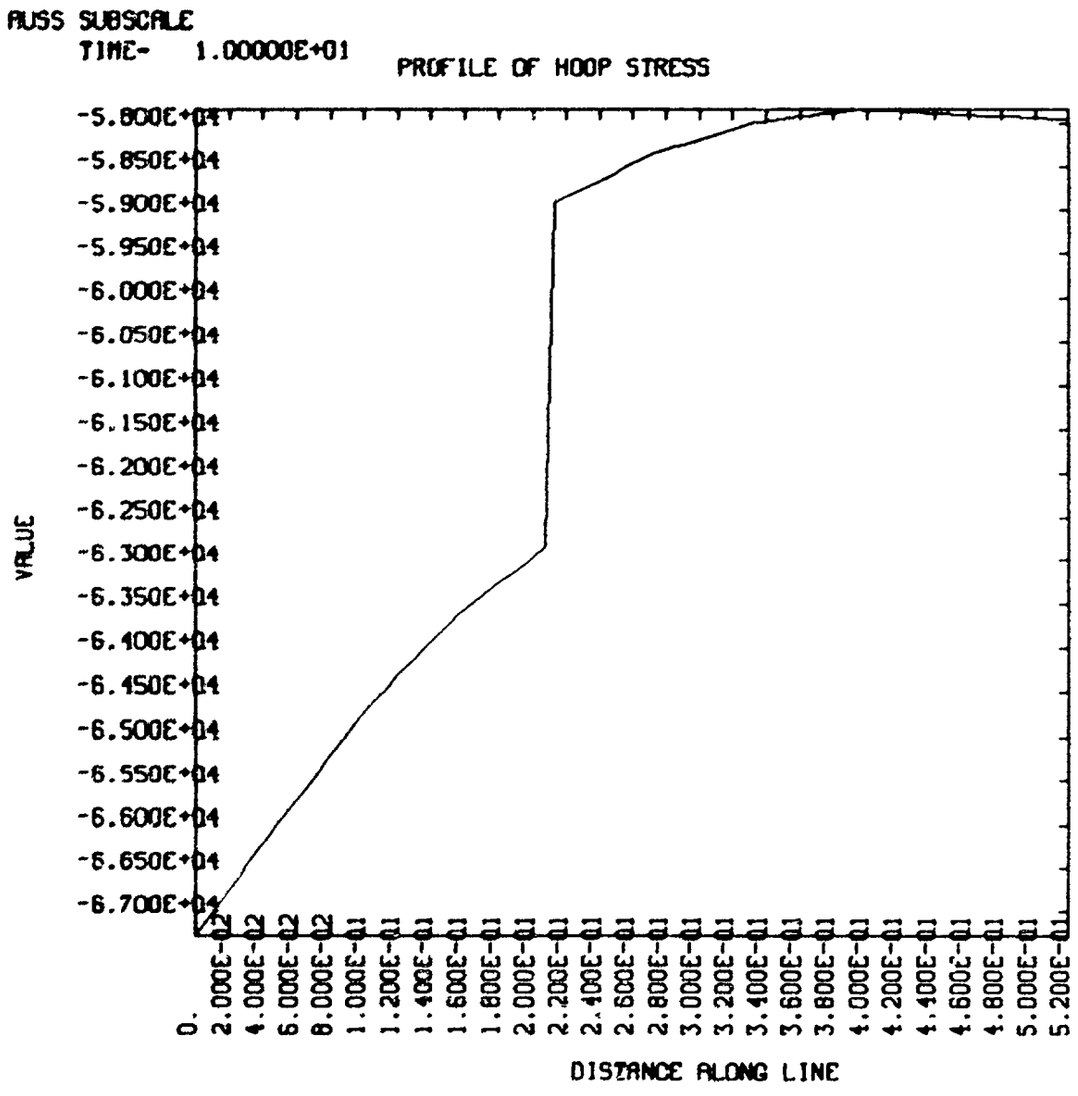

DESIGN CASE

Location: Cylinder, midbay

Pressure: 10,000 psi

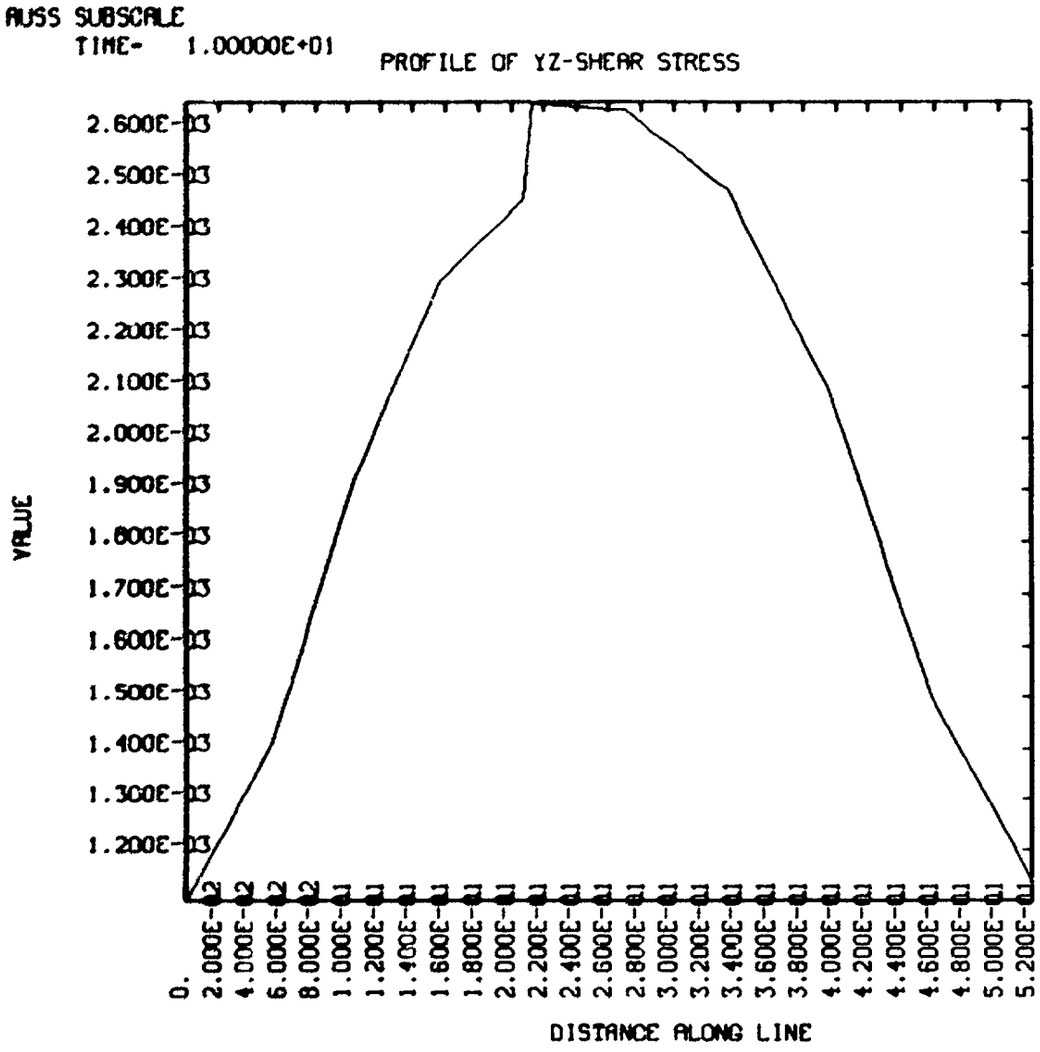

DESIGN CASE

Location: Cylinder, midbay

Pressure: 10,000 psi

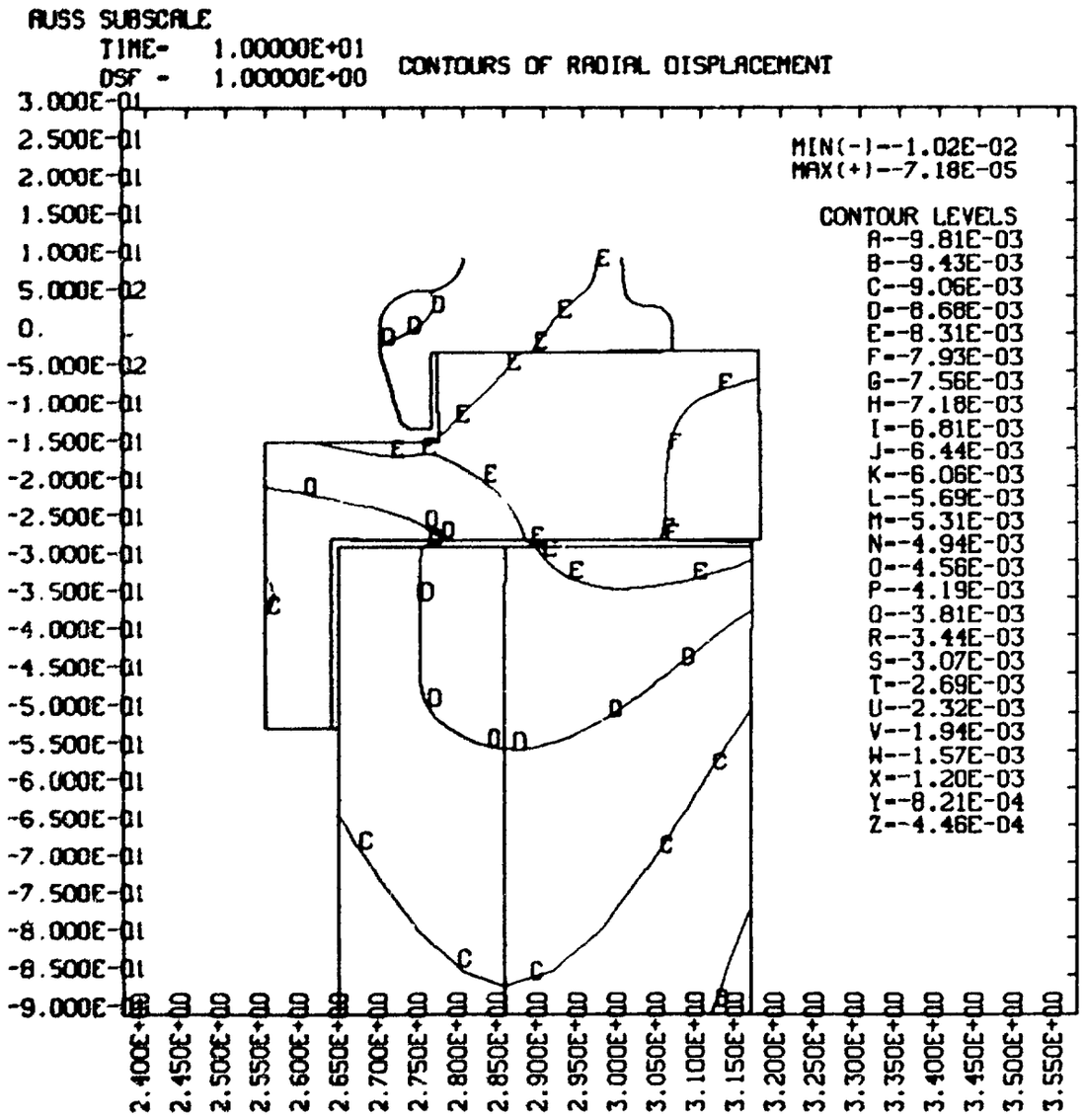

DESIGN CASE

Location: Cylinder, end

Pressure: 10,000 psi

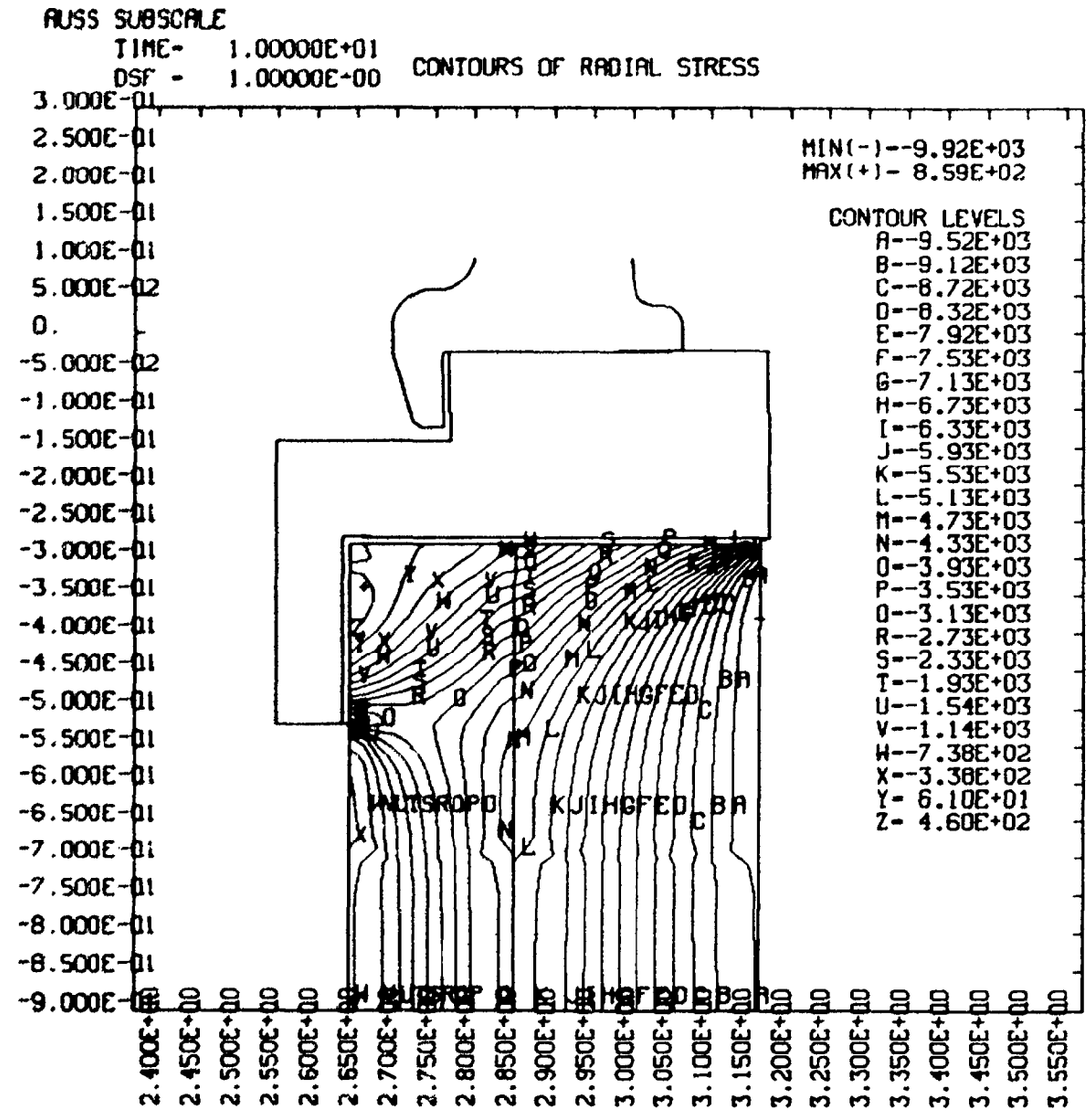

DESIGN CASE

Location: Cylinder, end

Pressure: 10,000 psi

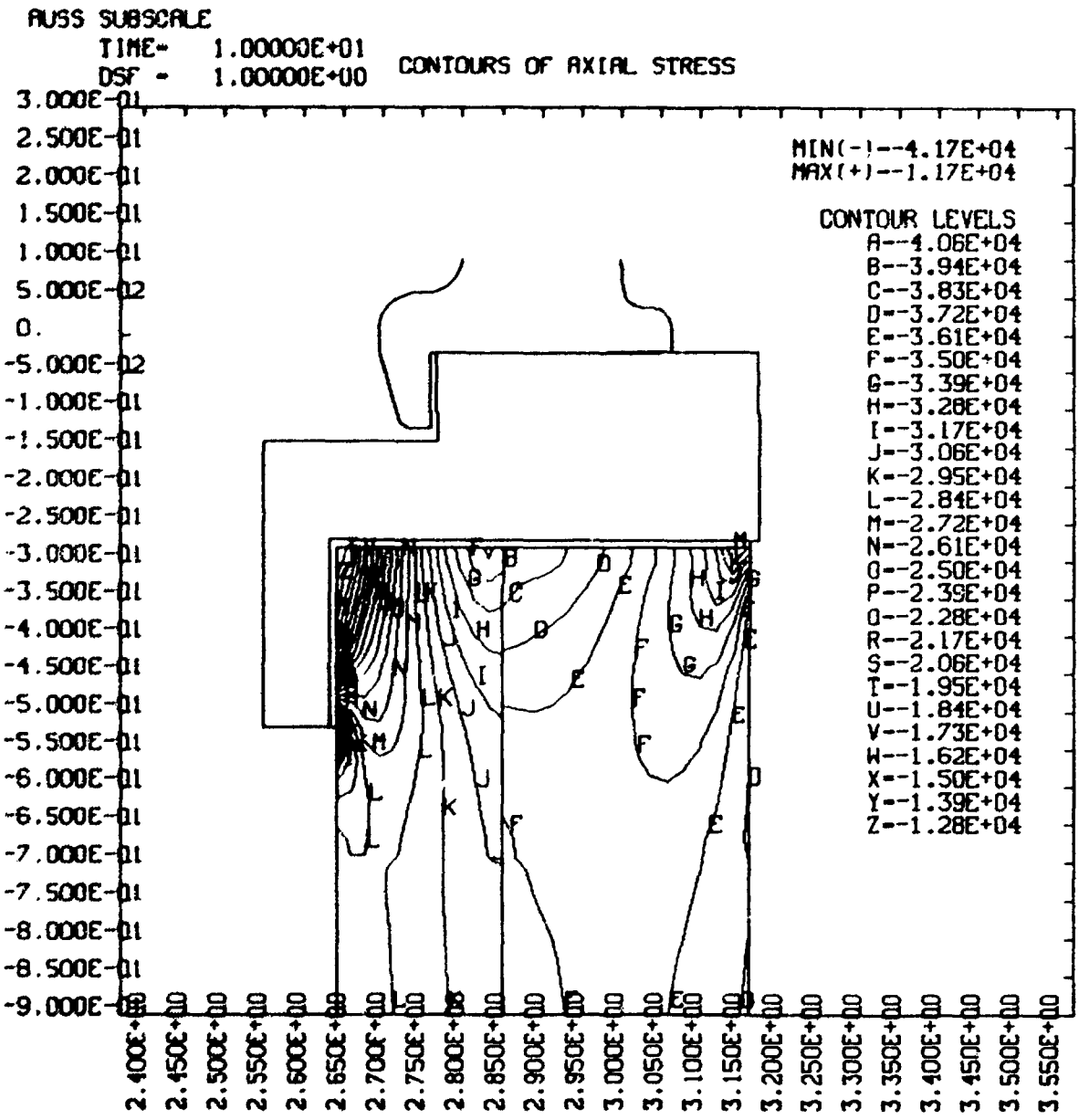

DESIGN CASE

Location: Cylinder, end

Pressure: 10,000 psi

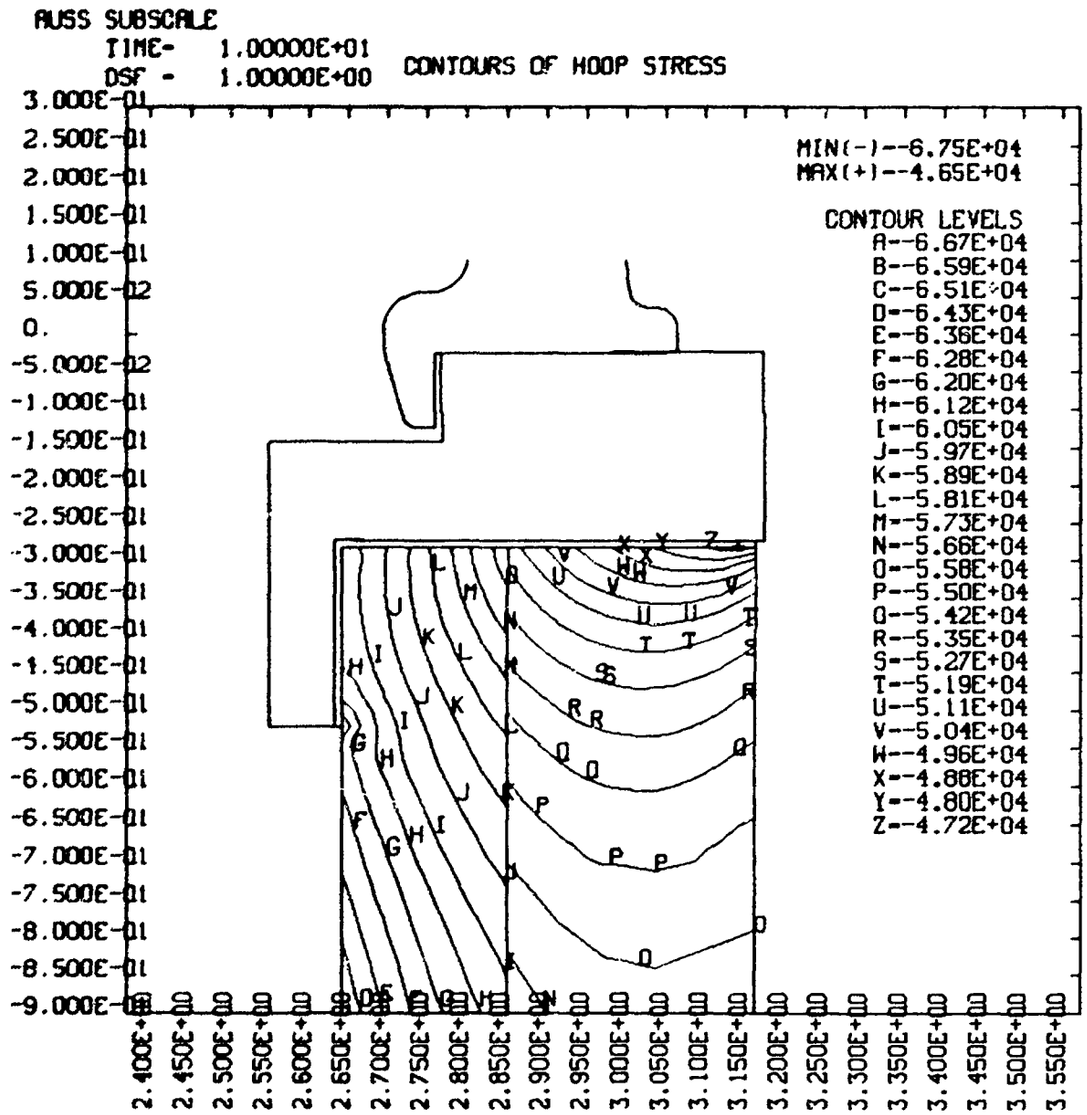

DESIGN CASE

Location: Cylinder, end

Pressure: 10,000 psi

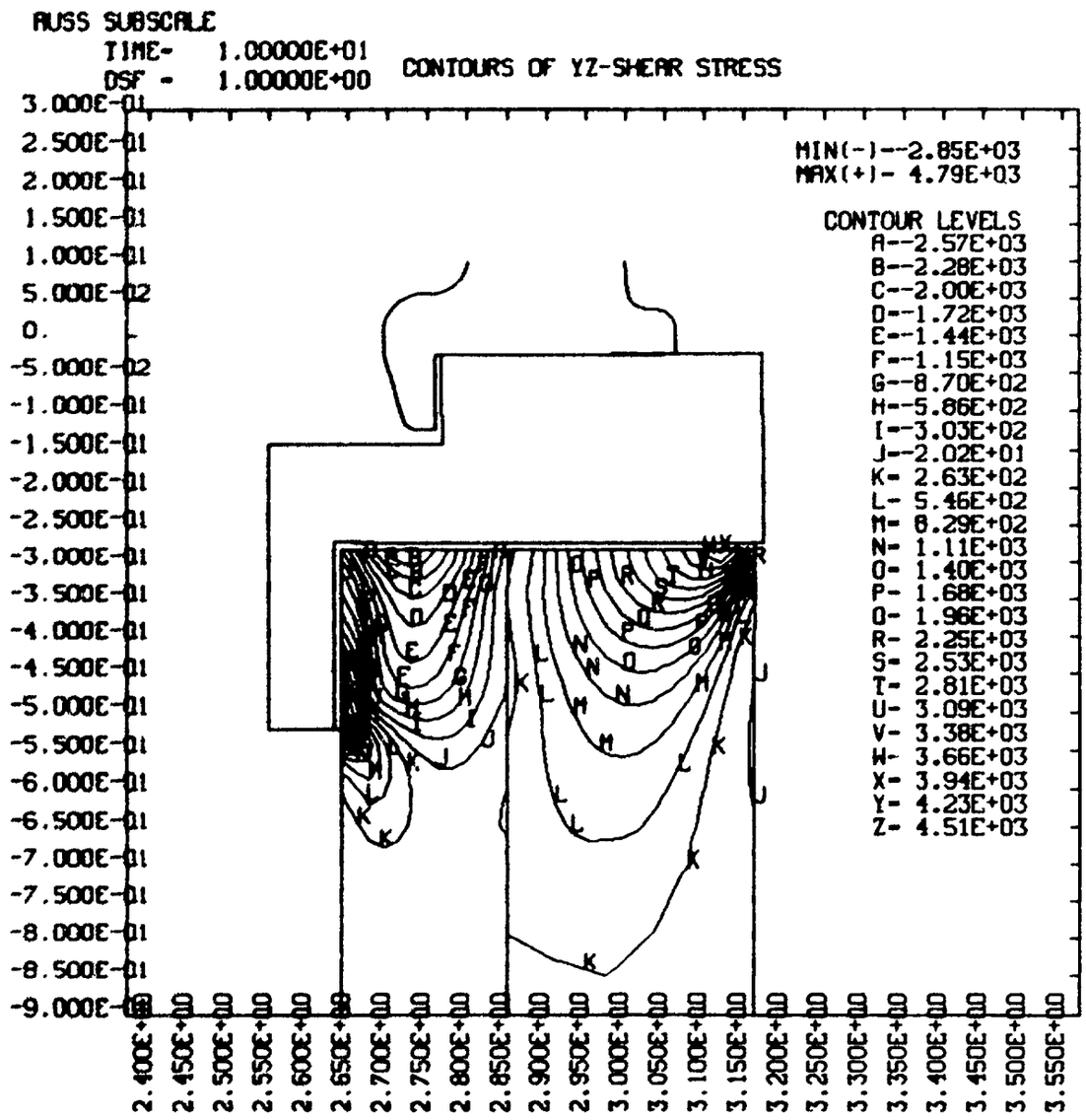

DESIGN CASE

Location: Cylinder, end

Pressure: 10,000 psi

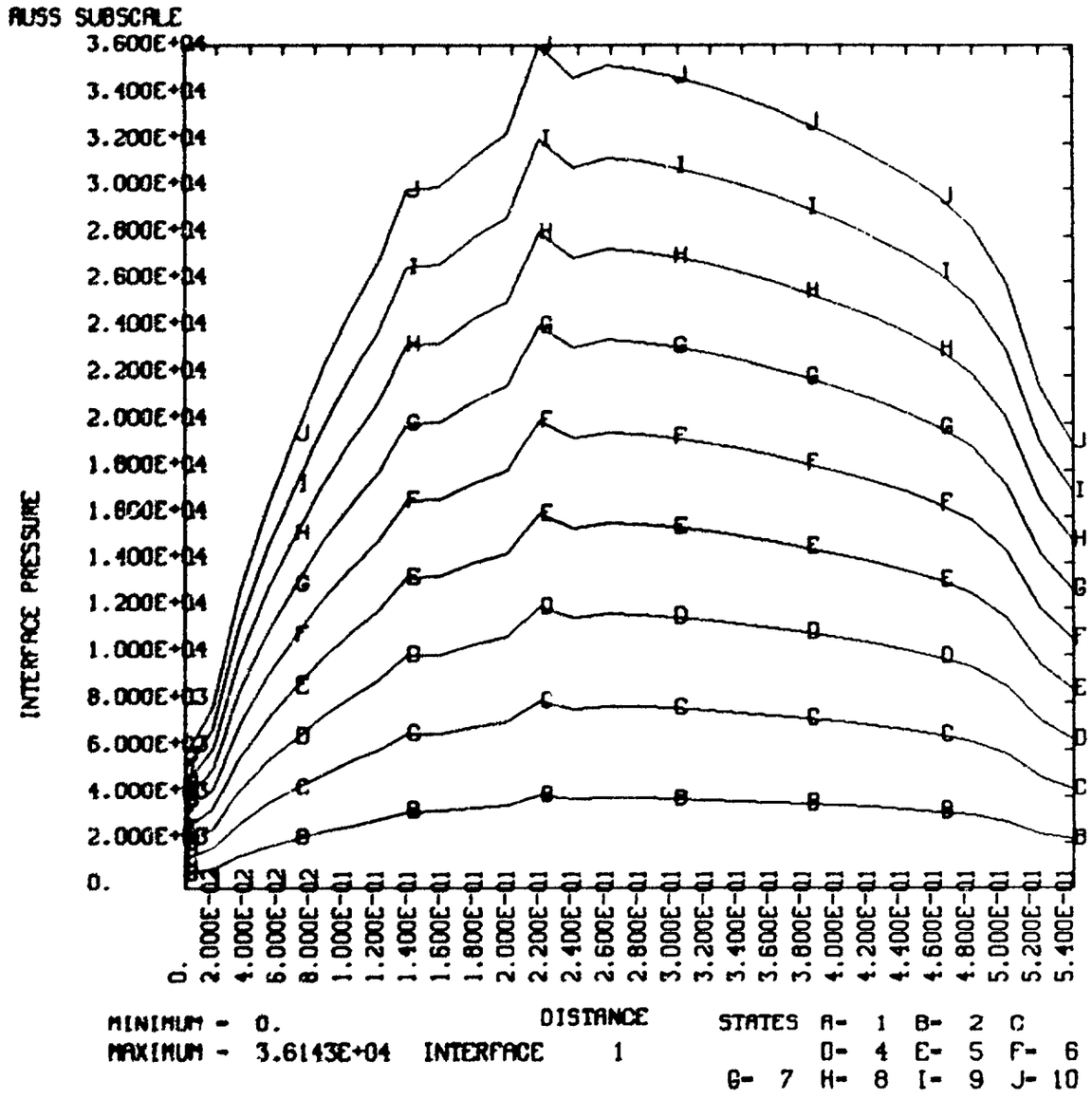

DESIGN CASE

Location: Bonding surface on titanium ring

Pressure: A state = 1000 psi

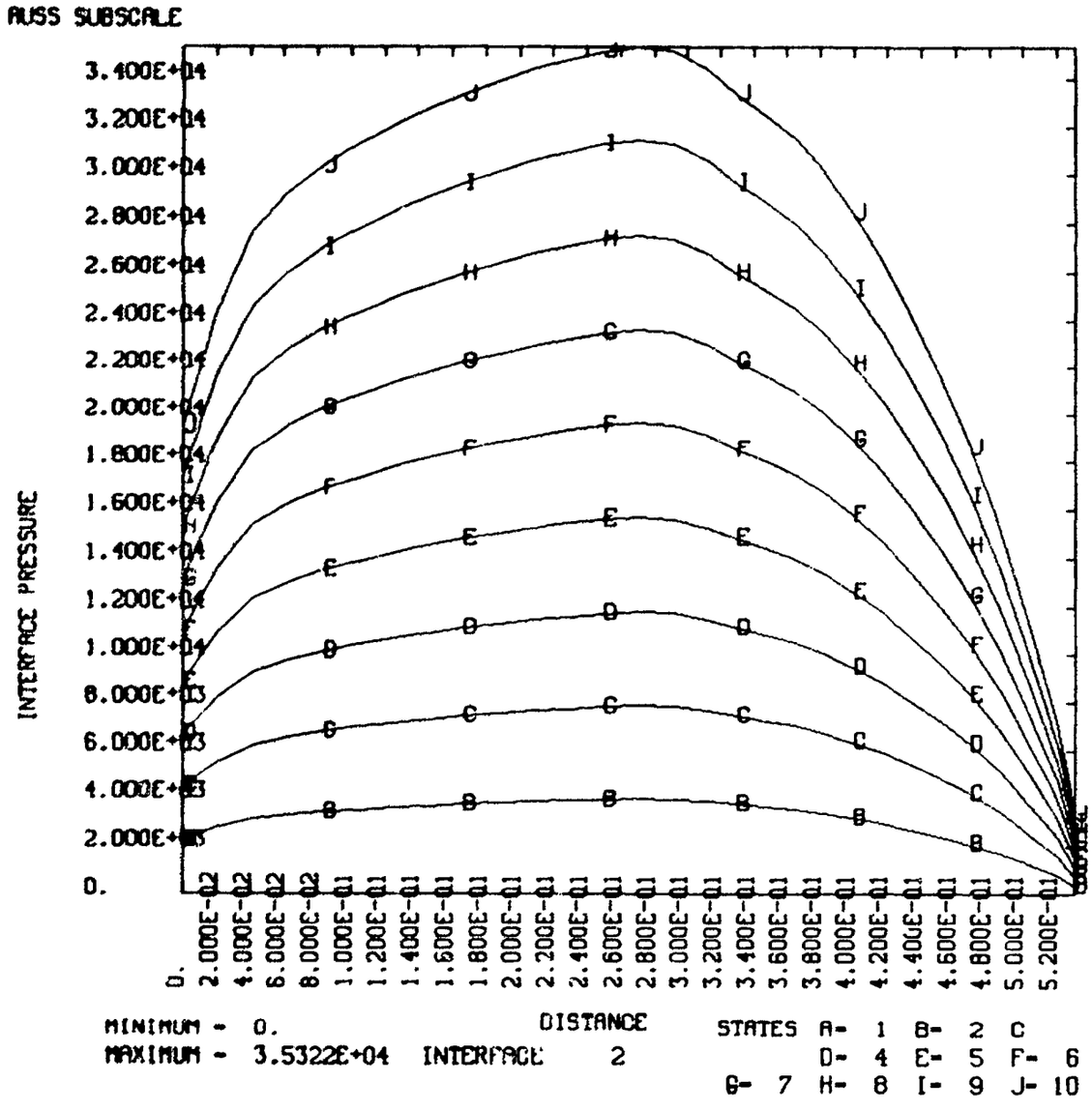

DESIGN CASE

Location: Epoxy adhesive layer on titanium ring

Pressure: A state = 1000 psi

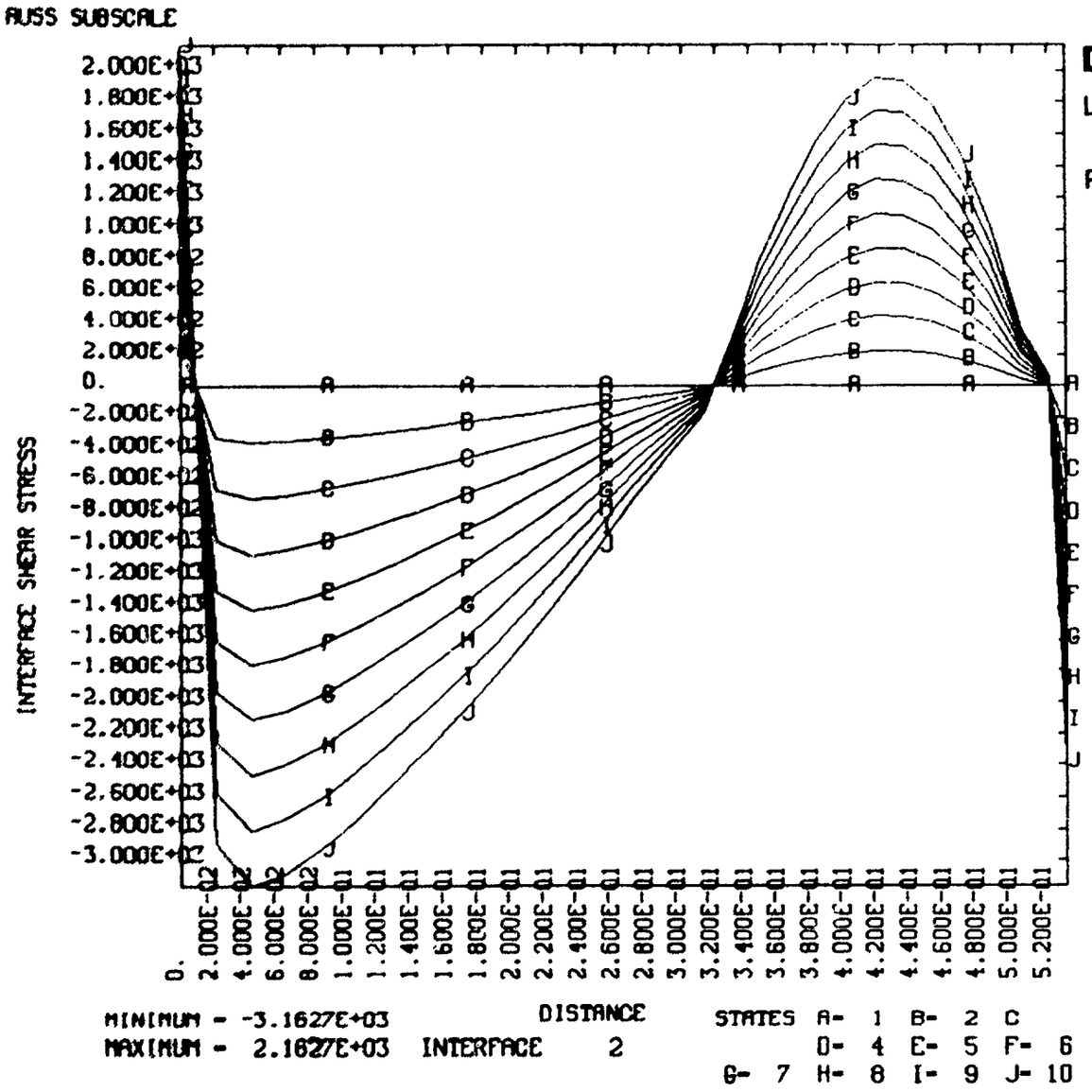

DESIGN CASE

Location: Epoxy adhesive layer on titanium ring

Pressure: A state = 1000 psi

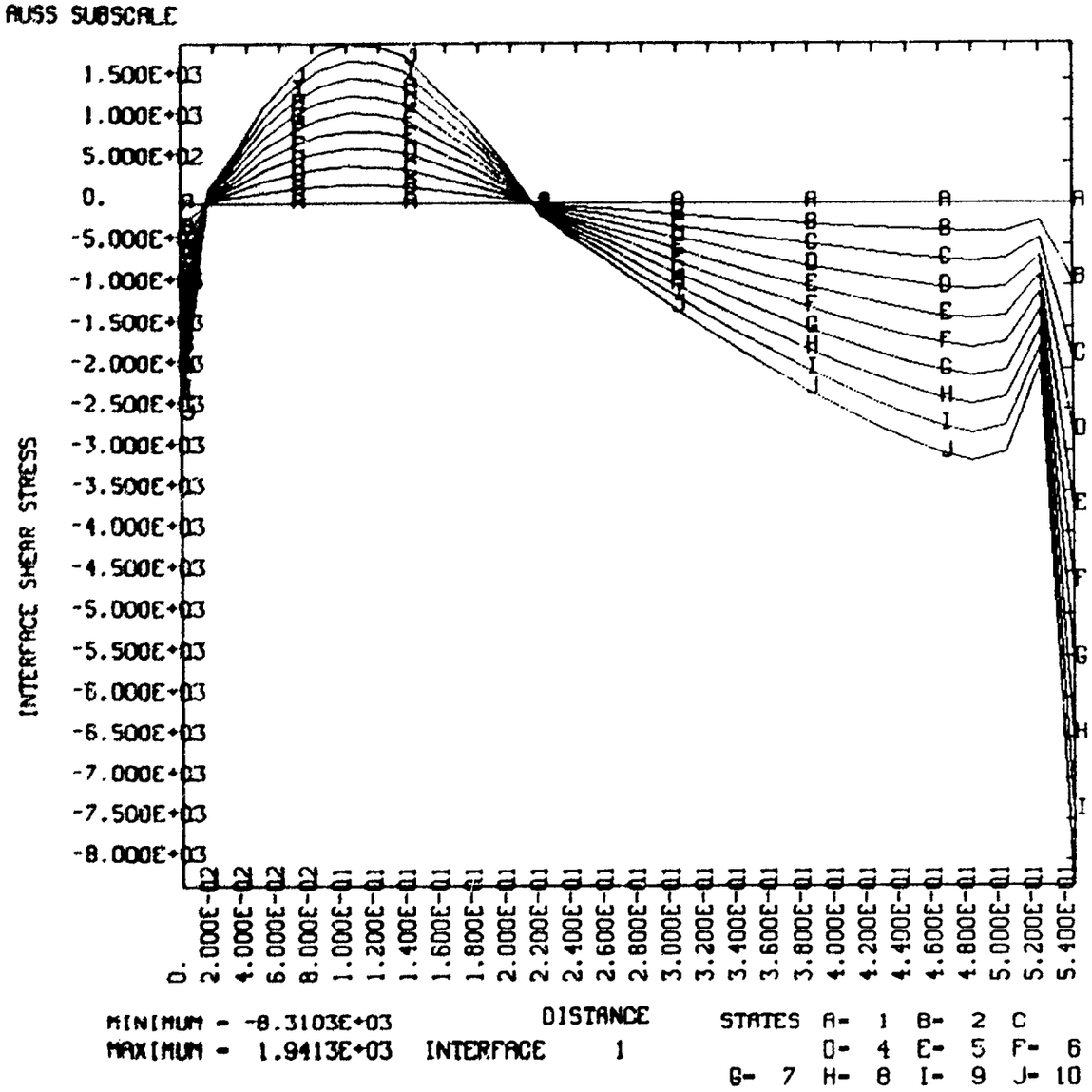

DESIGN CASE

Location: Bonding surface on titanium ring

Pressure: A state = 1000 psi

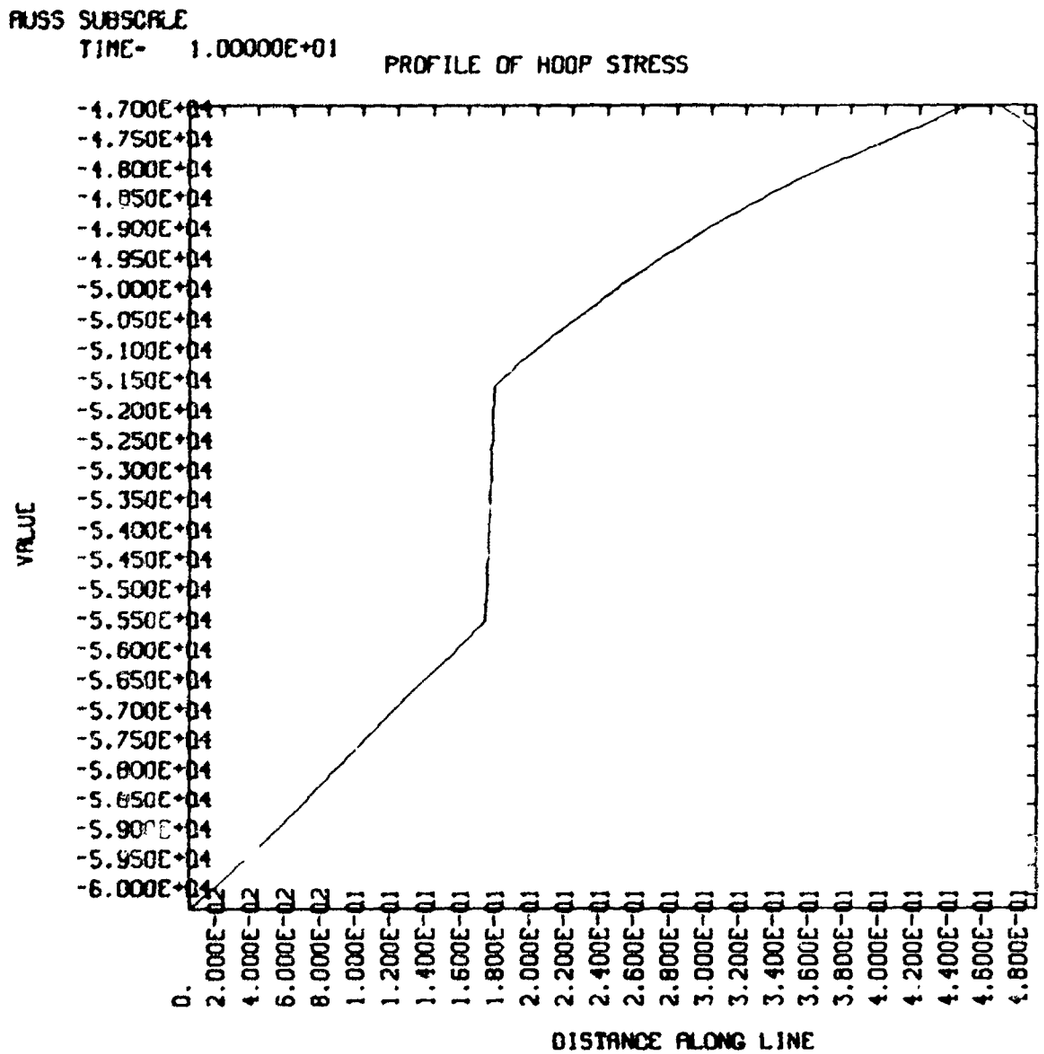

DESIGN CASE

Location: Cylinder, edge

Pressure: 10,000 psi

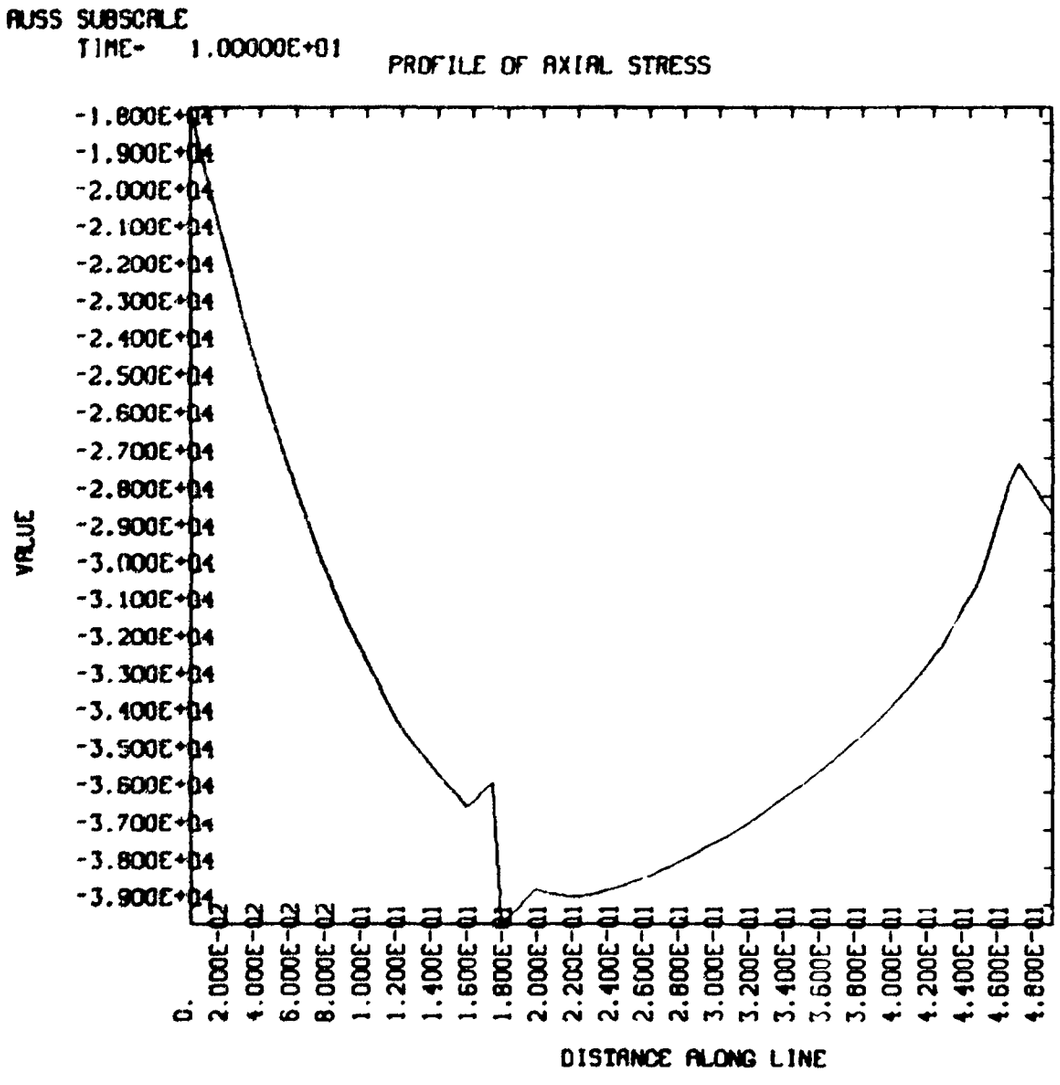

DESIGN CASE

Location: Cylinder, edge

Pressure: 10,000 psi

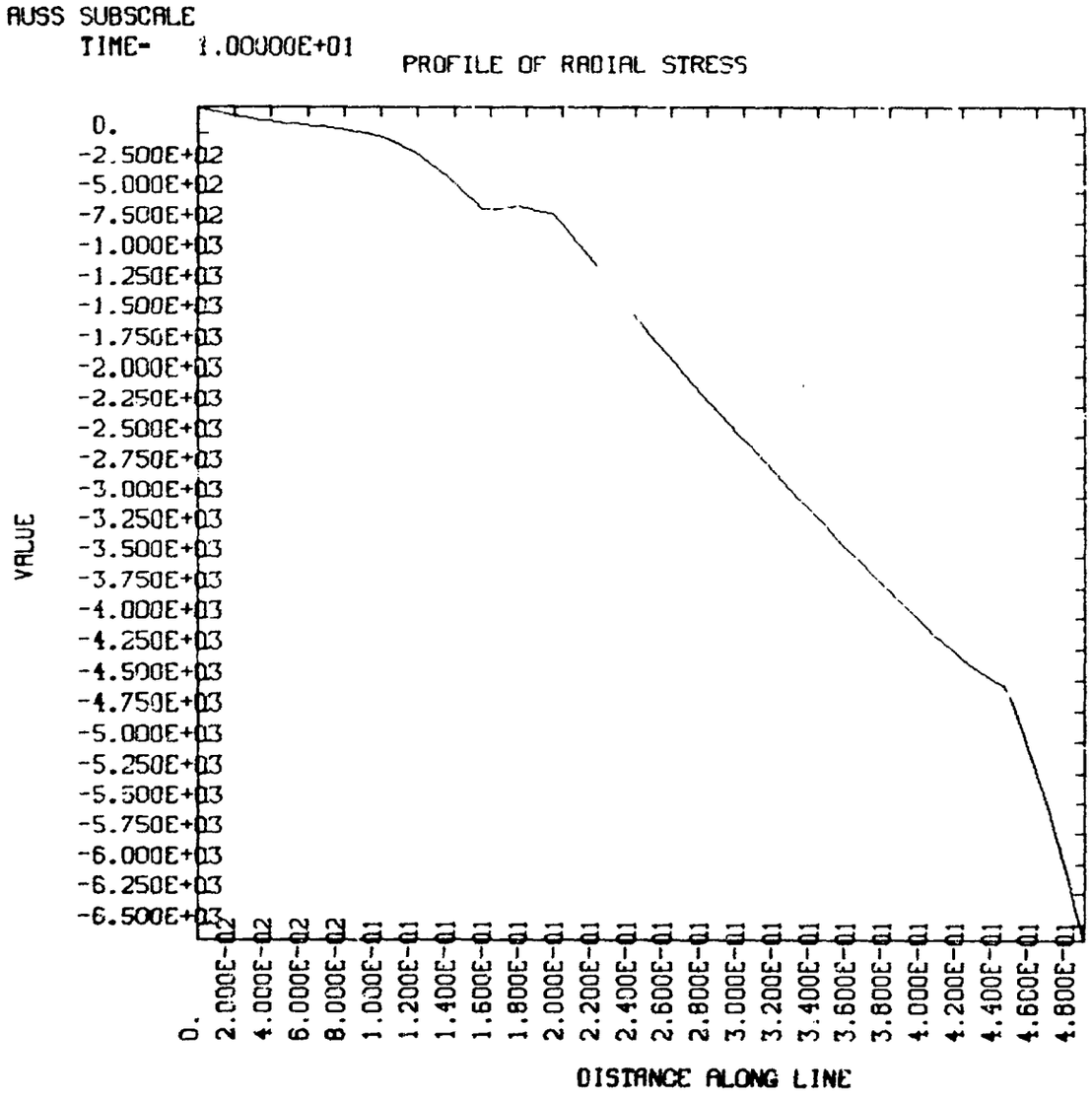

DESIGN CASE

Location: Cylinder, edge

Pressure: 10,000 psi

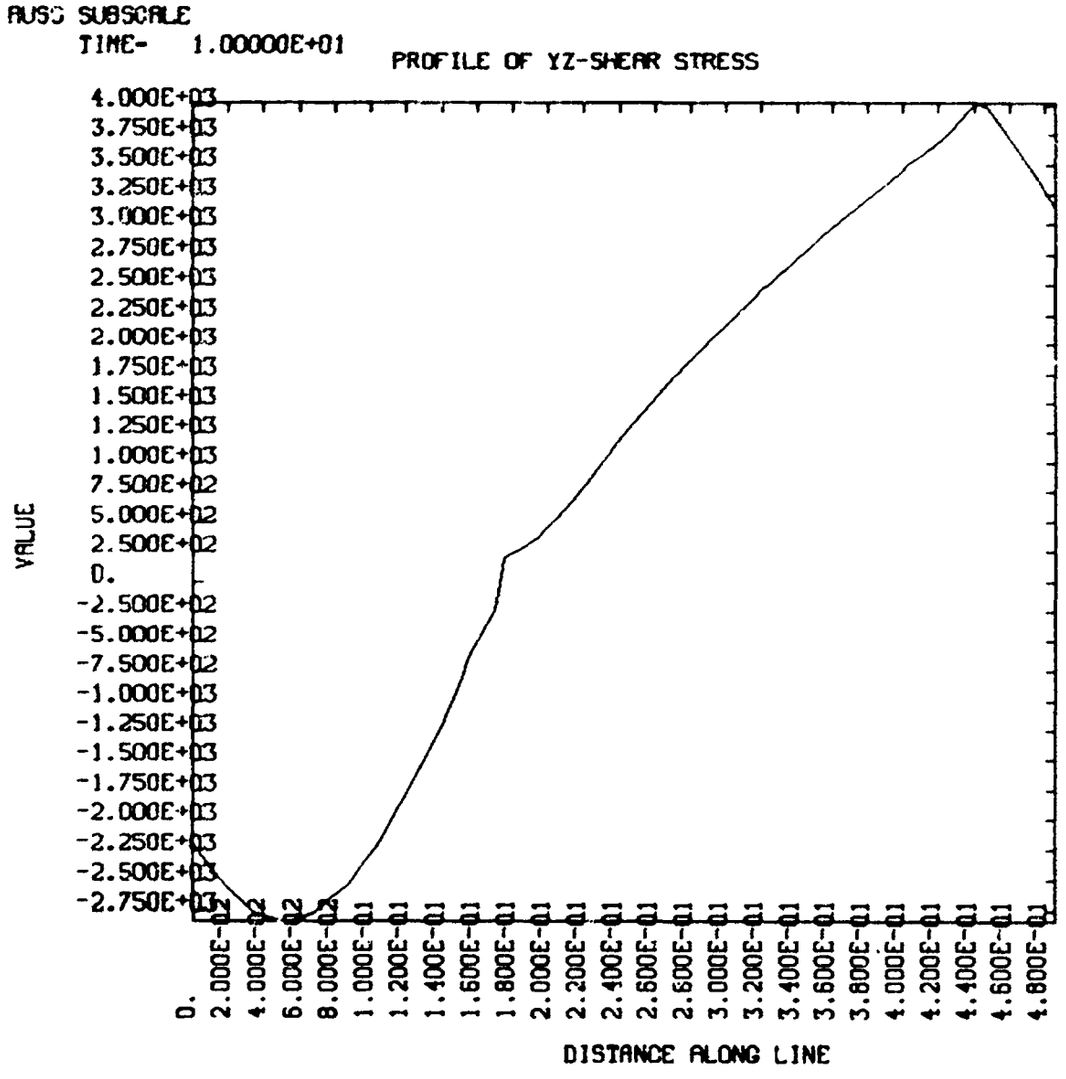

DESIGN CASE

Location: Cylinder, edge

Pressure: 10,000 psi

PART III

AS BUILT CASE

AS BUILT CASE

1. Layup ratios for fiber layers 2.5:1.0/2.0:1.0 with 90/0 degree orientations.
2. Thickness ratio of layup layers — 35:65.

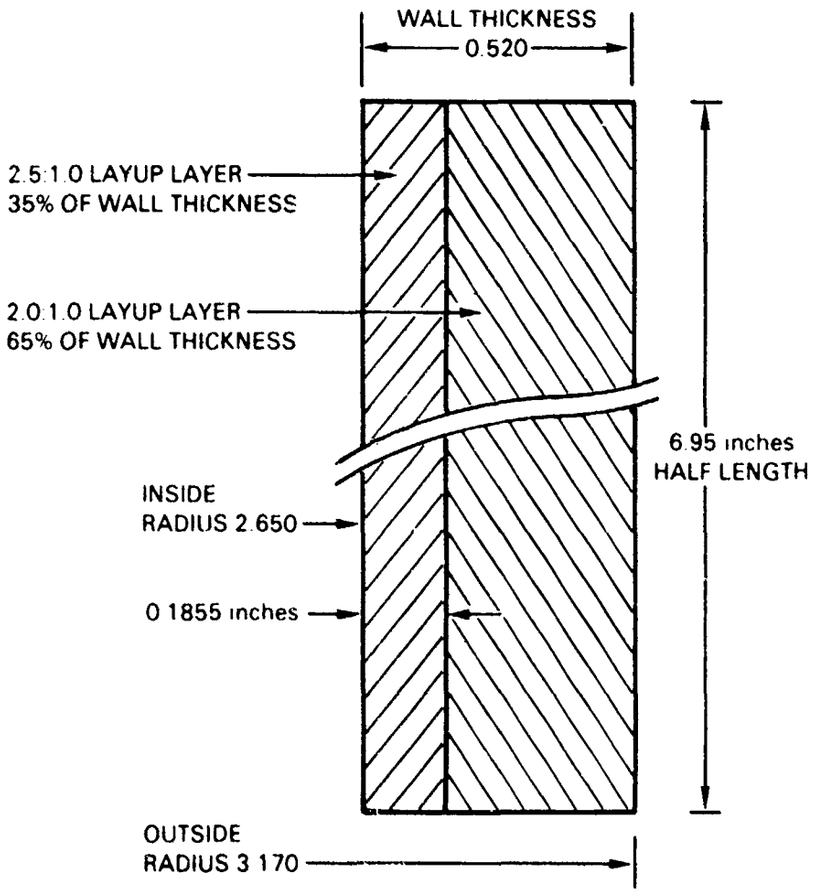

AS BUILT CASE

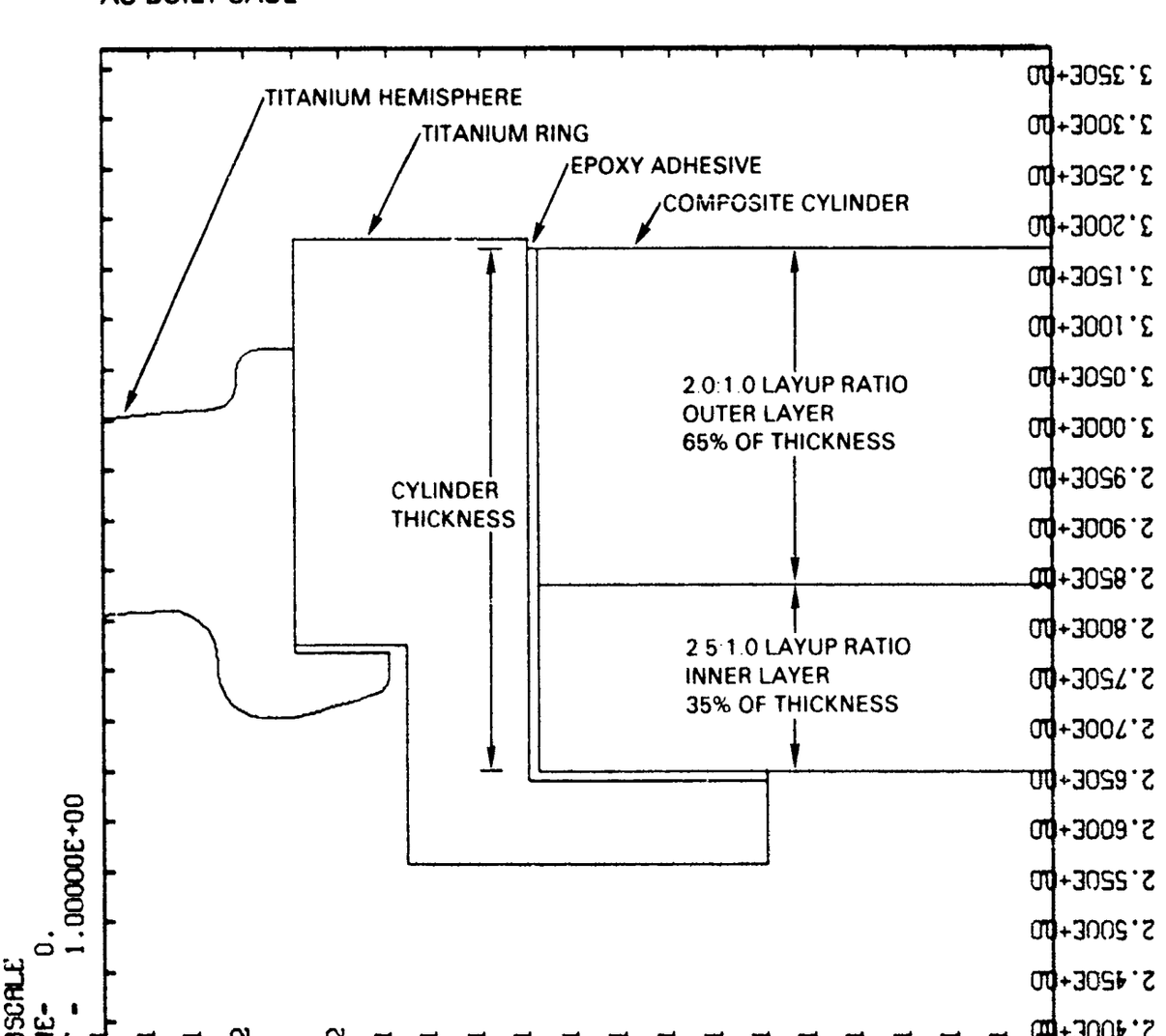

AUSS MODEL SCALE PRESSURE HULL CYLINDER FABRICATION INSTRUCTION

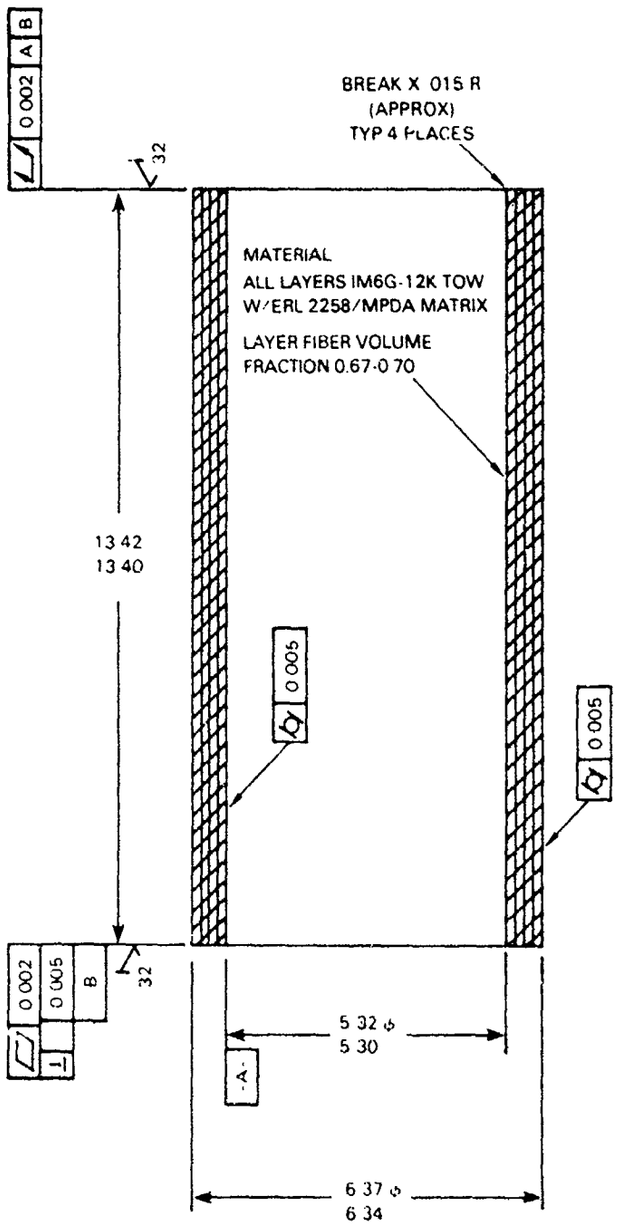

LAMINAS
HOOP 52
AXIAL 12

LAMINATE STACKING SEQUENCE

	Layer No	Orientation (deg)	Tension (lbs)	Thickness (in.)	Cumulative Thickness (in.)
1s LAYER	1	90	8	0.0069	0.0069
	2	90		0.0069	0.0138
	3	0		0.0136	0.0274
	4	90	12	0.0069	0.0343
	5	90		0.0069	0.0412
	6	90		0.0069	0.0481
	7	90		0.0069	0.0550
	8	90		0.0069	0.0619
	9	0		0.0136	0.0755
	10	90	12	0.0069	0.0824
	11	90		0.0069	0.0893
	12	90		0.0069	0.0962
	13	90		0.0069	0.1031
	14	90		0.0069	0.1100
	15	0		0.0136	0.1236
	16	90	12	0.0069	0.1303
	17	90		0.0069	0.1374
	18	90		0.0069	0.1443
	19	90		0.0069	0.1512
	20	90		0.0069	0.1581
	21	0		0.0136	0.1717
	22	90	16	0.0069	0.1786
	23	90		0.0069	0.1855
2nd LAYER	24	90	8	0.0069	0.1924
	25	90		0.0069	0.1993
	26	0		0.0136	0.2129
	27	90	12	0.0069	0.2198
	28	90		0.0069	0.2267
	29	90		0.0069	0.2336
	30	90		0.0069	0.2405
	31	0		0.0136	0.2541
	32	90	12	0.0069	0.2610
	33	90		0.0069	0.2679
	34	90		0.0069	0.2748
	35	90		0.0069	0.2817
	36	0		0.0136	0.2953
	37	90	12	0.0069	0.3022
	38	90		0.0069	0.3091
	39	90		0.0069	0.3160
	40	90		0.0069	0.3229
	41	0		0.0136	0.3365
	42	90	16	0.0069	0.3434
	43	90		0.0069	0.3503
3rd LAYER	44	90	8	0.0069	0.3572
	45	90		0.0069	0.3641
	46	0		0.0136	0.3777
	47	90	12	0.0069	0.3846
	48	90		0.0069	0.3915
	49	90		0.0069	0.3984
	50	90		0.0069	0.4053
	51	0		0.0136	0.4189
	52	90	12	0.0069	0.5258
	53	90		0.0069	0.4327
	54	90		0.0069	0.4396
	55	90		0.0069	0.4465
	56	0		0.0136	0.4601
	57	90	12	0.0069	0.4670
	58	90		0.0069	0.4739
	59	90		0.0069	0.4808
	60	90		0.0069	0.4877
	61	0		0.0136	0.5013
	62	90	16	0.0069	0.5082
	63	90		0.0069	0.5151
	64	90		0.0069	0.5220

AS BUILT CASE

3-D Orthotropic Elastic Constants
0/90 2.5:1.0 Layup (volume averaged)

E_R	= 1.68 Msi	ν_{R0}	= 0.038
E_0	= 17.39 Msi	ν_{0R}	= 0.396
E_Z	= 7.85 Msi	ν_{0Z}	= 0.059
G_{R0}	= 0.766 Msi	ν_{Z0}	= 0.027
G_{0Z}	= 0.875 Msi	ν_{ZR}	= 0.389
G_{RZ}	= 0.631 Msi	ν_{RZ}	= 0.083

ρ = 0.0571 lb/in^3

fiber volume = 0.67

AS BUILT CASE

3-D Orthotropic Elastic Constants
0/90 2.0:1.0 Layup (volume averaged)

E_R	= 1.68 Msi	ν_{RO}	= 0.041
E_O	= 16.33 Msi	ν_{OR}	= 0.396
E_Z	= 8.91 Msi	ν_{OZ}	= 0.052
G_{RO}	= 0.751 Msi	ν_{ZO}	= 0.028
G_{OZ}	= 0.857 Msi	ν_{ZR}	= 0.390
G_{RZ}	= 0.646 Msi	ν_{RZ}	= 0.073

ρ = 0.0571 lb/in^3

fiber volume = 0.67

AS BUILT CASE

Stress Values* at Cylinder Midbay

Radius	Hoop Stress (psi)	Axial Stress (psi)	H/A Ratio
Inside	-67,500	-29,000	2.33
Outside	-58,250	-35,800	1.63

Layup ratio between hoop and axial fibers

Inner Layer	2.5:1.0
Outer Layer	2.0:1.0

thickness ratio of inner and outer layers 35.65

*All stress values referred to 10,000 psig pressure

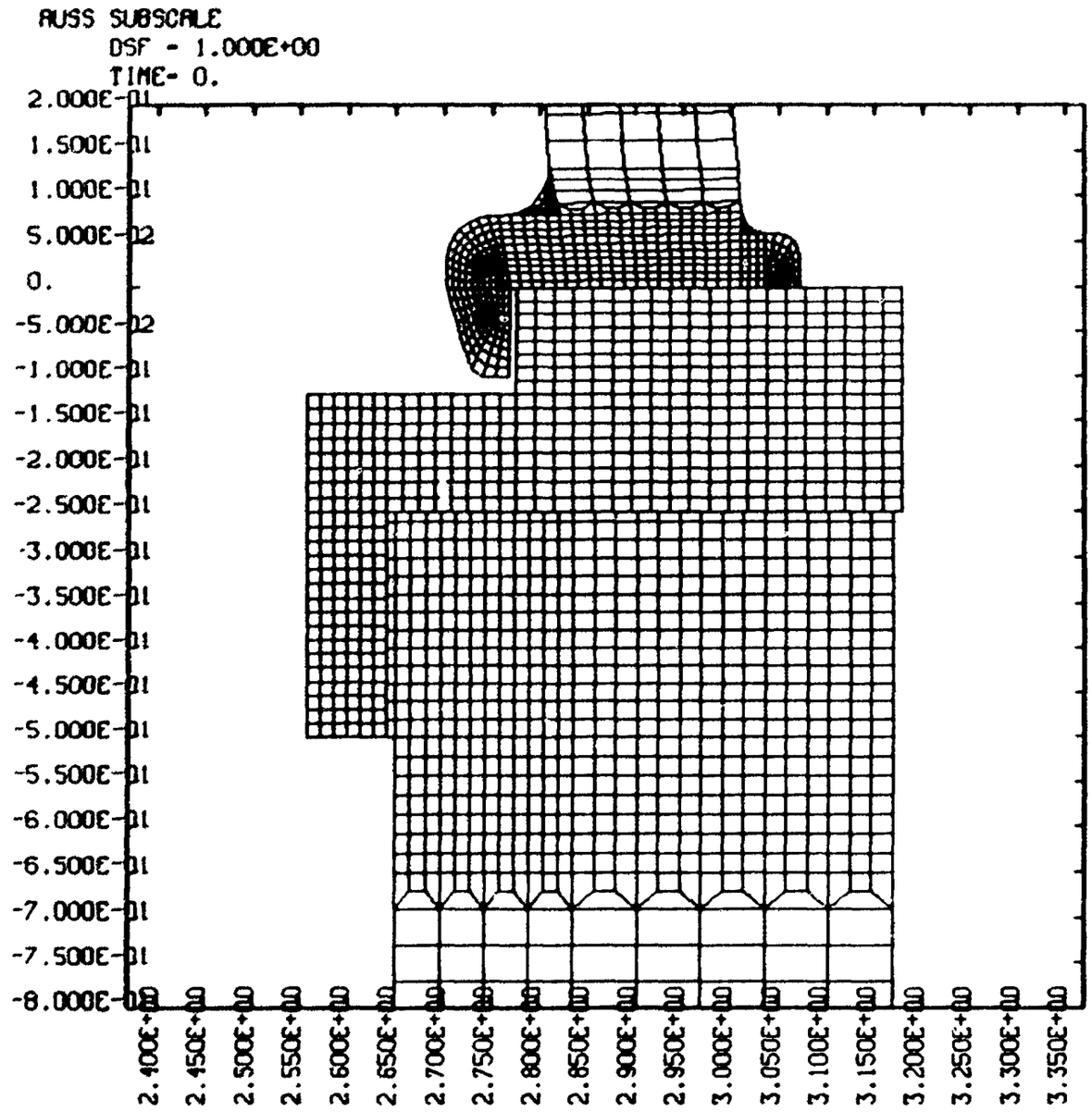

AS BUILT CASE

Location: Cylinder, end

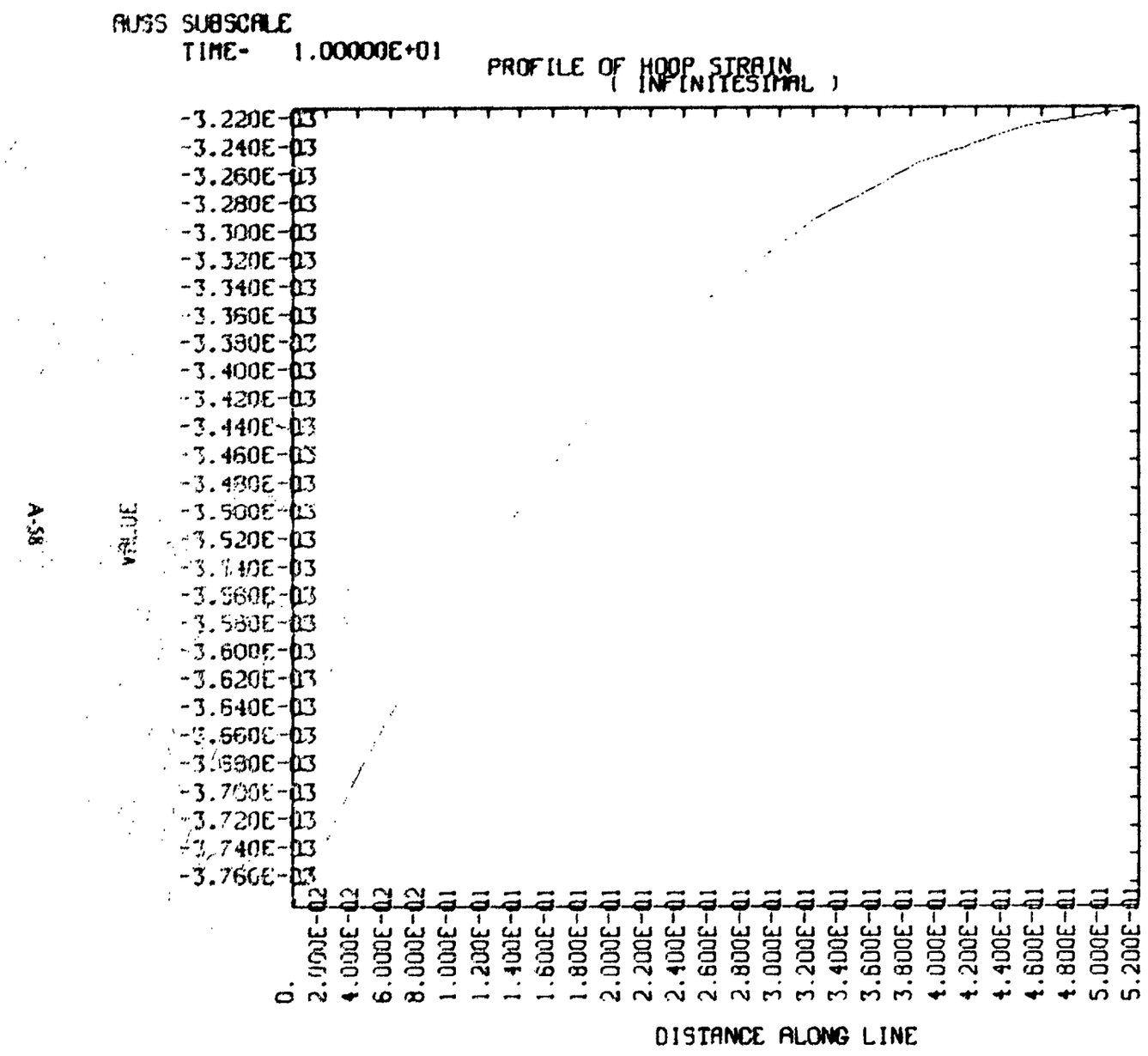

AS BUILT CASE

Location: Cylinder, midbay

Pressure: 10,000 psi

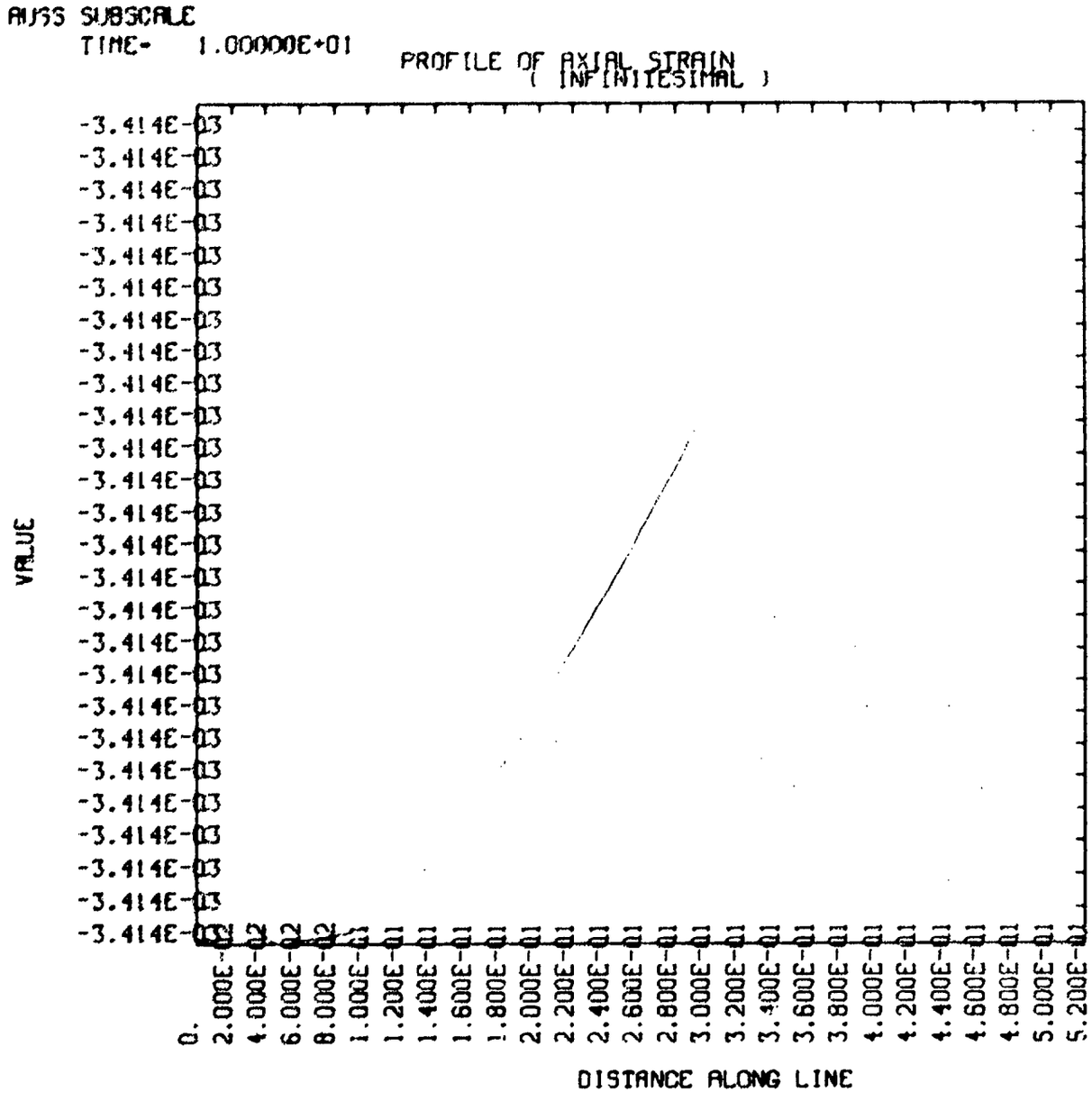

AS BUILT CASE

Location: Cylinder, midbay

Pressure: 10,000 psi

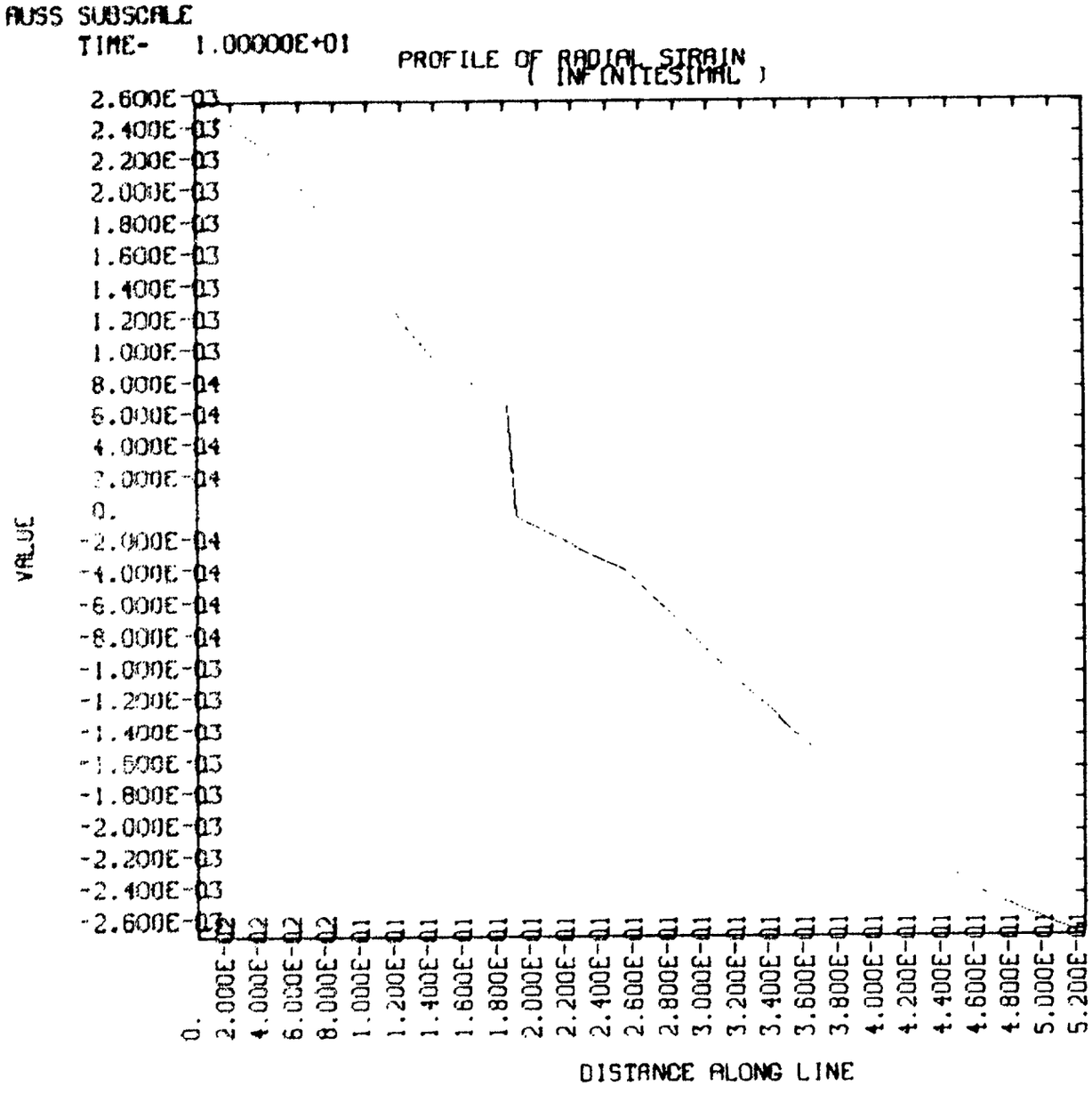

AS BUILT CASE

Location: Cylinder, midba

Pressure: 10,000 psi

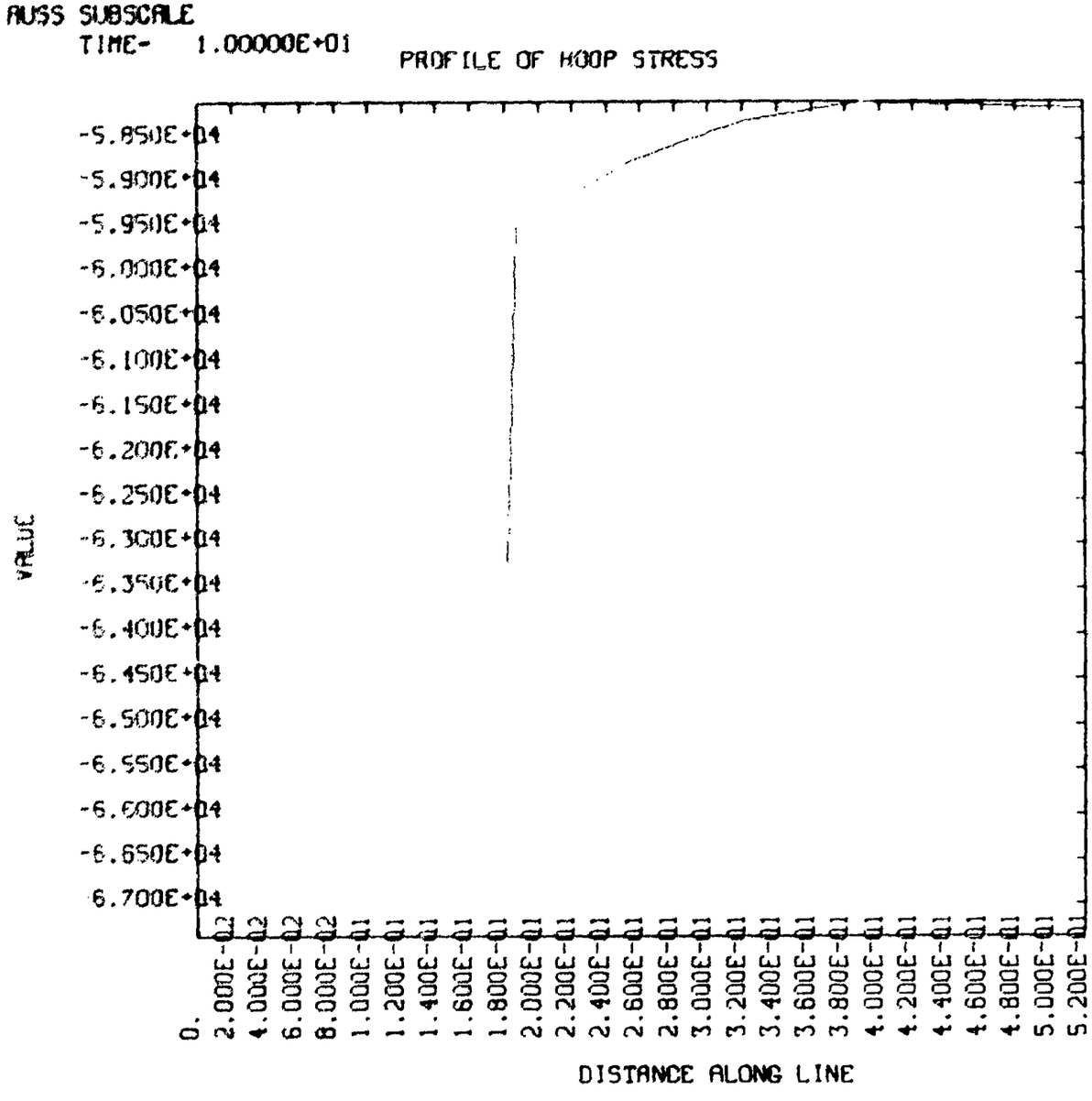

AS BUILT CASE

Location: Cylinder, mid

Pressure: 10,000 psi

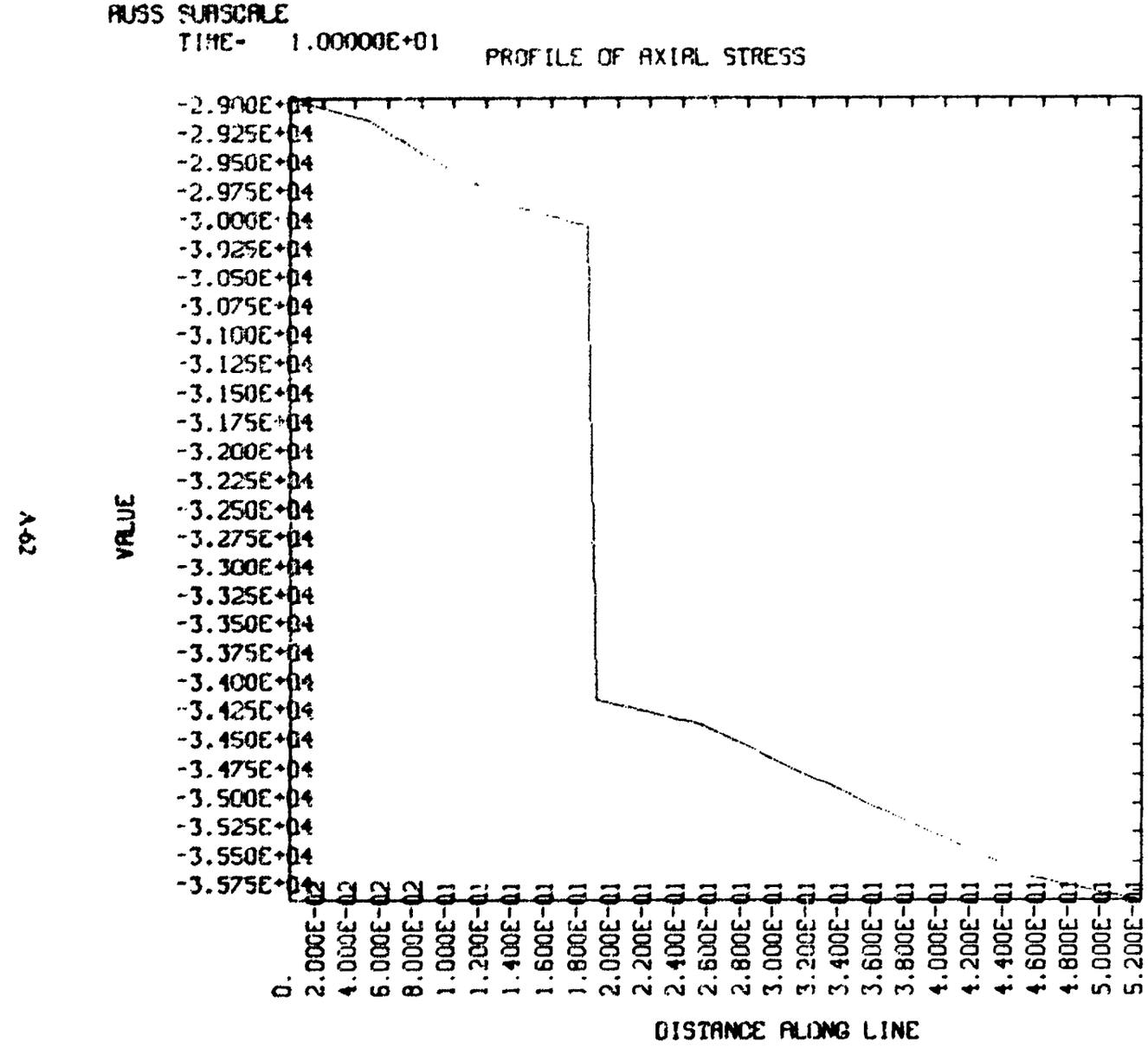

AS BUILT CASE

Location: Cylinder, midbay

Pressure: 10,000 psi

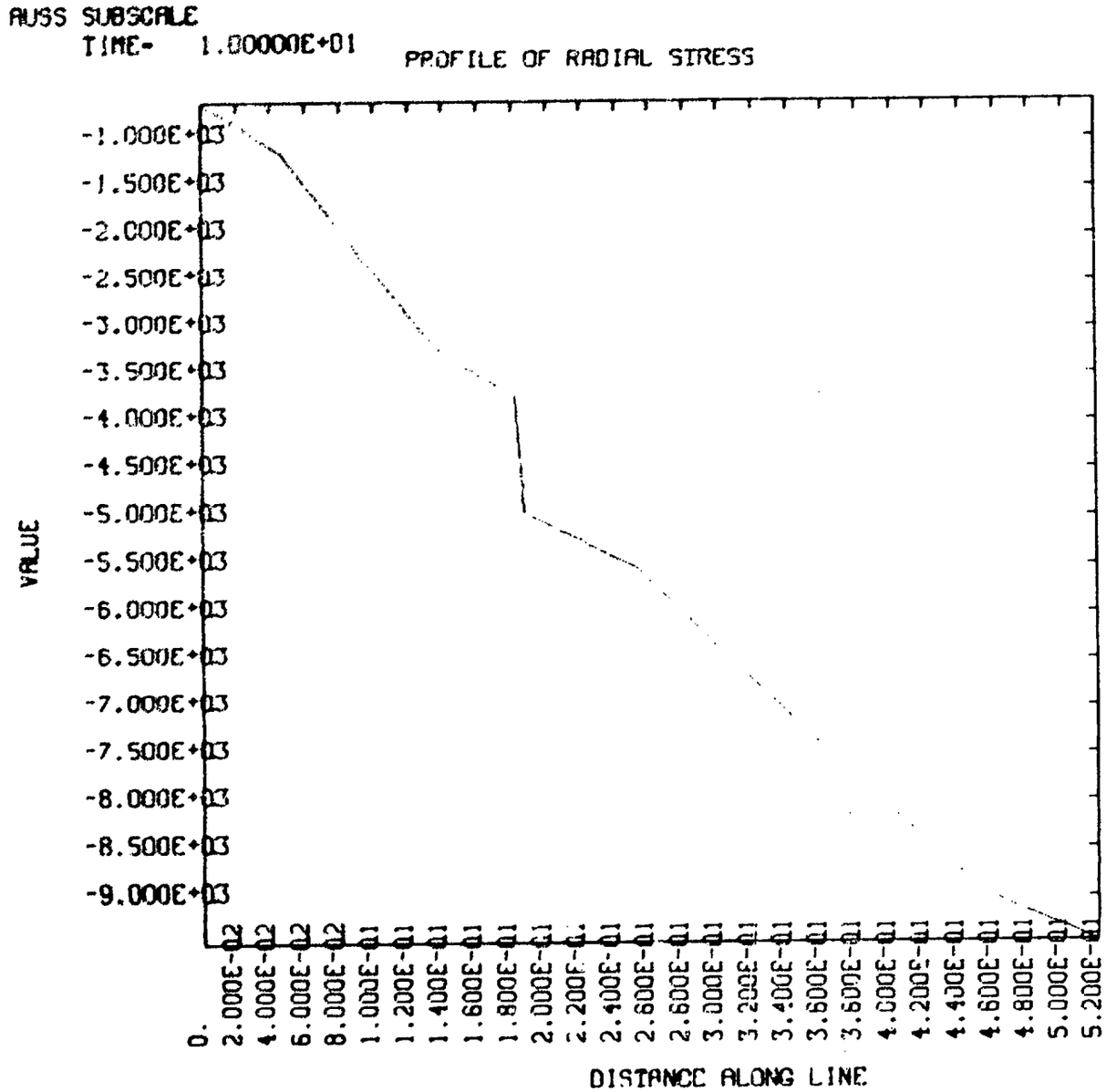

AS BUILT CASE

Location: Cylinder, midbay

Pressure: 10,000 psi

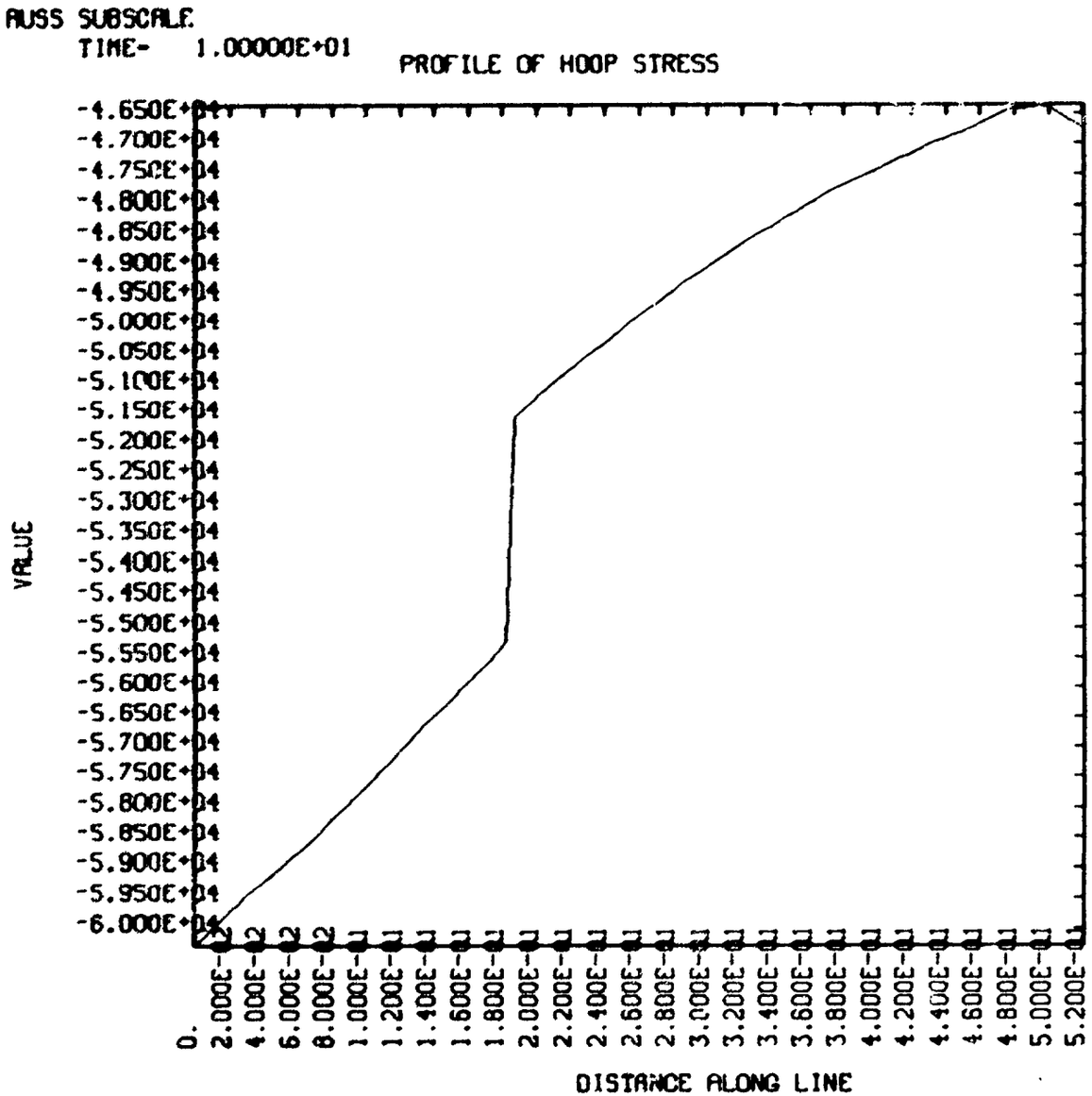

AS BUILT CASE

Location: Cylinder, edge

Pressure: 10,000 psi

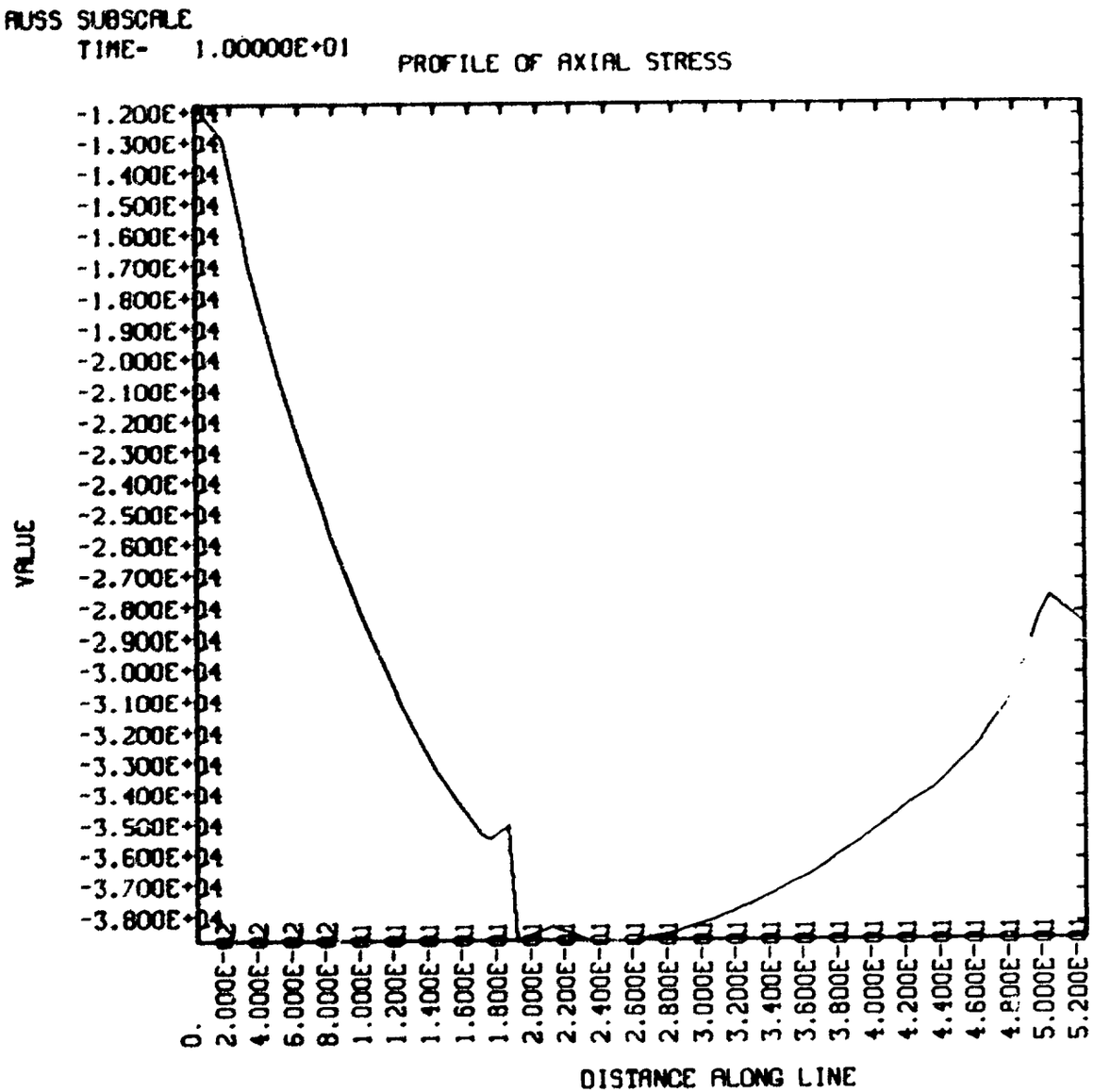

AS BUILT CASE

Location: Cylinder, edge

Pressure: 10,000 psi

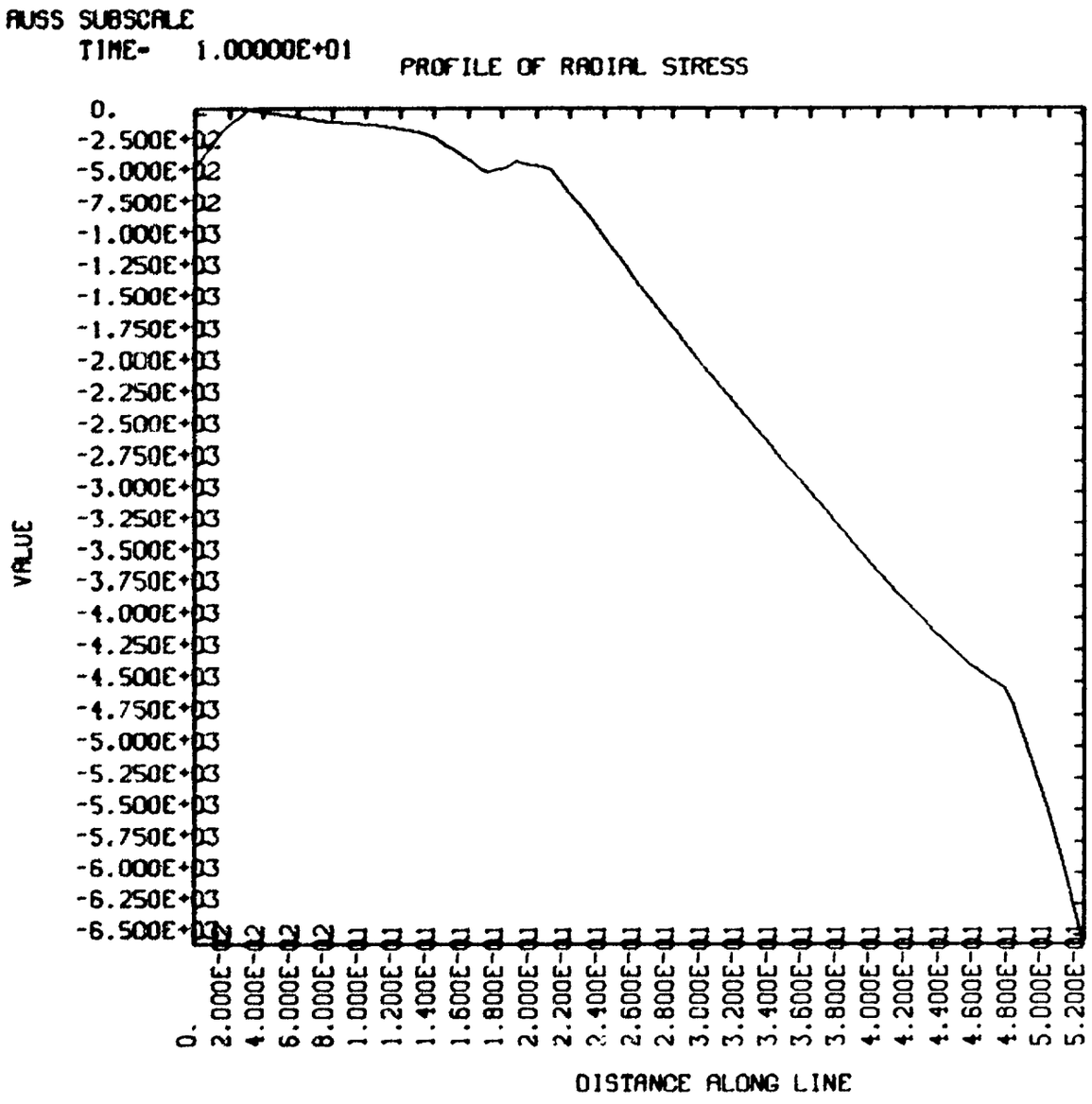

AS BUILT CASE

Location: Cylinder, edge

Pressure: 10,000 psi

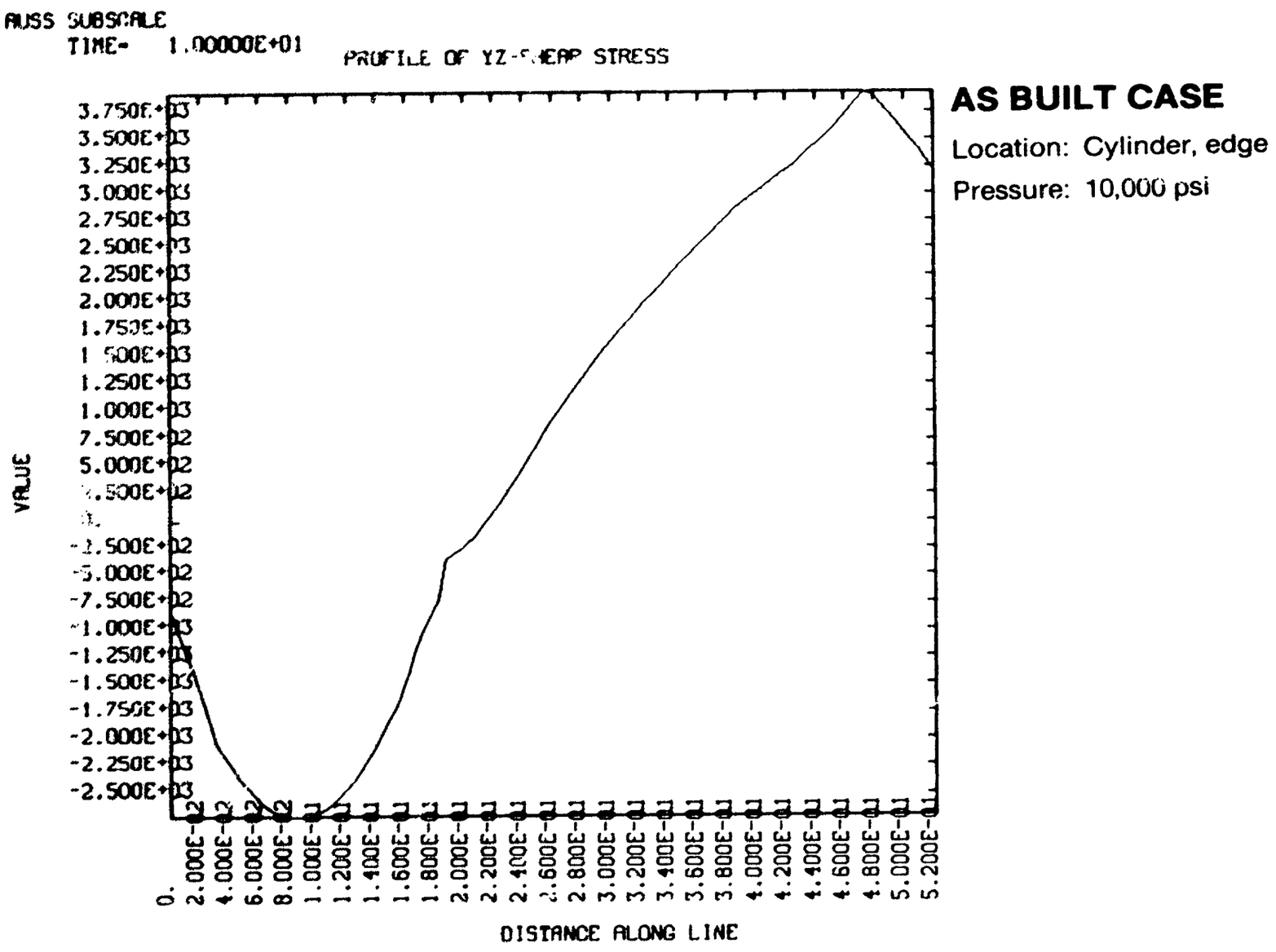

AS BUILT CASE

Location: Cylinder, edge

Pressure: 10,000 psi

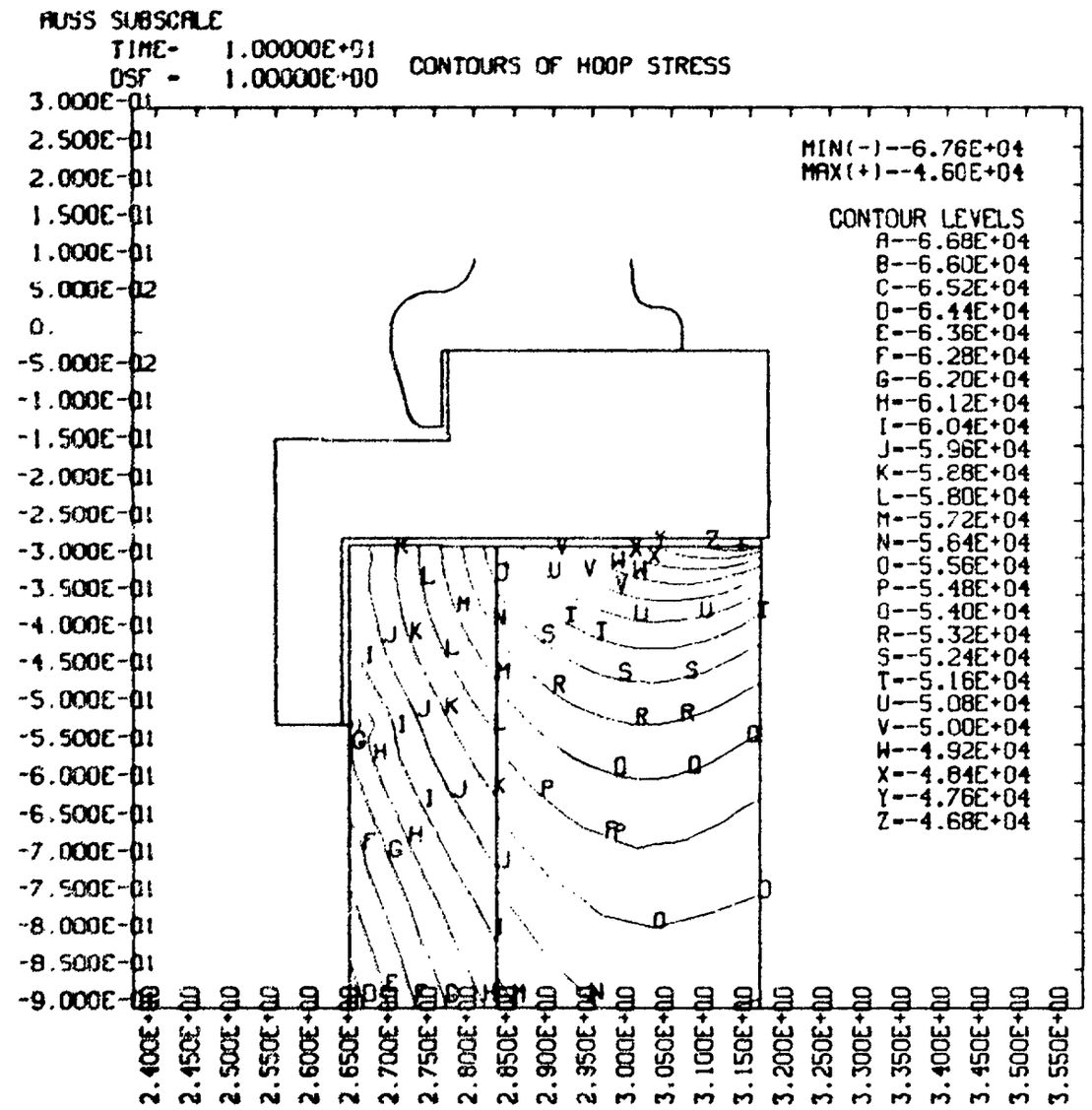

AS BUILT CASE

Location: Cylinder, end

Pressure: 10,000 psi

A-88

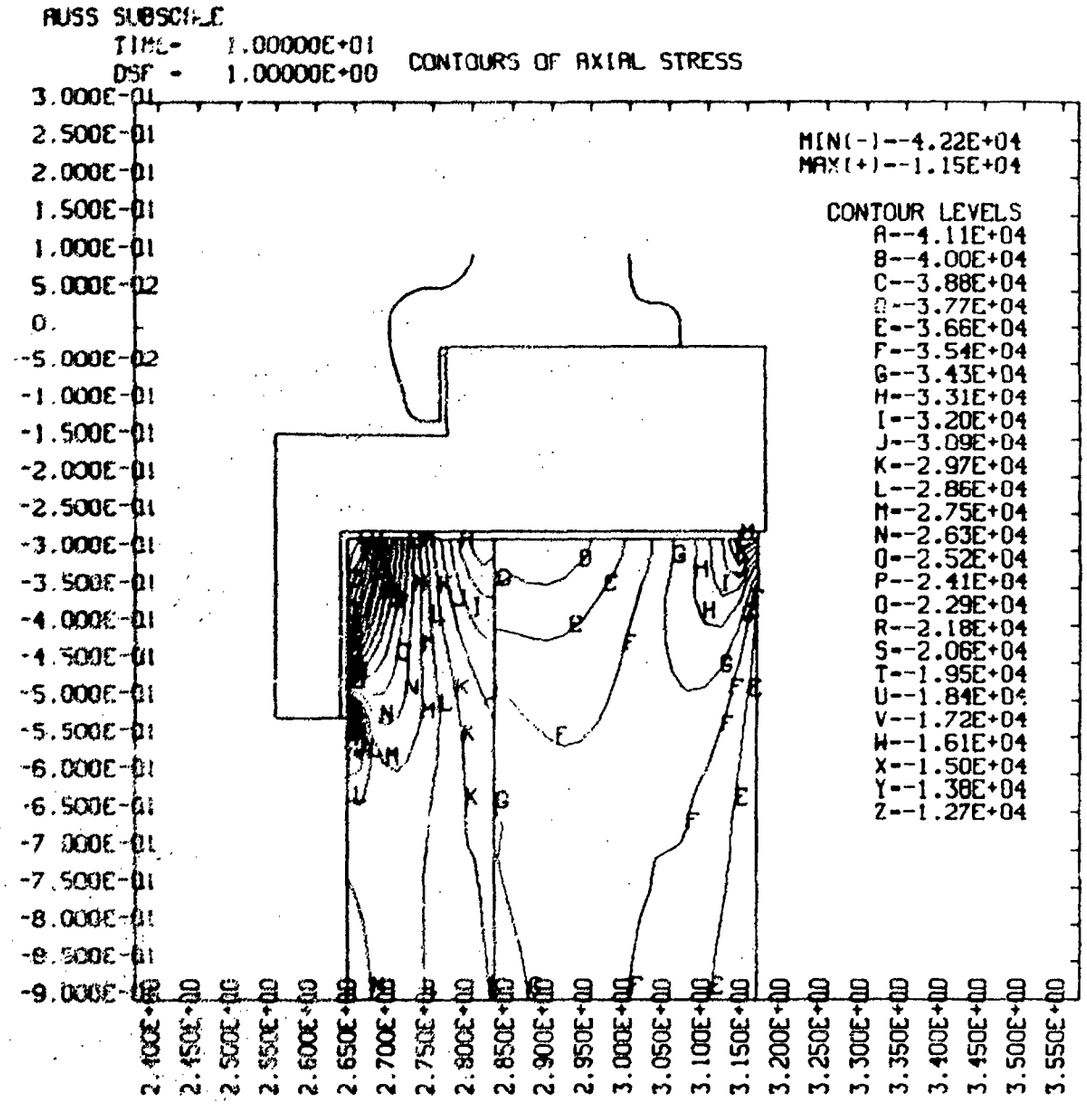

AS BUILT CASE

Location: Cylinder, end

Pressure: 10,000 psi

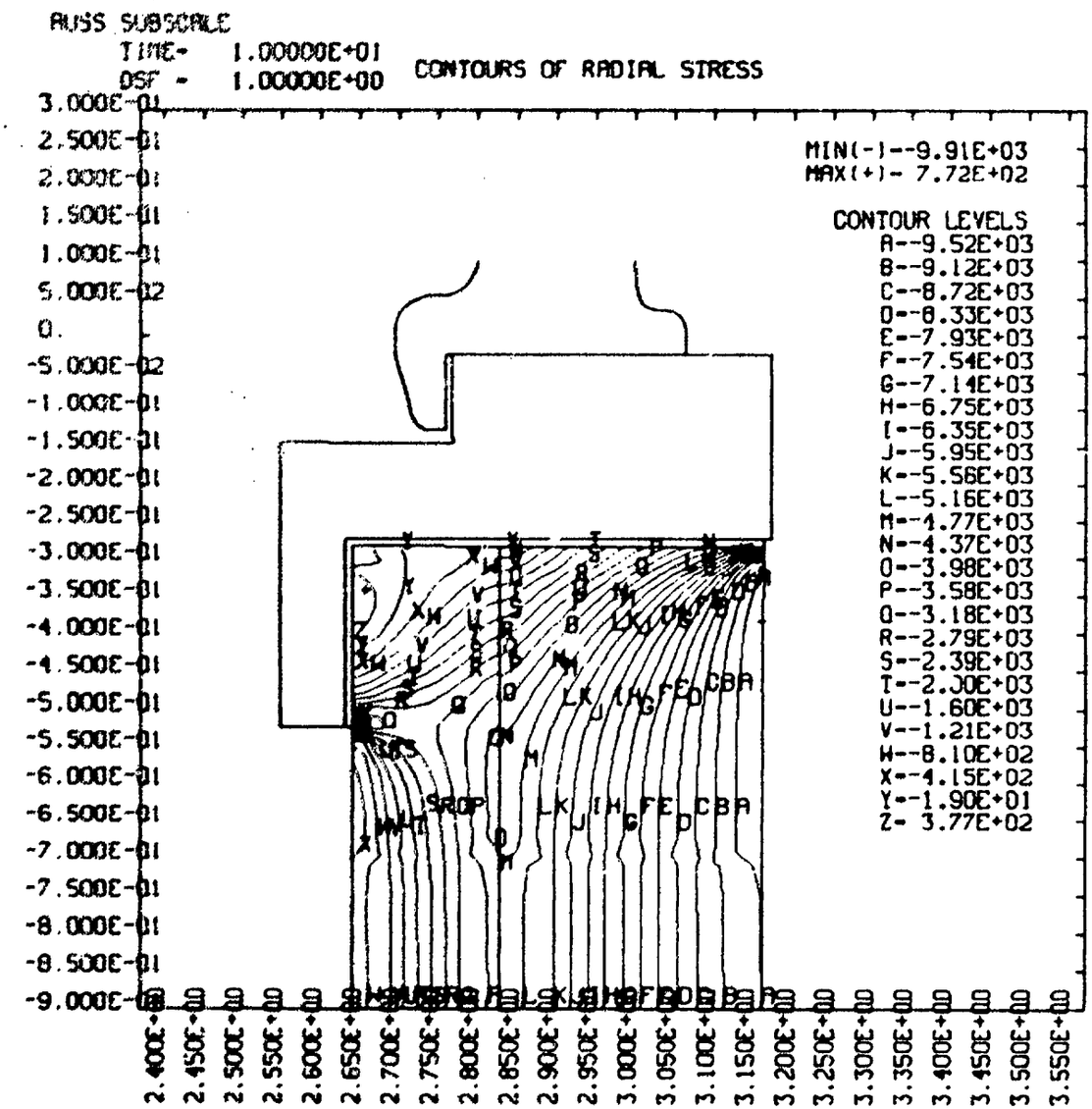

AS BUILT CASE

Location: Cylinder, end

Pressure: 10,000 psi

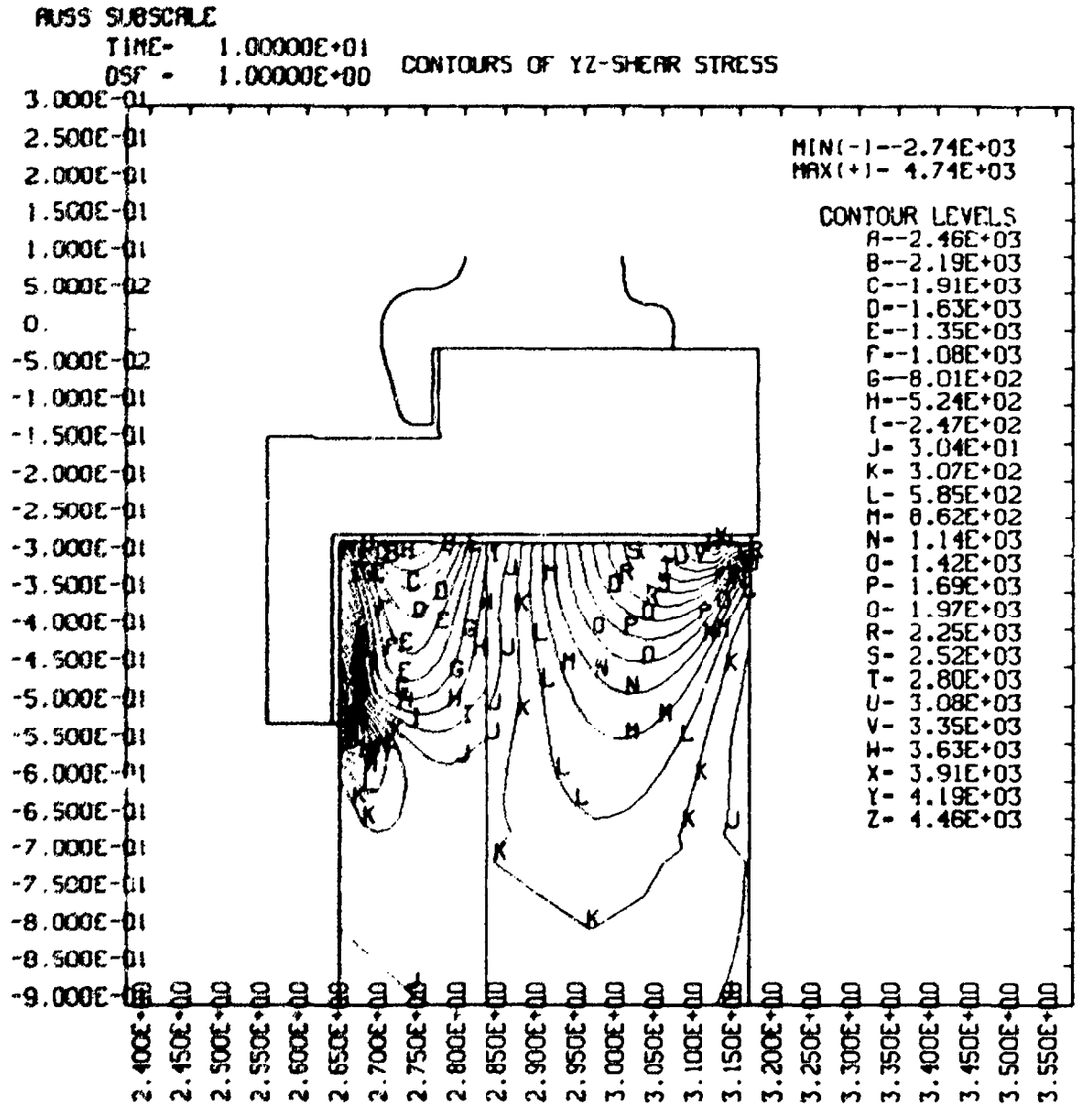

AS BUILT CASE

Location: Cylinder, end

Pressure: 10,000 psi

APPENDIX B

AUSS Model-Scale Pressure-Hull Cylinder from Glass-Fiber-Reinforced Plastic

Note: The calculations of layer, composite, and effective cylinder properties were obtained from H. Garala, NSRDC and R.G. Rudness, Oak Ridge National Laboratory

GENERAL

Although graphite-fiber-reinforced plastic (GFRP) was the prime candidate for fabrication of the cylindrical pressure hull in the AUSS vehicle, the glass-fiber-reinforced plastic (GRP) was also seriously considered for this application. To this end, a GRP model-scale pressure-hull cylinder was fabricated by Martin Marietta Energy Systems at Oak Ridge, TN, using the same tooling employed for the winding of the AUSS model-scale pressure-hull GFRP cylinder.

FABRICATION

The dimensions of the GRP model-scale cylinder were identical to those of the GFRP cylinder to facilitate direct comparison between structural performances of cylinders made from GRP and GFRP (Figure B-1). There was a difference, however, in the hoop-to-axial layup ratios. While the GFRP cylinder was wound with 2.5:1 hoop- to-axial ratio in the first 40 percent of thickness, followed by 2:1 ratio in the remainder of the thickness, the GRP cylinder was wound using only the 2:1 hoop-to-axial ratio (Figure B-2). The materials used in the winding of the GRP cylinder was S2 glass and ERL 2258-PDA epoxy resin (Figure B-3).

The computer-generated CLASS program compared the calculated physical properties of individual composite layers and of laminate with 2:1 hoop to axial ratio in GRP and GFRP cylinders (Table B-1). The calculated longitudinal and transverse moduli of elasticity indicated that the GRP cylinder should be elastically stable at design pressure of 9,000 psi without any radial end support. Furthermore, the laminate transverse (axial) modulus appears to be almost as large as the laminate longitudinal (hoop) modulus because the glass fiber is highly isotropic in both axial and transverse directions.

In this respect, the calculated GRP laminate 2:1 ratio properties are very different from the calculated GFRP laminate (2:1 ratio) properties (Table B-2). In the GFRP laminate, the transverse (axial) modulus is, approximately, only 54 percent of the longitudinal (hoop) modulus because the structural properties of GFRP fibers are highly directionally oriented (27,400,000 along fiber versus 1,550,000 psi transverse).

Based on the review of calculated laminate moduli ratios in GFRP and GRP composite cylinders, one can conclude that the 2:1 hoop-to-axial layup ratio does not represent the optimum layup ratio for maximizing resistance to circumferential elastic instability without increasing the axial stresses to dangerous levels. For GRP, the ratio should fall into the 3 to 5 range, while for GFRP it should be in the 2.2 to 2.5 range. The actual layup ratios chosen for the AUSS model-scale pressure-hull cylinders were 2.19:1 for GFRP and 2:1 for GRP constructions. Obviously, the ratio chosen for GFRP is closer to the optimum layup ratio than the one for GRP.

The GRP cylinder was wound in two stages. After winding half of the thickness, the composite was jelled by heating it to between 120° to 130°F for 16 hours while rotating on the aluminum mandrel. After jelling, the winding was continued until the full thickness was attained. The fully wound cylinder was again heated to between 120° to 130°F for 16 hours while slowly rotating on the mandrel. The completely jelled cylinder was now cured in an oven for 4 hours at 300°F while still

Table B-1. Calculated properties of GRP used in design of model-scale AUSS pressure-hull cylinder.

*****LAYER PROPERTIES *****

pppppppppppppppppppppppppppppppppppppppppppppppppppppppppppppppppppppppppppppp

LAYER identification is number 6

The LAYER has been named S2/2258/.79VF

Layer Axial Modulus is .... 9.800E+06
Layer Transverse Modulus is .... 4.900E+06
Layer Axial Poisson's Ratio is 0.2500
Layer Transverse Poisson's Ratio is 0.2800
Layer Axial Shear Modulus is .... 2.000E+06
Layer Axial Thermal Expansion Coeff. is 1.750E-06
Layer Transverse Thermal Expansion Coeff. is 7.000E-06
Layer Axial Tensile Strength is .... 2.900E+05
Layer Axial Compressive Strength is .... 2.000E+05
Layer Transverse Tensile Strength is .... 1.400E+04
Layer Transverse Compressive Strength is .... 4.200E+04
Layer Shear Strength is .... 2.800E+04

Layer Density is 7.800E-02

LAMINATE THERMOELASTIC PROPERTIES

pppppppppppppppppppppppppppppppppppppppppppppppppppppppppppppppppppppppppppppp

MATERIAL IS :
M6/T.3333/0/T.0833/90/-90/S

LAMINATE LONGITUDINAL MODULUS (0)	(E xx)	=	8.193E+06
LAMINATE TRANSVERSE MODULUS (90)	(E yy)	=	6.554E+06
LAMINATE SHEAR MODULUS (in plane)	(G xy)	=	2.000E+06
LAMINATE MAJOR POISSON'S RATIO	(NU xy)	=	0.1875
LAMINATE LONGITUDINAL BENDING MODULUS	(D xx)	=	8.015E+05
LAMINATE TRANSVERSE BENDING MODULUS	(D yy)	=	4.234E+05
LAMINATE SHEAR BENDING MODULUS	(D xy)	=	1.666E+05
LAMINATE DENSITY		=	7.850E-02
LAMINATE LONGITUDINAL EXPANSION COEFFICIENT	(' xx)	=	2.915E-06
LAMINATE TRANSVERSE EXPANSION COEFFICIENT	(' yy)	=	4.485E-06
LAMINATE SHEAR EXPANSION COEFFICIENT	(' xy)	=	1.484E-36
LAMINATE THERMAL CURVATURE COEFFICIENT	(k xx)	=	1.079E-20
LAMINATE THERMAL CURVATURE COEFFICIENT	(k yy)	=	-2.124E-20
LAMINATE THERMAL CURVATURE COEFFICIENT	(k xy)	=	-9.915E-29

Table B-2. Calculated properties of GFRP used in design of model-scale AUSS pressure-hull cylinder.

***** LAYER PROPERTIES *****

pppppppppppppppppppppppppppppppppppppppppppppppppppppppppppppppppppppppppp

LAYER identification is number 4

The LAYER has been named IM6/2258/.68VF

Layer Axial Modulus is .... 2.740E+07
Layer Transverse Modulus is .... 1.551E+06
Layer Axial Poisson's Ratio is 0.3110
Layer Transverse Poisson's Ratio is 0.3300
Layer Axial Shear Modulus is .... 9.260E+05
Layer Axial Thermal Expansion Coeff. is .... -3.000E-07
Layer Transverse Thermal Expansion Coeff. is 1.300E-05
Layer Axial Tensile Strength is .... 4.700E+05
Layer Axial Compressive Strength is .... 3.500E+05
Layer Transverse Tensile Strength is .... 7.700E+03
Layer Transverse Compressive Strength is .... 2.300E+04
Layer Shear Strength is .... 1.300E+04

LAMINATE THERMOELASTIC PROPERTIES

pppppppppppppppppppppppppppppppppppppppppppppppppppppppppppppppppppppppppp

MATERIAL IS : M4/T.3333/0/T.0833/90/-90/S IM6/2258/.68VF

LAMINATE LONGITUDINAL MODULUS (0)	(E xx)	=	1.887E+07
LAMINATE TRANSVERSE MODULUS (90)	(E yy)	=	1.021E+07
LAMINATE SHEAR MODULUS (in plane)	(G xy)	=	9.260E+05
LAMINATE MAJOR POISSON'S RATIO	(NU xy)	=	0.0474
LAMINATE LONGITUDINAL BENDING MODULUS	(D xx)	=	2.207E+06
LAMINATE TRANSVERSE BENDING MODULUS	(D yy)	=	2.093E+05
LAMINATE SHEAR BENDING MODULUS	(D xy)	=	7.712E+04
LAMINATE DENSITY		=	0.000E+00
LAMINATE LONGITUDINAL EXPANSION COEFFICIENT	(' xx)	=	2.542E-07
LAMINATE TRANSVERSE EXPANSION COEFFICIENT	(' yy)	=	1.237E-06
LAMINATE SHEAR EXPANSION COEFFICIENT	(' xy)	=	-1.051E-35
LAMINATE THERMAL CURVATURE COEFFICIENT	(k xx)	=	-1.891E-22
LAMINATE THERMAL CURVATURE COEFFICIENT	(k yy)	=	8.947E-21
LAMINATE THERMAL CURVATURE COEFFICIENT	(k xy)	=	-9.029E-28

Press Any
Key

CHECK SUPPLIED CONDITIONS

pppppppppppppppppppppppppppppppppppppppppppppppppppppppppppppppppppppppppp

mounted on the now nonrotating mandrel. After cure, the composite cylinder was removed from the mandrel and trimmed to length.

The fabrication process for GRP model-scale cylinder was significantly shorter (52 hours) than for the GRFP model-scale cylinder (96 hours) because of the two additional intermediate curing cycles used in fabrication of GFRP cylinder. This makes the fabrication of GRP cylinders substantially more economical than GFRP cylinders. When one adds to this a 4:1 price differential in cost of fiber, the overall production cost of GRP cylinders can be projected to be less than 50 percent of GFRP cylinders.

Microscopic inspection of the fabricated GRP model-scale cylinder disclosed the laminate to be of good quality. The layers were of uniform quality with only minor dispersed resin-rich inclusions (Figure B-4).

TESTING

PRESSURE-TESTING SETUP

The testing of the model scale GRP cylinder was identical to the testing of the GFRP cylinder. For proof testing to 10,000 psi, the GRP cylinder was equipped with titanium end rings and capped with titanium hemispheres (Figures B-5 through B-10). These metallic components provided the GRP cylinder with only a minimum of radial end support, which minimized flexure and shear stresses at cylinder ends.

For pressurization above 10,000 psi, the titanium hemispheres (which would fail at 11,500 psi) were replaced with flat steel closures capable of withstanding pressures to 20,000 psi (Figures B-12 and B-13). The same flat end plates were used previously for implosion testing of the GFRP model-scale cylinder.

Prior to pressure testing, the interior of the GRP cylinder was instrumented with ten 90°F straingage rosettes and a single acoustic-emission transducer with 150-kHz natural frequency (Figure B-11). Both the straingages and the acoustic-emission transducer were to provide advance warning of impending implosion and, thus, an opportunity to terminate pressurization prior to destruction of the model-scale pressure hull.

PRESSURE-TESTING PROCEDURE

The AUSS model-scale GRP cylinder was subjected to the same test procedure as the GFRP cylinder (Appendix A). First, the test assembly consisting of the cylinder capped at both ends with titanium hemispheres (Figure B-7) was prooftested at 10,000 psi while the strains were read at 1,000-psi intervals. Following the prooftest, the same assembly was pressure cycled ten times to 9,000 psi. The strains were read again at the completion of 10-pressure cycles to determine if any creep took place during cycling.

After successful completion of pressure cycling, the test assembly was removed from the pressure vessel and disassembled. The GRP cylinder was now mated with the flat-steel end plates (Figures B-12 and B-13) and placed back into the pressure

vessel. The pressurization of this test assembly proceeded at 700 psi/minute rate with 30-second pauses for taking strain readings at 1000 psi intervals. Pressurization was terminated at 17,500 psi when it appeared that implosion was imminent. This decision was based on exponential rise of acoustic-emission events during the pressurization interval from 17,000 to 17,500 psi. Upon removal from the pressure vessel, the GRP cylinder was inspected for any visual signs of damage. None were observed.

TEST FINDINGS

The hoop and axial strains recorded by straingages on the interior of the GRP cylinder (Table B-3) increased linearly with pressure to 10,000 psi (Figures B-14 and B-15). The average hoop and axial strains recorded at *midbay* were –7592 and –3608 microinches/inch; at the ends, the strains decreased to –5485 and –3086 microinches per inch, respectively. The significant decrease in hoop strains at the ends indicates that the titanium hemispherical end closures (Figure B-10) provide considerable radial support to the ends of the GRP cylinder and generate significant shear stresses whose magnitude, unfortunately, cannot be determined from available strain data.

The recorded strains were used to calculate the effective moduli of elasticity in hoop and axial directions (Table B-4). Suprisingly, the hoop (7,690,000 psi) and axial (6,860,000 psi) moduli of elasticity were of about the same magnitude even though the fiber layup ratio between 90 and 0 degree orientation is 2:1. Based on this finding, one can postulate that the layup ratio chosen for the AUSS model-scale GRP cylinder is *too low*. A higher layup ratio would increase resistance to circumferential buckling and material failure in hoop direction, *the prime modes of failure*, without significantly decreasing the resistance to axial buckling and material failure in axial direction, a *potential secondary mode* of failure.

Table B-8. Strains on the interior surface of AUSS model-scale pressure hull cylinder made of glass reinforced plastic.

	:<---------- 0.5L ---------->				<---- 0.4L ---->				<---- 0.31L ---->	
	Orientation									
Pressure	Hoop	Axial	Hoop	Axial	Hoop	Axial	Hoop	Axial	Hoop	Axial
0	0	0	0	0	0	0	0	0	0	0
1000	-739	-345	-737	-352	-744	-353	-733	-354	-732	-359
2000	-1395	-657	-1394	-667	-1410	-666	-1391	-668	-1392	-677
3000	-2174	-1032	-2175	-1045	-2202	-1041	-2172	-1045	-2174	-1059
4000	-2917	-1396	-2929	-1413	-2956	-1406	-2916	-1412	-2916	-1431
5000	-3682	-1780	-3710	-1802	-3736	-1791	-3686	-1799	-3687	-1824
6000	-4449	-2156	-4509	-2167	-4534	-2155	-4428	-2168	-4433	-2180
7000	-5237	-2542	-5300	-2522	-5303	-2492	-5374	-2792	-5282	-2592
8000	-6018	-2957	-6074	-2936	-6076	-2894	-6225	-3270	-6045	-3010
9000	-6775	-3354	-6863	-3323	-6871	-3285	-7043	-3736	-6833	-3429
10000	-7508	-3735	-7616	-3408	-7653	-3681	-7795	-4151	-7550	-3815

	<---- 0.21L ---->		<---- 0.12L ---->		:<---------- 0.015L ---------->					
Pressure	Hoop	Axial	Hoop	Axial	Hoop	Axial	Hoop	Axial	Hoop	Axial
0	0	0	0	0	0	0	0	0	0	0
1000	-735	-353	-745	-281	-603	-225	-502	-262	-580	-273
2000	-1390	-660	-1407	-531	-1121	-496	-927	-515	-1081	-549
3000	-2166	-1029	-2198	-832	-1740	-826	-1430	-818	-1680	-885
4000	-2910	-1389	-2956	-1126	-2333	-1145	-1906	-1107	-2255	-1210
5000	-3688	-1768	-3742	-1434	-2950	-1478	-2400	-1406	-2857	-1554
6000	-4455	-2145	-4527	-1155	-3506	-1842	-2881	-1698	-3485	-1819
7000	-5262	-2546	-5306	-2231	-4063	-2215	-3396	-2027	-4194	-2110
8000	-5958	-2911	-6070	-2342	-4622	-2566	-3850	-2328	-4792	-2450
9000	-6764	-3338	-6853	-2661	-5243	-2944	-4327	-2558	-5421	-2795
10000	-7446	-3719	-7628	-2976	-5822	-3321	-4652	-2818	-5983	-3121

PRESSURE HULL:

Scale Factor:	4.85
Outside Diameter:	6.360 in
Inside Diameter:	5.320 in
Length:	13.40 in
Weight (without end rings):	10.4 lbs
Weight (with end rings):	11.2 lbs

INSTRUMENTATION:

90 Degrees Rosettes: CEA-13-125WT-350
Gage Factor: 2.165
Gage Size: 1/8 inch

TEST CONDITION:

Cylinder end rings radially supported by Titanium hemispherical end closures

Table B-4. Calculated* stresses and moduli of elasticity in glass-fiber-reinforced plastic (GRP) model-scale AUSS pressure-hull cylinder.

Calculation of Moduli:

Hook's Law for an othrotropic material in cylindrical coordinates is as follows:

$$Strn(c) = 1/E(c)\ [Strs(c) - V(cz)\ Strs(z) - V(cr)\ Strn(r)]$$
$$Strn(z) = 1/E(z)\ [Strs(z) - V(zc)\ Strs(c) - V(zr)\ Strn(r)]$$
$$Strn(r) = 1/E(r)\ [Strs(r) - V(rc)\ Strs(c) - V(rz)\ Strn(z)]$$

Initial Data:

Outside Radius, R(o)	=	3.22 in.
Inside Radius, R(i)	=	2.68 in.
Pressure, p	=	10000 lb/in^2
Poisson Ratio, V(cz)	=	0.145
Poisson Ratio, V(zc)	=	0.107
Poisson Ratio, V(rc)	=	0.124
Poisson Ratio, V(cr)	=	0.256
Poisson Ratio, V(zr)	=	0.275
Poisson Ratio, V(rz)	=	0.180
Average Strains in Hoop Direct. @ 0.5L, Strn(c)	=	7592 u in/in
Average Strains in Axial Direct. @ 0.5L, Strn(z)	=	3608 u in/in

Stresses in thick-walled cylinder:

$Strs(ci) = \{ 2 R^2(o)\ p \} / \{ R^2(o) - R^2(i) \}$	=	62976 lb/in^2
$Strs(co) = \{R^2(o) + R^2(i) * p\} / \{ R^2(o) - R^2(i) \}$	=	52976 lb/in^2
$Strs(zi) = \{R^2(o)\ p\} / \{ R^2(o) - R^2(i) \}$	=	31488 lb/in^2
$Strs(zo) = \{R^2(o)\ p\} / \{ R^2(o) - R^2(i) \}$	=	31488 lb/in^2
Strs(ri) =		0 lb/in^2
Strs(ro) =		10000 lb/in^2

Calculated Moduli from Strains:

Modulus in the hoop direction at inside of the cylinder, E(ci) =

$$E(ci) = 1/Strn(ci)\ [Strs(ci) - V(cz)\ \ Strs(zi) - V(cr)\ Strn(ri)]$$
$$= 7.69E+06 \text{ lb/in}^2\text{/in/in}$$

Modulus in the axial direction at inside of the cylinder, E(zi) =

$$E(zi) = 1/Strn(zi)\ \ [Strs(zi) - V(zc)\ \ Strs(ci) - V(zr)\ \ Strn(ri)]$$
$$= 6.86E+06 \text{ lb/in}^2\text{/in/in}$$

* Calculations are based on average hoop and axial strains *measured* on the interior surface of AUSS model-scale pressure hull cylinder subjected to 10,000 psi external hydrostatic pressure loading.

COMPARISON OF TEST DATA FROM GRP AND GFRP CYLINDERS

When one compares strains recorded during hydrostatic testing of GFRP cylinder (Appendix A) with strains recorded on the GRP cylinder, several interesting observations can be made.

(1) The titanium hemispherical end supports are better matched to GFRP than GRP cylinders, as evidenced by the fact that the hoop strains at midbay and at ends of GFRP cylinder (Table B-5, Figures B-16 and B-17) are approximately the same magnitude while in the GRP cylinder they differ significantly (Table B-6, Figures B-14 and B-15).

(2) The hoop and axial strains in the GFRP cylinder are fairly well matched while those in the GRP cylinder differ by a factor of two. This would seem to indicate that the 2.19:1 layup ratio in GFRP cylinder is *close to optimum* value while the 2:1 layup ratio in GRP cylinder is far from optimum; increasing the layup ratio in the GFRP cylinder to 2.5:1 would probably optimize graphite-fiber-reinforced composite cylinders for external pressure. In GRP cylinders, the layup ratio needs to be increased to at least 3:1 before the hoop and axial strains start approaching in magnitude.

(3) The effective moduli of elasticity in GFRP cylinder differ by, approximately, a factor of two indicating a well balanced design that maximizes circumferential resistance to buckling while at the same time providing adequate resistance to axial buckling (Table B-7). This is not the case with GRP cylinder where the effective moduli in hoop and axial directions are close to being the same (Table B-3). The design of the GRP cylinder can be significantly improved by placing more fibers in the hoop direction which would raise the circumferential resistance to buckling, while still providing adequate resistance to axial buckling.

(4) The performance of the GRP cylinder was superior to that of GFRP cylinder, as shown by its ability to withstand 17,500 psi of external pressure without implosion. The GFRP cylinder imploded at 12,600 psi. This large disparity in critical pressures is amazing, when one considers that the 2.19:1 layup ratio of the GFRP cylinder was close to the optimum value for graphite-fiber-reinforced cylinders under external pressure, while the 2:1 layup ratio of the GRP cylinder was far from the optimum value for glass-fiber-reinforced cylinders.

Table B-5. Predicted strains on the interior surfaces of AUSS model-scale pressure-hull cylinder at 10,000-psi external hydrostatic pressure loading.

AUSS Model-Scale GFRP Pressure-Hull Cylinder

APPLIED LOADING		LAMINATE MID-PLANE STRAINS AND CURVATURES LOAD INDUCED response		TEMPERATURE INDUCED response	
N xx =	-1.0000D+03	e xx =	-5.1757D-05	e xx =	0.0000D+00
N yy =	-5.0000D+02	e yy =	-4.6469D-05	e yy =	0.0000D+00
N xy =	0.0000D+00	e xy =	1.0410D-26	e xy =	0.0000D+00
M xx =	0.0000D+00	k xx =	6.1032D-12	k xx =	0.0000D+00
M yy =	0.0000D+00	k yy =	3.4303D-11	k yy =	0.0000D+00
M xy =	0.0000D+00	k xy =	-6.9863D-19	k xy =	0.0000D+00

AUSS Model-Scale GRP Pressure-Hull Cylinder

APPLIED LOADING		LAMINATE MIDPLANE STRAINS AND CURVATURES LOAD INDUCED response		TEMPERATURE INDUCED response	
N xx =	-1.0000D+03	e xx =	-1.1063D-04	e xx =	0.0000D+00
N yy =	-5.0000D+02	e yy =	-5.3413D-05	e yy =	0.0000D+00
N xy =	0.0000D+00	e xy =	3.7132D-28	e xy =	0.0000D+00
M xx =	0.0000D+00	k xx =	1.6350D-11	k xx =	0.0000D+00
M yy =	0.0000D+00	k yy =	1.3114D-11	k yy =	0.0000D+00
M xy =	0.0000D+00	k xy =	-2.4919D-20	k xy =	0.0000D+00

YY = AXIAL ORIENTATION
XX = HOOP ORIENTATION

Table B-6. Strains on the interior surface of AUSS model-scale pressure-hull cylinder made of graphite-fiber-reinforced plastic.

					Mid-bay					
Pressure	GAGE 1		GAGE 2		GAGE 3		GAGE 4		GAGE 5	
(PSI)	Axial	Hoop	Axial	Hoop	Axial	Hoop	Axial	Hoop	Axial	Hoop
0	0	0	0	0	0	0	0	0	0	0
1000	-334	-358	-325	-376	-326	-379	-338	-391	-338	-402
2000	-685	-746	-688	-764	-668	-767	-678	-783	-688	-809
3000	-1025	-1122	-997	-1141	-996	-1138	-999	-1157	-1013	-1185
4000	-1362	-1489	-1320	-1505	-1312	-1500	-1315	-1526	-1338	-1364
5000	-1713	-1879	-1663	-1900	-1655	-1894	-1656	-1927	-1689	-1975
6000	-2064	-2271	-2008	-2299	-2001	-2291	-2000	-2330	-2041	-2391
7000	-2416	-2666	-2354	-2700	-2347	-2691	-2343	-2735	-2394	-2812
8000	-2780	-3084	-2770	-3127	-2714	-3115	-2707	-3164	-2766	-3260
9000	-3158	-3510	-3099	-3573	-3095	-3560	-3086	-3611	-3154	-3733
10000	-3498	-3881	-3418	-3951	-3415	-3935	-3403	-3987	-3479	-4135

					Mid-Bay to Ring A					
Pressure	GAGE 6		GAGE 7		GAGE 8		GAGE 9		GAGE 10	
(PSI)	Axial	Hoop	Axial	Hoop	Axial	Hoop	Axial	Hoop	Axial	Hoop
0	0	0	0	0	0	0	0	0	0	0
1000	-341	-407	-345	-398	-340	-392	-338	-383	-337	-370
2000	-689	-815	-694	-801	-682	-796	-672	-787	-638	-760
3000	-1009	-1193	-1017	-1176	-998	-1171	-983	-1162	-925	-1120
4000	-1332	-1574	-1341	-1552	-1315	-1548	-1295	-1538	-1218	-1482
5000	-1679	-1987	-1690	-1959	-1656	-1956	-1631	-1945	-1535	-1873
6000	-2030	-2405	-2043	-2372	-2001	-2370	-1971	-2359	-1857	-2269
7000	-2380	-2827	-2396	-2789	-2346	-2787	-2311	-2774	-2180	-2666
8000	-2753	-3278	-2771	-3235	-2713	-3233	-2672	-3218	-2521	-3090
9000	-3138	-3751	-3160	-3702	-3093	-3701	-3046	-3682	-2872	-3571
10000	-3462	-4155	-3487	-4099	-3412	-4098	-3359	-4077	-3166	-3905

PRESSURE HULL:
- Scale Factor: 4.85
- Outside Diameter: 6.360 in
- Inside Diameter: 5.320 in
- Length: 13.40 in
- Weight (without end rings): 7.0 lbs
- Weight (with end rings): 7.8 lbs

INSTRUMENTATION:
- 90 Degrees Rosettes: CEA-13-125WT-350
- Gage Factor: 2.165
- Gage Size: 1/8 inch

TEST CONDITION:
- Cylinder end rings radially supported by Titanium hemispherical end closures

Table B-7. Calculated* stresses and moduli of elasticity in graphite-fiber-reinforced plastic (GFRP) model-scale AUSS pressure-hull cylinder.

Calculation of Moduli:

Hook's Law for an othrotropic material in cylindrical coordinates is as follows:

$$Strn(c) = 1/E(c) \quad [Strs(c) - V(cz)\ Strs(z) - V(cr)\ Strn(r)]$$
$$Strn(z) = 1/E(z) \quad [Strs(z) - V(zc)\ Strs(c) - V(zr)\ Strn(r)]$$
$$Strn(r) = 1/E(r) \quad [Strs(r) - V(rc)\ Strs(c) - V(rz)\ Strn(z)]$$

Initial Data:

Outside Radius, R(o)	=	3.182 in.
Inside Radius, R(i)	=	2.66 in.
Pressure, p	=	10000 lb/in^2
Poisson Ratio, V(cz)	=	0.052
Poisson Ratio, V(zc)	=	0.028
Poisson Ratio, V(rc)	=	0.040
Poisson Ratio, V(cr)	=	0.393
Poisson Ratio, V(zr)	=	0.386
Poisson Ratio, V(rz)	=	0.072
Average Strains in Hoop Direct. @ 0.5L, Strn(c)	=	3922 u in/in
Average Strains in Axial Direct. @ 0.5L, Strn(z)	=	3444 u in/in

Stresses in thick-walled cylinder:

$Strs(ci) = \{ 2 R^2(o)\ p \} / \{ R^2(o) - R^2(i) \}$	=	66405 lb/in^2
$Strs(co) = \{R^2(o) + R^2(i) * p\} / \{ R^2(o) - R^2(i) \}$	=	56405 lb/in^2
$Strs(zi) = \{R^2(o)\ p\} / \{ R^2(o) - R^2(i) \}$	=	33202 lb/in^2
$Strs(zo) = \{R^2(o)\ p\} / \{ R^2(o) - R^2(i) \}$	=	33202 lb/in^2
Strs(ri) =		0 lb/in^2
Strs(ro) =		10000 lb/in^2

Calculated Moduli from Strains:

Modulus in the hoop direction at inside of the cylinder, E(ci) =

$E(ci) = 1/Strn(ci) \quad [Strs(ci) - V(cz)\ Strs(zi) - V(cr)\ Strn(ri)]$

= 1.65E+07 lb/in^2/in/in

Modulus in the axial direction at inside of the cylinder, E(zi) =

$E(zi) = 1/Strn(zi) \quad [Strs(zi) - V(zc)\ Strs(ci) - V(zr)\ Strn(ri)]$

= 9.10E+06 lb/in^2/in/in

* Calculations are based on average hoop and axial strains *measured* on the interior surface of AUSS model-scale pressure-hull cylinder subjected to 10,000-psi external hydrostatic pressure loading.

DISCUSSION

Since both cylinders were fabricated by the same team at Martin Marietta Energy Systems of Oak Ridge, TN, using the same epoxy resin system, winding equipment, and mandrels, one can postulate that the only reason for the large disparity in critical pressures is inherent to the fiber material itself (i.e., S2 glass fibers are better suited to carry compressive stresses than IM6 graphite fiber). If this is the case, it may be feasible for a GRP cylinder to match the *weight* of a GFRP cylinder by increasing the thickness of the GFRP cylinder until it also implodes above 17,500 psi, which would be due to material failure. If such an approach is taken, the weight-to-displacement ratio of both GRP and GFRP cylinders would be approximately the same (about 0.625). For many applications, including AUSS, such a weight-to-displacement ratio is not acceptable, and a different approach would have to be taken.

A less conservative approach would be to reduce the critical pressure requirement for all composite pressure hulls on unmanned vehicles with 20,000-foot design depth. In such a case, the critical pressure of the GRP cylinder could be reduced until it matches that of the AUSS model-scale GFRP cylinder. This would be accomplished by reducing the thickness of the GRP cylinder until its critical pressure due to material failure decreases to 12,600 psi. Because of reduced thickness, the weight-to-displacement ratio of the cylinder would decrease to about 0.415, the same ratio as the GFRP cylinder.

CONCLUSIONS

The structural performance of the GRP model-scale AUSS cylinder was significantly superior to that of a GFRP cylinder of identical dimensions (Table B-8). The GRP model-scale AUSS cylinder met the 18,000-psi critical pressure requirement specified by NSRDC for composite pressure hulls with 9,000-psi design pressure, while the GFRP cylinder, which failed at 12,600 psi, did not meet this requirement.

There appears to be higher potential payoff for the U.S. Navy to focus the composite pressure-hull development program on GRP rather than GFRP composite since glass fibers seem to be better suited for carrying compressive stresses than graphite fibers in epoxy matrices of external pressure hulls in underwater vehicles.

RECOMMENDATIONS

An experimental program should be initiated for design and winding of AUSS pressure-hull GRP cylinders with the same weight-to-displacement ratio as the existing GFRP cylinder.

Table B-8. Test results of subscale models of AUSS cylinder.

	MODELS	
	SUBSCALE MODEL 1	SUBSCALE MODEL 2
MATERIAL SYSTEMS	IM6/2258	S2/2258
FIBER ORIENTATION	(90°/0°)	(90°/0°)
FIBER DISTRIBUTION	2.5:1 FIRST 40% OF T 2.0:1 LAST 60% OF T	2.0:1 FULL THICKNESS
FIBER CONTENT BY VOLUME	68%	74.9%
FABRICATION PROCESS	WET WINDING	WET WINDING
NUMBER OF CURE CYCLES	3	2
DIMENSIONS: I.D.; THICKNESS; LENGTH	5.30"; 0.52"; 13.4"	5.30"; 0.52"; 13.4"
WEIGHT OF THE CYLINDER (LB)	7.0	10.4
W/D RATIO		
• CLYLINDER ONLY	0.415	0.626
• WITH TI END-RINGS	0.480	0.685
• WITH TI END-RINGS AND HEMI-HEADS	0.529	0.695
MAXIMUM PRESSURE, PSI	12,600	17,500
MAXIMUM STRESSES, PSI	83,674	116,214
CALCULATED MODULI, PSI		
• HOOP DIRECTION	16,500,000	7,690,000
• AXIAL DIRECTION	9,100,000	6,860,000
AVERAGE PLY THICKNESS, IN		
• HOOP DIRECTION		0.024
• AXIAL DIRECTION	0.014	0.012
REMARKS	MODEL FAILED	MODEL IS NOT BROKEN YET
TESTING CONFIGURATIONS	MODEL WAS PRESSURE CYCLED 100 TIMES WITH TITANIUM HEMI-HEADS TO 9,000 PSI AND THEN TESTED TO FAILURE WITH FLAT PLATE END CLOSURES	MODEL WAS TESTED WITH TITANIUM HEMIHEADS TO 9,000 PSI AND THEN TESTED TO FAILURE WITH FLAT PLATE END CLOSURES

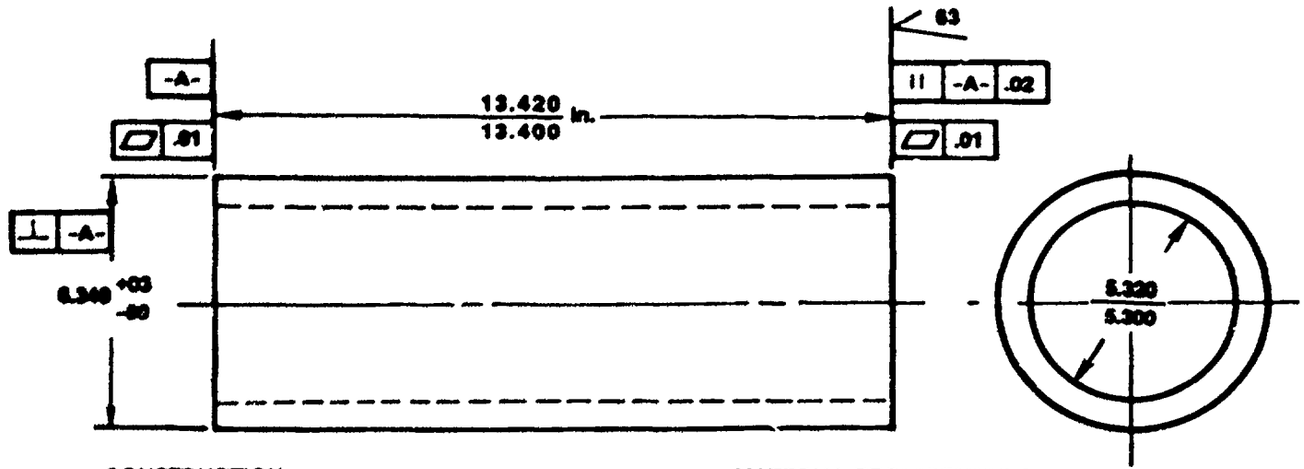

CONSTRUCTION:

FIBER EPOXY COMPOSITE
2:1 BIDIRECTIONAL FIBER ORIENTATION

STRUCTURAL PERFORMANCE REQUIREMENTS:

DESIGN PRESSURE 9000 psi
IMPLOSION PRESSURE > 13,500 psi
(WITH RADIAL END SUPPORTS)

MATERIAL REQUIREMENTS:

COMPRESSIVE PROPERTIES

HOOP	> 100,000 psi
AXIAL	> 50,000 psi
RADIAL	> 120,000 psi
E-HOOP	> 7.5×10^6 psi

FLEXURAL PROPERTIES

HOOP	> 160,000 psi
AXIAL	> 80,000 psi

Figure B-1. AUSS model-scale pressure-hull cylinder.

CONCEPTUAL CASE

1. Layup ratio for fiber layers 2.0:1.0 with 90/0 degree orientations.

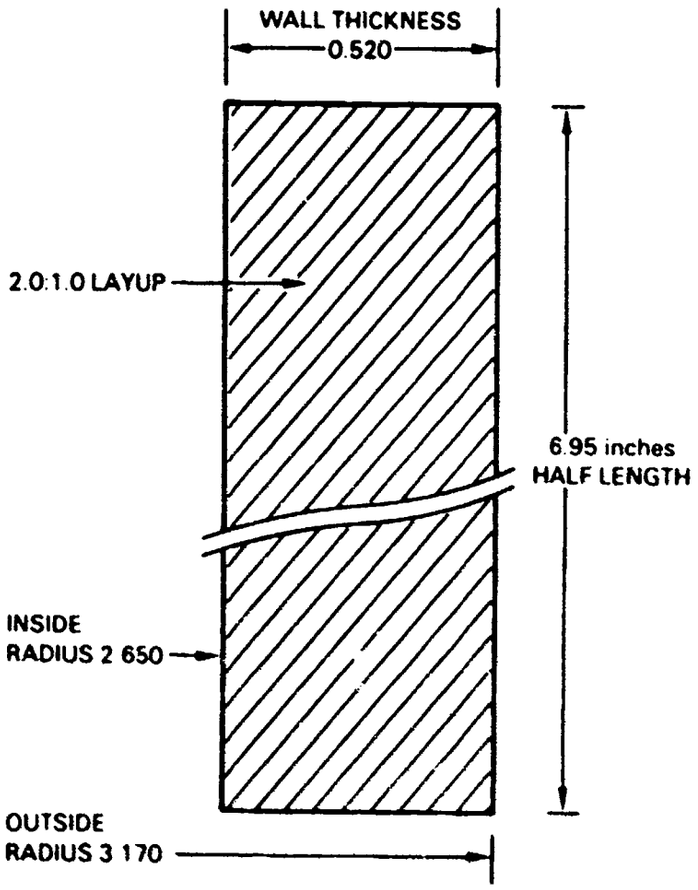

Figure B-2. Layup ratio selected for AUSS model-scale pressure-hull cylinder made from GRP.

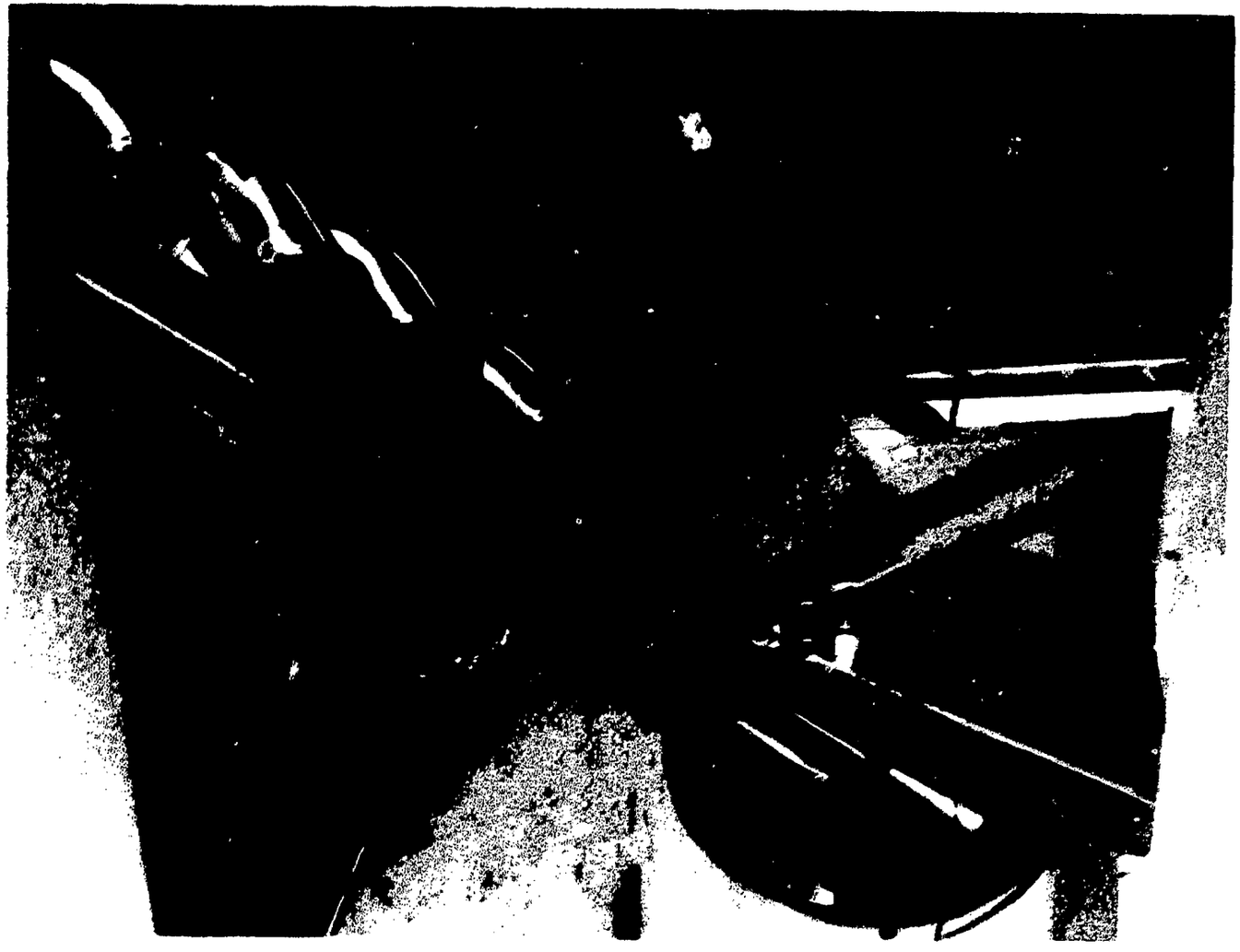

Figure B-3. Winding arrangement used in fabrication of AUSS model-scale pressure-hull cylinders.

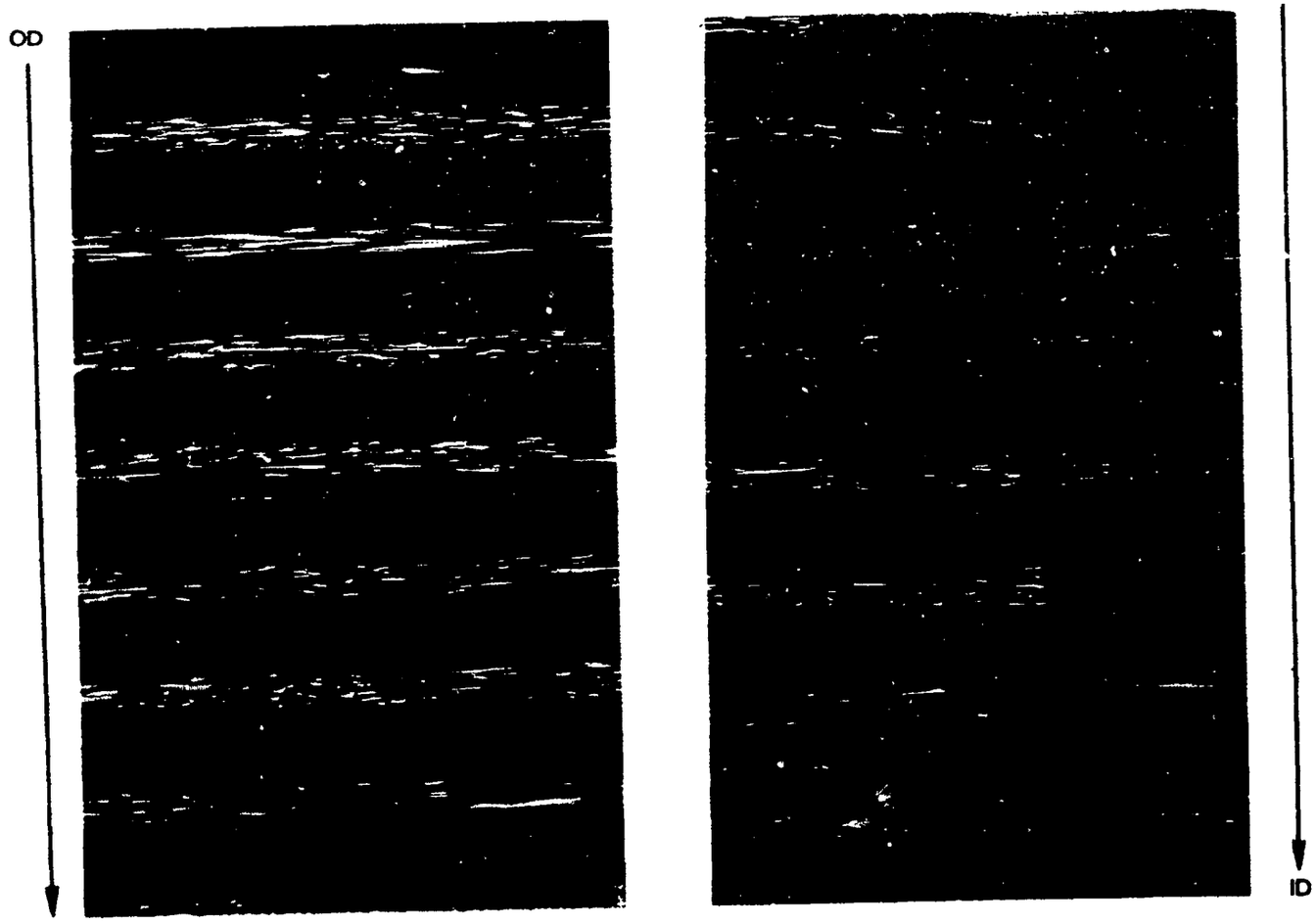

Figure B-4. Cross-section of model-scale GRP cylinder under 20 X magnification; average layer thickness is 0.024 in hoop and 0.124 in axial.

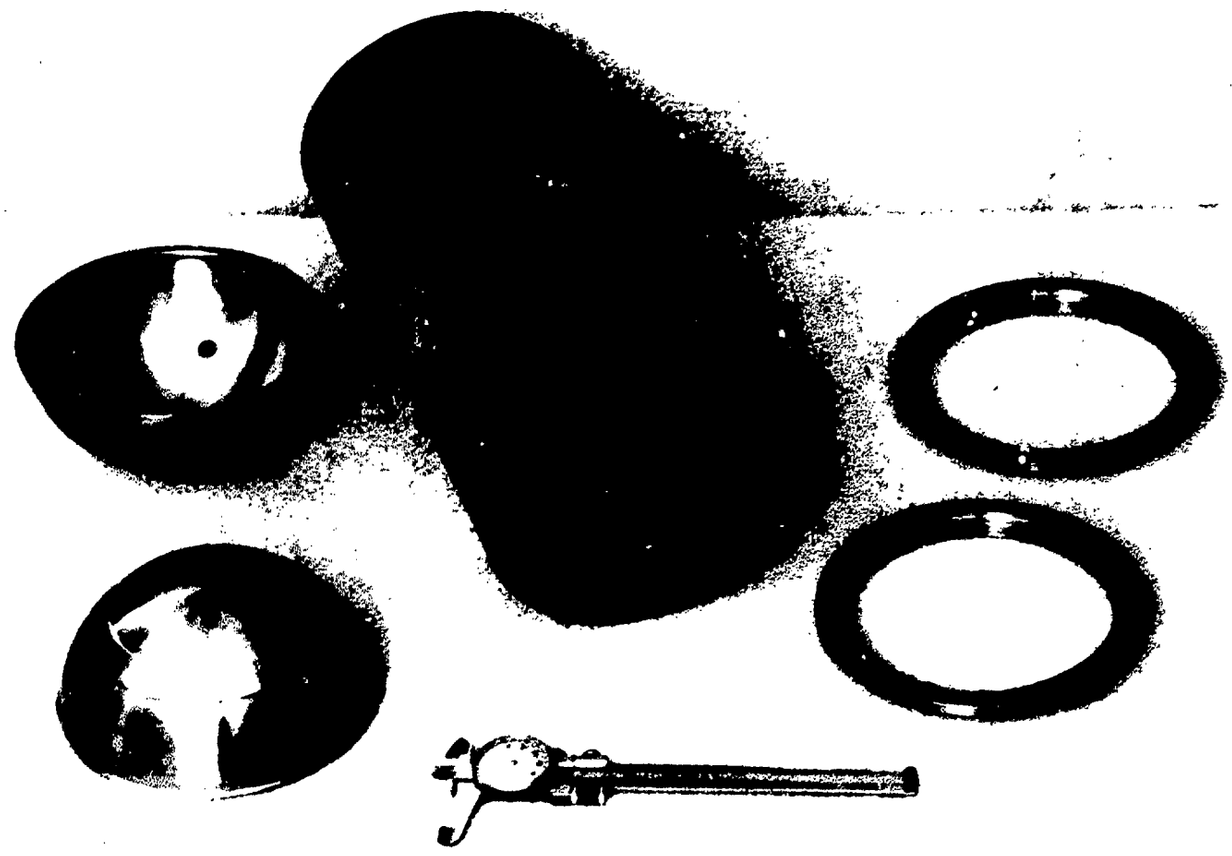

Figure B-5. Components of the GRP model-scale pressure housing before assembly for testing.

Figure B-6. AUSS model-scale pressure-hull assembly utilizing the GRP cylinder.

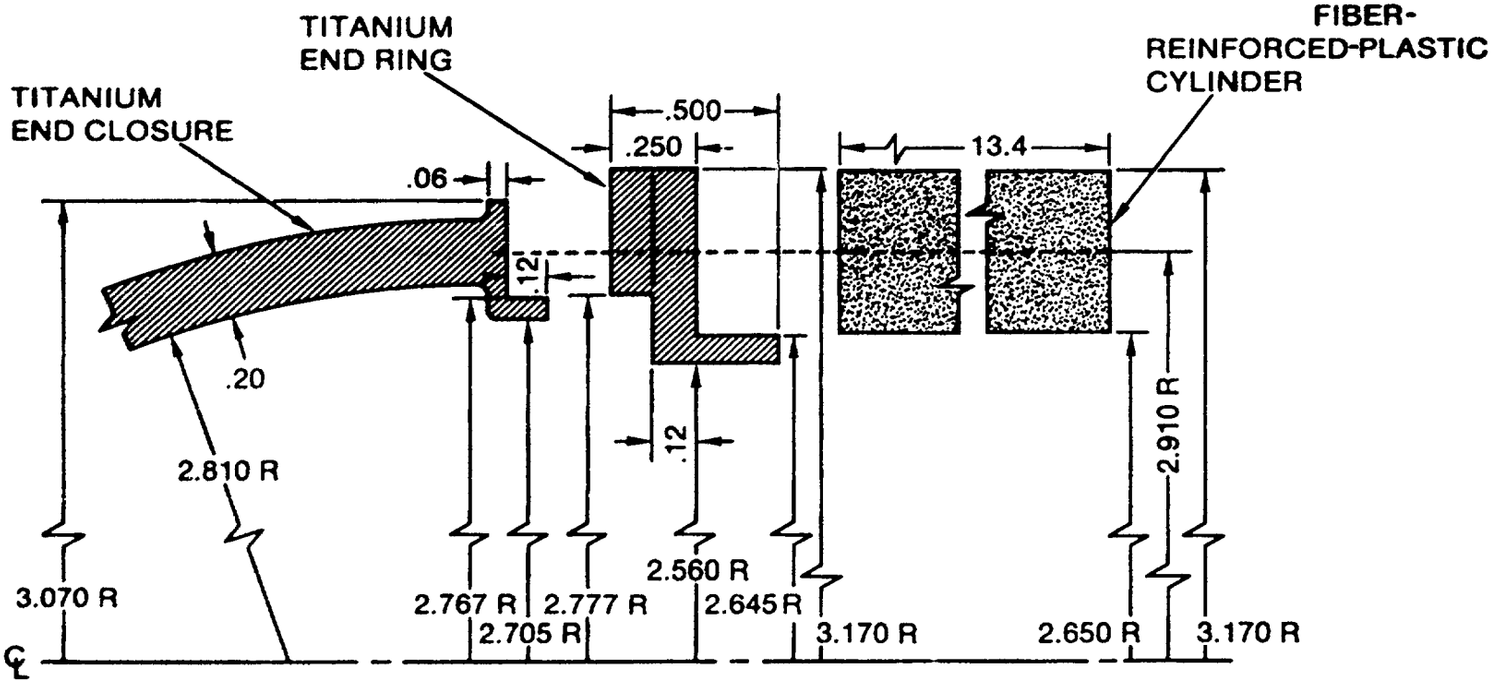

Figure B-7. Hydrotest arrangement AUSS model-scale pressure hull.

CONCEPTUAL CASE

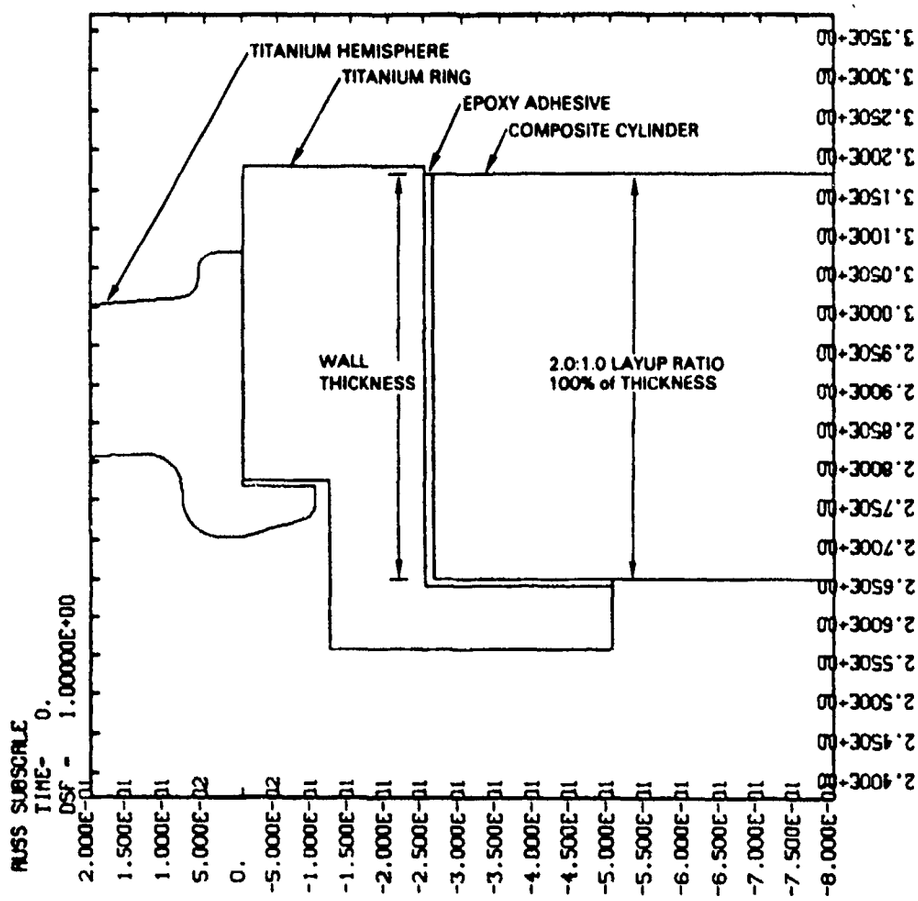

Figure B-8. Detail of cylinder end support utilized in finite element stress analysis.

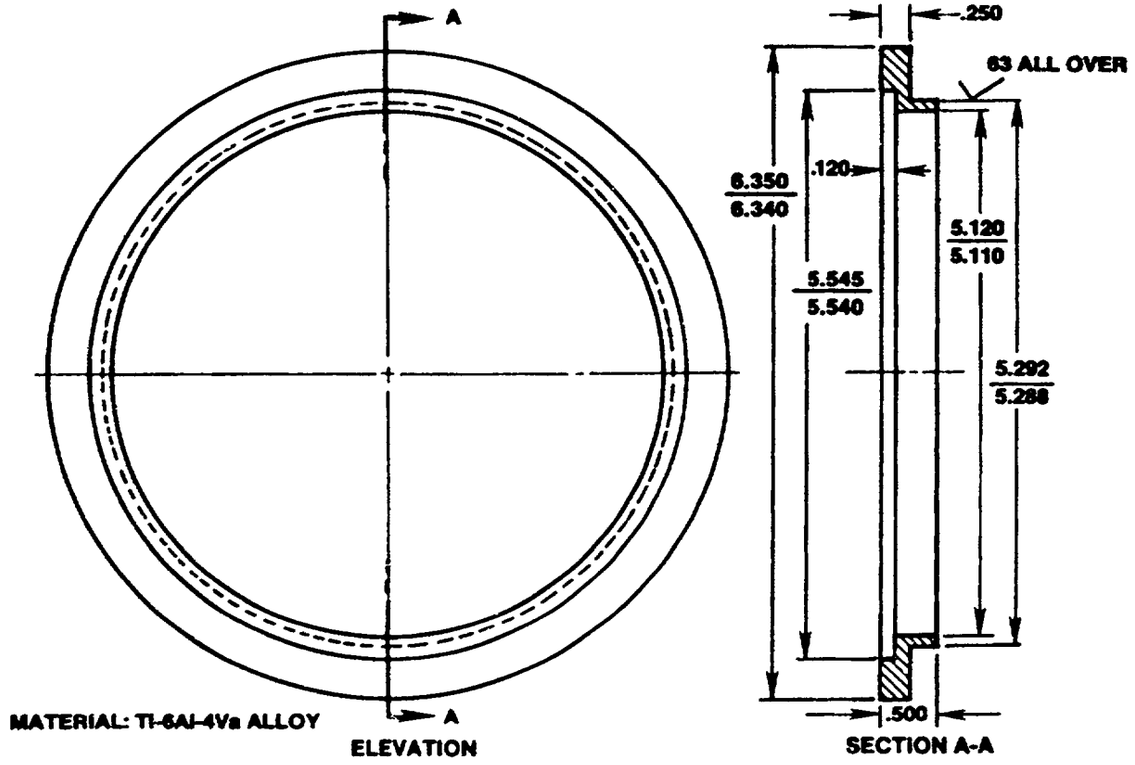

Figure B-9. AUSS model-scale pressure-huil end ring.

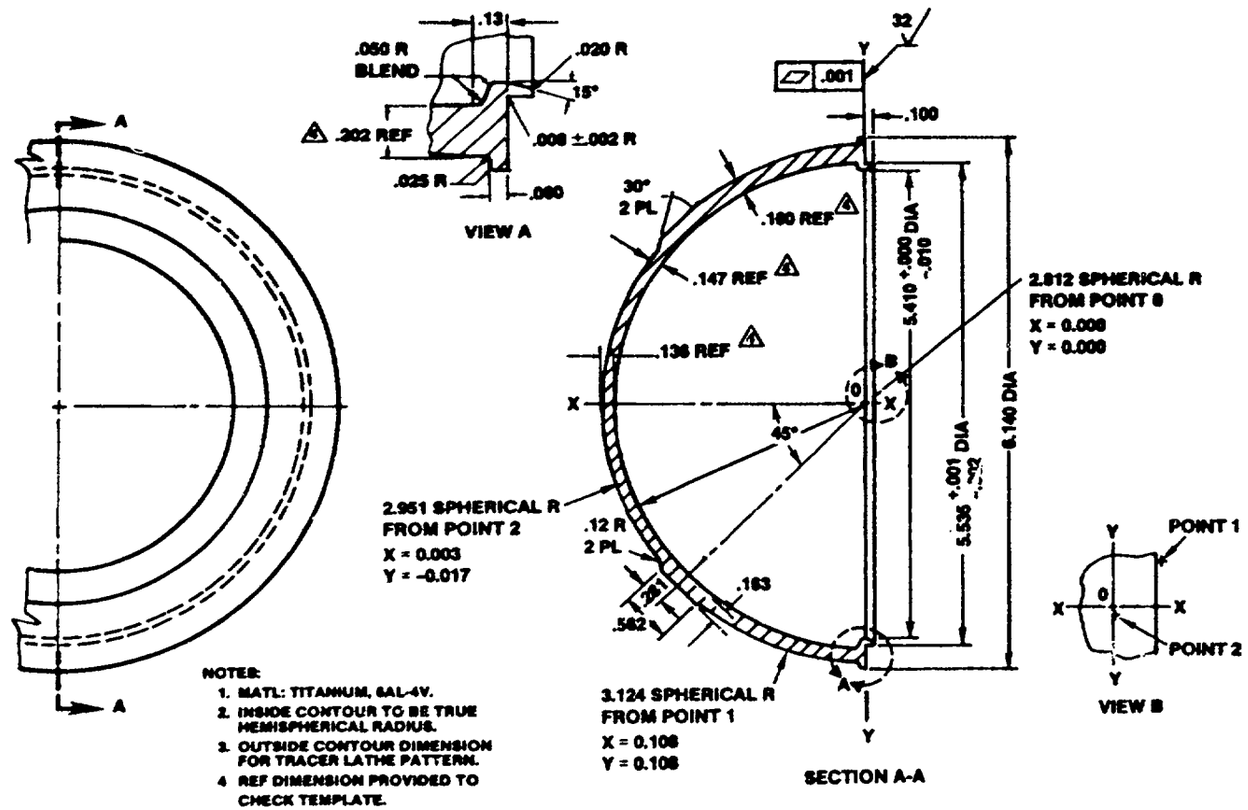

Figure B-10. AUSS model-scale pressure-hull end closure.

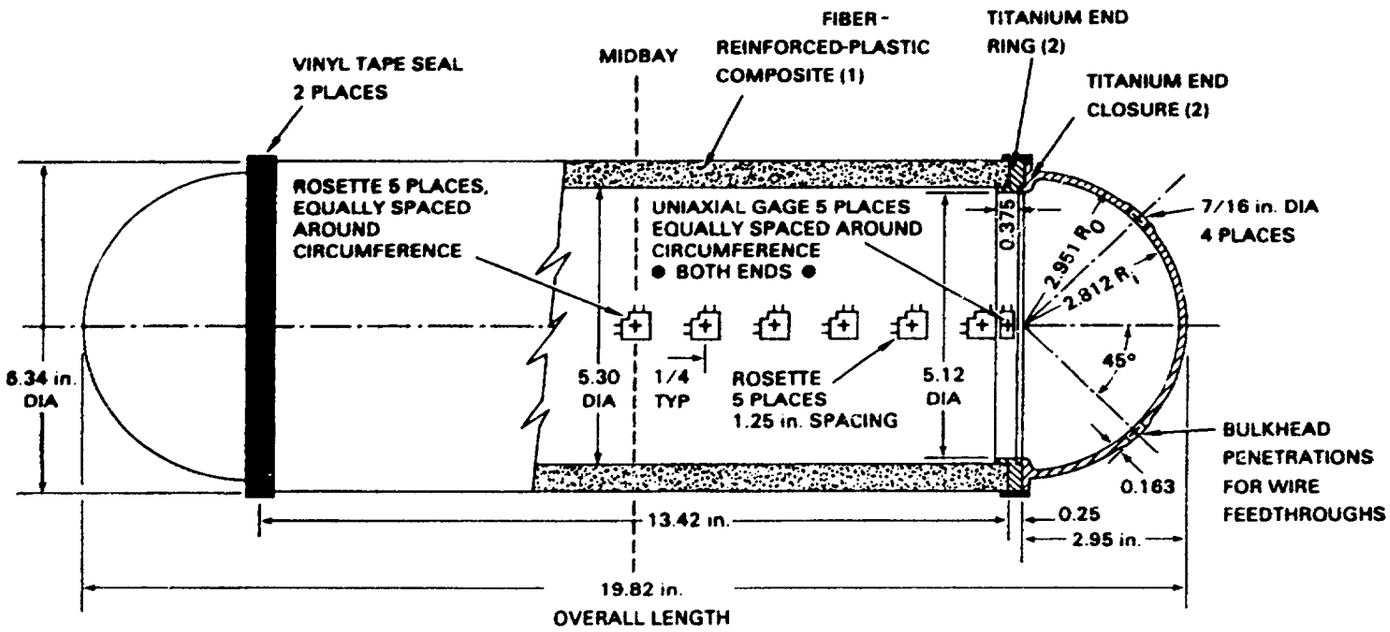

Figure B-11. Location of straingages on AUSS model-scale housing assembly.

Figure B-12. AUSS model-scale pressure-hull cylinder mated with flat plate end closures for hydrotesting to implosion: details of end closures is shown in Figure B-13.

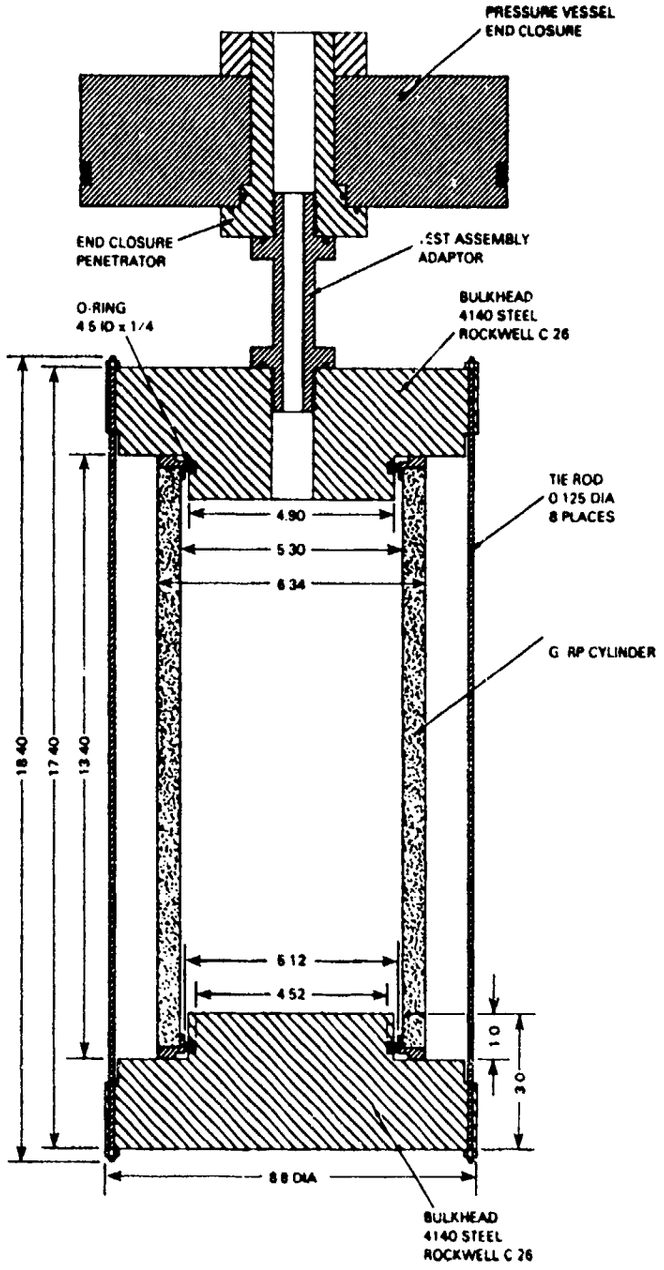

Figure B-13. Assembly test fixture.

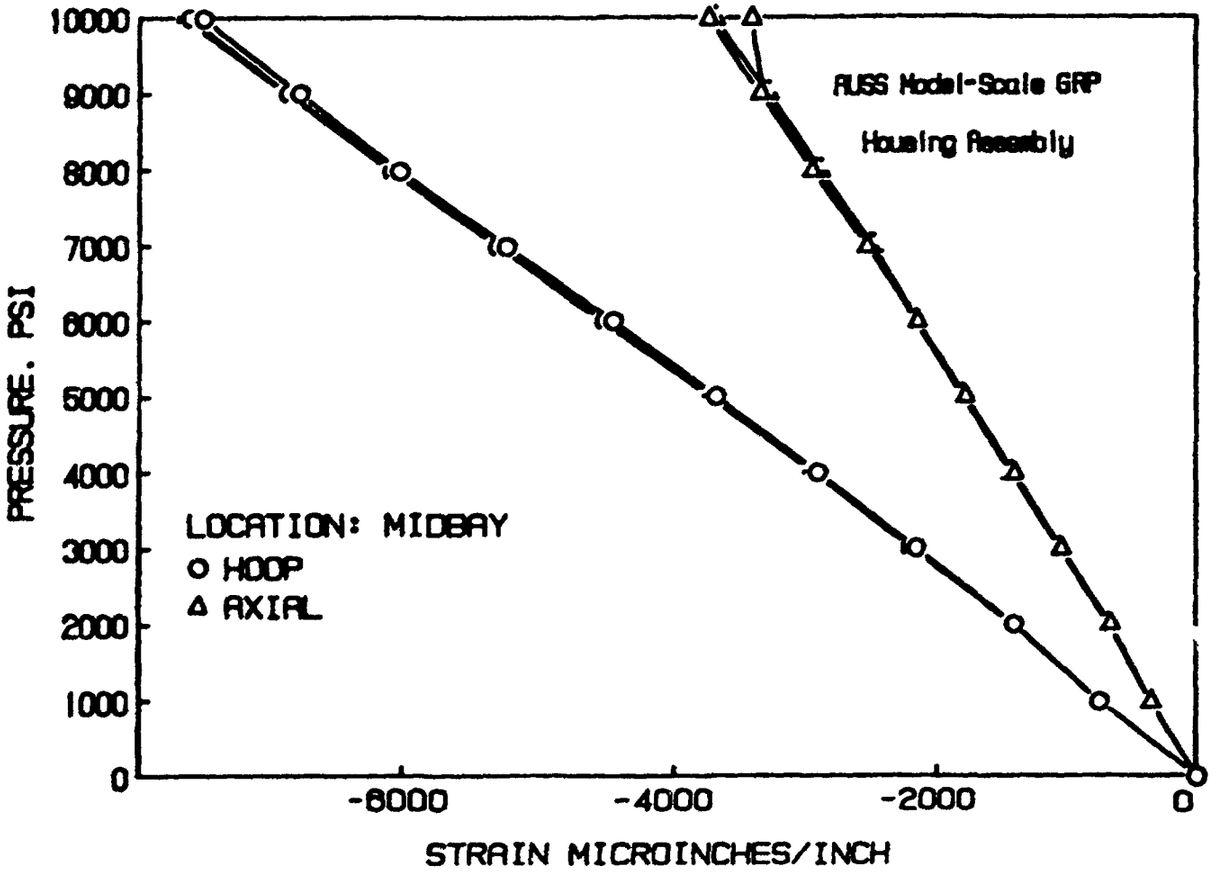

Figure B-14. Strains on the interior surface of AUSS model-scale pressure-hull GRP cylinder.

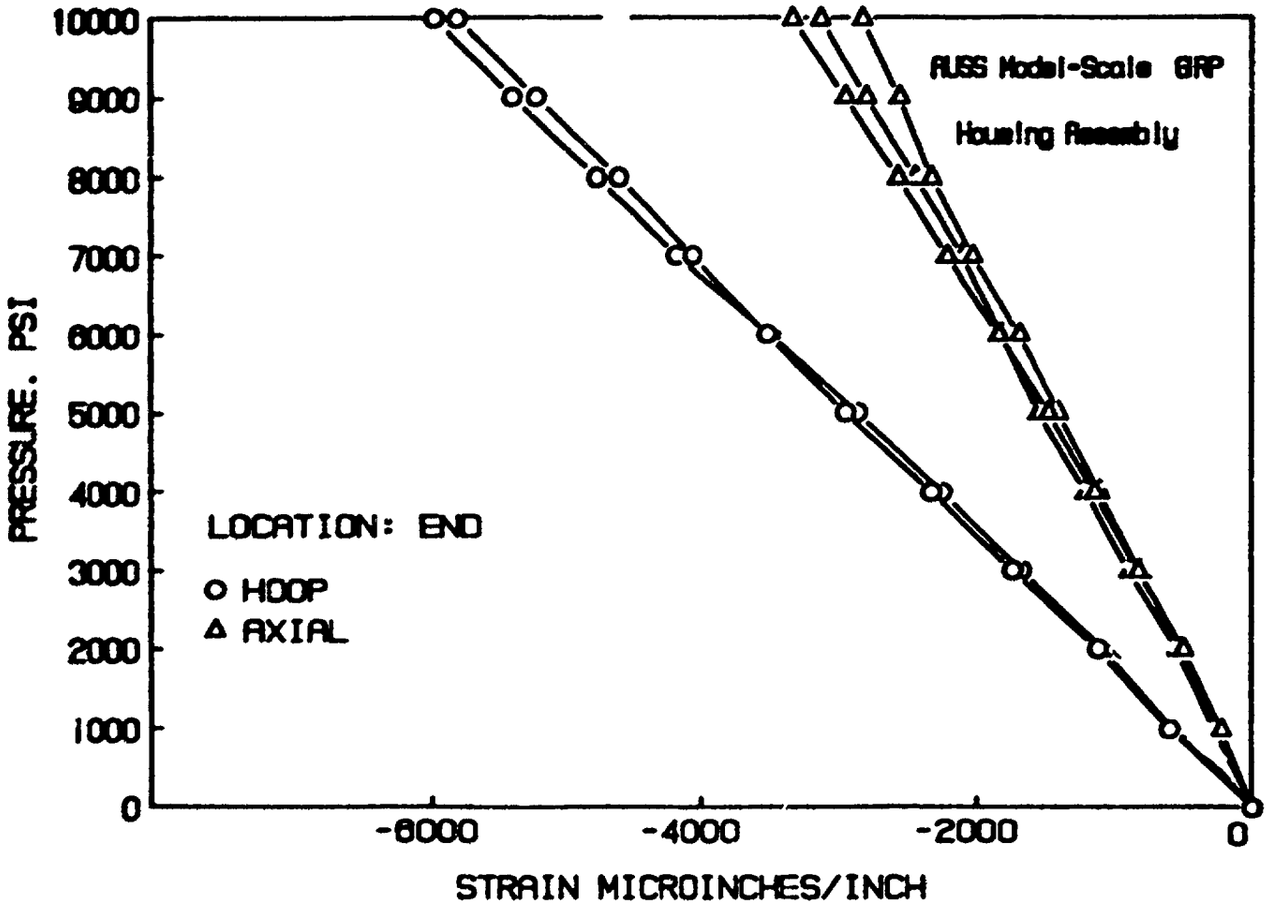

Figure B-15. Strains on the interior surface of AUSS model-scale pressure-hull GRP cylinder.

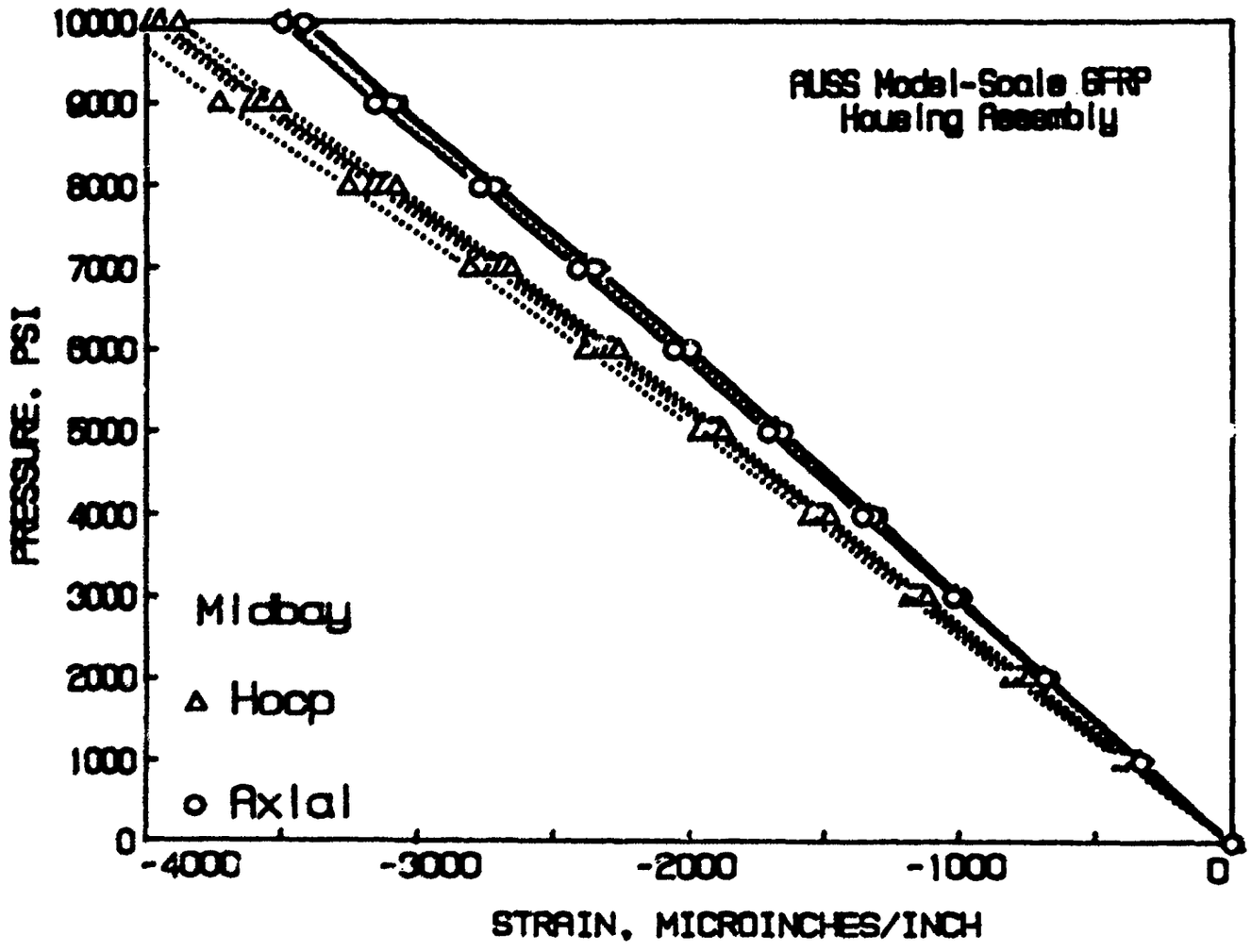

Figure 8-16. Strains on the interior surface of AUSS model-scale pressure-hull GFRP cylinder.

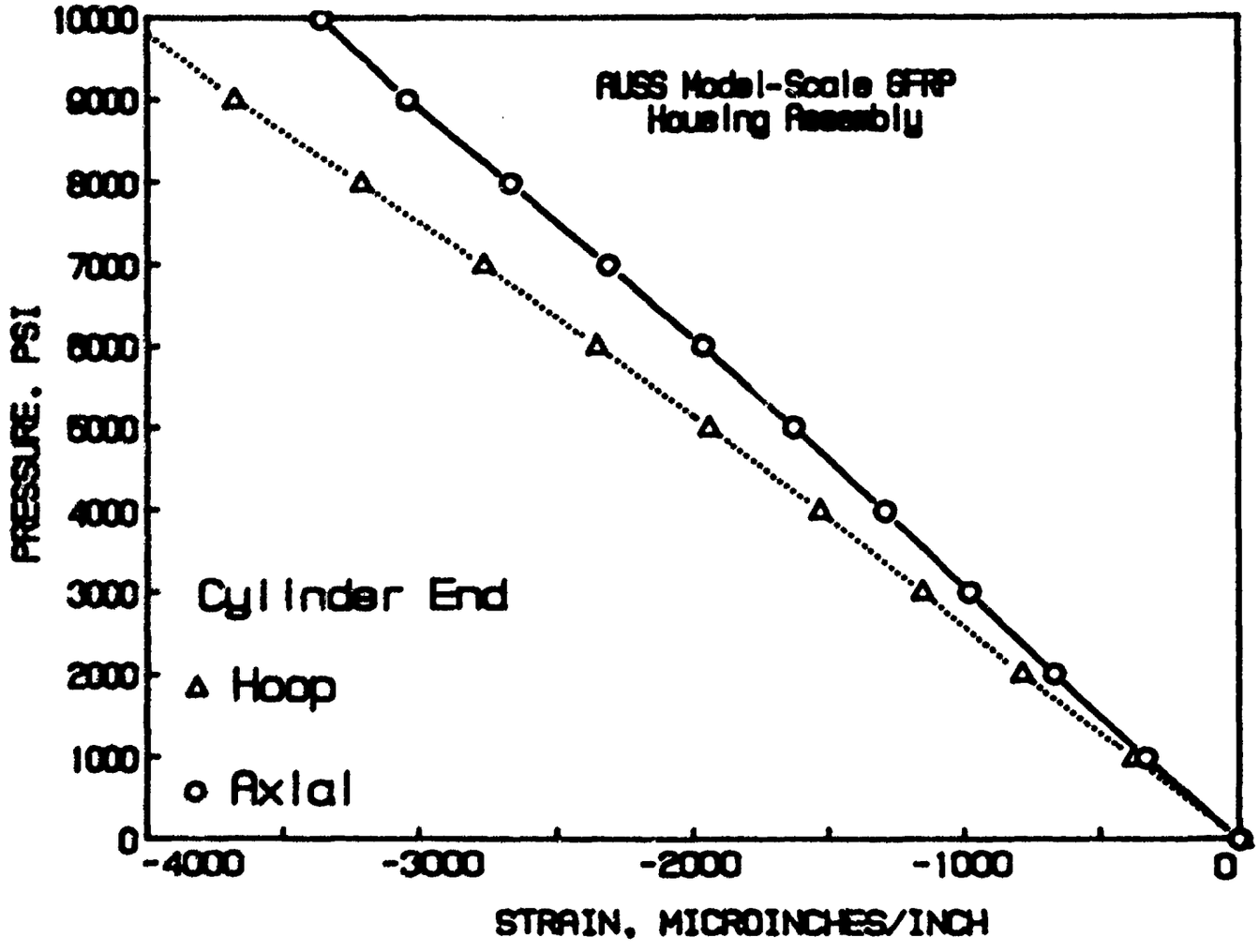

Figure B-17. Strains on the interior surface of AUSS model-scale pressure-hull GFRP cylinder.